PART I

A WF$_6$ BUBBLE CHAMBER

PART II

PHYSICS OF BUBBLE CHAMBERS AND

APPLICATIONS TO ADVANCED DESIGNS

Thesis by

Joe Hill Mullins

In Partial Fulfillment of the Requirements

For the Degree of

Doctor of Philosophy

California Institute of Technology

Pasadena, California

1959

ABSTRACT

Part I

The role of bubble chambers in photoproduction studies is considered in the light of experimental problems, and arguments for use of heavy liquid chambers are presented. Successful operation of a small WF_6 chamber in conjunction with the C.I.T. electron synchrotron is described and experimental results are given. Design, construction and operation of a 12 inch hydrostatically supported bubble chamber for use with hydrocarbons, Freons, or WF_6 is described. The chamber is operated with a unique "resonant" expansion system employing large valves of a special design, resulting in a very fast operating cycle with small energy input.

Part II

The mechanism of formation and growth of bubbles in a bubble chamber is investigated, and the results of calculations concerning growth and collapse in propane are given. Mechanisms which have been proposed dealing with the nucleation of bubbles by charged particles are examined with the intention of determining their probable validity, and the influence of some additional processes is discussed. A technique is suggested which may allow construction of large bubble chambers, particularly of the heavy liquid variety, with very fast expansions and recompressions, or very rapid cycling rates.

TABLE OF CONTENTS

PART I: A WF$_6$ BUBBLE CHAMBER

APPENDICES

PART I

A WF$_6$ BUBBLE CHAMBER

INTRODUCTION

A. Bubble Chambers - General Considerations

A pertinent starting point for a discussion of bubble chambers is an evaluation of their role as a tool for investigation in high energy physics. The capabilities and limitations of the devices are subject somewhat to specific design, but there are general characteristics which are common to most types of chambers. For example, a bubble chamber of any type is a visual instrument, and possesses the general features of such devices. In the first place, visual instruments allow one to examine very complicated single events, e.g., those with many reaction products, in great detail, and thus are often of value in identifying processes which might appear ambiguous to other means of detection. Such visual instruments are particularly useful for making general surveys of the order of magnitude of total cross sections for the types of reactions or processes occurring in a given range of energy and incident particle type.

It is also of interest to compare the properties peculiar to bubble chambers with those of other visual particle detectors, such as nuclear emulsions and cloud chambers. In general, the density of the bubble chamber medium is intermediate between that of cloud chambers and of nuclear emulsions. There is, in fact, a wide and still growing range of choice, e.g., from 0.05 gm/cm^3 for H_2 to about 2.5 gm/cm^3 for xenon or WF_6. This is one of the distinctions of bubble chambers, in that an experimenter can to some extent choose a liquid with characteristics he requires. A pertinent feature of bubble chambers which they share with expansion cloud chambers is their ability to limit background and achieve limited time resolution by examining a single pulse only of an accelerator in a given

picture, as opposed to the large number of pulses in the equivalent volume of nuclear emulsions.

Moreover, bubble chambers appear to have inherently a higher repetition rate than expansion cloud chambers, as bubble chambers with satisfactory expansion systems return to equilibrium comparatively quickly upon recompression. This enables one to operate them as often, say, as once per second, corresponding to the repetition rate of some of the large accelerators. In fact, Professor Lord's group at the University of Washington (1) have operated a small propane chamber at 15 cycles per second, and a 10 c.p.s. chamber employing Freon has been constructed by a Russian group (2). We have suggested (Chapter II-2) techniques for constructing large bubble chambers to operate at rates as high as 30 to 60 cycles per second. The high rate of picture output, combined with the large solid angle available in many experiments and the good spacial and angular resolution typical of visual instruments, make bubble chambers potentially high data yield devices.

However, as with any experimental technique, there are drawbacks to bubble chamber work. For example, scanning, although a less serious problem than in emulsions, is still a major undertaking. More laborious and difficult than scanning in most cases is the analysis of events in bubble chamber pictures, i.e., the determination of angles, ranges, momenta, etc. Although much progress has been made recently toward automating the analysis of bubble chamber pictures, the time and effort involved is still the major impediment to the attainment of good statistical accuracy.

The limited time resolution, particularly for photoproduction experiments, poses another problem. Whereas with counter techniques, one has available the time resolution provided by very fast electronics

(1 - 10 mμ sec.) to reduce background, this degree of discrimination is not available to bubble chambers. Of course, in many cases one can substitute good spacial resolution for time resolution, but there is a limit to this. Furthermore, because of the short lifetime of the bubble nucleii (Chapter II-1), the expansion of a conventional bubble chamber cannot be counter-controlled.* Consequently, it is highly probable that most bubble chamber experiments, especially those employing photon machines, will be background-limited.

Not among the least of their disadvantages is the fact that bubble chambers are complicated and expensive devices, and require extensive engineering and special techniques to construct and operate.

However, there is one major point which perhaps outweighs many of the limitations of the technique. This concerns the philosophy that there should be available an experimental approach which is divorced from those used in magnet-counter or counter-telescope methods. Such a visual technique provides a very important check on and complement to the counter experiments, and in cases of doubt allows the repeat of a given experiment in a manner whose systematic errors are quite different.

In summary, owing to its large solid angle of acceptance and other characteristics noted above, a bubble chamber, provided the backgrounds are not prohibitive, is inherently well fitted for extracting total cross sections for photoproduction and for the study of complicated processes involving angular correlation functions. On the other hand, for simple reactions, counters are probably superior for finding differential

* There is, of course, the possibility of using a high repetition rate bubble chamber (one which expands for each machine cycle) and using counters to control the flash and camera. This technique is being considered by many groups. In this connection see Chapter II-2.

cross sections to high statistical accuracy without the need for time
consuming scanning and analysis.

B. Specific Considerations - Experiments and Accelerator

The characteristics of a bubble chamber which would be most
desirable for studies with a Bev electron synchrotron must be examined
in the light of the specific experiments that could and should be done
with such a visual instrument.

Let us first consider π-meson photoproduction experiments.
The single production cross sections of π-mesons in the reactions
$\gamma \neq n \rightarrow n \neq \pi$, where n is a nucleon, are doubtlessly best measured
with the use of counter or counter-magnet techniques (3 - 15). Nonethe-
less, there are features about this process for which a bubble chamber
might be useful. In studying the production process, for example, around
the "second resonance" at 700 - 800 Mev (16,17), one would be helped
greatly in knowing the polarization of the emitted nucleon (18). In fact,
in the study of many processes, polarization experiments may play an im-
portant role. There is at least one technique which can be used in bubble
chambers to ascertain polarization of protons. This is in the study of
the asymmetry of the elastic scattering from carbon or other complex nu-
clei in the chamber liquid for which the analysing property is known.

The study of pair production of π-mesons such as $\gamma \neq P \rightarrow$
$P \neq \pi^{+} \neq \pi^{-}$ (and the neutral modes to a lesser extent) has been under-
taken at the California Institute of Technology, Cornell, and Stanford
with a diffusion cloud chamber, nuclear emulsions, counter telescopes, or
counters and a magnetic spectrometer (19 - 25). However, for these reac-
tions and those of higher multiplicities as well, it would seem that a

bubble chamber might be especially useful. In these experiments it is highly desirable to determine unambiguously the degree of multiplicity and kind of particles involved, as well as a sufficient number of the many kinematic parameters to determine the energy of the incident photon. The measurement of the angular correlation of all particles involved also is useful for comparison to the theoretical prediction from a specific production model.

Because one needs also to study the multiple production of π^0 mesons (with or without charged pions), it is desirable to have a medium which can detect γ-rays from the decay $\pi^0 \rightarrow 2\gamma$ with high efficiency as well as charged pions or nucleons. For this purpose a chamber liquid with a short radiation length is preferable.

Other straightforward photoproduction experiments within the energy range of the California Institute of Technology Synchrotron are the measurements of the cross sections for the processes of the form $\gamma + n \rightarrow Y + K$, where n is a nucleon, Y is a hyperon and K is a K-meson. Of these reactions, at the present writing, only those involving K^+ production from a proton have been studied using counters and a magnetic spectrometer, both at the California Institute of Technology and Cornell (25 - 31). There is perhaps a use for a bubble chamber in the study of the backward center of mass angles of the K^+, since here the K^+ is slow and has a short decay length, requiring a device which can examine the region close to the point of origin of the K^+.

Concerning the neutral production, the place of a bubble chamber becomes more prominent still. Study of the process $\gamma + p \rightarrow \Sigma^+ + \theta^0$ is difficult with any technique under the present energy limitations of the synchrotron because of the low cross section, the short life of both

particles, and the small laboratory angles at which the products emerge.
The forward angles, of course, are very badly contaminated with background,
due principally to electron-positron pairs. From the lifetime of the Σ^+
and the θ_1^0, (50% of the θ^0 particles), one finds that the expectation
zones for decay are at most limited to within a few centimeters of the
point of production. Thus, here is a possible use for a bubble chamber,
which with the proper experimental arrangement can examine the region close
to the point of production. Identification of the θ^0 particle would be
made by its decay. A similar argument can be advanced for other production
processes in which the neutral particle is the only one kinematically avail-
able for examination, for example the reactions $\gamma + n \rightarrow \Lambda^0 + \theta^0$,
$\gamma + n \rightarrow \Sigma^0 + \theta^0$. Here one needs the almost unique ability of a visual
instrument to identify the neutral particles by their decay and to employ
measurements on the daughter products to determine the energy of the neutral.

With the foregoing experimental problems in mind one can examine
in some detail the advantages and disadvantages of various bubble chamber
types. The kinds we have considered are liquid hydrogen, hydrocarbon, and
heavy liquid bubble chambers from the viewpoint of experiments with an
electron accelerator.

From the outset, it is clear that a hydrogen chamber has certain
advantages over all other types. In particular, the sensitive liquid is,
for high energy experiments, essentially a free-proton target, allowing
direct studies of reactions with single nucleons, uncomplicated by inter-
actions in nucleii. In hydrocarbon chambers, such as those using propane,
one also has free-proton targets, but the situation is complicated by the
necessity of separating the carbon events from the hydrogen ones. At the
expense of losing visibility of the point of interaction, one may

alternatively employ separate gaseous (or possibly liquid) hydrogen targets built into or adjacent to the chamber.

When one considers the use of any bubble chamber with a photon beam, however, a very important consideration arises. This is the very high background, especially in the forward direction, of electrons and positrons from pair production and Compton recoils. The situation is so bad, in fact, that only rudimentary calculations are necessary to indicate that chamber liquids other than hydrogen are probably impossible for any but electrodynamic experiments when used as targets for a bremsstrahlung beam.

To study experimentally the extent of this background problem in liquid hydrogen, J. M. Teem and E. D. Alyea, Jr. (32) used the 4 inch Berkeley hydrogen chamber in the bremsstrahlung beam of the 300 Mev U.C.R.L. electron synchrotron. For those processes whose end results are heavily ionizing particles (e.g., threshold pion production), it was shown feasible to operate the chamber at lower temperature and sensitivity and thus "bias out" a large amount of the electron contamination. However, it would appear that a hydrogen chamber has fairly severe limitations for the study of photoproduction processes for those cases in which one must detect minimum or near minimum ionizing particles. Teem and Alyea observed that in such cases, even using LiH as a filter to remove low energy photons from the beam, the practical necessity of obtaining a reasonable counting rate requires a beam intensity so high that the central portion of the chamber (the beam line) is obliterated by background. If the origin of events is obscured, and separate tracks are visible only in the region away from the beam, a hydrogen chamber loses some of its attraction. Under such conditions, there is no particular advantage in using hydrogen as a sensitive

liquid in the surrounding region (at least for production experiments).
One is therefore compelled to consider separately the characteristics of
a chamber liquid for use as a detector as distinguished from a target.

A possibility worth considering is that of a heavy liquid chamber
surrounding a high pressure gas target (H_2, D_2 or possibly even T_2). The
features possessed by heavy liquids that are of particular interest as a
detector are both their high stopping power for charged particles and
their short radiation length, that is, their ability to "materialize"
photons. The higher stopping power gives one an opportunity to identify
charged particles and measure their energy by allowing them to stop in the
chamber and decay. The higher density, of course, almost inevitably rules
out easily obtained macroscopic magnetic fields (10 - 15 Kg) as a momentum
measuring technique because of the large multiple Coulomb scattering. The
latter, however, somewhat compensates for the loss by giving the experi-
menter an opportunity to use the nuclear emulsion technique of measuring
momentum times velocity by observing the scattering. Such heavy liquids
thus possess the ability to detect and measure the energy of both charged
particles and γ-rays.

These are some of the considerations that led to our choice of
a heavy liquid as a bubble chamber medium. The idea was first proposed by
Glaser (33), who suggested several possible liquids, among which were
$SnCl_4$, WF_6 and xenon. Subsequent to this, Glaser and his co-workers con-
structed a small xenon chamber (34) and now have an operating 12 inch one.
Because of the high cost and scarcity of xenon, the bubble chamber group
at the California Institute of Technology under the direction of J. M. Teem
constructed a small chamber to test other heavy liquids (35). Although
two such liquids were found radiation sensitive ($SnCl_4$ and WF_6), tungsten

hexafluoride has several more appealing features. Among these are higher density, shorter radiation length, and lower operating temperature. Therefore, fairly extensive exposures were carried out with the WF_6 chamber in the C.I.T. synchrotron beam to explore the possibilities of the liquid (see Chapter I-2). On the basis of these tests, WF_6 was chosen as the eventual heavy liquid to fill our 12 inch chamber when completed. However, since WF_6 has certain handling problems, we intend to use a compromise liquid in the initial experiments. Some of the Freon type compounds such as CCl_2F_2 have been studied as bubble chamber fluids (36), and the heavier ones of this family (notably CBr_2F_2) are sufficiently dense and have short enough radiation lengths to make them useful heavy liquids.

The really unique feature of heavy liquids lies in their very high efficiency for photons. For example, the radiation length in WF_6 at the operating point is about 3.5 cm. Thus, the probability of seeing both photons from a π^o decay (or any photon) within the chamber is high. Here, however, one must note that a shorter radiation length also invites additional trouble from background photons. Whether this difficulty offsets the advantages of π^o sensitivity is not fully determined as yet. However, although the heavy liquid will unquestionably yield higher backgrounds than the lighter liquids, the situation is perhaps not quite so bad as may be supposed at first thought.

Let us consider briefly the sources of background around a photon machine. The background effect of all charged particles except electrons and positrons (protons, π-mesons, etc.) is clearly essentially the same for all liquids. For electrons and positrons produced in the beam line or target region and which enter the sensitive liquid, the situation differs primarily in that they cascade in the heavy liquid and not in the lighter

ones. However, this does not necessarily imply that the background is worsened by the cascade. Most of the bothersome electrons are in the energy range ($<$ 30 Mev) which would stop in, say, a hydrocarbon chamber anyhow, and the total number of bubbles produced is roughly proportional to the total energy of the particles. Thus an electron or positron can deposit no more bubbles in a heavy liquid through a cascade than it can in a hydrocarbon (or hydrogen) by simply stopping. In fact, the number of bubbles produced in the heavy liquid is likely to be fewer, if anything, since the sensitivity of a chamber is set from practical optical considerations to be about the same number of bubbles per centimeter for minimum particles in any kind of sensitive fluid. The shorter particle range in a heavy liquid thus indicates that the number of bubbles per unit total energy lost by a particle is smaller in the heavier liquid. It is true that the cascade distributes the background bubbles differently, but the worst feature here is the lateral spread of the shower, with the result that regions at wider angles from the beam line are obscured than would be the case if the usually forward-moving electron continued in a straight line. This effect, however, would seem to be no worse and is probably to be preferred over the bending of low energy electrons into the wide angular regions by the magnetic field that almost always must be used with the lighter liquids in order to determine charged particle momentum.

Another background source which is worse for heavy than for light liquids is the general spray of fairly low energy photons found around a photon machine which come from points outside the chamber. These will in general materialize to a much greater extent in a heavy liquid than in a light one. This problem, however, can be alleviated by adequate shielding, and extensive provisions have been made for this purpose on our chamber.

Thus the processes which yield worse background in a heavy liquid chamber would appear to reduce to essentially one: the production of π^0's, which is the very process we wish to be able to detect. If we assume that the background from pair and Compton produced electrons and positrons is the worst source, (perhaps by an order of magnitude), then that from π^0 mesons may not be too serious. Its effect is roughly to quadruple (because of the production of two pairs from every π^0) the background contribution which in a lighter liquid comes from charged pions. The primary difficulty here is probably that numerous stray electron-positron pairs in a picture make it difficult to follow a particular cascade from a photon of interest. In any case, the background situation is sufficiently complex to make it impossible to determine accurately without experiment.

The availability of a heavy, high atomic number liquid in a bubble chamber gives rise to the possibility of some experiments which could be broadly labeled "electromagnetic." Although some of these may not have the interest attached to them that have experiments such as strange particle production, the availability of a highly energetic photon beam plus a photon sensitive medium make them plausible experiments. The most obvious of these is a straight-forward shower experiment, in which a highly energetic electron (e.g., 1 Bev) is selected by a momentum-analysing magnet and fed directly into the chamber material. A 12 inch WF_6 bubble chamber contains 8 useful radiation lengths of material across its diameter. Thus a quite respectable shower could be developed and photographed in the chamber. In fact, because of the need for finding the best parameters to use in order to estimate the energy of a photon from its shower, this experiment should probably be done as early as possible.

For purposes of comparison, Table 1 lists a number of bubble

chamber liquids and some of their relevant characteristics. All liquids
in this list have been operated as bubble chamber media except those noted,
and the latter are almost certain to be usable because of their chemical
and physical similarity to liquids already tested. In this case also the
operating temperature is only an estimate, but probably a reliable one.

TABLE 1

Liquid	Oper. Temp. °C	Oper. Press psi	Oper. Density gm/cm³	Rad. Length (cm)	Stopping Power Rel. to Al.	Range of 100 Mev π (cm)	Nuclear Int. Length (cm)	Mult. Scatt. Coeff.
H_2	-246	70	0.06	1000	0.055	223	279	0.24
C_3H_8	60	308	0.43	109	0.22	57	86	1.06
CF_3Cl	8	240	0.97	28.1	0.38	33	68	2.30
CF_2Cl_2	67	256	1.15	20.9	0.43	29	62	2.71
CF_3Br	30	264	1.50	11.0	0.57	22	54	3.89
CF_2Br_2*	148	286	1.60	8.5	0.60	21	60	4.49
SeF_6*	42	255	1.7	10.9	0.63	20	46	3.80
$SnCl_4$	270	294	1.4	8.8	0.45	28	73	4.43
C_3H_8-CH_3I**	120	350	1.4	7.5	0.48	26	57	4.87
Xe	-19	370	2.3	3.5	0.66	19	63	7.15
WF_6	138	353	2.5	3.6	0.78	16	41	7.08
Nuclear Emulsion			3.8	3.0	1.04	12	25	7.64

* Denotes estimated operating conditions only.

** For mixture 50 - 50 by volume at room temperature. This implies a molar ratio of 1 propane to 1.41 methyl iodide.

Multiple scattering coefficient defined as $\sqrt{(\rho/M)\sum n_i Z_i^2}$ where ρ is density, M is molecular weight, n_i is the number of atoms with atomic number Z_i in the molecule.

"Stopping power" refers only to range of 100 Mev π.

Nuclear Int. Length based on geometrical cross sections.

CHAPTER I-2

EXPLORATORY WORK WITH SMALL BUBBLE CHAMBERS

A. Introduction

In the earlier phases of the bubble chamber program, it was decided to construct initially a small ($\sim$ 1 inch diameter) chamber. The purpose of this was twofold. First, it was necessary for us in the group to gain some experience with bubble chambers using a small, easily managed piece of apparatus. The primary goal, however, was to attempt to find a satisfactory high density liquid for a much larger chamber. At the time, the only heavy liquid which was being investigated was xenon (34) whose very high cost and scarcity seems to preclude its wide use as a bubble chamber fluid.

B. Earlier Work

The first chamber constructed was a small cylindrical all-glass chamber, whose sensitive region was approximately 1 inch in diameter and $2\frac{1}{2}$ inches long (Fig. 1). The chamber connected through a glass tube to metal expansion and filling systems. The chamber portion was immersed in a temperature controlling bath of Dow Corning 550 silicon oil. After the chamber had been tested with ether as an operating fluid, we were prepared to investigate heavier liquids. Following suggestions by Donald Glaser, we had planned to try $SnCl_4$ and WF_6, as well as some other fluids. Because of its availability the first liquid that we tested was $SnCl_4$. We obtained tracks from a Ra-Be source at a temperature of $270^{\circ}C$, where the vapor pressure of $SnCl_4$ is 20 atm and its density is 1.4 gm/cm^2 (Fig. 2). Radiation sensitivity was observed as low as $261^{\circ}C$. Because of the nature of the expansion system, the expanded pressure of the $SnCl_4$ was not known.

The success with $SnCl_4$ led us to try next the similar, but more

Figure 1

Schematic Diagram of Small Glass Bubble Chamber System

Employed for Testing $SnCl_4$.

Not shown in detail is the expansion apparatus, which was similar to that used on the small WF_6 bubble chamber shown in Fig. 3. Illumination for the glass chamber was light field.

Figure 1
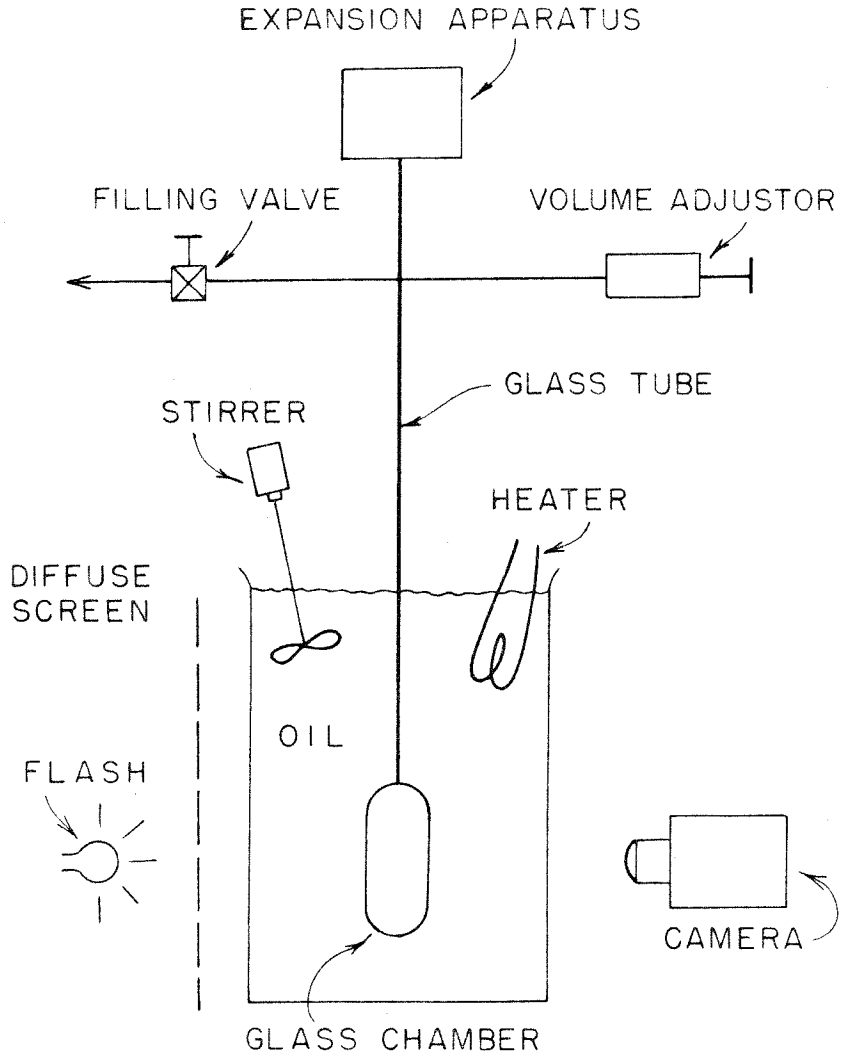
Figure 2

Bubbles in $SnCl_4$ Induced by Gamma Radiation

from a Ra-Be Source.

Typical ranges of Compton electrons produced by the photons are so short that distinct tracks are difficult to pick out.

Figure 2
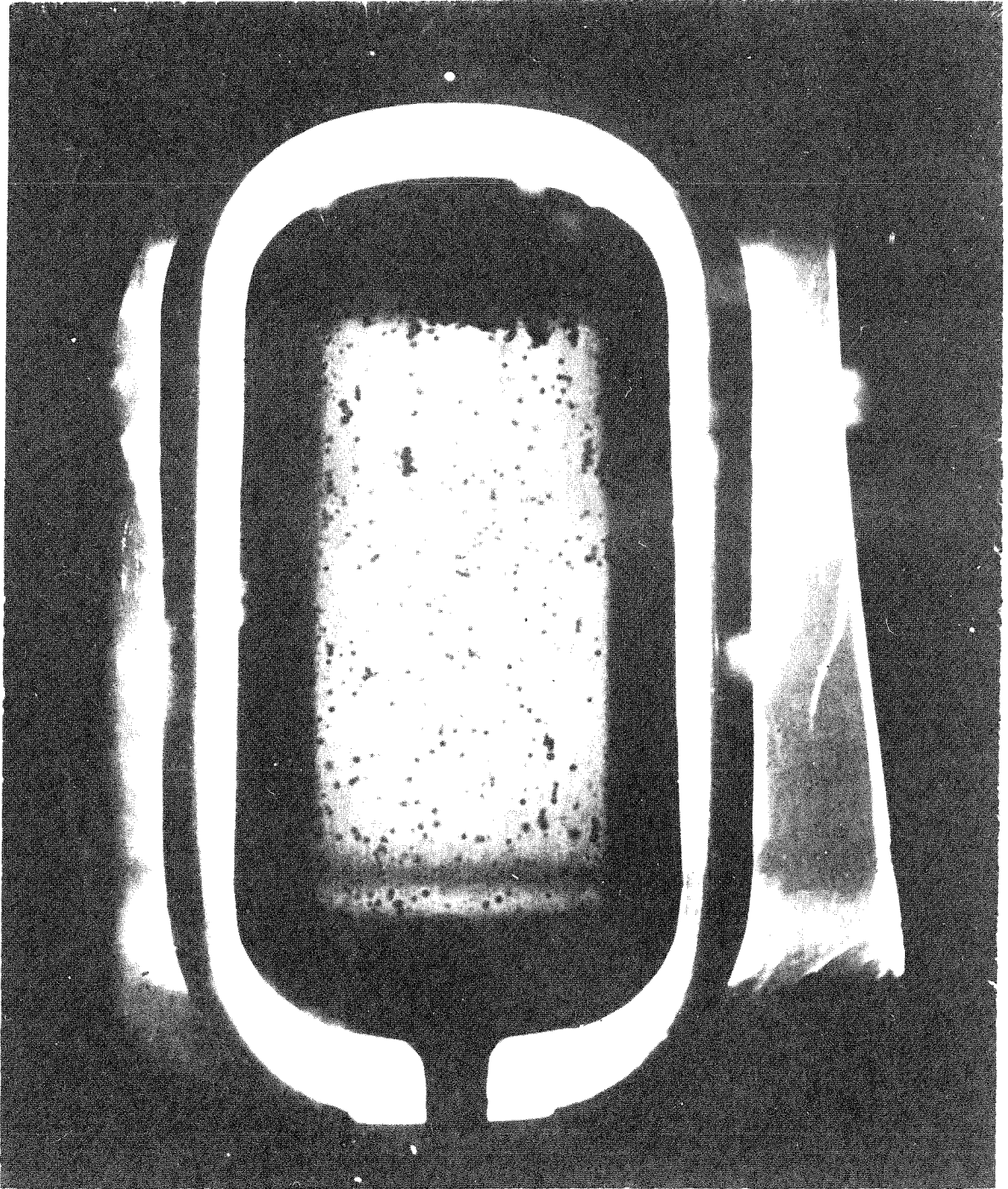
dense liquid $SnBr_4$. We estimated that this liquid would operate at a temperature between 380°C and 400°C. Breakage of the glass chamber delayed this test, and while a small metal chamber was being constructed we made a number of corrosion tests with $SnBr_4$ and WF_6. We found that among the metals, gold and rhodium were corrosion resistant to $SnBr_4$ at 400°C, while aluminum, copper, nickel, inconel, and stainless steel were attacked. A ceramic coating applied to these latter metals does provide corrosion resistance; however, we had some difficulty with chipping of the ceramic coating on sharp edges. Since the corrosion tests with WF_6 were more encouraging, the work with the tin compounds was suspended.

The purification of the $SnBr_4$ presented another difficulty. Whenever the liquid was vacuum distilled into a glass tube, sealed, and heated to 400°C, a black coating was deposited on the walls.* While the identity of this impurity was never determined, it apparently was removed by the heat treatment, because after redistillation no such effect was observed upon reheating the $SnBr_4$. The stannic bromide exhibits a greenish-amber color at temperatures above 250°C, but reverts to the colorless state upon cooling.

C. The Small WF_6 Chamber

The metal chamber constructed after breakage of the glass one was originally designed to test a variety of corrosive liquids, although the series of tests were stopped when success with WF_6 after the first trial made it apparent that the program had served its purpose.

---

* During operation of the glass chamber with $SnCl_4$, a thin, but similar black coating was observed to form on the walls, but this could have been a result of corrosion of the metal parts of the system.

The sensitive region of the chamber was a cylinder $1\frac{1}{2}$ inches in diameter and approximately 5/8 inches deep. Entering this chamber were two tubes, one from the top 3/16 inches in diameter and one from the bottom 5/16 inches in diameter. The latter led to the expansion apparatus 10 inches below (Fig. 3a).* Leading from the expansion tube were a filling valve and a piston (volume adjuster) which was used for adjusting and measuring liquid volume changes with a sensitivity of 0.004 cm^3. The top tube was originally intended as a filling tube for gases, in the event we wished to investigate gas (or two-component) bubble chambers. However, it was never employed for this end, and instead was used to introduce into the chamber purifying agents or metal samples for corrosion tests.

The windows were quartz plates $\frac{1}{2}$ inch thick and $2\frac{1}{2}$ inches in diameter. There were two window sealing arrangements, although only one was actually used. For WF_6, and, in general, for temperatures below $200^\circ C$, Teflon gaskets similar to "O" rings were used. For higher temperatures, there was provision for the use of flat gold gaskets between lapped metal surfaces and the windows. However, there was considerable difficulty with maintaining the seal without cracking the windows in the latter arrangement, so it was never employed. With the exception of the top tube, which was sealed with a gold plug**, all other seals were made at room temperature with Teflon "O" rings.

The expansion tube terminated in a Teflon diaphram - "O" ring combination which was machined from a single piece of Teflon. The flat

---

* From experience with forerunners of this chamber, we found that for a chamber of this size and construction an expansion tube of diameter greater than about 1/3 inch seems necessary for successful operation.

** We are indebted to D. F. Buckingham, D.D.S., for supplying this gold casting.

Figure 3

a. Diagram of Small WF_6 Bubble Chamber (to scale).

  Diaphragm - "O" ring (DO-ring) shown as it would appear under unbalanced pressure from the expansion valve side.

b. Schematic of Dark Field Lighting System (not to scale).
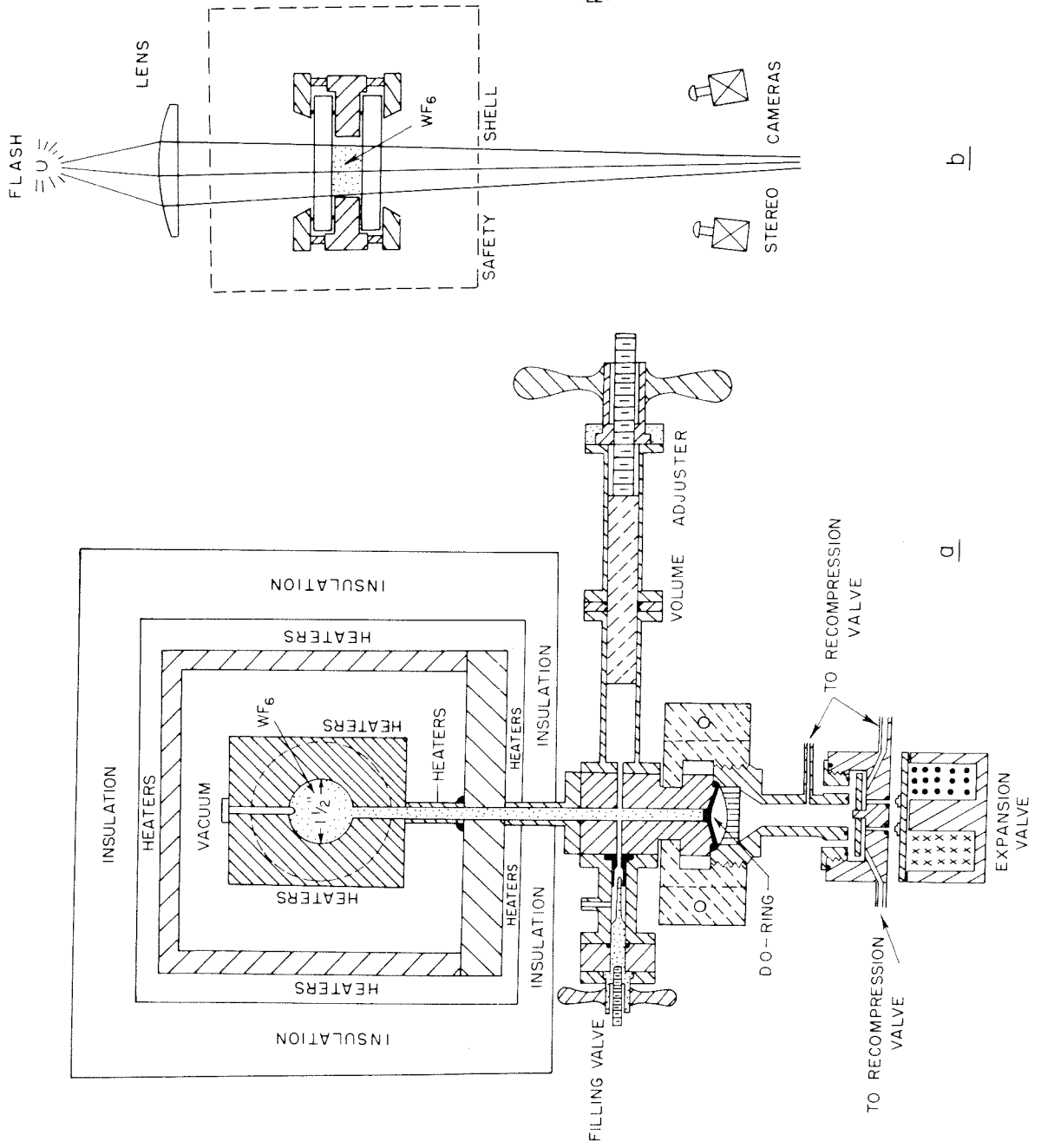
Figure 3

portion was about 0.030 inches thick and 1½ inches in diameter, and sep-
arated the liquid from the high pressure gas in the pop valve. The
diaphragm was backed by a **Hycar** rubber disk and a perforated polyethylene
piece. These were further supported by a perforated brass plate, which
limited the excursion of the composite diaphragm under unbalanced pressure
from the liquid side. The expansion system was fairly simple, consisting
of a gas "blow-off" valve of our own design energized by a D.C. solenoid
pilot. The large aperture and general mechanism of this valve allowed a
very fast (calculated) expansion time of roughly 3 milliseconds. A much
slower recompression was effected with a commercial A.C. solenoid valve.

Because of the toxic or corrosive nature of the fluids being
investigated, we took certain precautions for the safety of personnel, even
though the quantity of liquid involved was quite small. Although we had
not experienced leakage or breakage of this chamber, we adopted the prin-
ciple that any such chamber should be surrounded by an evacuated safety
vessel capable of containing high pressures in the event of a disaster.
The safety tank of this chamber was constructed of stainless steel with
quartz windows and designed to hold 40 atm. A fast closing, solenoid
operated valve would isolate the safety vessel from the vacuum pump should
the pressure rise above a preset value (typically 100 microns).

The chamber heaters (see Fig. 3a) were controlled by thermistor
regulated thyratron power supplies, temperatures being measured with iron-
constantan thermocouples placed at appropriate points. The thermocouple
which monitored the liquid temperature was located in the chamber wall
within about 1/15 inch of the liquid.

While the bulk of the chamber was constructed of stainless steel,
coatings on the inner walls provided further corrosion resistance. The

heated portions of the chamber were gold plated to a thickness of about
0.0008 inches. The valve, expansion cavity, and volume adjuster (with
the exception of its monel piston) were ceramic coated to a thickness of
about 0.002 inches. This system of coatings, however, on the basis of our
later experience, is not the best for WF_6. Specifically, the gold plating
was unnecessary and the ceramic actually undesirable. These coatings
would probably be necessary to prevent corrosion by $SnCl_4$ or $SnBr_4$, and
were applied for that purpose.

The chamber was photographed with dark field illumination by a
stereographic system consisting of two 16 mm movie cameras (Fig. 3b). Un-
fortunately, some light reflected from the edge of the safety tank window
entered the cameras, causing an annoying light ring in the photographs
shown below. This defect was later corrected by painting of the window
flanges, but further difficulties prevented us from obtaining a good series
of pictures with this optical improvement.

D. Purification of Tungsten Hexafluoride

Like many metal hexafluorides, WF_6 hydrolyzes when exposed to
water vapor, in this case forming HF and WOF_4. HF will, of course, attack
glass, forming, typically, SiF_4 and more H_2O, thus initiating a chemical
chain reaction. Since any bubble chamber requires transparent windows, we
were initially hesitant to consider operation with WF_6. However, our ex-
perience has shown that with proper techniques one can avoid this diffi-
culty. First, initial outgassing at high temperatures will remove essen-
tially all the water vapor from the system. Second, the distillation process
employed greatly reduces any HF contamination in the WF_6. Finally, sodium
or potassium fluoride may be placed in contact with the WF_6 to act as a
getter for HF, and certain other materials in the chamber tend to remove

the HF without becoming involved in the chain.

The purification system for the WF_6 employed three stages of vacuum distillation through tubes filled with NaF pellets. (Fig. 4) Except for the steel WF_6 storage cylinder in which the WF_6 was supplied by the manufacturer* and its connecting Cu tube, the entire system was constructed of monel or nickel. During distillation the liquid (or solid) was evaporated at a temperature of about 0^oC and condensed at -80^oC. Between distillations the WF_6 was kept frozen at -80^oC while the system was evacuated through a cold trap at -196^oC for about 10 minutes to further remove HF. (Some WF_6 was lost in this process.) Unless the NaF is thoroughly dry, it probably does more harm than good in reducing the HF contamination. We heated it to 1040^oC in melting the powder into pellets and, furthermore, outgassed the entire system thoroughly at temperatures above 150^oC before beginning the distillation. As a further precaution, we had NaF pellets in contact with the WF_6 after it was in the chamber. The monel volume adjuster piston was hollowed out from the liquid side, and filled with NaF pellets. The end was covered with a fine mesh monel screen to prevent the particles of NaF or NaF·HF from getting into the chamber.

This system seemed to produce satisfactory results for our initial experiments; however, an improved system, suggested by Weinstock (37) was adopted for the 12 inch chamber. (See Appendix III for details.)

---

* Supplied by General Chemical Division, Allied Chemical and Dye Corporation, 40 Rector Street, New York 7, New York. Price in 100 pound lots at the time purchase was made was $15.00 per lb.

Figure 4

Schematic Diagram of Purification System used with

the Small WF_6 Bubble Chamber

The NaF was in pellet form. All metal parts of the system after the copper tube were made of monel.
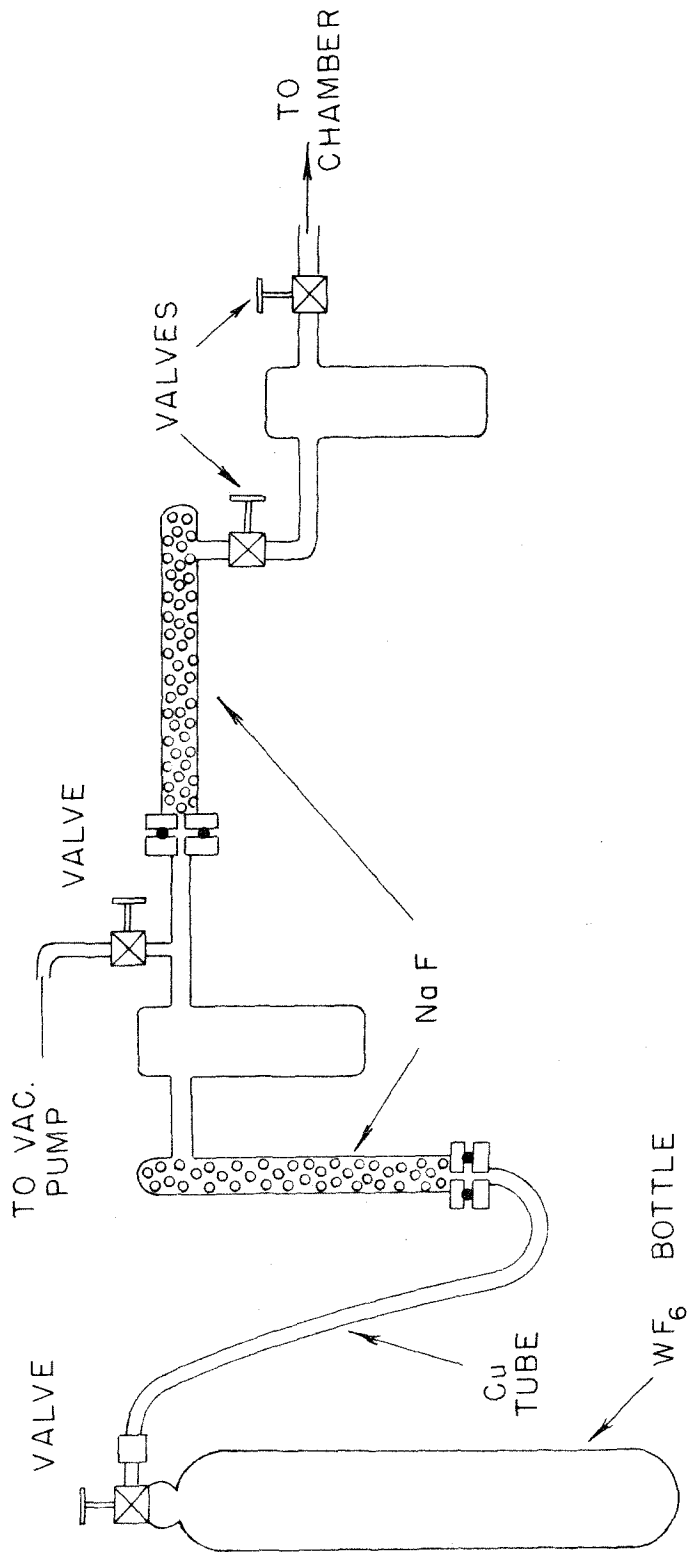
Figure 4

E. Chamber Operation with WF_6

The bubble chamber operated successfully with WF_6 on its initial trial, after the chamber was tested with n-butane. Satisfactory electron tracks from a Ra-Be source were observed over an operating temperature range from 136° to 150°C. The pictures shown (Figs. 5 and 6) were made at 149°C, at which temperature the bubble density for relativistic electrons was 45 - 50 bubbles/cm. Later, however, we found that the bubble density was almost as high at a temperature of around 140°C. The explanation appears to be connected with the violent boiling that can be seen in figure 5 which occurred around an inconel plug inserted in the top tube for corrosion tests.* This boiling probably caused self-recompression of the chamber to an extent which was dependent upon the operating temperature. Consequently, although the gas in the expansion valve dropped to one atmosphere in about three milliseconds, the pressure change in the liquid was not known, but almost surely was smaller at higher temperatures. Probably with no violent boiling and a superior expansion system, WF_6 would operate at a temperature considerably lower than those quoted above.**

Figures 5 and 6 were taken from a run with the Caltech one Bev electron synchrotron. The chamber was placed 70 cm from a lucite target at an angle of 45° with respect to the one Bev bremsstrahlung beam. The average energy per pulse in the beam was probably around 10^{10} - 10^{11} Mev,

---

* Flash photographs taken early in the expansion cycle showed that the boiling originated in the space around the inconel plug, and not from the plug itself. A clean, smooth, inconel surface does not appear to nucleate bubbles from WF_6.

** Word has been received here (36) that a group at University College, England, have operated a WF_6 bubble chamber of size comparable to the one described herein. Due, apparently, to a much superior expansion system, they were able to obtain satisfactory electron tracks at 128°C.

Figure 5

Illustration of Low Energy Shower in WF_6

Point 1, γ-ray produces $e^\pm$ pair.

Point 2, One of $e^\pm$ suffers radiative energy loss. Nearby new $e^\pm$ pair created.

Point 3, One of new $e^\pm$ suffers radiative energy loss.

Also in this picture are energetic proton and stopping particle (probably π^-).

Figure 6

Illustration of Several Types of Particles in WF_6

1. π-meson, $P\beta c = 58 \pm 13$ Mev.

2. π (or μ)-meson, $P\beta c = 134 \pm 49$ Mev.

3. K (?)-meson, $P\beta c = 85 \pm 17$ Mev. Above data from multiple scattering measurements

4. $\pi^+ - \mu^+ - e^+$ decay.

5. Energetic $\gamma \rightarrow e^\pm$.

6. $\pi^+ - \mu^+ - e^+$.

7. π-meson (?).

8. π-meson (?).

9. Energetic proton.

10. Stopping proton.

-30-
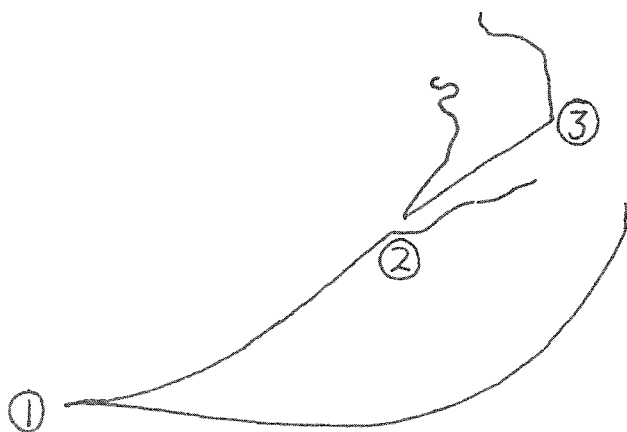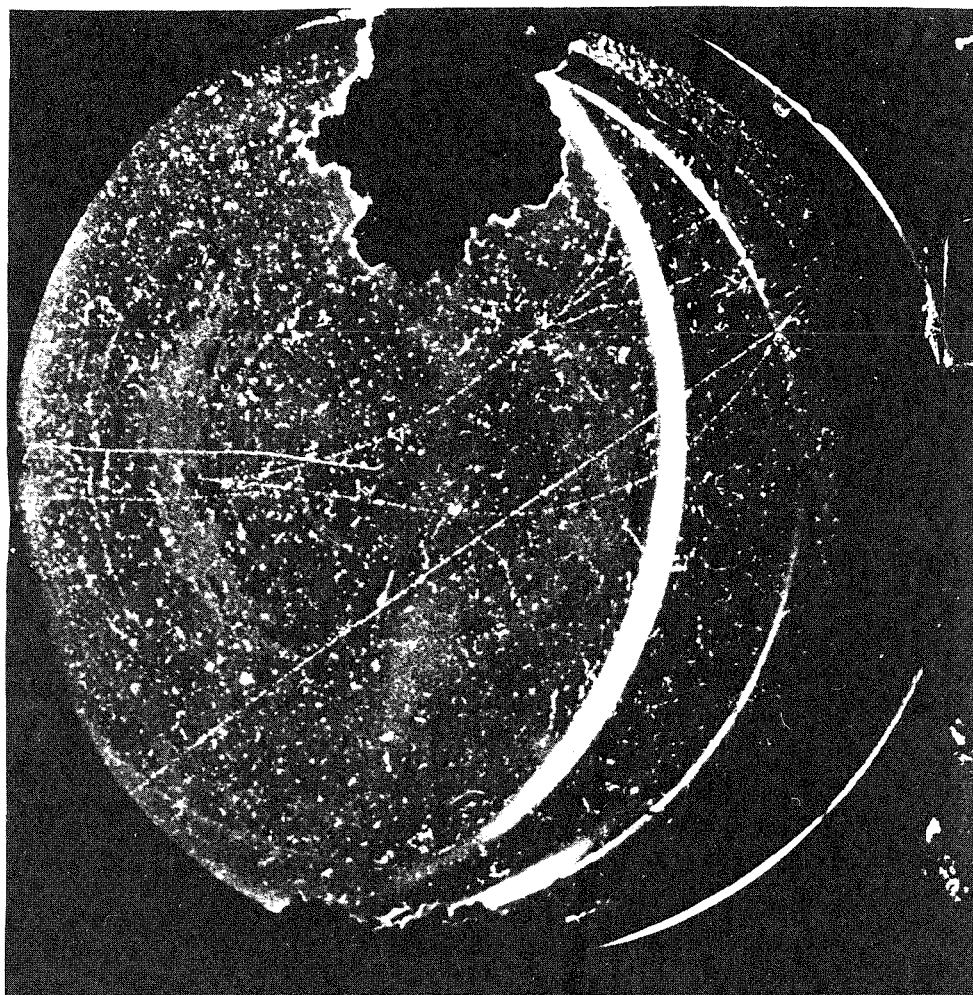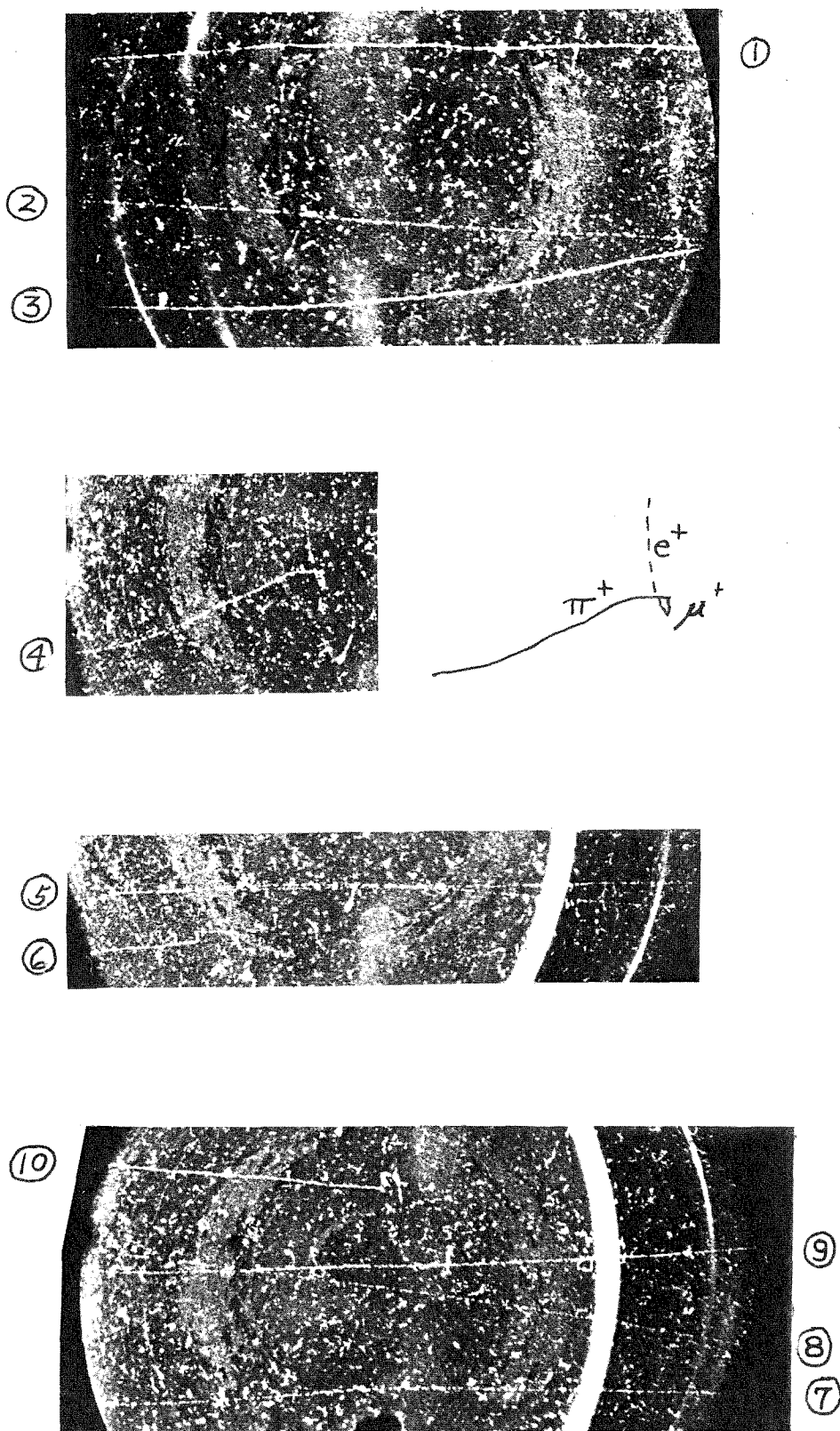
Figure 5

Figure 6

although no accurate calibration was made for this run. In addition, the dimensions of the target were significantly smaller than the beam at the point where the chamber was placed, and only about 10% of the beam actually impinged upon the target. Besides fairly extensive lead shielding of the chamber itself, no determined effort was made to clean up the beam, and it was probably considerably contaminated with charged particles from targets farther upstream.

The synchrotron was an ideal source for studying the chamber operation, since the X-ray beam could be extracted in 100 - 200 μs. By varying the timing of the beam dump with respect to the chamber expansion time, we were able to determine the sensitive time of the chamber as about 1.5 ms. Presumably the cut-off of the sensitive time was caused by self-recompression from the boiling described earlier. The rate of operation was once every 20 to 30 seconds, but it probably could have been greater, since the liquid appeared to reach thermal equilibrium in about 10 seconds.

The photographs illustrate the behavior of different kinds of particles in a WF_6 bubble chamber. Several features are worthy of note in these examples. Differences in Coulomb scattering and bubble density between pions and protons are obvious near the ends of their tracks. $\pi^{\pm}$-mesons are readily distinguished from π^--mesons through their characteristic decay.* The variation of bubble density with residual range is evident in these examples even though the operating temperature was so high that accurate bubble counting (or gap counting) measurements were impossible within our resolution. Many cases of pair production in the chamber liquid have been seen, of which the examples included readily

---

* Few π^- stars should be visible in WF_6 because of the short ranges of typical π^- star prongs.

illustrate the use of such an instrument for the detection of γ-rays and π^{0} mesons. The possibility of containing a shower for γ-ray energy measurement in a moderate size chamber is illustrated in the shower example.

F. Multiple Scattering Results

Some quantitative work was done with the pictures from this run with respect to multiple scattering by J. M. Teem and E. D. Alyea, Jr., during the writer's absence, and a summary of their results is given below. The analysis was undertaken in order to ascertain the feasibility of using the scattering technique in a heavy liquid chamber to determine particle momentum. Although there is good reason to believe that most of the bubbles originate precisely along the track of a particle (i.e., within $\sim 10^{-6}$ cm), there are many things which could cause a real or apparent displacement of the bubbles from their original positions. Nonuniform motion of the chamber fluid could cause a real distortion of the track in such a way as to give rise to false "scattering." Optical distortions arising from temperature inhomogeneities in the liquid could cause similar noise. Finally, there is a limit to how well one can determine the center of a finite sized bubble (of diameter ~ 0.1 mm), given the limited optical resolution of a typical bubble chamber photographic arrangement. All of these things can affect the usefulness of the multiple scattering technique for heavy liquid chambers.

For the analysis, two representative pictures were selected and enlarged. The enlargements were then projected onto tracing paper by means of Professor Leighton's anisotropic projector (39) used normally for determining curvatures of cloud chamber tracks. This projector magnifies one coordinate ten times more than the other, and the tracks in our pictures were arranged so that this additional magnification was used to

enlarge the scattering of the track. The tracing of the resultant image could then be analysed using ordinary drafting instruments. The multiple scattering theory used was that of Voyvodic and Pickup (40) based on the work of Williams (41,42), with the parameters adapted approximately to WF_6 rather than to nuclear emulsions.

The results of the measurements on four tracks of different types of particles and varying values of $P\beta c$ (= momentum X velocity) are shown in Fig. 7. The curves are least squares best linear fits to the points, taking into account the statistical errors shown. Identification of the particles was made from the multiple scattering measurements and the relative bubble density, or from the change of scattering with range.

Of particular interest in Fig. 7 is the value of noise (or spurious scattering) obtained. The multiple scattering theory predicts that the second differences in the scattering sagitta should be related to the cell length as

$$\bar{D}^2 = K^2(X_0)^3/(P\beta c)^2 \qquad (I-2-1)$$

where

$\bar{D}$ = mean second difference of scattering sagitta

X_0 = cell length

The quantity K is a slowly varying function of cell length, and over the range of cell lengths employed in this analysis changes only about 5%. Thus for a given track the plot of $\bar{D}^2$ vs. $X_0{}^3$ shown in Fig. 7 should be nearly linear and intercept at $\bar{D} = X_0 = 0$ if there were no noise or track distortion. Since random distortions or measurement errors are statistically independent of the real Coulomb scattering, they should be constant with respect to cell length and thus be given as a positive intercept of the curve with the $\bar{D}^2$ axis. It can be seen from Fig. 7 that all such

Figure 7

Results of Multiple Scattering Analysis

on Four Tracks in WF_6

A. Identified as π-meson. $P\beta c = 58 \pm 13$ Mev. Noise from mean square fit = 12.66 μ.

B. Tentatively identified (though improbable) as K^+. $P\beta c = 85 \pm 17$ Mev. Noise value 6.00 μ.

C. Identified as π or μ-meson. $P\beta c = 134 \pm 49$ Mev. Noise value = 14.29 μ.

Above three particles from first picture in Fig. 6.

D. Identified as proton. $P\beta c = 192 \pm 60$ Mev. Noise value 6.84 μ.

Average noise from above four values = 9.95 μ.

Figure 7
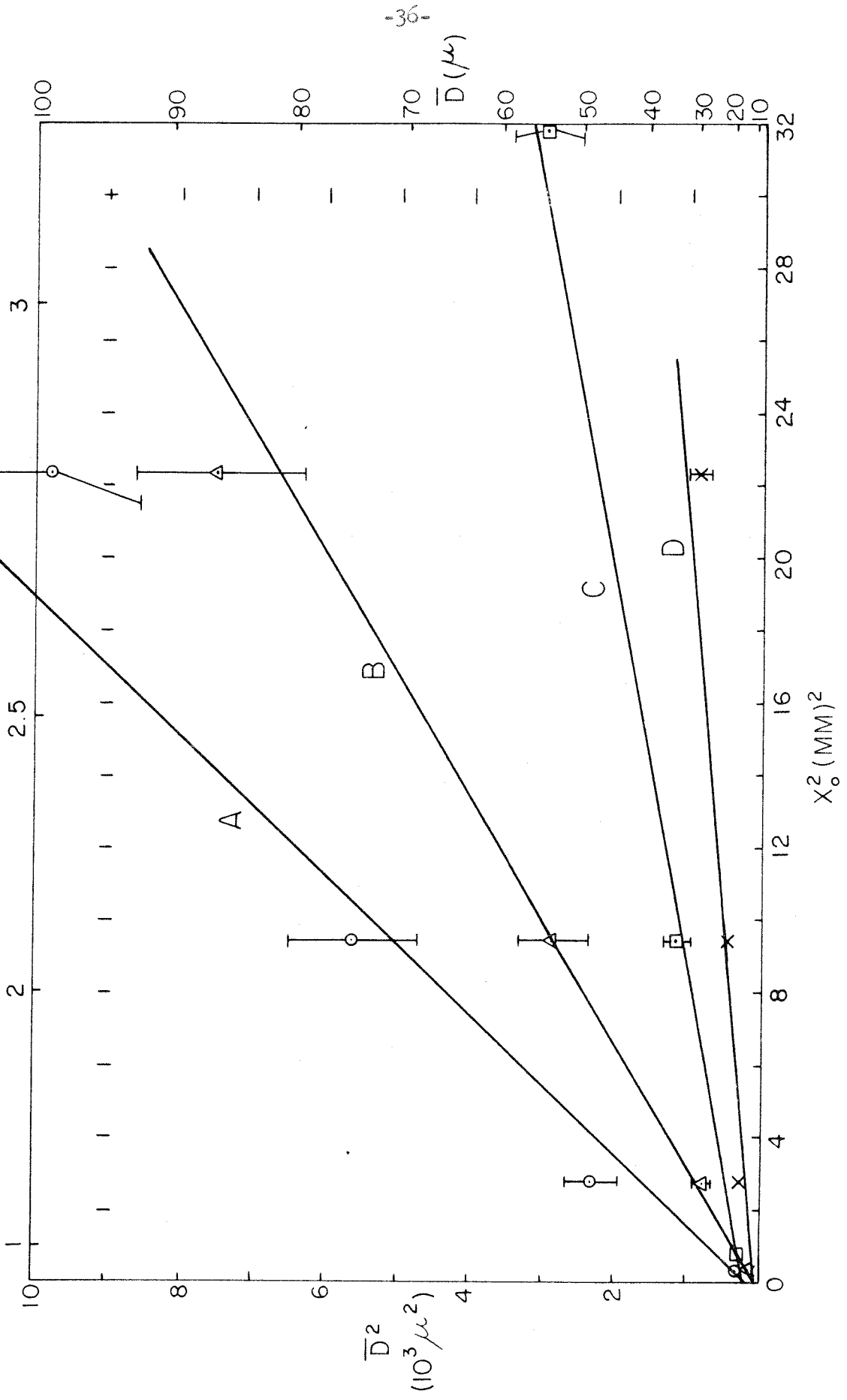
intercepts are less than $\bar{D}$ = 15 μ and the average is closer to 10 μ.*
This is quite remarkable considering that the bubbles themselves were prob-
ably of the order of 100 μ in diameter and the camera resolution comparable
to this. Also, within the statistics, there is no strong evidence of cur-
vature of the plots. A distortion of the particle track would almost cer-
tainly show up as a curvature in the graph, since there is no particular
reason why a distortion should have the same dependence on cell length as
the Coulomb scattering.

The results given above are extremely encouraging. It must be
remembered that the tracks used for this analysis were only about 3 cm
long because of the small size of the chamber. The errors assigned to the
Pβc values given in Fig. 7 are somewhat arbitrary and probably are over
conservative. A more careful investigation of the multiple scattering
theory suggests that a noise figure of 10 μ should enable one to measure
the Pβc of the worst case in Fig. 7 (~ 200 Mev) to better than 20% with
a 3 cm track. The much longer tracks available in a larger chamber should
give correspondingly better results. Of course, one might expect the
noise to be worse in a larger chamber, but perhaps not so much so as to
rule out multiple scattering measurements as a very useful technique.

* The actual noise figures for each track obtained from the least
squares fit are given in the caption.

CHAPTER I-3

DESIGN OF THE 12-INCH CHAMBER

A. Considerations Leading to Choice of the Design

One of the reasons for choosing the specific design of the 12 inch chamber described herein was to attempt to produce a multi-liquid chamber. That is, it was believed that it would be convenient to have available a choice of liquids with different properties, some of which might be corrosive or poisonous. Although one would expect the heavy liquid to be the most useful of the choices, there still remains the possibility that a hydrocarbon might be preferred for certain experiments. An example of this might be a case in which one wished to look for neutrons by observing the n-p recoils from free protons. Thus it would seem preferable to possess a chamber whose function was not strongly influenced by the peculiar chemical or physical properties of a given liquid.

One method to achieve the end described above is to place the liquid in a sealed, chemically resistant container whose only connection to another environment is through the necessary filler tubes. This is the technique adopted in our chamber. The original intention had been to employ a thin-walled cylindrical metal bellows chamber, with thin glass plates constituting the flat ends. This chamber was constructed and is, in fact, a part of the present system. However, the problem of severe boiling around the bellows (Chapter IV) has necessitated the insertion of a flexible sleeve inside the bellows chamber. Both the metal bellows chamber and the sleeve are hydrostatically supported by an inert fluid upon which the expansion apparatus acts.

Another requirement for flexibility is a temperature control that can cover a wide range of temperatures. The pressure controls need

some flexibility, though not so much as do the temperature controls. Most bubble chamber liquids (except H_2 and He) operate in roughly the same range of pressures.

Many of the bubble chambers that have been constructed suffer from a lack of reproducibility of sensitivity. We have strived in this chamber for a greater degree of precision than has been achieved in the past. By precision here is meant the ability to specify and reproduce accurately for each operation the conditions of expanded pressure and temperature. The chief appeal is that in a precise chamber, the bubble density as a function of particle velocity (Chapter II-1) should be the same from picture to picture. There then exists the opportunity to develop "bubble counting" into a quantitative technique for measuring particle velocity. To this end we have employed an elaborate and accurate set of thermal controls and a rather unique expansion system. Both of these items are discussed in detail later.

Another factor which affects the use of the chamber as a precision instrument is the degree of optical and turbulent distortion in the system. Optical distortions are usually caused by temperature inhomogeneities in the fluid through which the photograph must be taken and can be caused by sharp pressure gradients. Turbulent distortions are created by rapid fluid flow during the period of sensitivity, with the result that bubbles are displaced from their origins. There are two principal features in the chamber which are designed to keep down optical distortions. One is the very elaborate thermostating system, the other a very fast expansion and recompression. The function of the latter is to insure that the bubbles have very little time in which either to grow or to rise. Thus, when the bubbles are compressed out, they replace their heat of vaporization in

essentially the region from which it was drawn, allowing thermal equilibrium to be regained in a comparatively short time. (In this connection see Chapter II-1.) It is believed that in the present chamber turbulence will be kept low by the aid of the bellows and sleeve design, which should allow the expansion to take place uniformly.

An important consideration in achievement of reliable chamber sensitivity is the timing. With most expansion systems, although the pressure cycle may be quite reproducible, it is not uniform throughout the sensitive period of the operation. Thus, if reproducible results are to be expected with respect to bubble density, one must be able to control the time of introduction of particles quite accurately. It has been found that the C.I.T. Synchrotron beam can be "dumped" on command in a time of the order of 0.2 ms compared to the bubble chamber operation cycle of about 14 ms. Thus one can hope for good results with respect to timing.

A further requirement for a precision bubble chamber is a good optical system. There is an inflexible optical limit to the actual lateral resolution of the pictures once the geometry of the chamber has been established and the required depth of focus assigned. However, one has some degree of control over the resolution in depth, which is fixed by the stereo angle of the cameras. The greater the stereo angle, in general, the better the depth resolution, up to 90°, where it is equal to the "lateral" resolution. In this chamber the stereo angle is about 30°.

Incorporated into the present design are techniques that could be employed for the construction of much larger chambers. When one considers the construction of chambers several times the size of the present one, some items begin to loom as really prohibitive costs. Glass windows of good optical quality capable of safely standing 20 - 30 atmospheres of

pressure become exceedingly expensive for really large diameters (say, 1 meter) and in fact may not even be obtainable. Large, thick windows can be avoided entirely, however, if one uses the hydrostatic support method. With this technique, the heavy windows are replaced by fluid columns, one of which tapers down to small "peephole" windows for the cameras. Also one cannot hope to use liquids as scarce and expensive as xenon for much larger heavy liquid chambers, therefore the use of comparatively cheap WF_6 as a substitute. A third feature concerns the energy input to a chamber. To pressurize the device, a conventional expansion system employs compressed air which is released during expansion and replaced during recompression. This involves a large expenditure of energy, which goes up roughly as the cube of the chamber dimensions. Our chamber employs instead a non-dissipative expansion system which does not involve such a large energy input. Therefore it would be useful for larger chambers, as well as for those with very high repetition rates.

A prominent consideration which is present in all bubble chambers but particularly in this one, is that of personnel safety. The chamber under discussion is designed to contain a highly corrosive and thus also poisonous liquid at high temperatures and pressures. Hence it is important to take the utmost precautions against breakage of the chamber under those conditions which could dump the sensitive liquid into the room. This precaution must also be taken when a hydrocarbon is being used, for although the hydrocarbon is neither corrosive nor particularly poisonous, it presents an extreme fire hazard. The primary safety measure adopted for this chamber was to enclose the entire device in a very strong stainless steel outer tank, whose only visual entry is through small quartz camera ports. An additional precaution for use with WF_6 is to use a fluorinated support

liquid /heptacosafluoratributalymine $(C_4F_9)_3N$/ which is not only inert to WF_6, but which probably is also a fair solvent for the latter. Then in case of breakage of the thin inner vessel, the WF_6 should cause no damage in mixing with the support fluid.

B. Brief Description of Chief Features

The drawing (Fig. 8) illustrates the general features of the 12 inch chamber. The inner vessel contains the sensitive medium, and is a cylindrical chamber about 12 inches in diameter, to which the windows are attached by means of bellows. Both the windows and walls are of thin material, and are incapable of withstanding high pressures. The container is surrounded by an inert fluid which acts as a hydraulic medium, trans-mitting pressure to the walls of the support vessel and expansion apparatus.* The bellows chamber itself contains a hydrostatically supported lining, which is a flexible sleeve. This cylindrical bag is approximately 12 inches in diameter, and its ends are clamped between the windows and the metal flanges of the bellows chamber, affording a seal. The region between the lining and the bellows chamber is filled with the hydraulic medium.

The support vessel is a very strong cylindrical stainless steel tank, capable of withstanding very high pressures ($\sim$ 200 to 300 atm). To the lower end of the tank is sealed a glass window** of borosilicate crown. This glass disk is 4 inches thick and 15 inches in diameter, with a clear sight diameter of 12 inches, and is of superb optical quality. This win-dow should be capable of withstanding 1200 psi, and has been tested to

---

* At least one other chamber uses the hydrostatic support principle, and that is the 30 inch Berkeley propane chamber (43).

** Manufactured by Heyward Scientific Glass Co., Whittier, Calif.

Figure 8

General Layout of 12-inch WF_6 Bubble Chamber

Explanation of symbols

A. Safety shell
B. Bias cylinder
C. Radiant heating (and heat reflecting) shells
D. Expansion engine driving mechanism
E. Sleeve valve of expansion engine
F. Hydrostatic support vessel
G. Piston
H. Expansion cylinder
I. To loss pump
J. From loss pump
K. Illumination system mirror
L. Flash tube
M. Inner (bellows) chamber
N. Flexible insert (sleeve)
O. Target tube
P. Filling line for inner vessel
Q. Thick high pressure window
R. Support fluid filling line
S. Camera port
T. Camera
U. Film
V. Recording picture counters
W. Stand

Figure 8
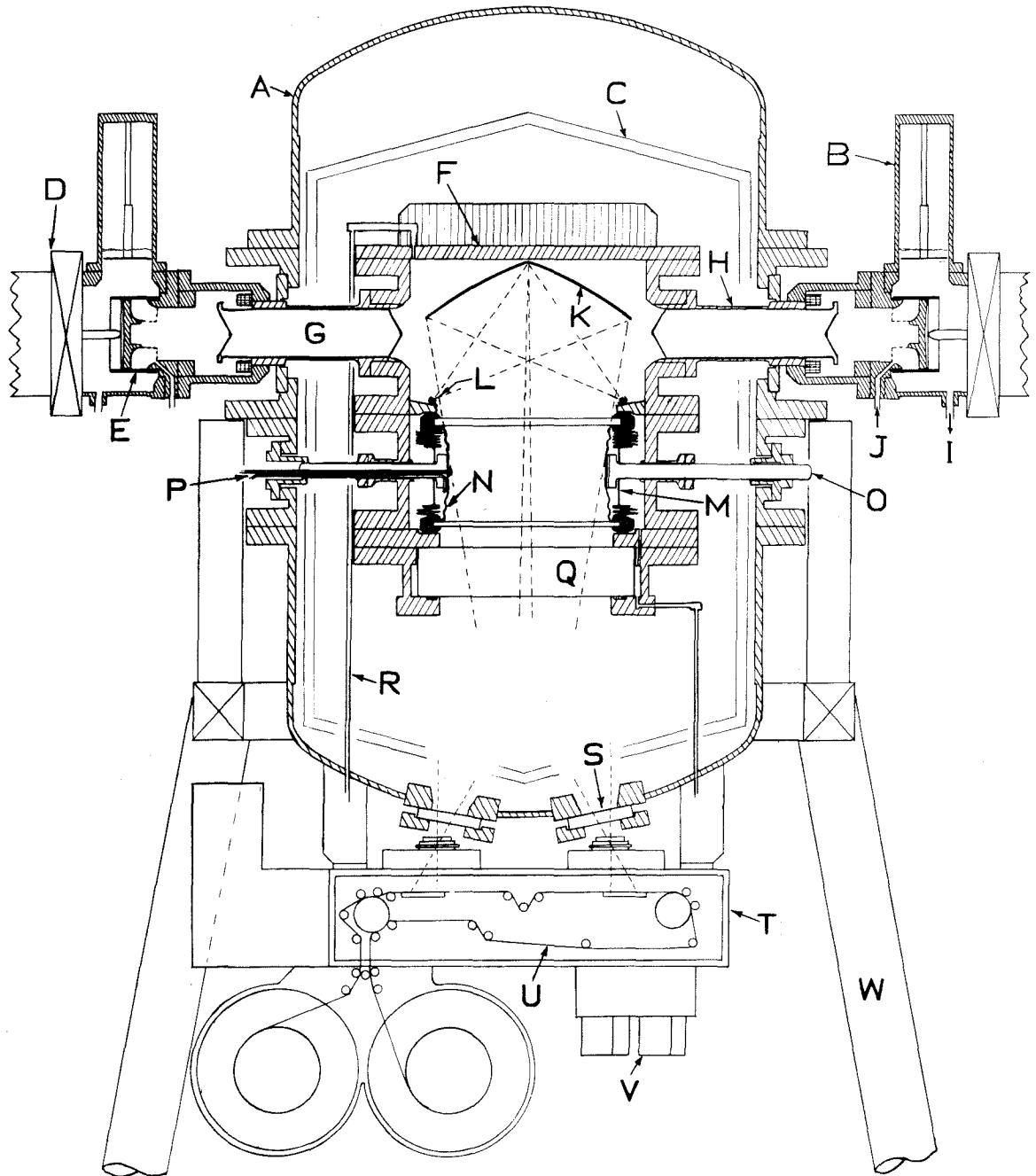
600 psi, although the maximum pressure we intend to employ is less than 500. The upper portion of the vessel contains the flash system (immersed in the hydraulic fluid) and the expansion cylinders which also serve as the mechanical support for the vessel.

Surrounding the entire support tank is the safety vessel, a large stainless steel cylinder capable, also, of containing high pressure, high temperature, corrosive fluid in case of a disaster. The region between the safety and support vessels may be kept evacuated, and contains the main radiant heating system as well as two heat reflecting steel shells outside the heaters. Sealed to the lower end of the safety vessel are the camera windows, which are quartz disks 3/4 inches thick with a clear sight diameter of $2\frac{1}{2}$ inches.

The expansion system transmits pressure to the hydraulic fluid through the four symmetrically placed expansion cylinders. In these cylinders are hollow, evacuated, free pistons $3\frac{1}{2}$ inches in diameter which act as thermal barriers between the fluid and the room. They are sealed to the walls of the cylinders with sliding "O" rings, and have mechanical limits to their motion. They thus act also to seal off the internal system and to provide positive stops to its volume excursion. The region of the cylinder outside the piston is filled with an ordinary oil, in which the expansion engines operate. The overall expansion system is unconventional, and is described in more detail later in this chapter and in Appendix I.

Temperature control is provided by the radiant heaters, plus a number of conductive heaters placed at the principal points of heat leak to the outside. All heaters are thermistor controlled.

Particles can be brought into the chamber through a number of routes. There is provision for a high pressure gas target running through

the center of the chamber itself, plus a similar one running tangent to the inner vessel. These targets are designed primarily for photon beams. There are in addition two steel charged particle "windows" directed radially inwards.

The lighting system is dark field, employing two "line source" flash tubes and two cylindrical mirrors. The stereoscopic camera uses 65 mm perforated film, and can handle 1000 foot rolls.

This chamber is also intended to be easily transportable, so the entire assembly is placed on a sturdy stand, including all plumbing, liquid storage tanks, pumps, purification systems, and so forth. The racks of electronics and power equipment, of course, are separate, but even they are mounted on casters. The system is thus compact and complete, and requires but one 220 v, 3 phase input line for operation. The stand also is designed to hold 30,000 pounds of lead shielding around the chamber.

C. The Inner Chamber

The bellows chamber (Fig. 9) is in the form of a short cylinder about 13 inches in diameter. The fully extended length is 6 3/4 inches, the compressed length 6 inches. The bellows is divided into two sections, one adjacent to each window. The upper one is the longer of the two, containing 10 leaves, each of which is an annular ring 1 13/16 inches wide. The extended length of this bellows section is 15/16 inches. The lower bellows contains four leaves, with an extended length of 3/8 inches. Because of hydrodynamic considerations, the upper bellows is expected to do most of the moving during expansion and recompression. The metal parts of the chamber are constructed of inconel X, a hardenable alloy about 70% nickel, which is an excellent spring material and has very high corrosion

Figure 9

Inner (Bellows) Chamber

Explanation of symbols

A. Upper stop
B. Upper ($\frac{1}{2}$ inch) window
C. Support vessel
D. Flexible (sleeve) insert
E. Upper bellows
F. Inner support fluid
G. Outer support fluid.
H. Sensitive (bubble chamber) fluid
I. Inner vessel wall
J. Sensitive fluid filling valve (shown in open condition)
K. Inner support fluid filling line
L. Central target tube
M. Lower bellows
N. Lower (3/8 inch) window
O. Lower stop
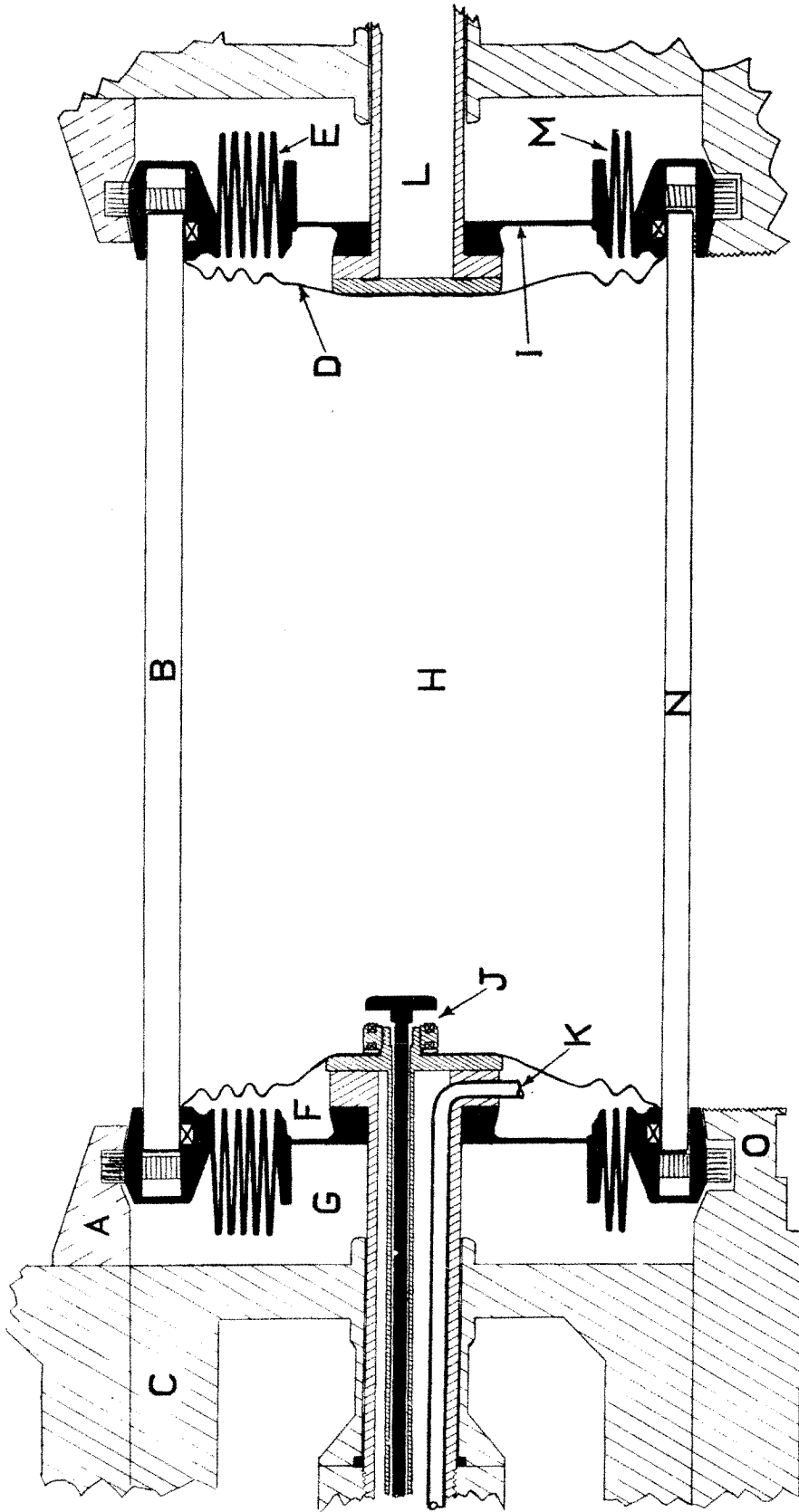
Figure 9

resistance, particularly to HF and WF_6. The windows, 3/8 inch to $\frac{1}{2}$ inch

thick, are of Pyrex or Vycor, the latter in particular for WF_6, since it

is more resistant to etching. In the original design, it was intended that

the windows be sealed to the metal chamber with Teflon "O" rings. However,

since it became necessary to add the flexible insert (see below), the seal

can be effected by the sleeve itself instead of the Teflon "O" ring. The

maximum useful diameter of the chamber is fixed by the inner diameter of

the bellows and the window flange, which is approximately 12 inches.

For the purpose of observing the position of the windows, there

are position transducers attached to the upper and lower window flanges.

These are variable reluctance devices excited by an audio oscillator. The

position of the windows must be known accurately during filling (and opera-

tion) in order to determine if the chamber contains the correct volume of

fluid. The position devices are also useful dynamically, in that they pro-

vide a monitor on the motion of the windows during expansion and recompres-

sion.

There are advantages to the bellows chamber system. One is that

the corrosive sensitive liquid is completely contained, and no complicated

sliding seals or other expansion apparatus is in contact with it. Also

the available area for expansion of the fluid is very large, allowing both

high speed and small actual fluid motion. Furthermore, since the material

of the chamber walls and bellows is metal and only 0.031 to 0.043 inches

thick, the thermal contact between the interior of the container and the

surrounding fluid is quite good. This helps in maintaining a constant

temperature in the chamber proper. Such a thing aids in maintaining uni-

form and constant sensitivity in a bubble chamber fluid.

However, there is a serious difficulty associated with the

bellows design, at least for the flat bellows configuration which we have employed. During the initial runs with the chamber (Chapter I-4), it was evident that violent boiling was occurring around the bellows themselves. The exact cause of this boiling is not completely understood, although some possible causes are discussed in Chapter I-4. Rather than attempt to solve this problem directly, we chose to avoid it by putting the inert fluid in contact with the bellows. Therefore we added the cylindrical flexible insert mentioned earlier. The sleeve used for the initial runs with propane was made of a sheet of 1/16 inch thick Hycar rubber, and was slipped over the edges of the windows. Hence when the windows were clamped down the rubber sealed by being pressed between each window and a rubber "O" ring in the appropriate flange of the bellows chamber. The filler tube was brought into the bag by means of a metal device which clamped to the edges of a 3/8 inch hole in the rubber bag. To this device was attached a flexible plastic tube for filling. The region between the bellows and the rubber was filled with the support fluid, brought into the system by a metal filling line. The test results are given in Chapter I-4.

Obviously one cannot hope to use Hycar rubber to contain WF_6 because of temperature and chemical considerations. For WF_6 we hope to use a Teflon sleeve, and at this writing work is in progress upon its fabrication.

The use of an insert as described above has certain advantages. The walls of the chamber are then smooth, and if the material of the sleeve (rubber for hydrocarbons, Teflon for WF_6 or Freons) is wetted by the sensitive fluid, we may hope for a relatively "clean" chamber, with little or no boiling from the walls. The test results given in Chapter I-4 indicate that this hope has good experimental basis. The sleeve also tends to smooth

out the rapid local fluid motion around the opening bellows leaves, reducing turbulent distortions.

There is one distinct drawback, however. The excellent thermal contact of the sensitive liquid with the support fluid is materially reduced, both by the sleeve itself and by the layer of trapped support fluid between the insert and the bellows chamber walls. How serious this effect is remains to be determined.

D. Support Tank and Fluid

As can be seen with the aid of Fig. 8, the support tank contains the normal operating pressure of the chamber (about 500 psi). At the lower end of the cylindrical structure is the large, high pressure window described earlier. This window has a pressure-assisted "O" ring seal. That is, the seal is made between the bottom of the window and an inverted flange on the vessel. The high pressure in the chamber forces the glass down against the flange, so that the seal is kept tight. The actual load from the window, however, (about 70,000 pounds) is borne by a padded "Flexitallic" gasket adjacent to the "O" ring.

The inner vessel connects to the support tank by a diametral tube, which serves as a mechanical support for the inner vessel. This tube carries the filling lines to the inner chamber, and also constitutes the outer portions of a gas-filled target that passes through the center of the chamber in some experimental arrangements.

Above the inner vessel are the four symmetrically placed expansion cylinders and four bellows, whose purpose is explained later. In order to reduce heat loss to the outside these cylinders have been made as thin-walled as possible commensurate with their required strength, for they must not only withstand the high pressure, but must also carry the

weight of the support vessel and its contents. The $3\frac{1}{2}$ inch diameter pistons (described earlier) in the expansion cylinders were limited to a stroke of about 1 5/8 inches in the original arrangement, but in a modification now completed have adjustable limits of stroke from 2 inches to $3\frac{1}{2}$ inches.

The illumination system, including the two flash tubes and two mirrors, are attached to the lid of the support tank so that they may be removed as a unit, preserving their adjustment.

In the initial run, we found that we were given some trouble by the "stretching" of the support tank in the vertical dimension, using some of the piston stroke in the volume change of the vessel itself. This stretching was probably caused primarily by loose bolts in some of the flanges, since a number of them are very difficult to reach in order to tighten. We solved this problem by running eight long bolts through the flanges from the lid to the window flange and prestressing them. Since the total force provided by the eight prestressed bolts is greater than the force on the ends of the support tank when it is at maximum pressure, and since the tank is extremely rigid in compression, there can now be little stretching of the tank under pressure. Results of this improvement are given in Chapter I-4.

One attribute of the support system should be noted. With this chamber the high pressure window could be eliminated. It is possible, in principle, to replace it with a continuation of the support vessel, at the end of which are only small camera windows, comparable to the ones now being used on the safety vessel. Such a procedure was not adopted for this chamber, since windows of the size of our high pressure window are not prohibitively expensive, and we were concerned that optical distortions in the support fluid between the camera and chamber should cause trouble.

However, for much larger chambers the gamble would probably be worth it for the reasons noted earlier.

An interesting possibility which we have not as yet exploited, but may later, is that the support fluid could be stirred and perhaps filtered continuously, providing a really effective uniform temperature bath, free of the dirt particles which often lighten the background of our dark field illumination system.

A final point concerns the geometry of the chamber. As Fig. 8 illustrates, all windows on the chamber are horizontal, and the optical path through the chamber approximately vertical. There are both advantages and drawbacks to this arrangement, as we have discovered during the construction and testing of the chamber. Among the advantages is the fact that such a geometry tends to reduce the optical distortions in the system that arise from temperature differences in the chamber. One expects that any static thermal (and thus density) gradients in the fluids will be vertical, due to convection. A ray of light traveling parallel to a gradient in the index of refraction will be undeviated, whereas those traveling normal to it will be refracted, causing a change in the apparent position of an object. The almost vertical sight path possible in a horizontal chamber thus tends to minimize these distortions.

One the other hand, there are reasons why the vertical geometry may be preferred. The horizontal design requires that glass windows, which have poor thermal conductivity, constitute the top and bottom of the chamber, thus maintaining vertical thermal gradients instead of helping to destroy them. Particularly in a bubble chamber with bad boiling or a slow recompression system such that residual bubbles rise to the top of the chamber after an expansion, it is very bad to use a medium of poor thermal

conductivity for the top of the vessel. The residual bubbles in such a case compress out slowly, for they must deliver their heat of vaporization to the surrounding fluid. If the top of the chamber is glass, the excess heat is not readily carried away, and after a few expansions the fluid may become much hotter at the top than at the bottom.

From a practical standpoint there is another difficulty with horizontal windows. It is essentially impossible to avoid getting some dirt into the chamber, and this invariably either settles or possibly rises. In any case it usually ends up on the windows, a situation particularly bad when dark field illumination is being employed.

2. Expansion System

The system for expanding and recompressing this chamber is, as was previously stated, quite a departure from the conventional approach. The entire system is caused to behave in a manner much like a "single-shot" mechanical resonator. On the outside of the expansion pistons previously described are large normally-closed valves (the expansion engines). Beyond these valves and extending above the level of the fluid in which they operate are large gas reservoirs (bias cylinders) (Fig. 8), which are pre-pressurized to some value lower than the starting pressure in the chamber. The closed valves normally hold the pistons in check, retaining the starting pressure (typically about 500 psi). It is instructive in any complex mechanical resonator to examine the sources of energy storage and those of kinetic energy. The sensitive fluid of any bubble chamber at the temperature at which it operates is a comparatively compressible liquid. Thus the primary energy storage in this system is in the sensitive fluid itself. To a lesser extent, energy is also stored in the compression of the support

fluid, and in the small spring in the chamber walls. Energy, of course, is also stored in the bias cylinders through the medium of the pressurized gas. The kinetic energy or mass elements of the resonator are in the mass of the pistons and oil in the expansion cylinders primarily (since these will have the highest velocity when the sensitive liquid is expanding) and to a lesser extent in the distributed mass of the rest of the support fluid and the sensitive liquid itself.

For the moment it is convenient to consider the volume of gas in the bias cylinders infinite, so that there is no change of pressure in them during expansion. Now consider what occurs when the large valves are opened. Let the initial pressure in the chamber be P_0 and the pressure in the bias cylinder P_1, where $P_1 < P_0$. For simplicity consider the system lossless and the compressible media in the chamber linear. (The latter is very nearly true.) When the valves are opened, the chamber media expand, forcing the pistons back. The expansion does not stop when the chamber pressure becomes equal to the bias cylinder pressure because of the kinetic energy in the motion of the inertial elements. The motion stops when the pressure in the chamber drops to $2P_1 - P_0$, for then the usable stored energy in the chamber has been transferred to the bias cylinders. This is most simply seen in the following manner:

We define a compression constant K for the chamber as viewed from the pistons by $K \equiv dV/dP$, where V is the volume. The energy stored in the chamber when the volume changes an amount ΔV is given by

$$\int_0^{\Delta V} P dV.$$

If now ΔV is the volume change in going from pressure $2P_1 - P_0$ to P_0, the energy storage is

$$\int_{0}^{\Delta V} P dV = \int_{2P_1 - P_0}^{P_0} KP^2 dP = 2KP_1(P_0 - P_1).$$

During the change ΔV the energy stored in the bias cylinders is

$P_1 \Delta V = KP_1 \Delta P = 2KP_1(P_0 - P_1)$, which is equal to the above.

When the motion has stopped, the chamber is fully expanded, so particles are introduced and the picture taken. Now the cycle continues, the motion reverses itself and stops (in the lossless case) when the original conditions are restored and the chamber recompressed. At this time the valves are closed, stopping the oscillation after one cycle.

It need not be said that the above is idealized, for it is obvious that a bubble chamber liquid, by its very nature, is not a lossless medium. In fact, the energy losses during a cycle would be expected to be quite substantial, since the fluid attempts to boil when the pressure is low. However, if the cycle is fast enough and the chamber sufficiently clean, the bubbles are not allowed time to grow to a size sufficient to prevent the recompression, as is indicated by the test results in Chapter I-4. In actual operation, while the vapor pressure of the sensitive liquid is only 300 psi, the starting chamber pressure is about 500. Hence there is excess stored energy in the beginning, since the final chamber pressure is required merely to be above 300 psi. Fairly large losses can be tolerated. The loss pump, described later, restores the chamber pressure to its initial value during the "dead time" of the system.

Evidently the chamber can be made to recompress no matter what the losses, if the initial pressure is made sufficiently large, or, stating it another way, if the initial energy storage is big enough. However, there are mechanical limitations to the pressure one may safely employ, determined chiefly by the strength of the high pressure window. Therefore

a modification was made in the system (Fig. 10), whose purpose is both to allow more initial energy storage and to speed up the cycle. The change consists of a group of springs at the inner stop of each piston, with an available compression of about 3/8 inch, providing a total force of up to 3700 pounds at each piston. The springs act as a substitute for additional compression of the chamber media, so that we may store more energy in the system without raising the starting pressure dangerously high. The springs also give a larger starting impulse to the pistons, speeding up the over-all cycle. Another reason for making this modification was to compensate for the fact that the fluorocarbon support fluid proved to have a consid-erably higher compressibility than we had at first expected. The springs are thus required in order to regain the speed that was lost by the anom-alous compressibility. A quantitative treatment of the expansion-recom-pression cycle is contained in Appendix I.

The loss pump mentioned earlier forces the expansion engine fluid from the bottom of the bias cylinder gas reservoir to the trapped region between the pistons and the large valves, driving the pistons inward and restoring the initial pressure in the chamber and initial energy storage in the springs (Fig. 10). This operation is not required to be fast, as it need only be done before the chamber is next expanded.

The bellows mentioned before, which occupy the symmetric four positions between the expansion cylinders, are called "mechanical diodes," and they were designed to flatten the bottom or low pressure portion of the expansion cycle. They consist of re-entrant bellows which are collapsed against solid outer stops by large internal pressures, and can contain such pressures without damage. However, if the chamber pressure drops below the external pressure, the bellows open freely inwards. The intention is to

Figure 10

Expansion Piston and Bias Cylinder

Explanation of symbols

P. Piston
C. Expansion cylinder
S. Booster springs
B. Bias cylinder
M. Piston position monitor
L. Oil level
D. Splash damper
V. Expansion engine sleeve valve
I. To input of loss pump
O. From output of loss pump

Arrows (other than those concerned with lettering) indicate the direction of oil flow during expansion and recompression or pump up.

Figure 10
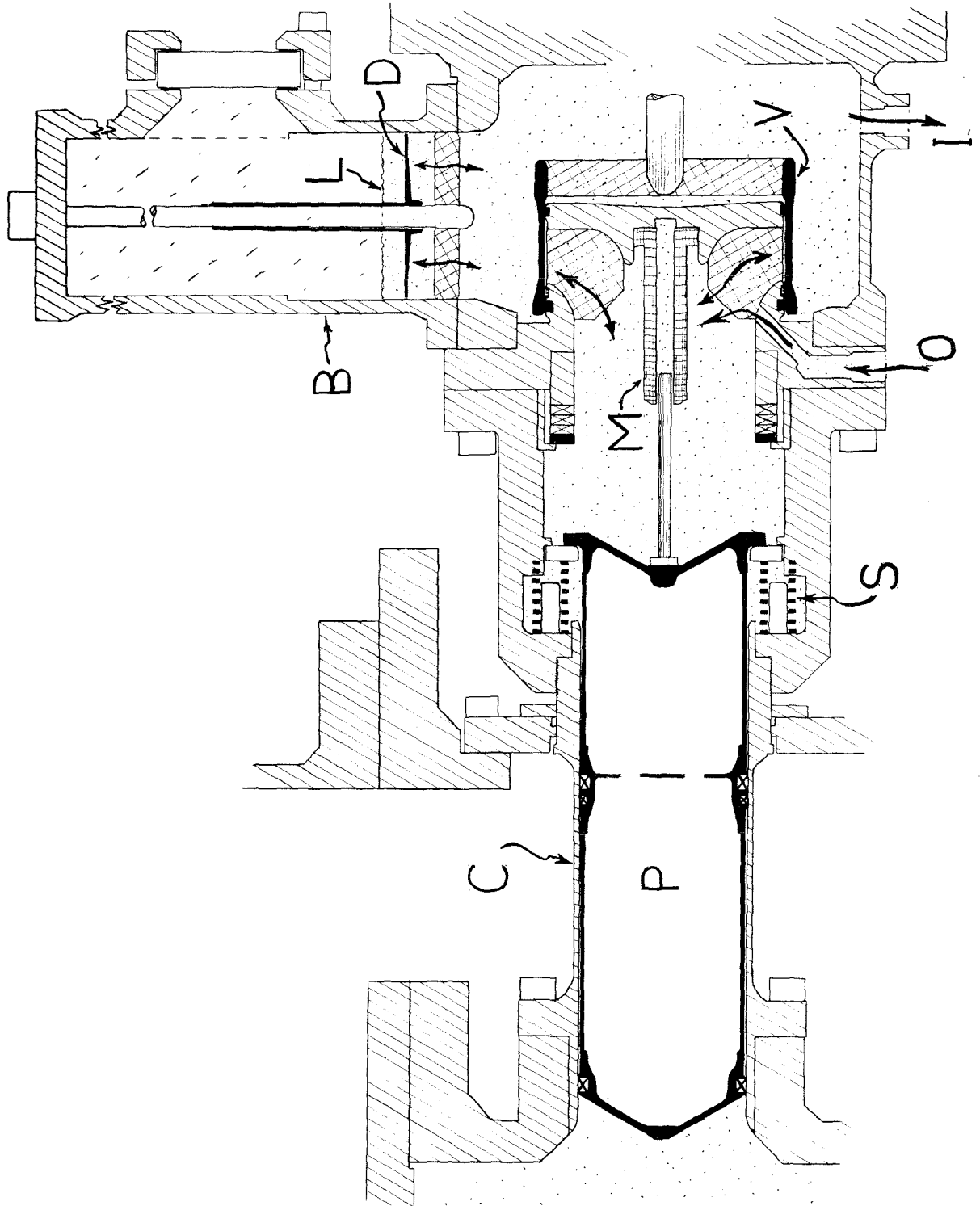
pressurize each bellows from the outside, constituting the external pressure previously mentioned, to some value such as 100 psi. Then the expansion cycle will be adjusted to drop the chamber pressure below this value, and the bellows, it is hoped, will function to flatten the bottom of this pressure cycle, yielding a longer period of constant pressure conditions. These devices have not been tested, however.

In order to adjust the volume of the support fluid to the correct value, one must be able to ascertain the position of the free pistons. The pistons used in the tests described in Chapter I-4 had alnico magnets attached to them which could be followed with the aid of a compass from the outside, through the non-magnetic stainless steel of the cylinders. This technique is crude and clumsy, but worked, if not well, then at least well enough. The new pistons (Fig. 10) have superior position measuring devices of the variable reluctance variety, which can also be employed dynamically.

It is now pertinent to review the reasons for choosing an expansion system such as described above. One was to obtain a very fast expansion cycle, with an equally quick recompression in order to reduce the thermal input to the chamber caused by the irreversible boiling process. The limitation on the speed of this one is primarily in the unavoidable mass of the fluid and pistons in the exit orifices (expansion cylinders), and this effect has been reduced to a comparatively low value by the use of a much larger exit area (40 in^2 for the four cylinders together) than is usually employed in a chamber this size.

F. Expansion Engines

The large valves in the expansion system whose function is outlined above constitute the expansion engines. When the system was first

proposed, we did preliminary calculations (Appendix I) to determine the
requirements on the valves. We found that we needed to be able to open
an orifice for liquid flow about 40 in^2 in area in a time comparable to 3 ms,
allow it to remain open for some 10 ms, and close again in another 3 ms.
We further needed control over the overall period to either lengthen or
shorten it, in order to allow flexibility in choice of bubble chamber and
support fluids and in case our preliminary calculations were inaccurate.
(Some of the relevant quantities were not accurately known.) In addition,
we had to be able to handle differential pressures up to about 300 psi,
under an internal absolute pressure of up to 500. We decided to relax our
requirements to the extent of dividing the task among four such valves,
each with an orifice of about 10 in^2. Then we also required accurate syn-
chronizability of the devices to less than 1 ms, as well as an overall
timing accuracy of this order.

Unfortunately, we found no commercial valves answering to this
description without extensive modification, and even then requiring large
inputs of compressed air to operate. Therefore we designed our own. The
result was a set of devices which, although they still have defects invari-
ably inherent in such a new design, do perform the required function quite
satisfactorily.

For the valve proper we chose a sleeve design (Fig. 11) from the
following considerations. Because of the large pressures involved, we
thought it better to have a rigid mechanical structure. However, we also
wanted the moving part to be light, since high speeds were required of it.
Among the rigid valve configurations, the sleeve probably has the best
orifice to weight ratio. An additional dividend of this type of structure
is that the force created by the differential pressure across the valve

Figure 11

Expansion Engine

Explanation of symbols

B.   Bouncer
D.   Driver
P.   Gas "spring" piston
RS.   Rear drive shaft
FS.   Front drive shaft
C.   Coupling between shafts
MMA.   Moving magnet assembly
FM.   Fixed portion of magnet
VH.   Valve housing
DP.   Dash pot
S.   Sleeve (of valve)
SP.   Spider on sleeve
ST.   Valve "seat" (solid disk)
SS.   Static seal
DS.   Dynamic seal
R.   Ribs which attach "seat" to body of valve
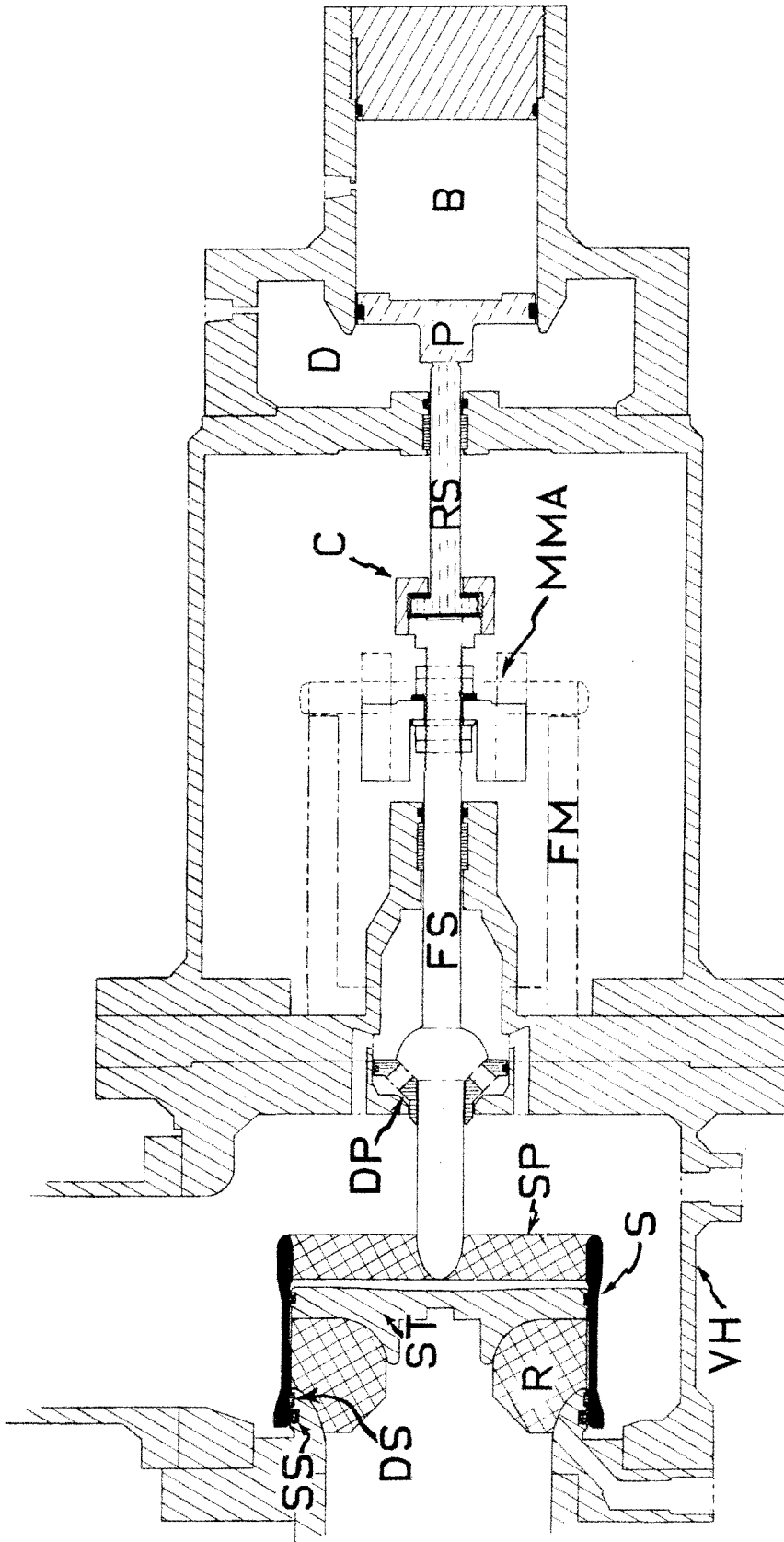
Figure 11

port is directed normal to the direction of travel of the moving piece, and consequently does not influence its motion. Any differential pressure up to the breaking strength of the parts themselves can be used in a sleeve valve without appreciably affecting the force required to open or close it. Another feature of this particular valve is that it has two seals or seats. The first one disengaged during the opening stroke of the valve is a rubber "O" ring, which is a good static seal. The second, a Teflon ring which is still a fairly good dynamic seal, is not broken until the valve has traveled about $\frac{1}{2}$ inch and thus acquired speed. The feature insures rapid effective opening times of the valve, even though the moving piece starts slowly.

The principle of operation of these valves is quite annlagous to that of the expansion system itself. The moving portion of the valve constitutes the mass of a mechanical oscillator which is driven by "springs" consisting of the double gas reservoir seen in Fig. 11. The natural period of oscillation of the system (and hence the open time of the valve) is adjusted by means of the pressure in the gas reservoirs, effectively determining the spring constant of the oscillator. (Actually, "constant" is the wrong term to use here. The characteristics of a gas "spring" are quite nonlinear.) The equilibrium position of the moving piece is arranged to be at some point between the closed and fully open positions, and in the quiescent state the valve is held closed against the restoring force of the "springs" by means of a powerful electro-magnet. Upon release of the magnet, the valve structure swings out to the open position and back to the closed, completing the cycle we require. For a lossless system it would be necessary merely to revive the current in the magnet at the end of the cycle in order to keep the valve closed. However, there are

unavoidable mechanical energy losses, so that a means must be provided to replace them. This is accomplished by the use of a large pulse of current which flows through the magnets and an auxiliary coil attached to the moving structure. The extended pulling force of the holding magnet plus the action in the magnetic field of the moving coil are sufficient to overcome the losses and drive the valve closed.

For reliable operation, it is not adequate to give the valves just barely enough energy to return. Instead, they must be given sufficient excess energy to take into account various mechanical fluctuations in the operation. However, if too much excess energy is applied, the valves will reach their closed position with considerable velocity, closing the holding magnets with a damaging mechanical shock. This difficulty is overcome by the use of a "dash pot" which operates in the oil of the valves, and absorbs the shock of closing.

The construction and operation of the expansion engines as well as their actual performance is considered in much greater detail in Appendix II.

G. Heating and Temperature Monitoring

Since the sensitivity of a bubble chamber liquid is a strong function of temperature, it is quite important to have an accurate and reliable temperature controlling system. Other reasons for wanting good temperature control have been given earlier. Great stress (perhaps too great) has been laid upon this point in the design of our chamber, and the heating and temperature monitoring systems are quite elaborate.

The uniformity for which we initially asked was about $0.1^{\circ}C$ throughout the chamber. Actually such extreme accuracy is probably not

required for the size and geometry of our present chamber, but it might be needed in a large, completely hydrostatically supported chamber, at least from the standpoint of optical distortions. In our chamber the optical path includes only an inch or so of support fluid, but in a completely hydrostatically supported chamber the path length through the support fluid may have to be closer to a meter. Optical distortions may then present a problem, and trouble of this kind has been encountered in the Berkeley 30 inch propane chamber (43).

A good starting point for any device which is to possess constant and uniform temperatures is to provide excellent thermal insulation. In this chamber we have employed the time-honored technique of vacuum plus heat reflecting surfaces whenever possible. For example, such an approach is used in the main insulation, that between the support vessel and the safety tank.* In those places where metal connections to room temperature cannot be avoided, we have used stainless steel, and that in the thinnest form possible compatible with strength requirements.

The primary heating of the chamber is done with radiant heaters placed inside the reflecting shields in the vacuum between support and safety vessels. The idea is that radiant heating is basically uniform, and should develop no hot spots in the support vessel. These heaters are divided horizontally into four channels, each with a separate thermistor control. In addition, on all those points where metal parts lead from the support vessel to the outside are placed individually controlled conduction heaters. The heater controls the temperature at the point of heat loss,

---

* From considerations of safety, we have tried operating the chamber with one atmosphere of pressure inside the safety shell and found, at least at 60°C, that no serious harm was done to the temperature regulation.

keeping it equal to the temperature of the rest of the support vessel.

All heaters are individually operated by thermistor controlled power supplies. Thermistors (temperature dependent resistors) were chosen for the sensing elements by reason of their very high sensitivity, among other things. The ones we are using* have a resistance temperature coefficient of about 2.5% per degree centigrade at 140°C. They are also very small, have a short thermal time constant, and are relatively cheap.

However, since thermistors have an absolute resistance tolerance of 20%, they cannot be used to measure temperatures accurately unless individually calibrated. Therefore a different device is used to monitor temperatures. We have chosen thermocouples for this purpose. No doubt laboratory resistance thermometers are more accurate instruments, but they are bulky and quite expensive. Since we wished to measure temperatures in many places (our chamber has over 30 thermocouples), some of which are quite cramped for room, thermocouples seemed the logical choice.** However, we also wished to be able to read the temperatures in the chamber to 0.1°C. The standard technique with thermocouples is to display their output on a multipoint recording potentiometer. If one wishes to read to 0.1°C on the usual potentiometer scale, the full scale reading has to be only about 20°C (about 1 millivolt for copper-constantan). This implies that the cold junction must be within 20° of the chamber temperature or that a bucking voltage be used. The system we employ to solve the problem was worked out

---

* Victory Engineering Company, Type 55A2.

** It was found experimentally by L. R. Gallagher that welded copper-constantan thermocouples taken from a common batch of wire have all the same calibration to 0.1°C. These thermocouple materials are convenient for our purpose since the metals are resistant to oxidation, have relatively high voltage output, and can be obtained in batches of quite uniform composition.

by Gallagher. All thermocouples from the chamber terminate and have their cold junctions in a stirred silicone oil bath. The temperature of the bath is controlled by a thermistor regulated power supply of the type we employ for the chamber heaters, and is read on an accurate mercury thermometer with $0.1^{\circ}C$ divisions. The output of the thermocouples is then fed to a 16 point Wheelco recording potentiometer which reads 1 millivolt full scale, or about 20° C. Thus we have obtained our required reading accuracy as well as solving the thermocouple cold junction problem.

H. The Optical System

The illumination and photographic systems for this chamber were developed by E. D. Alyea, Jr., and are to be reported in detail by him. However, for the sake of completeness, a brief description will be given here. Figure 8 illustrates the broad features of the arrangement. Illumination is provided by two xenon flash tubes, each about 6 inches long and $\frac{1}{4}$ inch in diameter and forming approximate line sources. The light from each tube is collimated to an aluminized cylindrical glass mirror placed next to the lid of the chamber. These two mirrors focus the light in one dimension so as to fill the chamber but avoid the two camera windows as shown. Light from bubbles is thus scattered through small angles into the camera lenses, affording lighted bubbles against a dark background. An intricate system of vanes is employed in the flash tube holders to provide more uniform illumination and to avoid lighting of certain parts of the interior of the chamber.

A requisite part of this lighting system is its high efficiency. A large fraction of the light produced by the tubes is actually employed to illuminate the chamber, and the bubbles scatter very efficiently at

small angles. For our chamber, this feature is highly desirable, since most of the energy put into the flash tubes ends up as heat in the chamber and support tank, much of it in the vicinity of the tubes themselves. The less energy we are required to put into the tubes the better, for heat input, especially in the form of a "hot spot," may cause serious optical distortions.

The camera employed uses standard 65 mm. film and was designed to use to as great an extent as possible standard Mitchel Camera parts. The stereo pictures are both recorded on the same strip of film, along with the picture numbers. The lenses (Goerz Rectagon 3.5 inch) are spaced 12 inches apart, so that they line up with the extreme edges of the chamber. With the chamber-to-camera distance of about 26 inches, we have a stereo angle of something under 30°. It must be noted that different parts of the chamber are viewed by the camera at different angles through several thick layers of material of varying indices of refraction. Therefore the problem of reconstructing the actual position of a bubble from the two images on the film is not a simple one. This problem has been considered in great detail by Alyea and Fretwell, and the discussion of it is left to them.

I. Experimental Target Arrangements

Of course, a bubble chamber is essentially useless without a means for injecting high energy particles. The arrangements for particle entry into our chamber have been made with the characteristics of a bremsstrahlung beam in mind, and the primary target arrangements are passages for the x-ray beam. The "standard" target, as we have called it, is an unobstructed tube passing diametrally through the center of the

chamber. This tube is to be filled with high pressure gas, which will constitute the target material. For many experiments, one would expect to use H_2 gas, in particular for all investigations of photoproduction from single protons. This might be, for example, multiple meson production. One could also use deuterium in the tube, or possible even tritium, for studies of photoproduction from neutrons.

Another tube, parallel to the central one and in the same horizontal plane, passes through the safety and support vessels. This target passes closely beside and tangent to the inner chamber. It is also to be filled with high pressure gas, and will be used as a target in those experiments in which it is not necessary to see both sides of the target, but for which we require the stopping power of the full chamber diameter. Such an experiment, perhaps, might be the study of K^+ mesons produced at large center of mass angles.

Two additional target arrangements are provided. These are designed primarily for the entrance into the chamber of charged particles, although they could be used for neutrals as well. One is a series of comparatively thin windows about 2 inches in diameter through the safety and support vessels, comprising a total of about 4.83 gms/cm^2 between the outside and the sensitive fluid. The other is a much larger rectangular window 3 X 6 inches, with a total of 22 gms/cm^2. The thinner of these windows is to be used for the entry of lower energy charged particles. Both of these target windows would supposedly have their greatest utility when the chamber is used in conjunction with a momentum-analysing magnet.

The central tube target has not yet been tested, and the optimum shape for it is not fully determined. It seems clear that a simple

cylindrical shape is not best, from consideration of the generally cone-shaped spray of background electrons and positrons from pair (and Compton) production in the hydrogen. Figure 12, which was taken from the Berkeley hydrogen chamber run by Teem and Alyea mentioned in Chapter I-1, is an illustration of this spray. It would seem prudent to confine the worst part of the cone to hydrogen, rather than letting it emerge into the photon sensitive heavy liquid, where it would spread by cascade into wider angular regions. One would then envision the target tube as somewhat cone-shaped, reducing background at the expense of the availability of forward angles for observation. The problem is complicated, and the best solution will probably have to be found experimentally.

In order to reduce the background contribution from the numerous low energy photons in the bremsstrahlung beam, we intend to employ the "beam hardener" technique of Alyea and Teem, and which is used with some modification by the Cornell group with their hydrogen diffusion chamber (23). The method is to pass the beam through a long tube containing lithium hydride in a magnetic field, with a small exit collimator. The method functions because of the higher absorption cross section of LiH for low energy photons. Degradation of the beam through cascade processes is avoided by the combination of the magnetic field, multiple Coulomb scattering, and the collimator. Most of the photons from secondary processes are sufficiently deflected to miss the small opening in the collimator because of the multiple scattering or magnetic deflection of the electrons and positrons which produce them.

J. Plumbing Arrangements

The topic of the plumbing for our chamber merits special treatment

Figure 12

Bremsstrahlung Beam in Hydrogen

This picture taken with 4 inch Berkeley hydrogen chamber in 300 Mev bremsstrahlung. Part of spray of e$^{\pm}$ arises from entrance foil.

Figure 12

BEAM

-74-
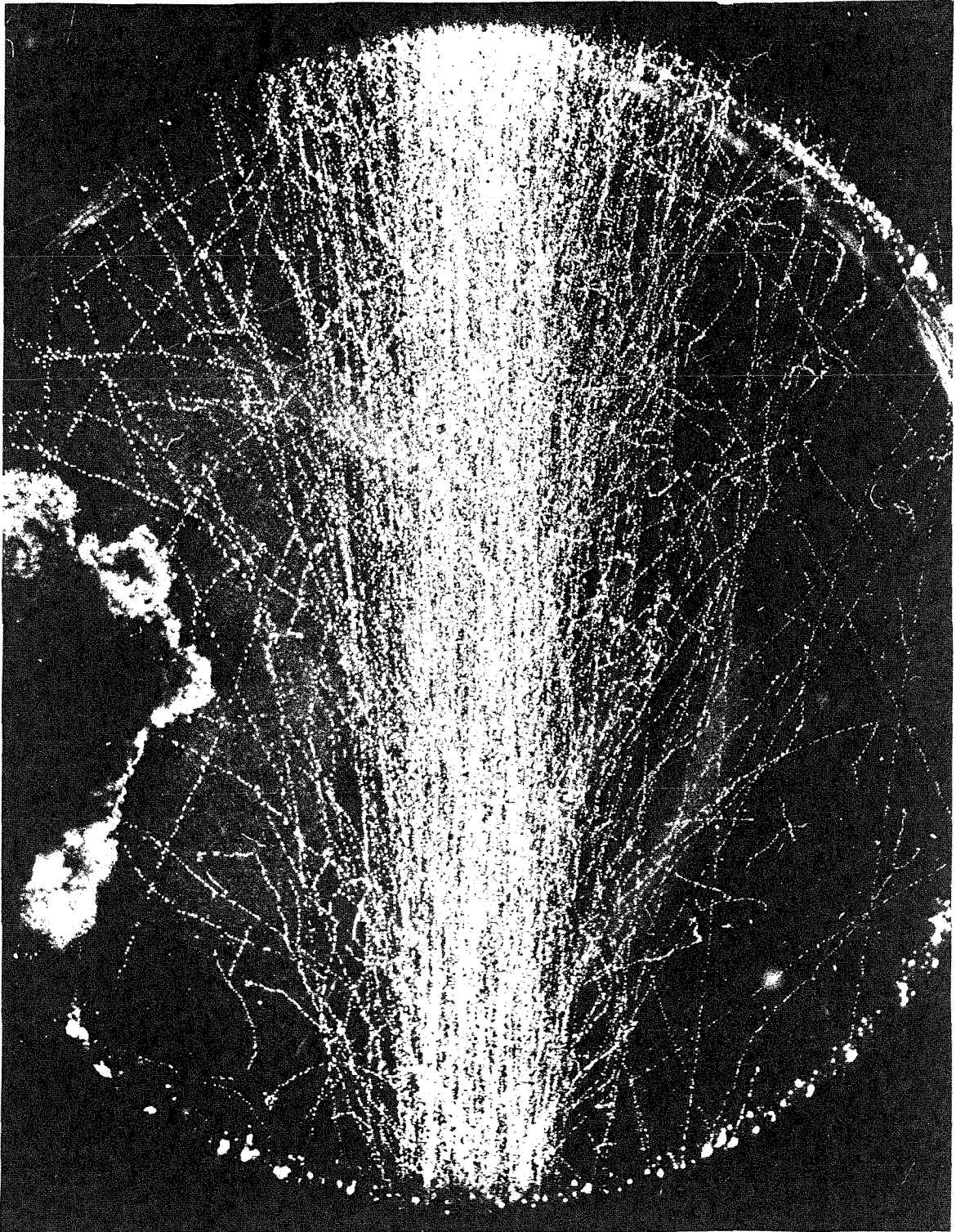
because of the number of separate systems involved. There are, in fact, six distinct sets of piping, each of which has its own special requirements.

We begin with consideration of the high pressure gas supply. Since all of the items but one requiring high pressure gas are essentially reservoirs needing no supply other than enough to make up leaks, we are able to use a single standard 220 cubic foot N_2 cylinder to supply all our needs. (Even the dissipative device, the three-way valve described below, consumes very little gas.) Excellent pressure regulation is maintained in the various devices with inexpensive single-stage regulators by the technique of using them to form what is, in effect, a two stage system. One regulator attached directly to the N_2 bottle supplies gas to a manifold at a regulated pressure of about 400 psi. The manifold furnishes a common input to the rest of the regulators, of which there are five.

The plumbing arrangement for the oil which fills the expansion engines is shown schematically in Fig. 13. The primary purpose of the external system is to provide means for pumping the chamber up to the starting pressure between expansions, as described earlier. When the system is quiescent, the loss pump circulates the oil around the low impedance closed loop shown, requiring very little power. Upon command, the three-way valve switches the flow through the pump so that it passes from the bias cylinders to the region between the pistons and the expansion valves. This drives the pistons inwards, building up the chamber pressure until a pressure transducer indicates the proper value, at which time an automatic control switches the three-way valve back to the quiescent condition. In the case of failure of the pressure transducer, control, or 3-way valve, a mechanical bypass is set to a differential pressure somewhat

Figure 13

Plumbing for Expansion Engine Oil (Schematic)

Explanation of symbols

HP.	High pressure side of sleeve valve
LP.	Low pressure side of sleeve valve
G.	Pressure gauge
V.	Manual valve
A.	To high pressure side of other engines
B.	From low pressure side of other engines
TWV.	Three way solenoid valve
P.	Gear pump (loss pump)
M.	One horsepower motor
T.	Dirt trap
BP.	Safety overpressure bypass valve
F.	Filling line.

Arrows indicate direction of oil flow.

Figure 13
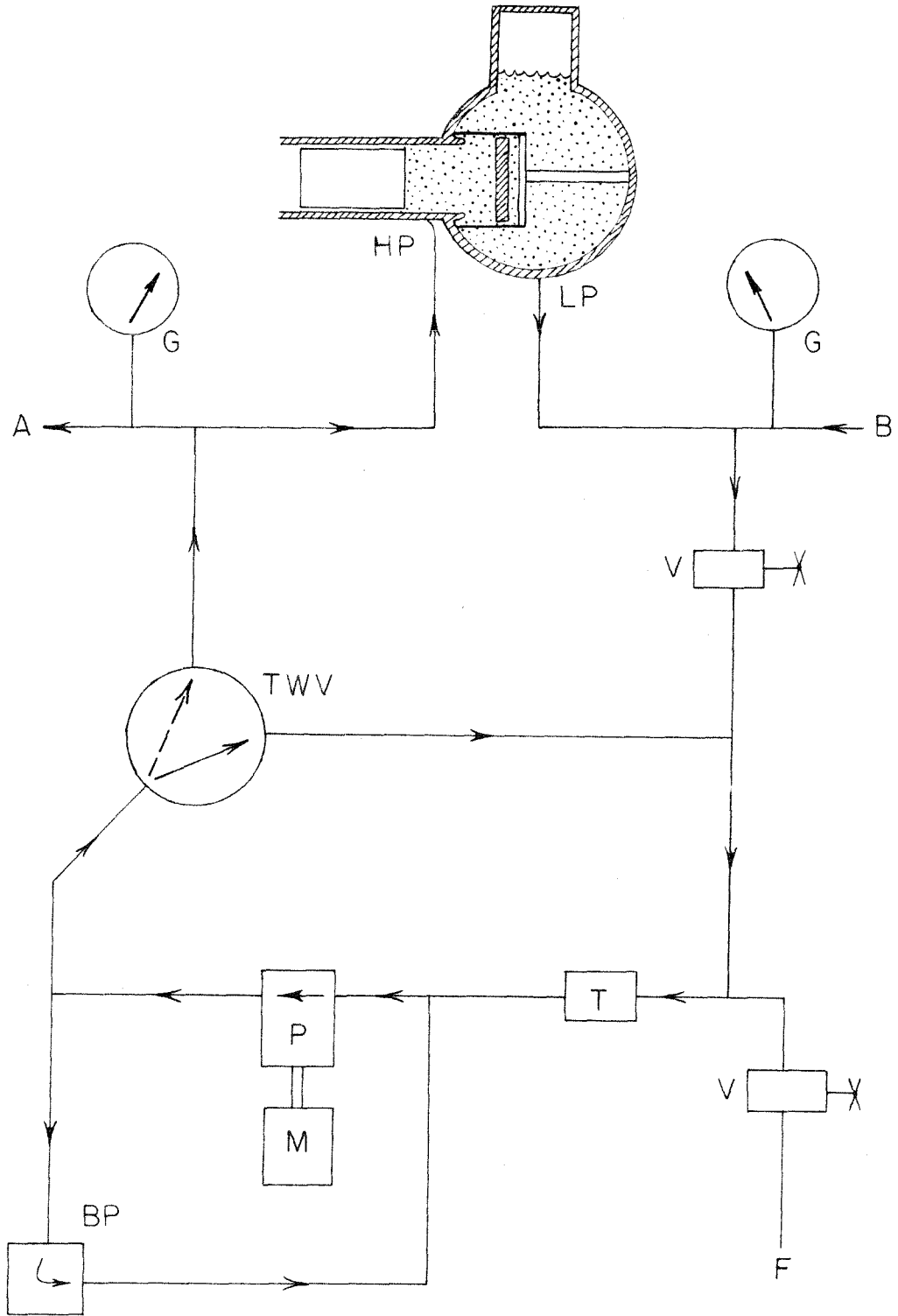
higher than the maximum normally employed, and acts to bypass the pump so that the pressure in the chamber does not exceed safe values. The pump itself is a simple efficient oil gear pump, driven by a one h.p. electric motor. The three-way valve is a pneumatic pilot-operated device, with a 3/4 inch equivalent orifice.

In order to ensure that the oil level in the bias cylinders remains the same on all four engines, the system is made common to the four through external pipes. Since the engines are all in the same horizontal plane, the oil is self-leveling in the bias cylinders. To avoid severe splashing of this oil during chamber expansion, a light, freely movable aluminum "damper" rides just below the oil level in each bias cylinder (Fig. 10). This guided horizontal disk moves with the oil during the rapid flow, and inhibits splashing.

The vacuum system, used primarily for keeping the safety shell evacuated, constitutes a third plumbing system. All main pumping lines are about 2 inches in diameter, and the pump used is a Welch 375 liters/min two-stage mechanical fore pump. The system contains, in addition, a large liquid N_2 cold trap, and a multitude of auxiliary input lines for pumping out other vessels during filling or purification operations. The vacuum attained is quite satisfactory for our purposes. While pumping on the cold trap and some of the smaller equipment, the fore pump has been observed to attain 8×10^{-5} mm Hg. A 2 inch air-cooled diffusion pump is also provided, but has not been used.

A safety feature included in the vacuum system is a large, high pressure, 2 inch pneumatic valve, placed between the safety vessel and the vacuum pump. This fast-acting valve is controlled by a sensing device

employing a Pirani gauge in the vacuum. Should the pressure in the system rise above a certain preset value, the 2 inch valve is automatically closed, isolating the safety vessel. This provides the necessary protection in case of leakage or breakage of the support vessel.

The plumbing array for handling the support fluid is a fourth separate system, shown in simplified form in Fig. 14. One of the practical problems in filling a hydrostatically supported bubble chamber is the necessity of getting the support vessel and fluid air free. Since the solubility for air in most liquids gets smaller as the temperature rises, we have had considerable difficulty with air which comes out of solution during the heating of the chamber and forms undesirable bubbles, increasing the effective compressibility of the fluid. Therefore we have had to allow provision for evacuating the portions of the support system not filled with fluid while the system is hot. (Of course the sensitive fluid cannot be in the chamber during this operation.) The technique is usually to leave the support system not quite filled, and to evacuate the region above the liquid level. Since the support system must be excluded from contact with air, the commercial high pressure accumulator shown is used to apply pressure to the support fluid for the purpose of adding liquid to the support tank (or removing it) when the sensitive fluid is in the chamber and hot.

Since there is a tendency for the support fluid to become dirty under some conditions, there is also provided a filtration technique. The Chempump shown is arranged to circulate the fluid through a sintered stainless steel filter.* This operation can be performed only under pressures

---

* Manufactured by Micrometallic Corporation.

Figure 14

Support Fluid Plumbing (Schematic)

Explanation of symbols

CST.   Chamber support tank (vessel)
FL.   Filling line (for support vessel)
DL.   Draining line (for support vessel)
V.   Manual valve
G.   Pressure gauge
ST.   Storage tank
Vac.   To vacuum system
A.   High pressure accumulator
N.   To high pressure N_2 supply
CP.   Chempump (Arrow indicates direction of flow)
HE.   Heat exchanger (for heating or cooling support fluid during circulation)
F.   Filter
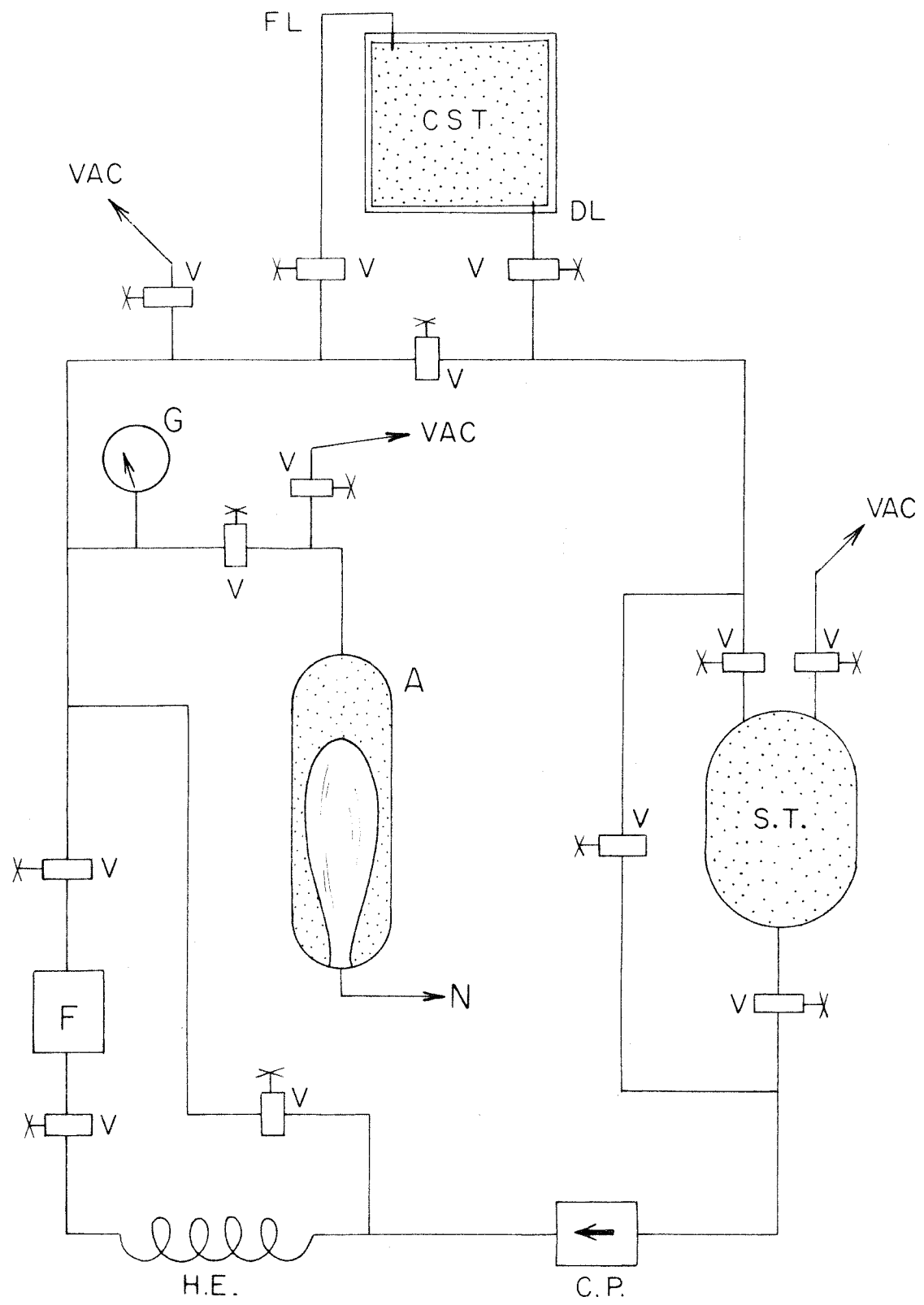
Figure 14

less than 150 psi because of the limiting strength of the pump housing. Thus we cannot filter the fluid when the chamber is filled with the sensitive liquid and hot. Higher pressure pumps are available, however, and it may be worthwhile in the future for us to purchase such a pump, so that it can act to stir the support fluid constantly, as suggested earlier. The Chempump may also be used to transfer support fluid from the storage tank to the support vessel when the system is evacuated or under low pressure. Otherwise the accumulator must be used.

The storage tank shown is normally employed for holding the support fluid when it is not in use. It is a high pressure stainless steel vessel, since it would also be used as a receptacle for the contents of the safety shell in case of a disaster.

For filling the chamber with a hydrocarbon (propane, butane, or isopentane) or a Freon (CF_2Cl_2 or CF_2Br_2), there exists a separate plumbing system. This is quite simple, and consists of a stainless steel storage tank with two filling lines and a quartz window for observation of the liquid level. In addition there is a "volume adjuster," which is a larger version of the piston described in Chapter I-2. The piston on this model is 1.6 inches in diameter and 12 5/8 inches long (Fig. 15). The piston is driven from the outside by means of its threaded shaft and a mating captured nut with handle attached. Double sliding seals are made with Teflon "O" rings. This device is designed to allow small adjustments to be made in the volume of liquid in the chamber under high pressure conditions.

The plumbing system for the WF_6 is, by reason of the corrosive and dangerous nature of the fluid, the most elaborate and carefully leak tested of all. The system includes the purification system which is

Figure 15

Volume Adjuster

Explanation of symbols

P. Piston
C. Cylinder
H. Handle
T. Threaded shaft (integral with piston)
N. Captured nut (attached to handle)
V. To vacuum system (for pumping out region between the double seals)
F. Fluid
K. Key (guide which prevents piston from rotating)
O. Teflon "O" rings
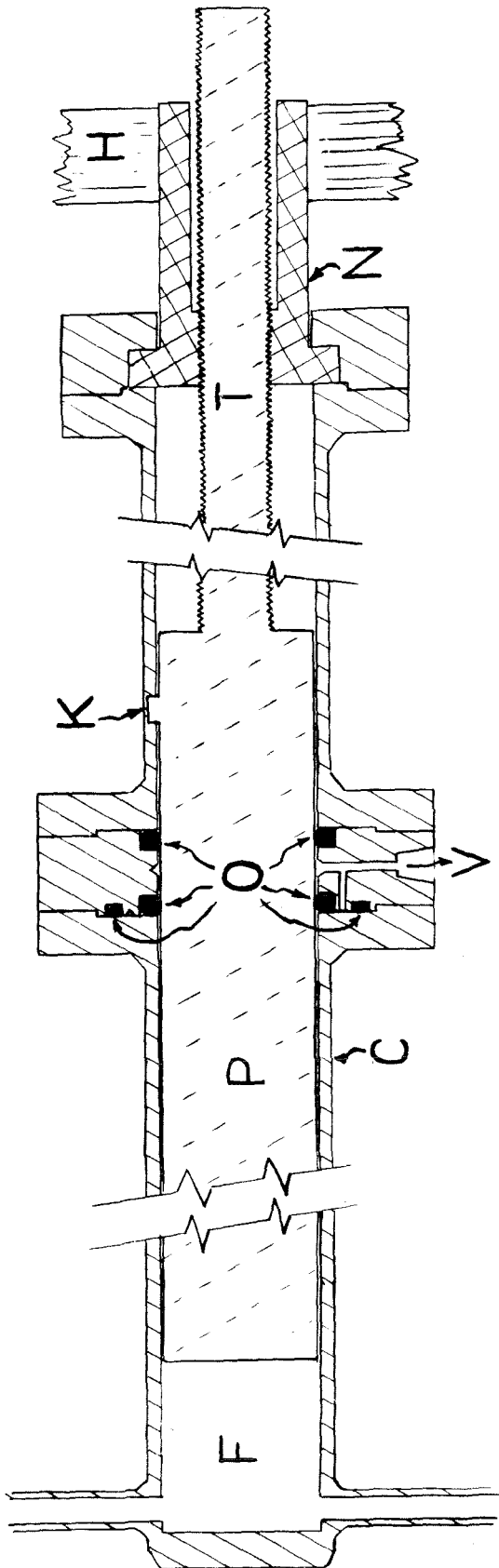
Figure 15

responsible for the majority of the complexity of the plumbing. The details of the purification system are reserved for Appendix III. We describe here only the parts of the system subsequent to purification of the liquid. In most respects, it is like the hydrocarbon system, with some notable differences. One is in the materials used. Whereas the hydrocarbon system is stainless steel with copper tubing, the WF_6 system is entirely monel, including the tubing. Seals at all joints are made with gold gaskets backed by Teflon "O" rings. No windows are used in order to see the liquid level in the storage tank; rather, a monel float arrangement is employed. The shaft of the float terminates in a nickel slug, and extends up a sealed-off inconel tube emerging from the top of the storage tank. Since the inconel is non-magnetic and the nickel magnetic, the position of the slug (and thus the float) can be followed from the outside with the aid of a differential transformer, using the nickel slug as the core. Many valves are required in the WF_6 plumbing, and these are all (with one exception), special monel (and inconel) valves of our own design. A volume adjuster like the one employed in the hydrocarbon system is used here as well, except that it is made of monel rather than stainless steel.

Provision is also made for filtration of the WF_6 without removal from the system through a sintered nickel plug. A similar plug is included in the hydrocarbon-Freon system.

CHAPTER I-4

OPERATION OF THE 12 INCH CHAMBER

A. Initial Run; Fluorocarbon-Butane

The first run with the 12 inch chamber was made before the light-
ing system was completed, and its primary purpose was to obtain information
relating to the overall operation of the expansion system. We used fluoro-
carbon $[(C_4F_9)_3N]$ as the support fluid and butane at $120^\circ C$ as the sensitive
liquid. The inner vessel was left as originally conceived, a metal bellows
chamber without the flexible sleeve or liner described earlier. We depended
upon the pressure transducer in the support liquid and the position trans-
ducers attached to the movable windows of the bellows chamber to provide
the data we required on the operation of the expansion system. Only a few
pulses of the chamber were actually made during this run, since a serious
leak that developed in the support tank resulted in a prohibitive rate of
loss of the expensive fluorocarbon. In addition, the final pulse of the
chamber was accompanied by a loud mechanical shock, so that we were afraid
that the pistons had struck their stops hard enough to cause damage. (This
was found later not to be true.) Unfortunately, the signals from the pres-
sure transducer were seriously masked by noise (which was later eliminated)
during these expansions, so the form of the pressure variation was not as
well established as we would have liked. In spite of the difficulties
encountered, however, some very useful information was gained during this
run. In the first place, it soon became clear that the compressibility
of the entire system as seen from the pistons was far greater than we had
expected. This fact made itself known both through the long period of
oscillation of the system (~ 25 ms) and the amount of motion required by
the pistons in order to raise the chamber pressure. The exact cause of

this anomalous compressibility was not then known but is now understood. For one thing, the actual compressibility of the fluorocarbon is much higher than we had anticipated. For the lack of better information, we had simply assumed that the fluorocarbon would have a compressibility comparable to that of a typical hydrocarbon, which is in the range of 50 - 100 x 10^{-6} per atmosphere. However, an extrapolation of lower temperature data (44) obtained later on this fluid indicates that the compressibility at $120^{\circ}C$ may be as high as 300 x 10^{-6} per atmosphere. Such a value, however, accounts for only half of the compressibility that was observed in excess of that of the sensitive fluid itself. It was found during the second run that a large part of the additional apparent compressibility came from the stretching of the support tank walls. No matter what its source, however, it was clear that this large compressibility would make operation of the chamber impossible with the piston stroke we had available.

A second difficulty which was indicated by the shape of the pressure and window position waveforms was that there was severe boiling in the chamber. The extent and origin of this was not determinable from the first run data, as we had no lighting system with which to obtain pictures of the boiling. However, the effect upon the pressure waveform was similar to that obtained in the second run, of which pictures are shown later.

B. Second Trial; Glycerine-Butane

The next series of chamber expansions was made for the purpose of determing the origin and extent of the boiling indicted in the first run. Therefore, the lighting system was completed and installed, and a temporary stereo camera using cut film was constructed, using the Goerz Rectagon lenses that had been purchased for the permanent camera. In an

effort to avoid the problems caused by the high compressibility of the
fluorocarbon, we changed to glycerine for the support fluid. Glycerine
has a high boiling point and the lowest compressibility of any known or-
ganic liquid, so it was a logical choice for a hydraulic fluid. The
viscosity is higher than we would have liked, but is down to about 10 -
15 cp at the 120° operating temperature of butane, so that it was consid-
ered usable. Other than the change in support fluid and the addition of
a lighting system, there were no major changes from the first run.

Several rather serious difficulties were encountered, having
primarily to do with the properties of glycerine. For one thing, the
glycerine turned out to be a fairly good electrical conductor at the
higher temperatures. This had a number of serious consequences. One
was that our flash power supply was short-circuited, and the current elec-
trolysed the glycerine. Our original intent had been to employ the con-
ventional technique of leaving the main condenser bank connected perman-
ently to the tubes. The 1 to 3 kilovolts from the main supply in itself
is insufficient to ionize the tubes, and an auxiliary high voltage trans-
former is used to apply a 10 to 15 kilovolt pulse to the tubes upon com-
mand to break down the gas. Only then does the main supply discharge its
condenser bank through the tubes. However, the glycerine in which the
tubes were immersed made this technique unusable, so we were forced to
resort to a more complicated system in which ignitrons are placed in series
with the flash tubes and the condenser bank. The ignitrons are triggered
in conjunction with the auxiliary pulse transformer, so that voltage is
applied to the flash tubes only during the time they are being pulsed.
Even with this system, we found that in order to get the tubes to fire,

excessive energy had to be supplied to the pulse transformer because of the low impedance presented by the glycerine. Another unfortunate effect which may have been at least partly due to the electrical conductivity of the glycerine was that our window position transducers changed their calibrations radically as the chamber was heated. This resulted in the breaking of one of the movable windows because the bellows chamber opened to its outer mechanical stop without our knowledge and allowed excessive differential pressure to build up between the inside and outside of the chamber.

Glycerine also proved to be a rather remarkable solvent at the higher temperatures. The evaporated aluminum reflective coating on the mirrors of our lighting system was quickly destroyed by the action of the glycerine. A change to inconel for the reflective coat was of little avail, since it, too, was eventually dissolved. In addition, after several days at high temperatures the glycerine became quite colored and cloudy, making it very difficult to obtain satisfactory pictures through it.

In spite of the various difficulties encountered, the second run was wholly successful in obtaining the information we wanted. We discovered in this run that a large contribution to the anomalous compressibility before mentioned came from the stretching of the support chamber. The total compressibility of the chamber as measured from the pistons at $120^\circ C$ was about 34 cm^3/atmosphere. The butane, with a volume of 13 liters and a compressibility of about 1.46×10^{-3}/atm, contributed 19 cm^3/atm. to this number, while the glycerine, with a volume of 54 liters and an estimated compressibility of only about 35×10^{-6}/atm, contributed less than 2 cm^3/atm. The amount contributed by the expansion of the support vessel is the remaining 13 cm^3/atm, and is almost equal to that arising from the compression of the sensitive fluid itself. Mr. C. L. Friswold of Central

Engineering suggested a method of largely eliminating the support tank expansion, and his technique, described in Chapter I-3, was adopted and employed with excellent results in the third run.

The results of the second run in terms of the pressure cycle and the motion of the bellows chamber windows is best seen in the sample oscilloscope traces shown in Fig. 16. The AC envelope of higher frequency and large initial amplitude is the output of the pressure transducer, and the amplitude is approximately proportional to pressure (except that zero pressure is not a null). The other, lower frequency AC envelope (whose initial value is zero) is the output of the window position transducer (the upper window), and the amplitude is quite proportional to the displacement of the window from its initial position. Expansions were made at 120.5°C and at 115°C. The oscilloscope traces shown in Fig. 16 were obtained during the 115° run, since the widest range of pressure conditions was attempted at this temperature. The analogous pictures at 120°C were quite similiar, with perhaps slightly more severe boiling effects and a somewhat longer period of 17.0 ms for expansions in which the pressure change was small. The vapor pressure of butane at 115°C is 297 psi. Table 2 lists the conditions appropriate to the pictures shown. Amplitudes of pressure and position should not be compared between pictures, as the oscilloscope gain was usually adjusted to yield a convenient trace amplitude. Table 2 gives the values of maximum and minimum pressures and maximum window positions, from which the calibration of the traces may be inferred. The horizontal scope calibration is 5 ms/cm.

A number of features are evident from this series of pictures. For small pressure swings such as those in Fig. 16a, b, c, it may be seen

Figure 16

Oscilloscope Traces of Expansion Waveforms

during Glycerine-Butane Run

Sweep speed of oscilloscope approximately 5 ms/cm. Higher frequency (20 KC) trace with large initial amplitude is proportional to pressure in support fluid just above the top window of bellows chamber. Lower frequency (1 KC) trace with small initial amplitude is proportional to displacement of upper window from initial position. For details on vertical trace calibration and chamber operating conditions, see Table 2 (and text).

a

b

c

d

e

f

g
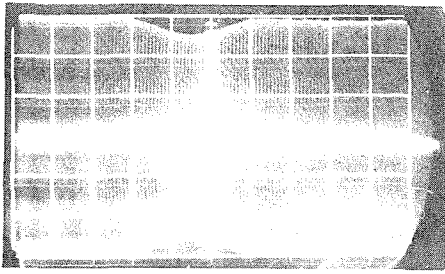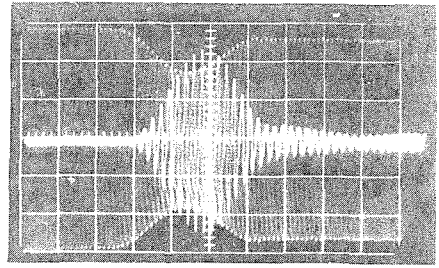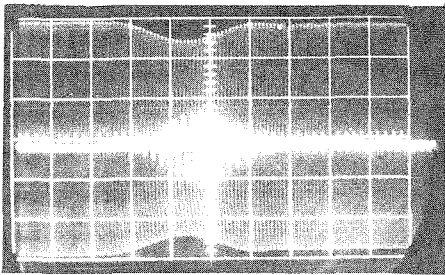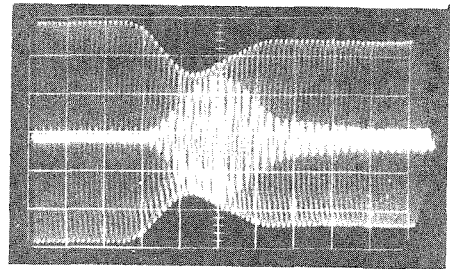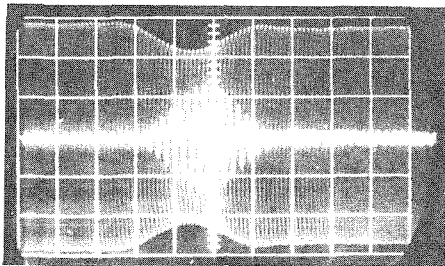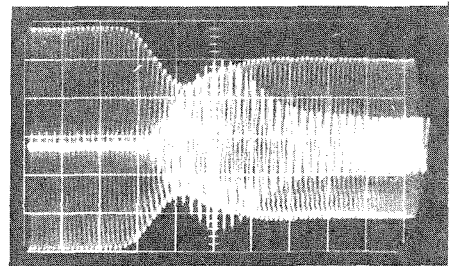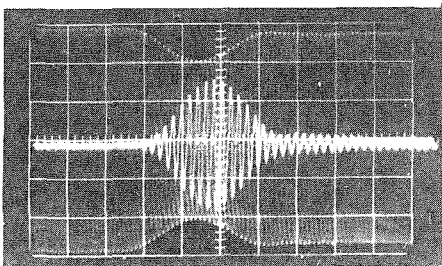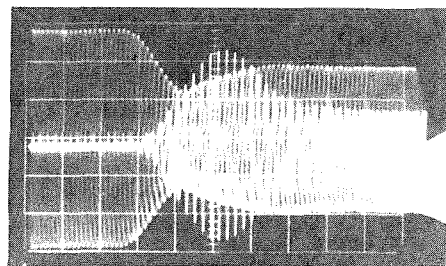
h

Figure 16

TABLE 2

Pict. No.	P_i	P_m	P_f	P_B	X_0	τ	Q	E_D
a	351	302	348	315	0.035	15.5	24.6	2.4
b	358	298	349	312	0.041	16.5	18.2	7.8
c	380	288	368	311	0.061	16.5	11.3	14.7
d	382	270	364	296	0.076	17.0	8.96	25.7
e	423	262	392	295	0.108	18.5	7.45	62.0
f	436	237	369	275	0.155	19.0	3.81	149
g	458	225	334	260	0.201	19.5	2.07	281
h	497	220	338	261	0.225	20.0	1.83	407

Explanation of symbols

Pict. No. refers to photograph in Fig. 16.

P_i = initial pressure of the system in psi.

P_m = minimum pressure obtained during expansion in psi.

P_f = final pressure (at end of cycle) (psi).

P_B = initial pressure in bias cylinders (psi).

X_0 = maximum displacement of upper window (inches).

τ = period of the pressure cycle in milliseconds

Q   defined in text.

E_D = energy dissipation during cycle in joules.

Oscilloscope sweep approximately 5 ms/cm

Butane vapor pressure = 297 psi.

that both pressure and window position are sinusoidal, almost in phase, and return nearly to their initial values at the end of the cycle. As can be seen from Table 2, for these pulses the minimum pressure drops little if any below the vapor pressure of the butane, so one expects little boiling. This may be interpreted as an indication that the viscous and turbulent losses in the system are small, and that the analysis given in Appendix I is valid at least for these cases. However, as the pressure excursion is increased (Fig. 16 d-h) and the minimum pressure falls farther below the vapor pressure, the character of the cycle begins to change. The sinusoidal shape, particularly of the pressure, begins to be altered, and neither the pressure nor the chamber window position returns to its initial value. In addition, there is a very distinct "phase shift" between the two, meaning that the minimum pressure and maximum window position occur at different times. Furthermore, the overall period is longer for the larger pressure excursions than for the smaller ones. All of these things one would expect if the butane were boiling violently. The failure of the pressure to return to its initial value is a consequence of thermodynamic losses in the boiling process. This process is quite nonlinear, so deviation from the harmonic pattern of the pressure and window position should be observed. The phase shift referred to before is also a consequence of the boiling. Once the vapor cavities become sufficiently large in the chamber, they can grow quite rapidly as long as the hydrostatic pressure is somewhat below the vapor pressure of the boiling liquid. Therefore the increase in volume of the contents of the chamber as a result of the formation of vapor drives the windows apart, increasing the pressure in the support tank. This is happening during the period shown in, e.g.,

Fig. 16h, when window position and pressure are increasing together. This process continues until the hydrostatic pressure becomes sufficient to halt further boiling, at which time the window has reached its maximum excursion. This, of course, occurs some time after the minimum of the pressure. The lengthening of the period can be looked upon as a result of the introduction of dissipation (as in an electrical oscillator) and the lowering of the "spring constant" as a result of the vapor cavities in the sensitive liquid. It should be made clear that this type of boiling is distinctly different from the growth of a single bubble in calm liquid as treated in Chapter II-1. The shape of the boiling envelope as shown in Fig. 17 indicates that the boiling occurs in a region of rapid fluid motion close to metal walls, with a result that the vapor cavity is kept supplied to a large extent with heat by conduction from the metal or by the introduction of fresh hot fluid. Thus the rate of evaporation should be much greater than that for a bubble in calm liquid, where the layer of cool fluid around the bubble limits the rate at which it can obtain heat. In fact, the pressure at which the expansion of the bellows chamber ceases is in some way a measure of the effect of the liquid motion. The curves in Chapter II-1 show that a single bubble ceases its growth very soon after the pressure begins to rise from its minimum value, whereas a vapor cavity which was freely supplied with the hot liquid or heat from metal walls would not likely stop growing until the hydrostatic pressure exceeded the vapor pressure of the fluid. An examination of Fig. 16h shows that the window position maximum occurs at about 291 psi, or (within the errors of measurement) essentially at the vapor pressure of 297 psi.

One indication of the severity of the boiling is shown in Table 2

Figure 17

a. Tracks from Ra-Be Source in Butane

This expansion of the 12 inch chamber was made using butane at 120.5°C. The pressure dropped to approximately 235 psi during the expansion. The tracks can be seen in the lower portion of the picture (only half of the chamber was lighted).

b. Illustration of Severe Boiling Around Bellows

Expansion conditions were about the same as in Fig. 16a, but flash was delayed slightly. The boiling can be seen clearly around the edges of the chamber in the lower (lighted) portion of the photograph.

Figure 17a
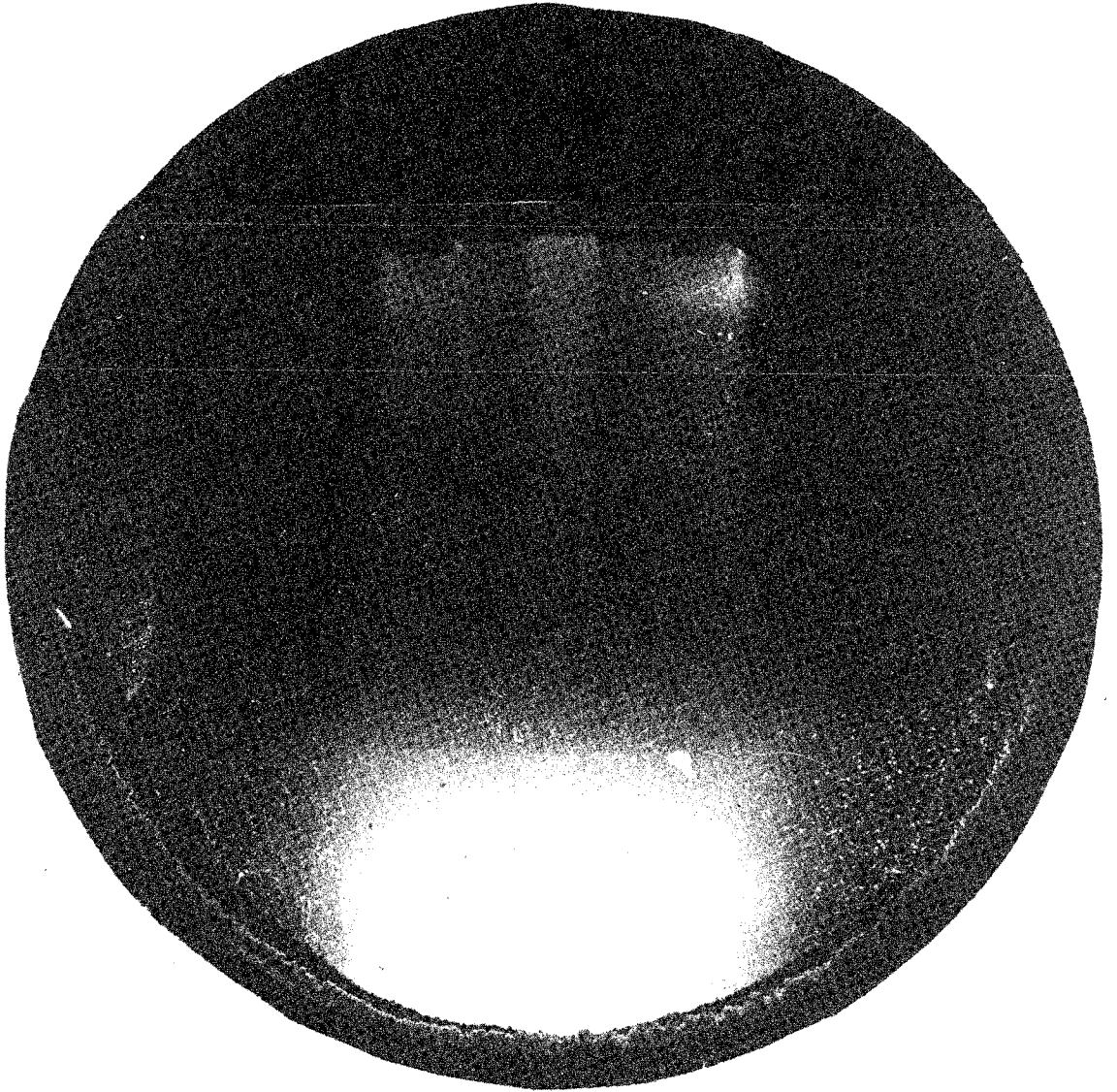
Figure 17b
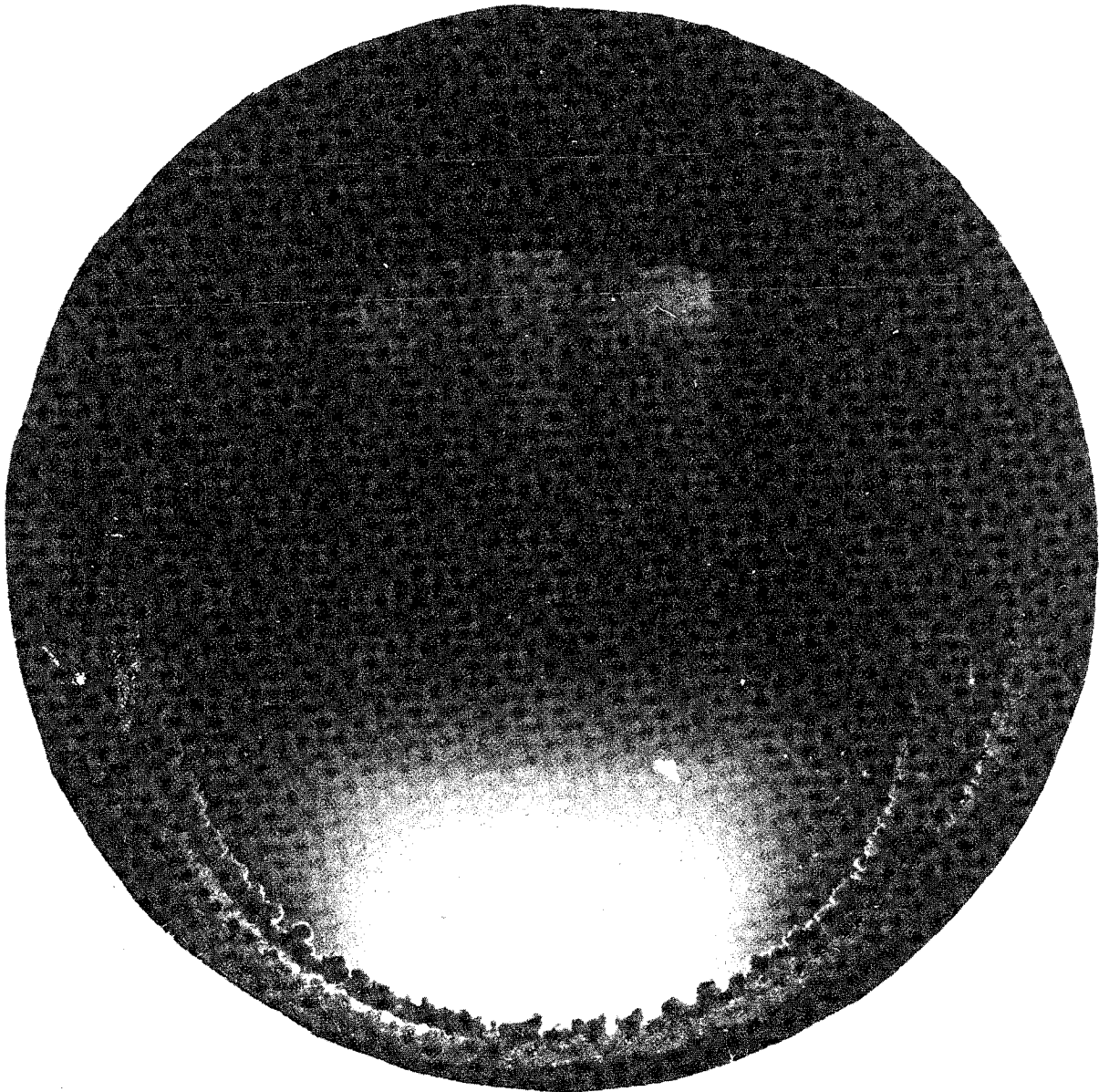
by the value of "Q." Of course, the concept of "Q" as used in electrical or mechanical harmonic oscillators is not quite applicable to our system, since the boiling process is inherently nonlinear. Therefore we have defined Q by

$$Q = \pi/2 \, \log \left[(P_i - P_m)/(P_f - P_m) \right] \qquad (I\text{-}4\text{-}1)$$

where

P_i = starting pressure

P_m = minimum pressure during the cycle

P_f = final pressure (at end of cycle)

This definition coincides with the conventional definition of Q for mechanical or electrical systems for the case of small losses (such as those in Fig. 16a,b) and the parameters are easily extracted from the photographs. For the cases of larger losses, where the comparison with a linear oscillator is no longer very meaningful, we merely consider "Q" as a parameter to indicate the degree of loss. Note the comparatively high Q (~ 20) for the pictures in which little boiling occurs.

Another revealing parameter is the total energy loss per cycle, which may be estimated in the following way. If the compressibility K of the composite system can be considered a small constant, then the energy stored in the chamber E_c can be written as $E_c = \frac{1}{2}KV_oP^2$, where P is the pressure, and V_o is the volume of the chamber. Then the energy removed from the chamber E_c' in a cycle is given by

$$E_c' = \frac{1}{2}KV_o\left[P_i^2 - P_f^2 \right].$$

This does not represent the dissipated energy, however, for we must account for the additional energy stored in the bias cylinders (Chapter I-3) as a consequence of that fact that the pistons do not return to their original

positions. Since the change in pressure of the bias cylinders is small during a cycle, this latter energy E_B is given approximately by $E_B = P_{BA} \Delta V$, where P_{BA} is average pressure in the bias cylinders and ΔV is the change in volume of the chamber contents between initial and final conditions. But for a linear system, by the definition of compressibility,

$$\Delta V = K V_o \Delta P = K V_o (P_i - P_f)$$

thus

$$E_B = K V_o P_{BA}(P_i - P_f)$$

and the dissipated energy E_D is given by

$$E_D = E_c' - E_B = K V_o \tfrac{1}{2} \sqrt{P_i^2 - P_f^2 \, \rfloor} - P_{BA} \sqrt{P_i - P_f \, \rfloor} \qquad \text{(I-4-2)}$$

Of course the above is not exact, since the chamber doubtlessly contained vapor bubbles at the end of the cycles in which bad boiling occurred, and the constant compressibility assumed above is incorrect. However, equation I-4-2 is sufficiently accurate for purposes of comparison, and the results of 37 expansions are illustrated in Fig. 18, where E_D is plotted against minimum pressure P_m. The two parameters under our control during the run were the initial pressure P_i and the initial bias cylinder pressure P_B. The solid curves in Fig. 18 are lines of constant bias pressure, whereas the dotted curves are lines of constant initial pressure.* To be noted especially is the very sharp increase in energy loss as the minimum pressure is lowered. It is evident that the extent of boiling increases very rapidly with decreasing expanded pressure.

Tracks from a Ra-Be source were observed in the chamber at a temperature of $120.5^{\circ}C$ and typical expanded pressures of around 230 psi.

---

* The calculations of the values of E_D and Q were made by E. D. Alyea, Jr., and J. T. Chang, to whom the writer is indebted.

Figure 18

Energy Loss per Cycle, Second Run (Glycerine-Butane)

P_m is minimum pressure (psi) attained in expansion cycle.

E_D (derived in text) is energy loss per cycle (joules).

P_1 is initial or starting pressure (psi).

P_B is pressure in bias cylinders at start of expansion.

Solid curves are lines of constant P_B, while P_1 is varied.

Dotted curves are lines of constant P_1, while P_B is varied.
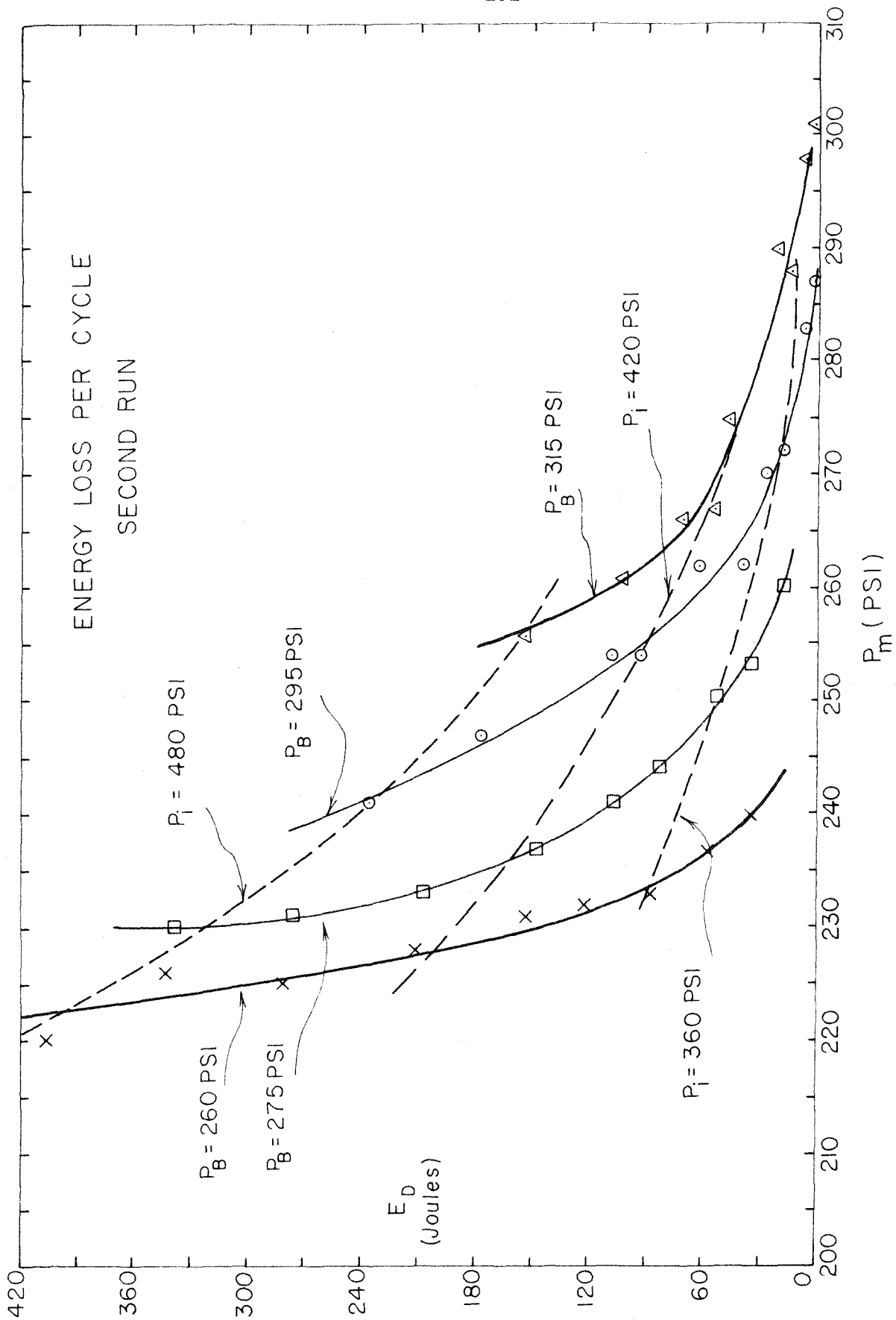
Figure 18

At this temperature the vapor pressure of butane is 326 psi. Some of these tracks may be seen in Fig. 17a. Violent boiling in the chamber is also evident in this picture as well as in Fig. 17b, and stereoscopic observation shows that the boiling originates in the bellows and not from the window gaskets. The annular "plume" extends into the chamber a distance of about 2 inches in some places, which illustrates the magnitude of the boiling. The pictures shown are of poor optical quality, and the cause of this was the cloudiness of the glycerine as well as the fact that the reflective inconel coating on the mirrors was almost gone. In addition, only one flash tube was operative in most of the pictures. A great deal of dirt may also be seen on the lower windows. This was found to consist mainly of fine abrasive which had come out of the bellows leaves, as explained below.

The boiling noted previously is of such a magnitude as to preclude operation of the chamber as the kind of precision instrument we had planned. Even though eventual recompression of the chamber after each pulse might be effected, it is doubtful that we could prevent the large vapor cavities from rising to the top of the chamber. This would result in a large heat input ($\sim$ 500 joules per pulse) at the top of the chamber, with the result that there would be several degrees temperature difference between top and bottom of the chamber during extended operating periods.

There are several things which may have caused such explosive rings of bubbles. When the chamber was constructed, we were concerned about getting the deep convolutions of the bellows free of an oxide coating acquired during a heat treatment. Chemical cleaning was tried without a great deal of success, so we had the bellows liquid honed. Apparently some abrasive from the liquid honing process wedged itself securely in the narrow cracks at the bottom of the bellows convolutions,

and resisted several determined efforts on our part to remove it. In addition, two glass windows on the bellows chamber were broken while the vessel was under vacuum, so that a large quantity of finely powdered glass apparently joined the liquid honing abrasive in the deep crevices of the bellows. When the apparatus was disassembled after the run, a large quantity of glass and abrasive was found lying on the bottom window of the bellows chamber which had obviously come from the bellows. Such fine particles of glass and aluminum oxide could very likely serve as nucleii for boiling, and as such might certainly have contributed to the violent plumes which we observed. However, that these particles could not have been the sole cause of the trouble is evident from the fact that the particles lying upon the window caused only slight boiling. The violence of the boiling must have been connected with environmental conditions. For one thing, since the bellows does not extend the full length of the chamber, liquid must rush into the leaves as they open. It is possible that the fluid flow is rapid enough around and in the bellows to promote cavitation in a metastable liquid such as one has in a bubble chamber. Either the foregoing or the abrasive particles mentioned previously could create bubble nucleii. In any case, bubbles created adjacent to the heated metal surface of the bellows would be expected to grow much faster than those near the center of the chamber, and it is certain that the rapid fluid flow would supply the newly formed bubbles with more heat as well. The situation is complicated enough to prohibit a very quantitative treatment, but certainly the above items should help explain in a qualitative fashion the boiling which we observed.

C. Test of the Sleeve Technique

It was not considered entirely impossible to find a more vigor-
ous chemical treatment to remove the dirt from the bellows. However, in
view of the fact that dynamical factors may have been the cause of our
boiling, we decided to eliminate this source of trouble in another way.
One possible method would be to discard the metal bellows chamber completely
and replace it with a flexible plastic (e.g., Teflon) container. Other
more radical changes could also be envisioned. However, because of the
difficult mechanical changes involved in an extensive modification of our
system, we were led to try the simpler flexible sleeve technique described
in Chapter I-3. Because of the relative ease of construction, we decided
first to try a simple Hycar rubber sleeve inside the bellows and to use
propane as a sensitive fluid so as to stay within the temperature capabili-
ties of Hycar. To avoid the troubles that had plagued us with glycerine,
we selected a clear light paraffin oil* as the support liquid, both between
the bellows and sleeve and in the main support tank. We also had constructed
and installed the prestressing bolts described in Chapter I-3 to reduce
the chamber stretching. These seemed to perform quite well, although there
remained a contribution to the anomalous compressibility which is not
satisfactorily explained. Quantitatively, the effect may be seen by a
comparison of the lengthening of the support tank under pressure with and
without the prestressing bolts. We measured the motion of the thick win-
dow (Fig. 8) as a function of pressure in the support tank, yielding the
lengthening of that portion of the tank below its point of suspension (the
expansion cylinders). Without the prestressing bolts, the window moved

* Whiterex Light - General Petroleum Co.

0.007 inches/100 psi, while with the bolts it moved only 0.001 inches/100

psi. Measurements on the total compressibility of the support tank plus

the support fluid (at room temperatures) yielded 11.2 cm^3/atm, of which

possibly as much as 5 cm^3 was due to the support oil. The resultant

6 cm^3/atm is substantially lower than the 13 which existed without the

prestressing bolts, but does not indicate as great a reduction as is im-

plied by the window motion. Part of the remaining anomalous compressibility

probably arises from the bowing of the lid of the support tank, but meas-

urements on this structure under pressure indicate that not nearly all of

the remaining anomalous compressibility can be so accounted for. The

smaller overall compressibility is evident in the shorter period (14 ms)

of the expansion cycle shown in Fig. 19 over those obtained in the second

run. However, part of the reason for the faster cycle is the slightly

smaller (1.2 x 10^{-3}) compressibility of propane at 60°C over that of bu-

tane and the fact that the actual volume of propane was smaller because of

the rubber sleeve.

Unfortunately, only a few expansions were made in the third run,

because the plastic tube used to connect the sleeve to the filling line

hardened under the action of the hot propane and slipped off, thereby

mixing the oil and the propane.* However, before this happened some very

interesting results were obtained. It was found that even at the operat-

ing temperature of 60°C, when the hydrostatic pressure of the propane was

---

* In a recent discussion with Professor Lord of the University of
Washington, we have learned that his group has experienced considerable
difficulty with violent boiling from the filler tube of their rapid cycling
(15 per sec.) 300 cc propane chamber. In fact, the shock wave generated
in the tube from the violent cavitation was powerful enough to straighten
out a bend in the copper tube. A similar shock wave doubtlessly played a
role in the disconnection of our filler line.

Figure 19

Oscilloscope Traces of Expansion Waveforms during Third Run

(Test of Sleeve Technique)

Sweep speed of oscilloscope approximately 5 ms/cm. Higher frequency (20 KC) trace with large initial amplitude is proportional to pressure in support fluid just above the top window of bellows chamber. Lower frequency (1 KC) trace with small initial amplitude is proportional to displacement of upper window from initial position. For details on vertical trace calibration and chamber operating conditions, see Table 3 (and text).

Figure 19
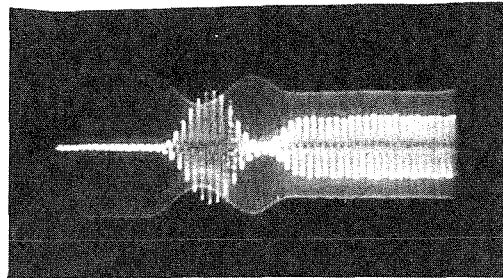
a
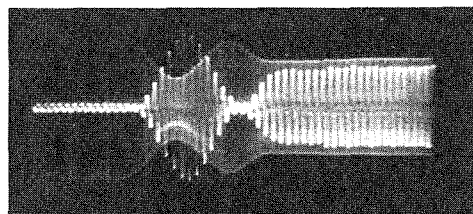
b
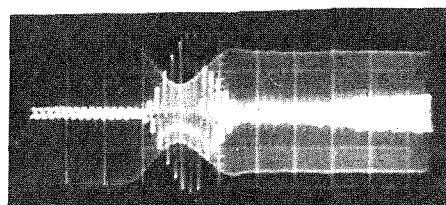
c

lowered slowly, it could be dropped as much as about 45 psi below the vapor pressure for several seconds before the propane erupted. This is an indication that, statically, the chamber was extremely "clean," and that the propane wetted all surfaces in the chamber. Apparently, Hycar rubber is very easily wetted by propane, which is perhaps not surprising considering their similar organic nature.

The oscilloscope pictures shown in Fig. 19 can be compared to the analogous ones for the second run. There is a very marked improvement in the harmonic character of the pressure and window position waveforms. The pictures in Fig. 19 go through more than one cycle because the expansion engine valves were not properly timed and stayed open too long, thereby allowing the chamber to begin a second expansion. The proper adjustments were being made when the leak described above developed. The quantities represented by the traces are as described before, and the relevant expansion conditions are listed in Table 3. Note in particular the value of Q and the minimum pressure. Even for the very large pressure swing represented in Fig. 19c, the Q is still 6.7, while the minimum pressure (143 psi) is 77 psi lower than was ever attained in the 115° butane run discussed before. In addition, the vapor pressure of the propane (305 psi) was even higher than that of the butane (297 psi). The improvement is quite striking, and is illustrated as well by Fig. 20, in which is plotted the energy dissipation E_D against minimum pressure in the manner of Fig. 18. The much smaller energy loss for equivalent minimum pressure is obvious. It would appear that the chamber is quite workable in the configuration used in the third run, as the final pressures noted in Table 3 are all well above the vapor pressure, so that recompression is assured.

TABLE 3

Pict. No.	P_i	P_m	P_f	P_B	τ	Q	E_D
a	444	228	423	309	14.0	15.3	31.1
b	445	160	402	265	14.0	9.6	80.1
c	448	143	384	250	14.5	6.7	124.4

For explanation of symbols see Table 2.

Oscilloscope sweep 5 ms/cm.

Vapor pressure of propane = 305 psi.

Pict. No. refers to Fig. 19.

Figure 20

Energy Loss per Cycle, Third Run

(Test of Sleeve Technique)

P_m is minimum pressure attained during expansion.

P_i is initial (starting) pressure in chamber.

P_B is pressure in bias cylinders.

E_D is energy loss in joules per expansion.

Curve shown is line of constant P_i = 445 psi, while P_B was varied
from 309 psi to 250 psi.
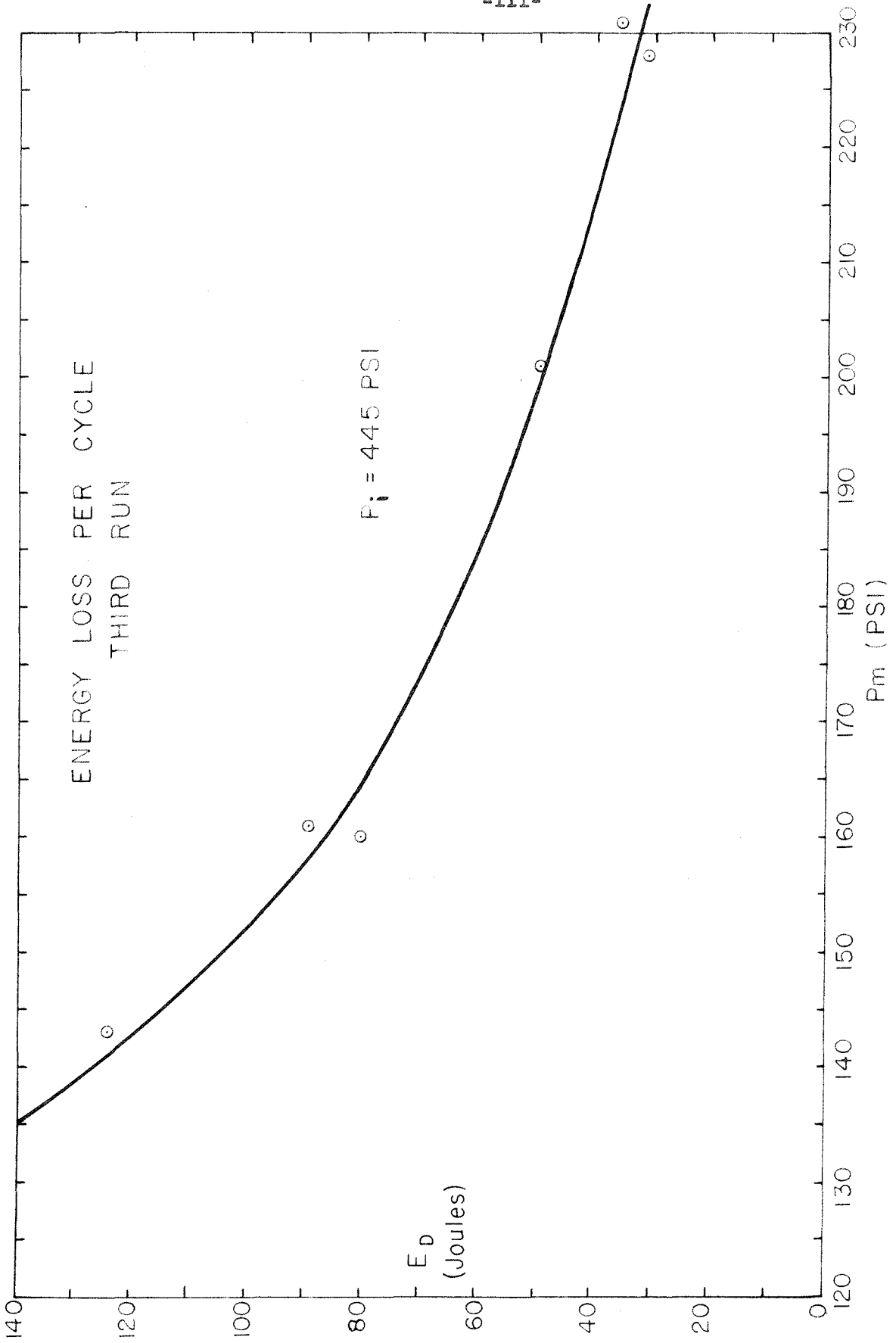
Figure 20

The pictures in Fig. 21 were taken during the expansions discussed previously. The optical quality is greatly improved over those from the second run owing to the clear oil and the new aluminum coating on the mirrors. Note that some boiling still exists, but is not from the region of the window. The boiling here comes only from the filling tube, and there appear to be only a few scattered small bubbles in the remainder of the chamber. The fact that the chamber was statically "clean," as mentioned earlier, is strong evidence that the filling tube boiling arose from dynamical effects, such as the rapid inflow of fluid when the chamber pressure dropped. A filling system which is to be installed for the next run should avoid this problem. The new filling valve is a smooth plate which seals the filling port from inside the chamber, thereby eliminating the filling hole in the side of the chamber and leaving a comparatively smooth wall everywhere. This valve is seen in Fig. 9. Some specular reflections from the flash tubes can be seen around the edges of the chamber which are caused by the rubber sleeve. The surface of the rubber used was quite smooth and shiny. Careful inspection of these pictures, particularly of Fig. 21a, reveals several short electron tracks, showing that the chamber was radiation sensitive as well. No source was employed when the pictures were taken, so the tracks noted presumably were from local and cosmic ray background.

D. Conclusions

The results of the runs with the chamber have demonstrated a number of things about bubble chamber design which are worth summarizing. The third run has shown clearly that the "resonant" expansion system is quite workable, and would appear to be a very satisfactory expansion

Figure 21

a. Expansion of Propane at 60°C.

The rubber sleeve can be seen as an uneven, smoothly bulging

surface around the perimeter of the chamber, from which the specular

reflections arise. Stereoscopic observation of this picture reveals

several short electron tracks. Note boiling from filler tube in

lower right corner of picture.

b. Second View of Filler Tube Boiling.

Plume from filler tube can be seen in upper left corner.

Note in both pictures that, although bubbles exist on rubber

sleeve, they are quite small in size, comparable to track bubbles.

Figure 21a
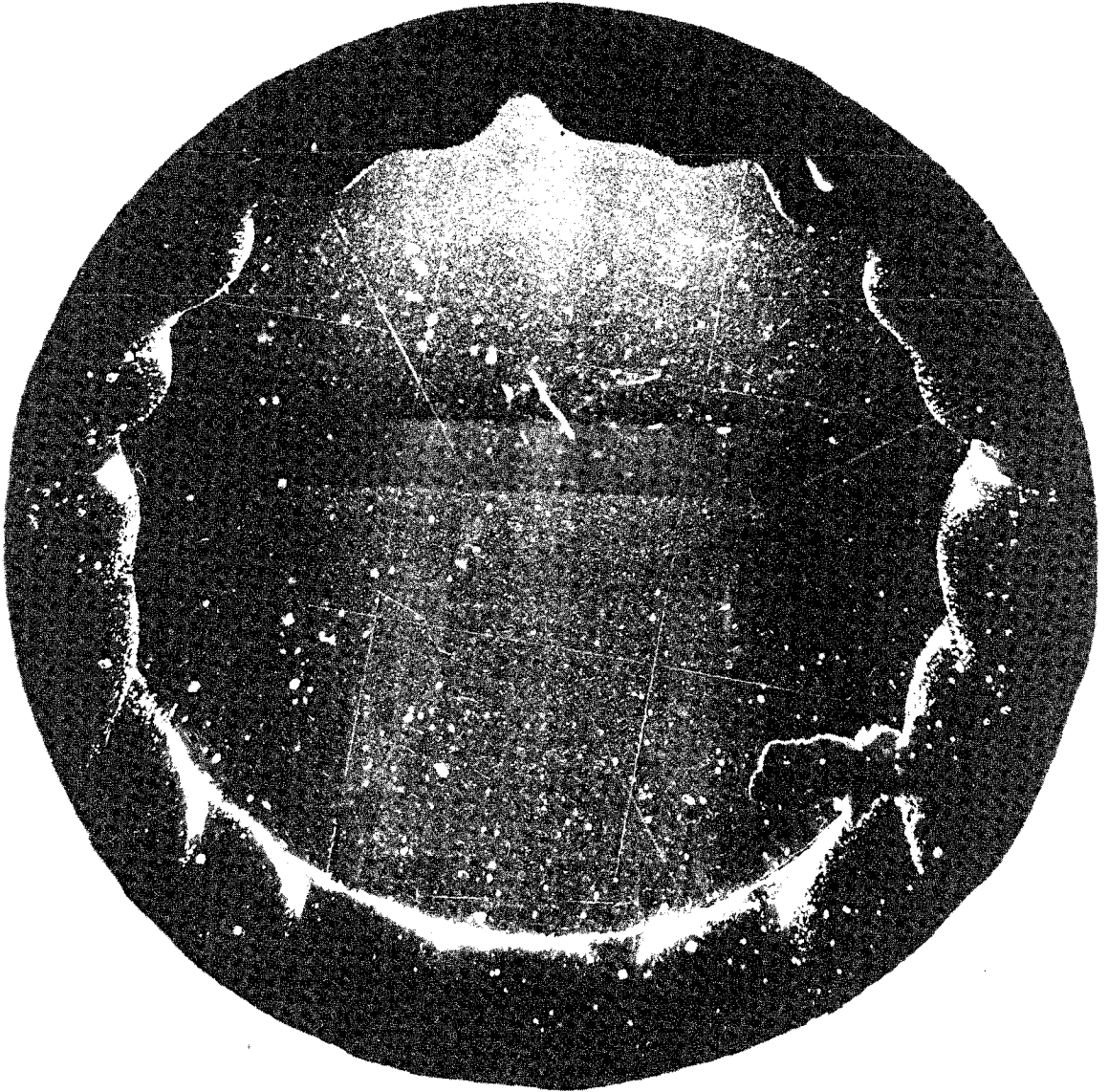
Figure 21b
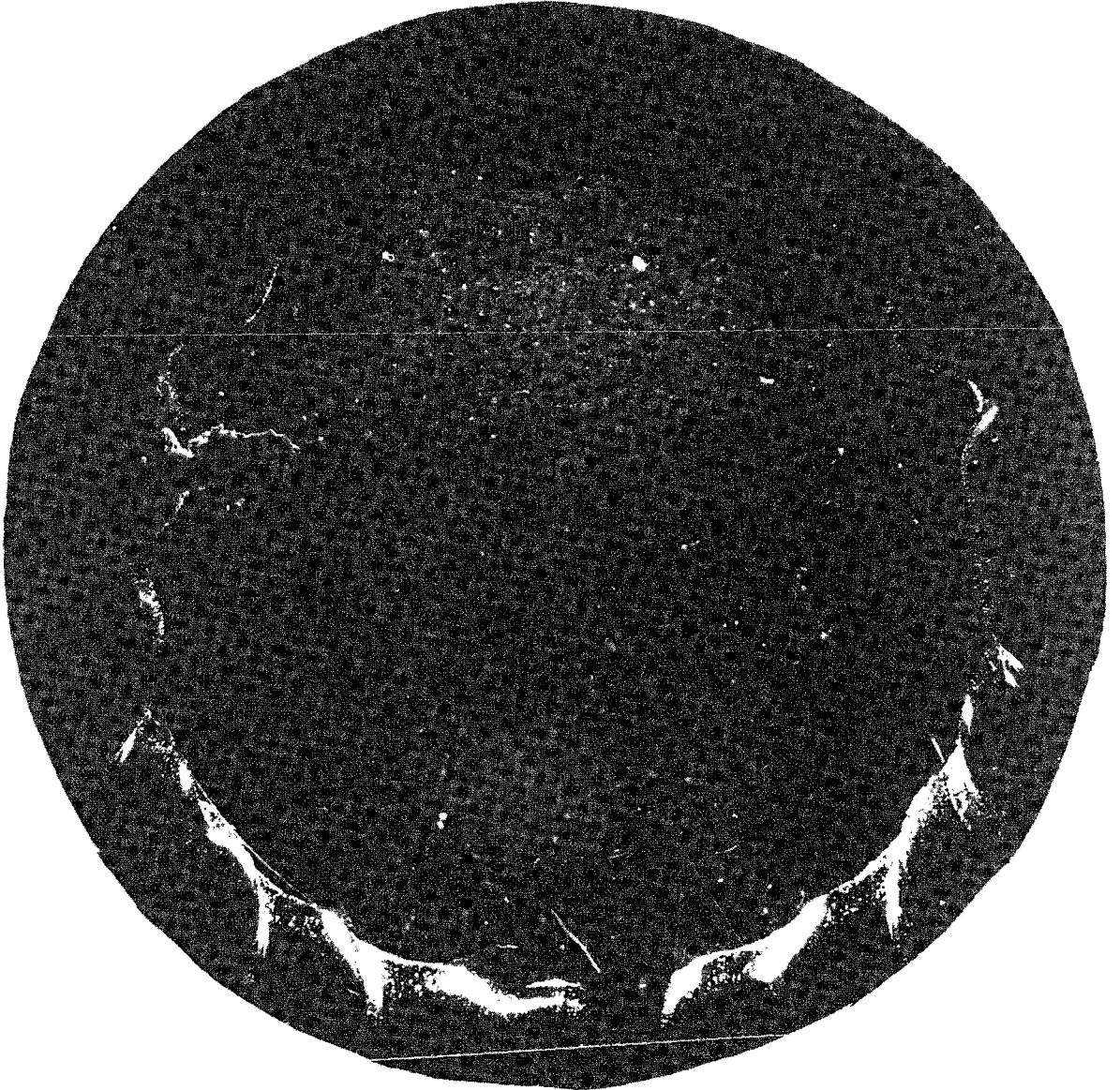
technique in spite of the additional mechanical complexity required to make it feasible. It is certainly faster than any other system on a chamber of comparable size known to the writer at present. For smaller, rapid-cycling bubble chambers employing lighter liquids (Chapter II-2), it may also offer a system whereby large repetition rates can be accomplished without the need for the huge external energy inputs required with purely dissipative systems.

Another important point has to do with chamber cleanliness. The experiment with the rubber sleeve has indicated a simple technique for making large bubble chambers which are "clean" without having to resort to the difficult all-glass construction used in previous "clean" chambers. The freedom from bad boiling around the walls of a chamber has obvious attraction from the point of view of maintaining uniform conditions as discussed in Chapter I-3. This cleanliness would seem to be vital for larger rapid cycling bubble chambers, since the heat input to a "dirty" chamber from the irreversible thermodynamic processes would probably be more than could be carried away by conduction through the sensitive medium. A similar observation has been made by Professor Lord's group (1) at the University of Washington, and they have had to reduce the volume of their 15 cycle per second chamber to 300 cc in order to be able to extract the heat from it during continuous operation. Their chamber is apparently quite "dirty." The sleeve technique would appear to improve chamber "cleanliness" in at least two ways. One is that the proper sleeve material is wetted by the sensitive liquid, reducing the probability of formation of bubbles on the walls. In addition, even if bubbles are formed the poor thermal conductivity of the non-metallic sleeve and its surrounding

support fluid limits the rate of input of heat to a bubble in much the same manner as does the layer of cool fluid surrounding bubbles formed near the center of the chamber. Therefore bubbles on the wall of the chamber grow very little more than those along particle tracks, and can be ignored in the practical case as a source of severe boiling.

With the insert and inside sealing valve mentioned previously, our 12 inch chamber should be fast and clean enough to yield us about the precision which we set out to achieve, and in this respect our project appears to be successful. Because of the required surface and chemical properties, however, it is certain that a Teflon sleeve must be used with WF_6. The permeability of the insert to WF_6 and its lifetime under the flexing caused by chamber expansion and recompression must be tested before we can be sure of its practicability.

PART II

PHYSICS OF BUBBLE CHAMBERS AND

APPLICATIONS TO ADVANCED DESIGNS

CHAPTER II-1

BUBBLE NUCLEATION AND GROWTH IN BUBBLE CHAMBERS

A. General

      The purpose of this chapter is to examine in some detail the phenomena of nucleation and of growth of bubbles in a bubble chamber. We will first discuss that portion of the process which occurs after the bubbles have attained the "critical" radius (defined below) in which they grow to visible size and then begin to collapse as the chamber is recompressed. From this discussion we will obtain valuable information relating to the operating cycle of bubble chambers such as the one described in Chapter I-3 as well as the more advanced chamber types discussed in Chapter II-2. We will then attempt to further our understanding of the process of generation of the microscopic bubble nucleii and their growth to critical radius. The underlying mechanism has been the object of speculation by several investigators (45 - 50), and we will utilize their work as well as a few considerations of our own. It is to be hoped that aside from purely academic interest in the phenomena themselves, the study of the formation and growth of bubbles will aid one in designing better bubble chambers.

      The bubble of critical radius is selected as the point of separation of the two processes described above, because this is the radius for which the internal (vapor) pressure just balances the collapsing force of the surface tension. More quantitatively, the critical radius is that for which

$$\pi R_c^2 \Delta P = 2\pi R_c \sigma$$
$$R_c = (2\sigma/\Delta P)$$

(II-1-1)

where R_c = critical radius

$\sigma =$ surface tension of fluid

$\Delta P = P_V - P_H$

$P_V =$ equilibrium vapor pressure of the fluid

$P_H =$ hydrostatic pressure in fluid

Any bubble larger than R_c should grow spontaneously to macroscopic size, while those smaller are expected to collapse in the absence of other effects.

B. Growth of Bubble to Macroscopic Size

1. Equations of Motion

The process of growth and collapse of vapor bubbles under certain conditions has been investigated by Zwick and Plesset (51,52) and more recently by Birkhoff, et al. (53). However, since their treatment was concerned with vapor bubbles under conditions of temperature and pressure quite different from those attained in bubble chambers, it is pertinent to redo the analysis in order to ascertain which approximations may be used.

The solution found by Zwick and Plesset for the growth of a vapor bubble is divided into three phases. The first and second concern the growth when the radius is still comparable to the critical radius. They consist of a "delay" period followed by a short interval of almost exponential growth. These need not concern us here, since in a bubble chamber, owing to the mechanism of formation (discussed later), there is quite likely to be an excess of heat in the vicinity of the bubble when it is formed, making these first two phases quite short. When the bubble has reached a radius large compared to the critical radius (still microscopic in a bubble chamber) the growth goes over into an "asymptotic" form with which we will

be concerned. The rate of growth of the bubble under these conditions is determined solely by the rate at which it can obtain heat. We will make the same assumptions as did Zwick and Plesset in their analysis, and then check to see if they are justified.

The first assumption is that the rate of heat transfer to the bubble is limited by the thermal conductivity of the surrounding fluid, and that most of the temperature drop in the fluid takes place in a layer surrounding the bubble whose thickness is small compared to its radius. It is further assumed that the vapor in the bubble is in thermal equilibrium with the liquid at the wall of the bubble. Under these assumptions we may derive the equations of motion for the growth and collapse of the bubble. The following development is different from that used by Zwick and Plesset, since we wish to include the possibility of large changes in the external pressures as well as large variations in the latent heat and density of vapor in the bubble. (As is shown later, these things occur in a typical bubble chamber cycle.)

If we imagine a surface surrounding the bubble an infinitesimal distance outside the vapor-liquid interface, we may write a differential energy equality:

$$-PdV - Hdt = d\mathcal{E} \qquad\qquad \text{(II-1-2)}$$

where

P = pressure in bubble

V = volume inside the surface

$\mathcal{E}$ = internal energy of bubble

H = rate of heat flow out of the bubble.

However,

$$\mathcal{E} = uV_v \rho_v + cV_\ell \rho_\ell \qquad (\text{II-1-3})$$

u = internal energy of the vapor per unit mass

$V_{v,\ell}$ = volume of the vapor and liquid, respectively

ρ_v = density of vapor

c = internal energy of the fluid per unit mass

ρ_ℓ = density of liquid

and

$$d\mathcal{E} = u\rho_v dV_v + V_v \rho_v du + uV_v d\rho_v + \rho_\ell cdV_\ell + V_\ell d(c\rho_\ell) \quad (\text{II-1-4})$$

There is, however, a constraint imposed by the conservation of mass inside the imaginary wall, so we may say

$$\rho_v V_v + \rho_\ell V_\ell = \text{constant, and}$$

$$\rho_v dV_v + V_v d\rho_v + \rho_\ell dV_\ell + V_\ell d\rho_\ell = 0.$$

This, in turn, leads to

$$dV_\ell = -\rho_v dV_v / \rho_\ell - V_v d\rho_v / \rho_\ell - V_\ell d\rho_\ell / \rho_\ell \qquad (\text{II-1-5})$$

and

$$dV = dV_\ell + dV_v = [1 - (\rho_v / \rho_\ell)] dV_v - V_v d\rho_v / \rho_\ell - V_\ell d\rho_\ell / \rho_\ell \quad (\text{II-1-6})$$

If we now equate the left side of equation II-1-2 with the right side of equation II-1-4 and substitute equations II-1-5 and II-1-6 for dV_ℓ and dV respectively, we have the required relation. If we also allow $V_\ell \rightarrow 0$, then the imaginary wall coincides with the real vapor wall. Dividing by dt, then, we obtain

$$\dot{V} = -V\dot{P} \frac{[u - c - (P/\rho_\ell)] (d\rho_v/dP) + \rho_v du/dP}{P[1 - (\rho_v/\rho_\ell)] + (u - c)\rho_v}$$

$$(\text{II-1-7})$$

$$- \frac{H}{P[1 - (\rho_v/\rho_\ell)] + (u - c)\rho_v}$$

The dot signifies differentiation with respect to time. In the above, we

have also used $\dot{\rho}_v = (d\rho_v/dP)\,\dot{P}$ and $\dot{u} = (du/dP)\,\dot{P}$. This is permissible, since the assumption of equilibrium between vapor and liquid allows only one thermodynamic degree of freedom, and both ρ_v and u are here considered functions of pressure only.

To simplify equation II-1-7, we may find the relationship between c and u in the following manner. Now we consider the same situation as above, except that H will be controlled in a way such as to keep the temperature and thus also the pressure of the bubble constant. Under such circumstances, the first term on the right vanishes, and we are left with, in time dt,

$$dV = -dQ/ \left\{ P\underline{/}1 - (\rho_v/\rho_\ell)\underline{\big]} \not = (u - c)\rho_v \right\}$$

where -dQ is now the heat added. However, by definition the latent heat of vaporization L is the heat required to vaporize unit mass of the fluid. Therefore $L = (dQ/\rho_v dV)$, which leads to

$$L\rho_v = P\underline{/}1 - (\rho_v/\rho_\ell)\underline{\big]} \not = (u - c)\rho_v \qquad (II-1-8)$$

If we now solve for u and differentiate with respect to pressure, we find

$$du/dP = dL/dP \not = (P/\rho_v^2)(d\rho_v/dP) - (1/\rho_v) \not = (1/\rho_\ell) \not =$$
$$dc/dP - (P/\rho_\ell^2)(d\rho_\ell/dP) \qquad (II-1-9)$$

By now using equation II-1-8, we find that the numerator of the first term on the right of equation II-1-7 becomes $\underline{/}L - (P/\rho_v)\underline{\big]}(d\rho_v/dP) \not = \rho_v(du/dP)$. By use of equation II-1-9, we may express the above as

$$Ld\rho_v/dP \not = \rho_v dL/dP - 1 \not = \rho_v/\rho_\ell \not = \rho_v dc/dP - (\rho_v P/\rho_\ell^2)(d\rho_\ell/dP)$$
$$= (d/dP)(L\rho_v) - 1 \not = (\rho_v/\rho_\ell)\left\{ 1 \not = \rho_\ell dc/dP - (P/\rho_\ell)(d\rho_\ell/dP) \right\}$$

If we employ the above plus expression II-1-8 substituted into the denominator of the terms in equation II-1-7, we find the expression for $\dot{V}$ is given by

$$\dot{V} = -\dot{VP}\left\{\varphi' - 1 + b(1 + \rho_\ell c' - P\rho_\ell'/\rho_\ell)\right\}/\varphi - H/\varphi \qquad \text{(II-1-10)}$$

where $\varphi = \varphi(P) = L\rho_v$, $b = \rho_v/\rho_\ell$, and the prime denotes differentiation with respect to pressure.

We must now relate the pressure in the bubble to the hydrostatic pressure in the fluid, the surface tension, and the effect of the inertia of the surrounding liquid. The differential pressure ΔP_I required to expand a spherical bubble of radius R against an incompressible fluid of density ρ_ℓ is given by (54)

$$\Delta P_I/\rho_\ell = R\ddot{R} + (3/2)\dot{R}^2 \qquad \text{(II-1-11)}$$

where the dot again signifies differentiation with respect to time. Since the pressure exerted by the surface tension is $P_T = (2\sigma/R)$, we may write

$$P - P_H = \rho_\ell R\ddot{R} + (3\rho_\ell/2)\dot{R}^2 + (2\sigma/R) \qquad \text{(II-1-12)}$$

where P_H is the hydrostatic pressure of the external fluid. As will be shown later, over the region of interest the terms on the right are quite negligible, and P may then be set equal to P_H.

The quantity H in equation II-1-10 is more difficult to assess, since it involves heat flow across an expanding (or collapsing) spherical wall. However, Zwick and Plesset (55) have found an approximate solution to this problem under the assumption (to be checked later) that the temperature drop takes place over a thin layer surrounding the bubble. This solution is

$$T - T_\infty = -[D/\pi]^{\frac{1}{2}} \int_0^t \left\{ \frac{R^2(x)[\partial T/\partial r]_{r = R(x)}}{\left[\int_x^t R^4(y)\,dy\right]^{\frac{1}{2}}} \right\} dx \qquad \text{(II-1-13)}$$

where

D = thermal diffusivity = $K/\rho_\ell c_\ell$

$K \equiv$ thermal conductivity of liquid

c_{ℓ} = specific heat of liquid

T = temperature at wall of bubble

T_{∞} = temperature at long distance from bubble.

The term in the numerator of the integrand above is related to the heat

flow out of the bubble since

$$R^2 \left[\partial T/\partial r\right]_{r \,=\, R} = H/4\pi K \qquad\qquad (II-1-14)$$

Expression II-1-13 can be inverted by multiplying both sides through by

$R^4(t)dt/\left[\int_t^{t'} R^4(z)dz\right]^{\frac{1}{2}}$ and integrating from o to t'. This leads to

$$\int_0^{t'} \frac{\tau(t)R^4(t)dt}{\left[\int_t^{t'}R^4(z)dz\right]^{\frac{1}{2}}} = \left[\frac{D}{\pi}\right]^{\frac{1}{2}} \int_0^{t'} \frac{R^4(t)}{\left[\int_0^{t'}R^4(z)dz\right]^{\frac{1}{2}}} \int_0^t \frac{F(x)R^2(x)dx\ dt}{\left[\int_x^t R^4(y)dy\right]^{\frac{1}{2}}}$$

where $\tau(t) = T_{\infty} - T(t)$ and $F(x) = \left[\partial T/\partial r\right]_{r \,=\, R}$ and D is considered a

constant. An interchange of the order of integration transforms the ex-

pression on the right to

$$\left[\frac{D}{\pi}\right]^{\frac{1}{2}} \int_0^{t'} F(x)R^2(x)\left\{ \int_x^{t'} \frac{R^4(t)\ dt}{\left[\int_t^{t'}R^4(z)dz\right]^{\frac{1}{2}}\left[\int_x^t R^4(y)dy\right]^{\frac{1}{2}}} \right\} dx$$

$$= \left[\frac{D}{\pi}\right]^{\frac{1}{2}} \int_0^{t'} FR^2 \left\{ \int_0^1 \frac{d\xi}{\left[1 - \xi\right]^{\frac{1}{2}}\xi^{\frac{1}{2}}} \right\} dx = -\pi \left[\frac{D}{\pi}\right]^{\frac{1}{2}} \int_0^{t'} FR^2\ dx$$

wherein we have employed the change of variables

$$\xi(t) = \frac{\int_x^t R^4(w)dw}{\int_x^{t'} R^4(w)dw}$$

Thus we have

$$\int_{o}^{t'} \frac{T(t)R^4(t)dt}{\left[\int_{t}^{t'} R^4(z)dz\right]^{\frac{1}{2}}} = \sqrt{\pi D} \int_{o}^{t'} FR^2 \, dx$$

Differentiation with respect to t' yields the result given below, in which we have changed the symbols used for the variables and employed relation II-1-14.

$$H(t) = -4K[\pi/D]^{\frac{1}{2}} [d/dt] \int_{o}^{t} \frac{R^4(x)T(x)dx}{\left\{ \int_{x}^{t} R^4(y)dy \right\}^{\frac{1}{2}}} \qquad (II-1-15)$$

It is convenient to expand the integral on the right. If we integrate by parts and take the time derivative explicitly, we have the following, where we have combined equations II-1-15 and II-1-10 and solved for $\dot{R}$,

$$\dot{R} = -R\dot{P} \left[\varphi' - 1 + b(1 + \rho c' - P \rho'/\rho)\right] / 3\varphi \qquad (II-1-16)$$
$$+ \left[R^2K/\varphi \sqrt{\pi D}\right] \left\{ T_o/S^{\frac{1}{2}} + \int_{o}^{t} \dot{T}(x)dx/\sqrt{S(t) - S(x)} \right\}$$

where $T_o = T(o)$; $\dot{T} = dT/dt$; $S(t) = \int_{o}^{t} R^4(y)dy$; and we have substituted

$V = 4\pi R^3/3$; $\dot{V} = 4\pi R^2 \dot{R}$.

The foregoing is the equation which must be solved. For the case which Zwick and Plesset considered, the hydrostatic pressure was held constant. If we can consider the terms on the right of equation II-1-12 negligible, then $\dot{P} = 0$. In this case the temperature at the wall is constant and has the value appropriate to an equilibrium vapor pressure equal to the external hydrostatic pressure. (This assumes, of course, that the

hydrostatic pressure is lower than the vapor pressure of the fluid far from the bubble, i.e., the liquid is metastable.) Also then φ is constant and $\dot{\tau} = 0$. Then equation II-1-16 reduces to

$$R = [R^2 K/\varphi\sqrt{\pi D}] [\tau_0/s^{\frac{1}{2}}] \qquad (II-1-17)$$

It can be shown by substitution that a solution which satisfies the above equation and the initial condition $R = 0$ at $t = 0$ is $R = At^{\frac{1}{2}}$, yielding $\dot{R} = \frac{1}{2}At^{-\frac{1}{2}}$ and $S = A^4 t^3/3$. By substitution, it is found that $A = (2K\tau_0/\varphi)\sqrt{3/\pi D}$. Therefore we have

$$R = [2K(T_\infty - T_{wall})/L\rho_v]\sqrt{3/\pi D}\ t^{\frac{1}{2}} \qquad (II-1-18)$$

which is the asymptotic solution found by Zwick and Plesset in a different way.

2. Validity of Approximations

Now it is pertinent to check the validity of the assumptions entering into the foregoing equations for typical bubble chamber conditions. The simplest procedure is to assume that the approximations are valid, and then to use the resultant motion of the bubble wall to evaluate the neglected terms. Since, in the cases we consider, the bubbles grow initially during a period of reasonably constant pressure, the simple expression II-1-18 may be expected to apply at first, and we may use it to estimate the effects of the approximations during the initial growth period.

We first check the assumption that the heated zone of fluid has a thickness small compared to its radius, the condition which is necessary for the validity of the Zwick-Plesset heat flow equation. This may be done by noting that the quantity $\sqrt{Dt}$ is a measure of the thickness of the heated zone. Then the ratio $\sqrt{Dt}/R = \sqrt{Dt}/A\sqrt{t} = \sqrt{D}/A$ is a measure of the validity of the heat flow equation during the initial growth period, when

equation II-1-18 applies. Table* 4 gives the values of quantities appropriate to propane for two different conditions of expanded pressure (the two used in the numerical calculations described later). In case I, the ratio $\sqrt{D}/A$ is 0.0278, while in case II it is 0.0824. Certainly under the initial growth conditions, the "thin thermal layer" approximation is well enough justified. For the later phases of bubble growth and collapse using the full equation (described later), the longest time considered is 7 ms. In case I, the bubble radius is then about 0.020 cm, while in case II it is about 0.0078 cm. The ratio $\sqrt{Dt}/R$ in these, the worst cases, is then 0.17 and 0.44 respectively. Since these numbers, especially the latter one, are not very small compared to unity, we may expect some error to be introduced by the use of the approximate heat flow equation during the later periods of growth and collapse. In fact, for case II, the error may be significant, and it would be useful to have a more quantitative measure of it. Further discussion of this point, however, is deferred until later.

One may also check without difficulty the justification for neglect of the inertial and surface tension effects given in equation II-1-12. If we employ the asymptotic solution II-1-18 with the values taken from Table 4, we find for case I

---

* Many of the quantities in Table 4 can be found in standard reference books, but some cannot and thus must be inferred from measurements on other hydrocarbons with the aid of the law of corresponding states. In particular, ρ, c, and K are all functions of temperature, but their dependence is comparatively weak, and the exact value for K and c is not known. Therefore their temperature dependence has been ignored, and average values used. This should not affect our calculations by more than about 10 to 20 percent.

TABLE 4

	Case I	Case II
Temp. of Fluid	$58.1^{\circ}C$	$58.1^{\circ}C$
Expanded Pressure	60 psi	120 psi
Temp. of Bubble Wall	$-4.7^{\circ}C$	$19.9^{\circ}C$
τ_0	$62.8^{\circ}C$	$38.2^{\circ}C$
K	4×10^{-4} cal/cm sec$^{\circ}$C	4×10^{-4} cal/cm sec$^{\circ}$C
ρ_l	0.4 gm/cm^3	0.4 gm/cm^3
c_l	0.6 cal/gm	0.6 cal/gm
D	1.67×10^{-3} cm^2/sec	1.67×10^{-3} cm^2/sec
$1/L\rho_v$	2.92×10^{-8} cm^3/erg	1.63×10^{-8} cm^3/erg
A	1.47 cm/sec$^{\frac{1}{2}}$	0.496 cm/sec$^{\frac{1}{2}}$
σ	10.0 dynes/cm	7.42 dynes/cm

$$R\ddot{R} + (3\rho_\ell/2)\dot{R}^2 + 2\sigma/R = P - P_H = \boxed{\rho_\ell A^2/8t} + \boxed{2\sigma/A\sqrt{t}}$$
$$= \boxed{0.108/t} + \boxed{13.6/\sqrt{t}}.$$

In the cgs units used here, one atmosphere is approximately 10^6 dynes/cm^2,

so after only 10 microseconds the first term is about 0.01 atm., while the

second term is ~ 0.005 atm. Since we are interested here in growth periods

of several milliseconds, it is evident that the above is completely negli-

gible, and the equating of P to P_H represents a very good approximation

over the region of interest. The situation for case II is an order of mag-

nitude better still because of the lower value of A and σ. For the later

period of growth and collapse, $P - P_H$ is negligible to an even better ap-

proximation because of the much smaller values of $\ddot{R}$ and $\dot{R}$, and larger R.

To check the final assumption, that of thermal equilibrium of

the vapor in the bubble, we must know the thermal conductivity of the vapor.

This is a difficult number to obtain exactly, but some rough approximations

can be made by considering the vapor an ideal gas and computing its thermal

conductivity from kinetic theory. The latter unfortunately requires a

knowledge of the mean free path of molecules in the vapor, but this can

be estimated from data on other hydrocarbons (56). Therefore, if we use

an effective collision radius of 7.4×10^{-8} cm per molecule and a heat

capacity at constant volume of 15 R per mole, the simple kinetic theory (57)

predicts a thermal conductivity of $1.54\sqrt{T} \times 10^2$ ergs/cm sec^{o}C, where T

is the absolute temperature. If we further use the ideal gas relation to

find the density of the vapor, we have the diffusivity $D = K/\rho_v c_v =$

$10.27 \, T^{3/2}/P$. For two typical values, we find at 5 atm, $D = 0.922 \times 10^{-2}$,

while at 10 atm, $D = 0.527 \times 10^{-2}$. Now one may define a thermal "relaxa-

tion time" τ_R for a spherical region $\tau_R = R^2/4D$. The maximum bubble

radius in case I is about 0.041 cm (where the 5 atmosphere value for D is appropriate), and for case II is 0.016 cm (where the 10 atmosphere value for D is appropriate). This radius yields, for case I, τ_R = 46 ms, and for case II, τ_R = 12 ms. Neither of these two times, particularly the first, are short compared to the periods of interest, so it is evident that the thermal equilibrium hypothesis is not valid for these cases. However, it probably makes very little difference in the dynamics of the bubble for the following reasons. In the initial growth period, the hydrostatic pressure is very nearly constant, so the vapor evaporates into the bubble at essentially constant temperature and pressure. Thus no thermal gradients are created in the vapor to begin with. During the later phases of growth and collapse, however, the external pressure is changed (as the chamber is recompressed), and one might expect the poor thermal equilibrium to have a strong effect on the behavior of the bubble. However, for a fluid such as propane, with many internal degrees of freedom per molecule, this is probably not the case. It can be shown that for an ideal gas under adiabatic conditions (the case of very poor thermal conductivity), the dependence of bubble radius upon pressure is $R/R_o = (P_o/P)^{(1/3)(c_v/c_p)}$ where c_v/c_p is the ratio of specific heats at constant volume and pressure. For propane this ratio is quite close to one, being around 0.9. On the other hand, if one considers the gas to be in equilibrium with a thin layer of fluid on the walls, (and no heat loss or gain by the bubble) the relationship becomes* (approximately) $R/R_o = (P_o/P)^{1/3} - A \log (P_o/P)$ where A is a small constant < 0.1. Therefore the functional dependence of radius on pressure is not strikingly different whether or not there exists thermal equilibrium.

---

* The relations from which this approximate equation was derived are developed later.

3. Numerical Solution of Bubble Growth Equation

Since the simple analytical solution represented by equation II-1-18 is not valid when the external pressure changes, it cannot be used for calculating the later growth (and collapse) of bubbles in a typical bubble chamber, and the complete equation II-1-16 must be employed. The calculation has been carried out for two conditions of pressure assuming propane as the sensitive fluid, since the required empirical parameters are known about this liquid. The procedure and results of these calculations are given in the following.

The conditions of pressure for the two cases calculated are typical of the 12 inch chamber described in Chapter I-3. The pressure is assumed to behave like a cosine function with a period of 14 milliseconds, and particles are injected at the time of minimum pressure. The first case considers the pressure to reach a minimum of 60 psi, and rise to 400 psi in the half-period of 7 ms. The second case is identical except that the minimum pressure is taken as 120 psi. Because of the complex nature of the equations and the pressure dependent coefficients of various terms, it is not possible to find a simple analytic solution to equation II-1-16. In addition, during most of the period of growth and collapse, all terms are found to be comparable and none can be neglected. Therefore a numerical solution must be employed. However, approximate analytic expressions can be found for the coefficients of the two terms on the right of equation II-1-16, and it may be of some interest to display them here.

Let us first consider $\varphi = L \rho_v$. From the Clausius-Claperyon relationship (58), we may write, for a fluid in equilibrium with its vapor,

$$dP/dT = L_o / \Delta VT \qquad\qquad (II-1-19)$$

where L_o is the latent heat per mole and ΔV is the change in volume per mole of the substance upon vaporization. This may be rewritten in terms of unit masses as

$$dP/dT = L \rho_v / T(1 - [\rho_v / \rho_\ell])$$

or

$$\varphi = L \rho_v = T[1 - (\rho_v / \rho_\ell)] \, dP/dT \qquad (II-1-20)$$

Now it happens that the equilibrium vapor pressure of a fluid may be fitted over a comparatively wide range with fair accuracy (59) by the simple function

$$\log [P/P_c] = a[1 - (T_c/T)] \qquad (II-1-21)$$

where

$$a = [T_B/(T_c - T_B)] \log (P_c/P_B)$$

and T_B, P_B; T_c, P_c are two known points. Actually, these points can be as widely separated as the boiling and critical points and still retain accuracy of the order of 2 to 5% with most liquids. In our case, the empirical function was fitted more closely than this, as the points P_B and P_c were taken as 2 and 20 atmospheres, respectively.

Using equation II-1-21, we may now find

$$dP/dT = [a + \log(P_c/P)]^2 \, P/aT_c \qquad (II-1-22)$$

Now if we substitute equation II-1-22 into equation II-1-20 and eliminate T by aid of equation II-1-21, we find

$$\varphi = L \rho_v = P[a + \log(P_c/P)] [1 - (\rho_v / \rho_\ell)] \qquad (II-1-23)$$

For lower pressure ρ_v / ρ_ℓ may be neglected compared to unity. However, for higher pressures (~ 5 atmospheres) the error becomes significant and the term should be included. For our case ρ_v / ρ_ℓ was computed using Van der Waal's equation.

The first term on the right of equation II-1-16 may be similarly

evaluated, although it is algebraically involved. Omitting the details, we write

$$Y \equiv \varphi' - 1 \neq b(1 \neq \rho_\ell c' - P\rho_\ell'/\rho_\ell)$$
$$= f(1 - b) - 2(1 - b) - Pfdb/dP \neq bBaT_c/Pf^2 \qquad (II-1-24)$$

where

$$f = a \neq \log (P_c/P)$$

$$b = \rho_v/\rho_\ell$$

$$B = \rho_\ell c_\ell - \alpha P \approx \rho_\ell c_\ell = 10^7 \text{ ergs/cm}^3 \text{ (propane)}$$

α = thermal coefficient of expansion of liquid under equilibrium vapor pressure conditions.

For convenience in the numerical solution of equation II-1-16, it is advantageous to define new dimensionless variables $\zeta = t/t_o$; $v = S/R_o^4 t_o$ where $t_o = 10^{-3}$ sec; and $R_o = 10^{-2}$ cm. Written in the new variables, equation II-1-16 becomes

$$\ddot{v} = -\chi\dot{v} \neq \psi(\dot{v})^{5/4} \left[(\tau_o/v^{\frac{1}{2}}) - \int_o^\zeta Gdx/\sqrt{v(\zeta) - v(x)} \right] \qquad (II-1-25)$$

where $\chi = 4P\Upsilon/3\varphi$; $\psi = 4K\sqrt{t_o}/\varphi R_o \sqrt{\pi D}$; $G = -d\tau/d\zeta$ and the dot now denotes differentiation with respect to ζ. The function ψ is plotted in Fig. 22 as a function of pressure. The functions χ and G are also shown in Figs. 23 and 24, but for generality are plotted as $P\chi/P$ and $-Pd\tau/dP$, respectively. They must be multiplied by $(1/P)(dP/d\zeta)$ (shown in Fig. 25 for case II) to obtain χ and G.

Using the curves described above and the initial value for τ_o, the solution of equation II-1-25 is straightforward but quite tedious. The principal difficulty lies with the last term, which is an integral that must be evaluated at each step in the solution, or at least often

Figure 22

The Function ψ vs. Pressure for Propane

ψ is defined in the text.

Figure 23

The Function $P\chi/\dot{P}$ vs. Pressure for Propane

To obtain χ, this function must be multiplied by $\dot{P}/P = (dP/d\varsigma)/P$.

Figure 24

The Function PdT/dP vs. Pressure for Propane

To obtain the function G defined in the text, the above must be multiplied by $\dot{P}/P = (dP/d\varsigma)/P$.

$$\psi = \frac{4k}{\sqrt{\pi D}} \quad \frac{1}{\varphi} \quad \frac{\sqrt{t_0}}{R_0}$$

$$t_0 = 10^{-3} \text{ Sec.}$$

$$R_0 = 10^{-2} \text{ Cm.}$$

(SEE TEXT)
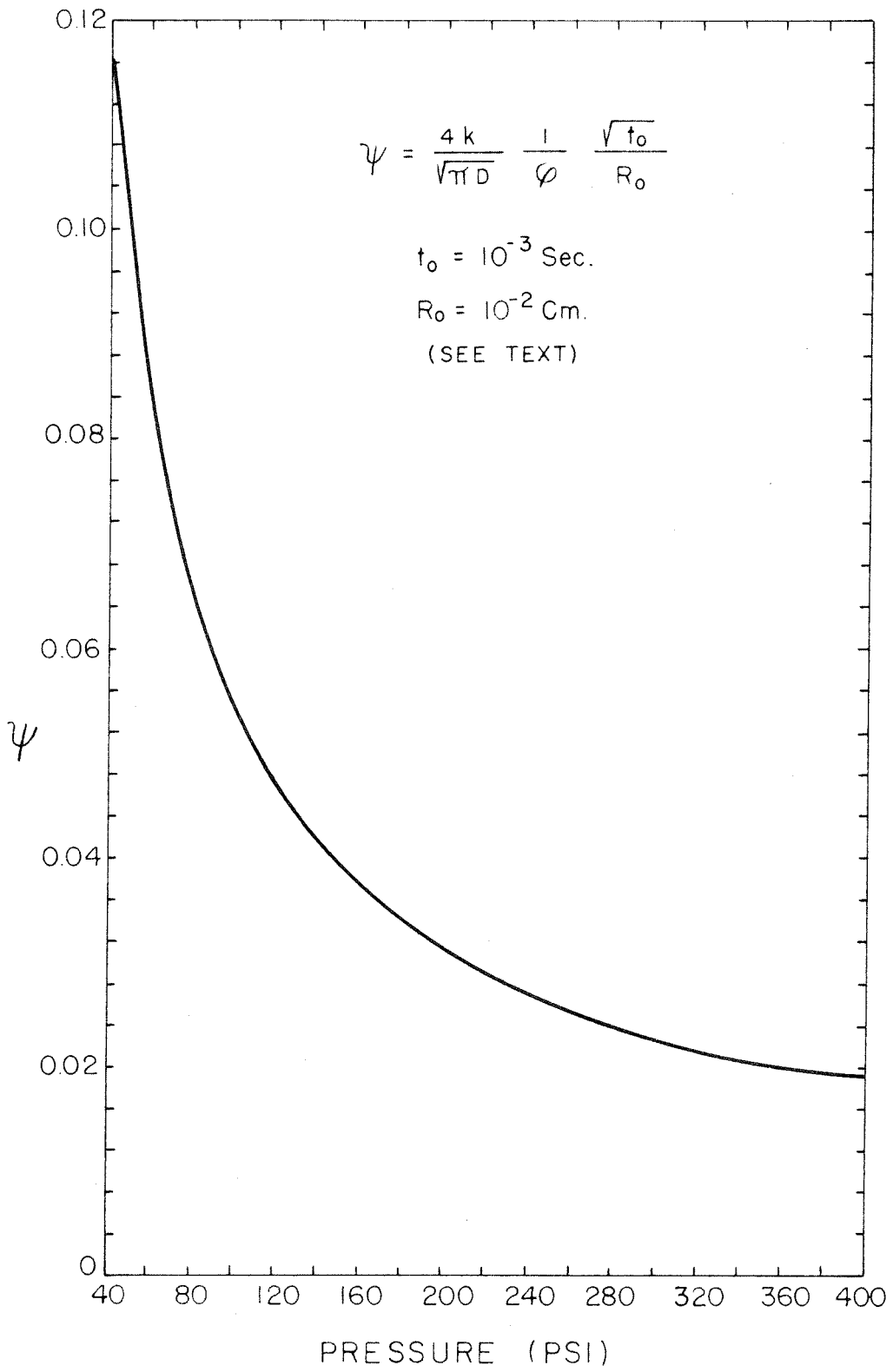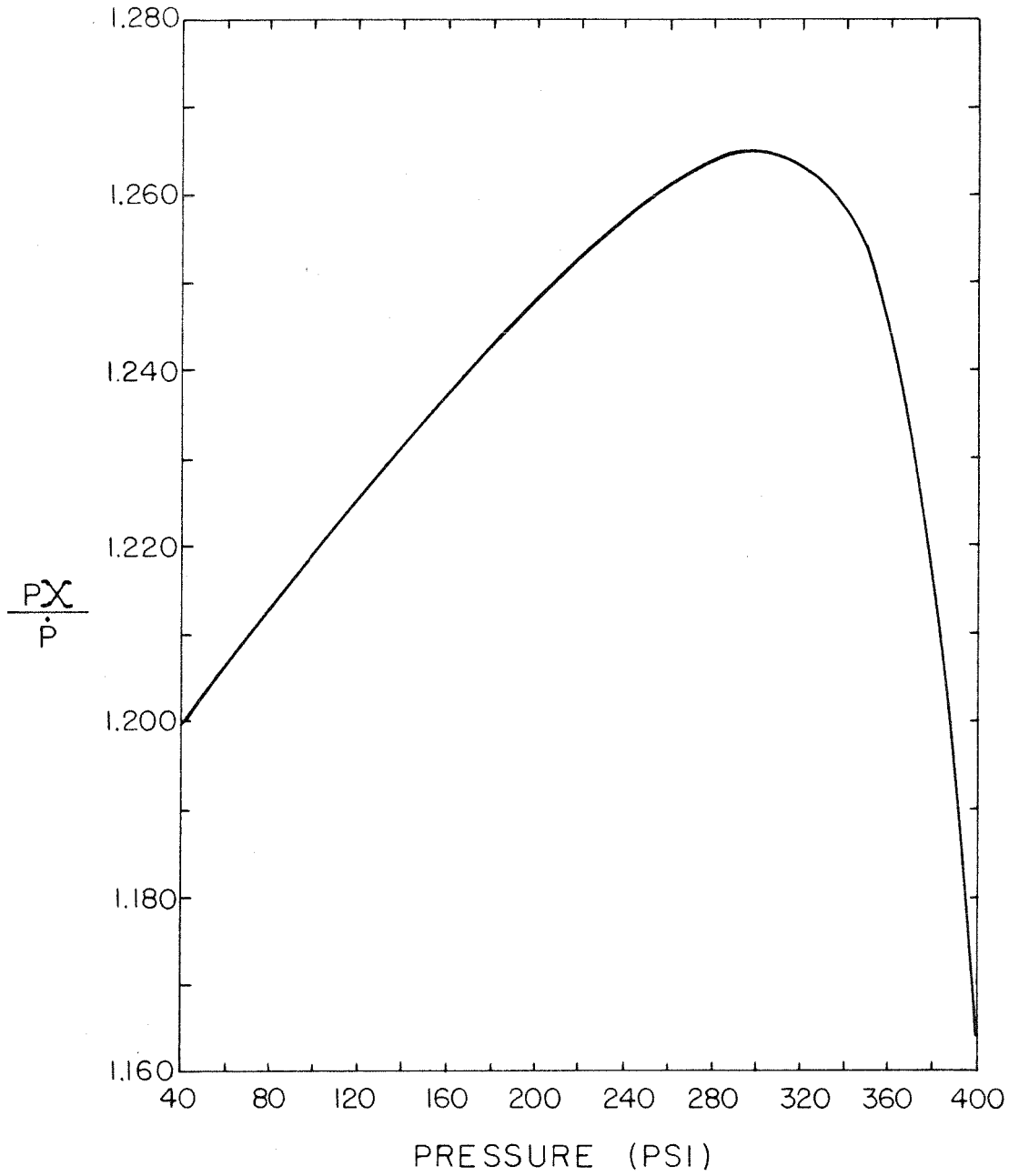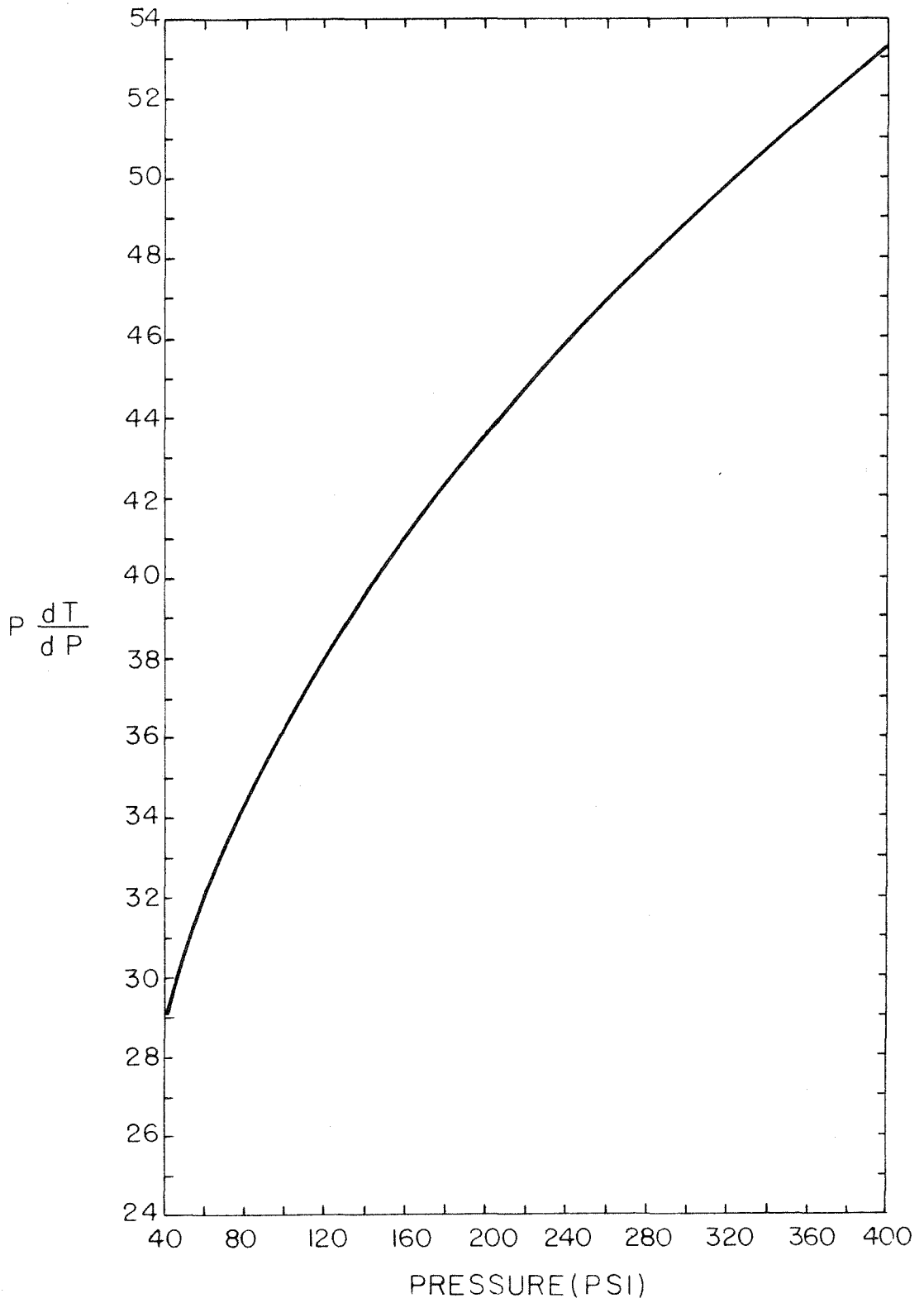
Figure 22

Figure 23

Figure 24

Figure 25

The Function $\dot{P}/P = (dP/d\varsigma)/P$ for Propane for Case II

Also shown is the actual pressure vs. time function assumed for the calculation of case II.

The analogous functions for case I are not shown.

Figure 25
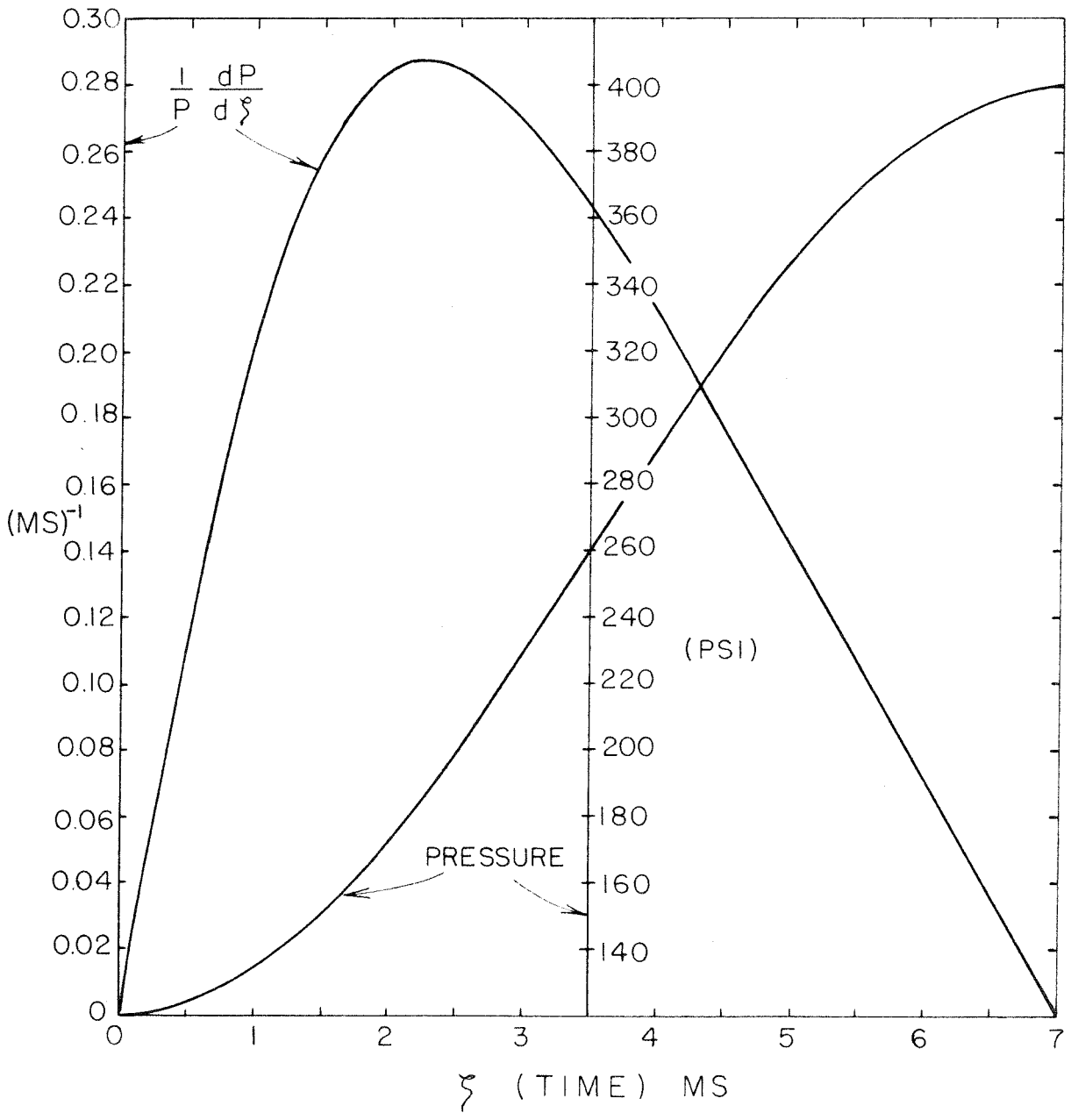
enough to make an extrapolation accurate. During the initial growth period, until about 0.4 ms after the origin of the bubble, the analytic solution given by expression II-1-18 is usable, but numerical solution must be employed afterward.

4. Results of Calculations

The behavior of a bubble in the two cases calculated is shown in Figs. 26 and 27. There are several features which may be noted. The most striking from the standpoint of the use of a bubble chamber as a precision instrument is the size and rapidity of initial growth of the bubbles in case I. In order to obtain precise locations of tracks and to allow the possibility of meaningful bubble counting, one would prefer bubbles as small as 0.1 to 0.2 mm diameter. Those in case I reach a maximum size of about 0.41 mm radius - much too large for use. The maximum radius in those of case II is somewhat better at 0.16 mm, but is still perhaps larger than one would like. The rapidity of growth also makes it difficult to use an early flash to obtain pictures when the bubbles are smaller, since the time of growth is comparable to the particle injection time for most accelerators. There seems to be little one can do about it. It would require a chamber with a much faster cycle than ours in order to prevent the large bubbles in case I when the pressure is dropped so low, and ours is sufficiently fast that troubles may already be encountered with the acoustical delay of pressure transmission. The solution is, of course, to operate the chamber with much higher minimum pressures, which is, in fact, the way most bubble chambers operate. The reason for the phenomenal rise in growth rate at lower pressures is easily seen in the simple growth equation II-1-18. The rate of change of vapor pressure with temperature

Figure 26

Bubble Growth in Propane, Case I

Ambient temperature assumed for this calculation is 58.1°C.
The pressure in the chamber is assumed to obey the function

$$P = \{230 - 170 \cos \omega t\} \,(\text{psi}),$$ t in seconds and $\omega = 449$

(Minimum pressure $= 60$ psi).

142-
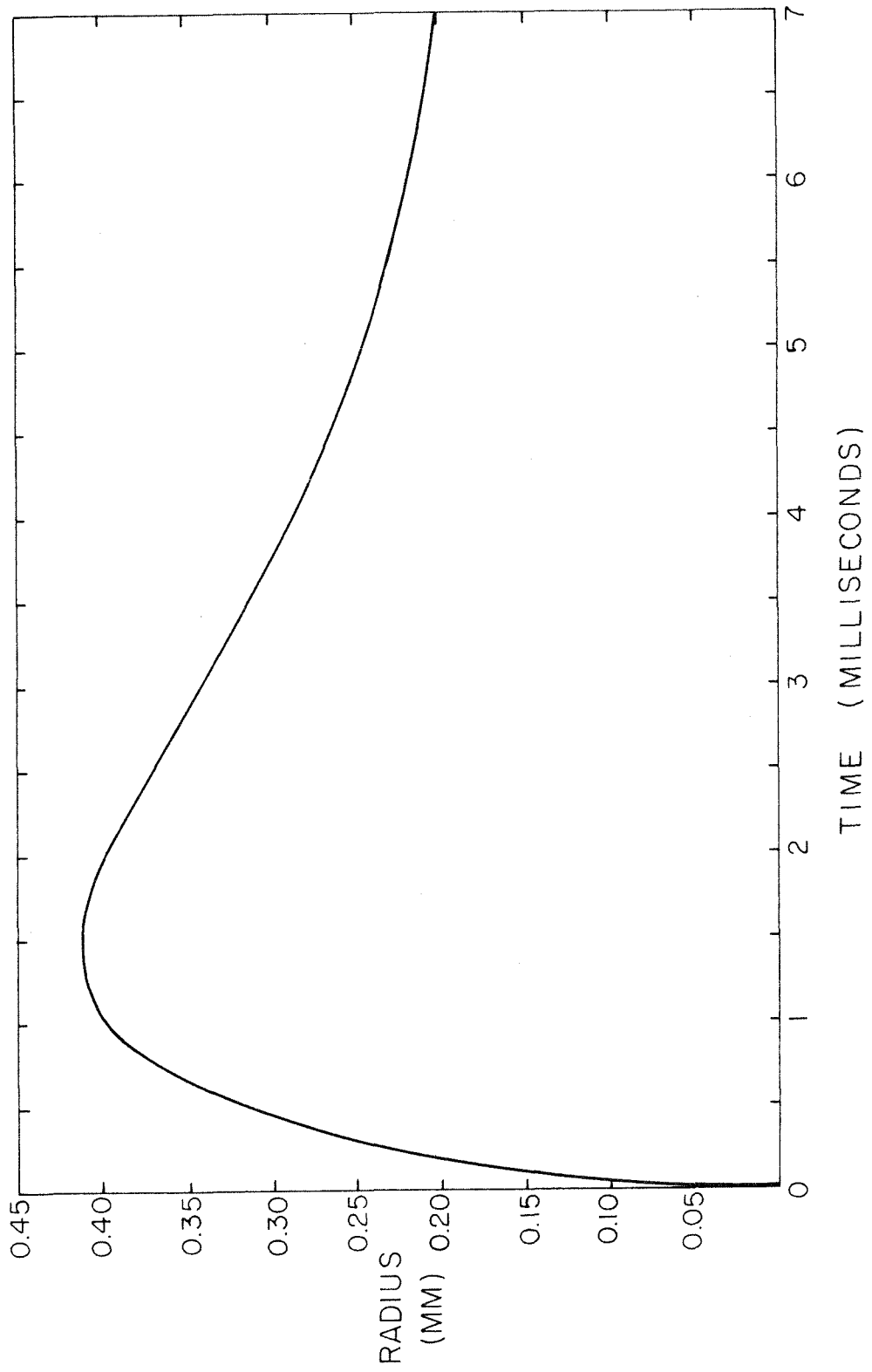
Figure 26

Figure 27

Bubble Growth in Propane, Case II

Ambient temperature 58.1°C.

Pressure in the chamber assumed to obey

$$P = \{260 - 140 \cos \omega t\}, t \text{ in seconds}, \omega = 449.$$

(Minimum pressure = 120 psi)
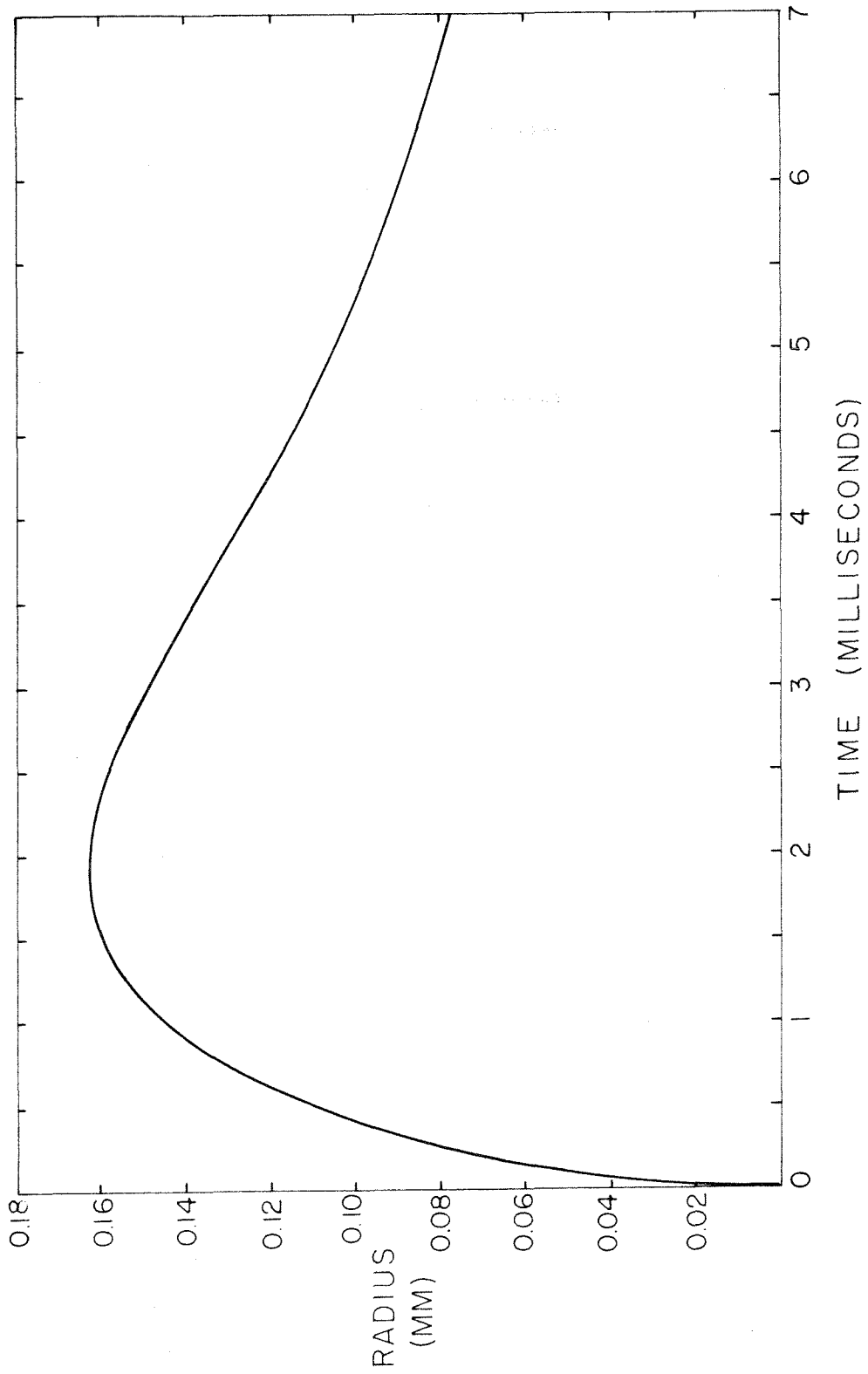
Figure 27

becomes quite small at lower pressures as can be seen by equation II-1-19.
In this relation L_0 is almost constant, while ΔV is essentially the volume
per mole of the vapor, and is (roughly) inversely proportional to the pres-
sure. Therefore as we lower the hydrostatic pressure of the fluid, the
temperature of the bubble wall drops with increasing rapidity, making the
numerator of expression II-1-18 large. In addition, the denominator con-
tains the term $L\rho_v$. Since we can consider L almost constant, we see that
this term varies like ρ_v, which is approximately proportional to pressure.
One then expects A to vary like $1/P_H^2$. What this is saying physically is
that the temperature gradient across the thin thermal barrier is larger,
increasing the heat flow, and the bubble is less dense, requiring less
heat per unit volume in order to grow. For illustration, the initial
growth coefficient A is plotted in Fig. 28. The very sharp dependence on
expanded pressure is evident here.

Another feature to be noticed is that there is a comparatively
long period when the bubble has a quite constant radius. This indicates
that flash timing is not at all critical with respect to obtaining uniform
sized bubbles. It is also to be remarked that in both case the bubble
begins to collapse well before the pressure has risen to the vapor pressure
of the fluid far from the bubble. This effect is caused by the combined
action of the pressure rise itself plus the fact that the bubble is sur-
rounded by a layer of cold liquid which it produced in expanding. The
latter acts as a heat sink for a short period during the collapse.

A further significant fact is that, in both cases, a residual
bubble exists even after the pressure has risen to 400 psi, 100 psi in
excess of the vapor pressure. Just when the actual collapse of the bubble
would occur is not clear, and it does not pay to continue the calculation

Figure 28

Initial Growth Coefficient for Bubbles in Propane

vs. Expanded Pressure

Ambient temperature assumed to be 58.1°C. The coefficient plotted
is the function A defined in text, such that $R = At^{\frac{1}{2}}$; R is radius of
bubble in cm and t is time in sec.

Figure 28

INITIAL BUBBLE GROWTH
RATE IN PROPANE

AMBIENT TEMP. =58.1°C

GROWTH RATE

$$\frac{CM}{(SEC)^{\frac{1}{2}}}$$

EXPANDED PRESSURE
(PSI)
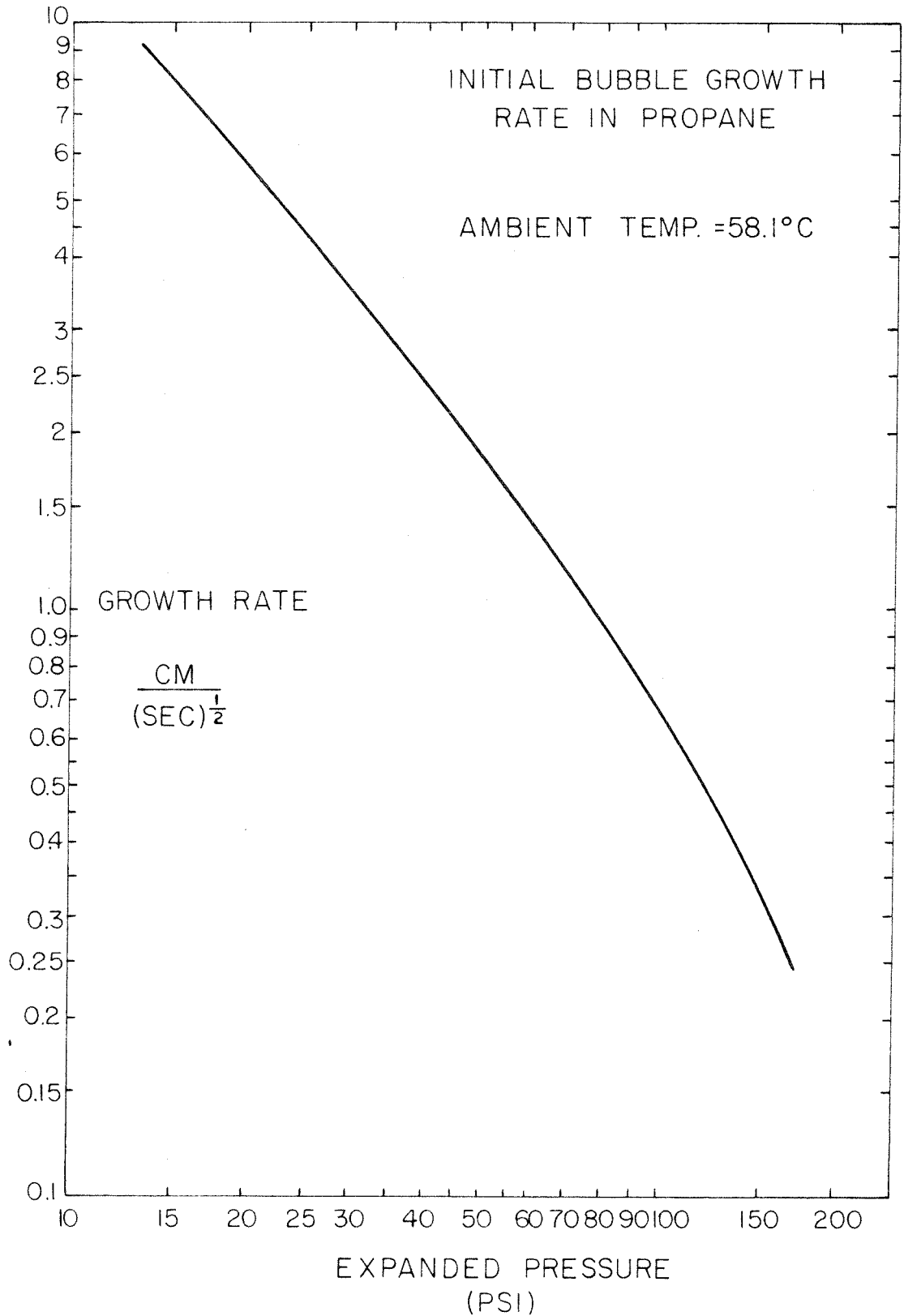
based upon equation II-1-25 for two reasons. One is that the approximate
heat flow equation, as mentioned earlier, almost surely begins to be sig-
nificantly in error. A rough estimate of the nature of the error can be
found in the following way. We note that during the latter portion of the
period of calculation of cases I and II, the rate of change in the bubble
radius is small. If we consider the radius constant, we can solve the heat
flow equation exactly, since then the nonlinear terms arising from the fluid
motion are not present. The solution is straightforward and the derivation
not presented here, but the result is that, for a bubble of unchanging
radius R, the heat flow as we have defined it is given by

$$H = -4\pi KR \, \mathcal{T}(t) - 4KR^2 \sqrt{\pi/D} \, \underline{[d/dt]} \int_0^t \mathcal{T}(x)dx/\sqrt{t-x}.$$

This is to be compared with the heat flow equation II-1-15. We note that
if R is considered constant in equation II-1-15, the result agrees exactly
with the foregoing except for the first term on the right of the above,
$4\pi KR\mathcal{T}$. The latter is just the steady state solution for $\mathcal{T}$ = constant and
$t \rightarrow \infty$. Therefore we may expect that the term $4\pi KR\mathcal{T}$ is a rough measure of
"curvature" error in the Zwick-Plesset solution for our case (although
there is no reason to believe that it represents an accurate correction).
It should be noted that the above "correction" varies as R whereas the rest
of the solution varies as R^2, so we expect the error to increase near the
end of the cycle, as the bubble radius decreases. Also the sign of the term
is such as to increase the rate of heat flow out of the bubble, and there-
fore to speed its collapse. The term $4\pi KR\mathcal{T}$ evaluated for the calculated
cases indicates an error in the rate of heat flow at the end of the period
of calculation of about 10% in case I and about 40% in case II.

Another source of error which is much more difficult to estimate
but which could be quite large is the physical rise of the bubble, bringing

it in contact with liquid cooler than its walls. At the end of the period

of calculation (7 ms), the bubble has already risen about 0.48 mm, which

is larger than the diameter of the heated zone.

It is to be noted that both of the above errors are of such a

nature as to speed the bubble collapse, and they may have a large effect.

Thus the foregoing calculations set an upper limit to the size of the

residual bubble, and it is conceivable that the actual bubble collapse may

occur quite rapidly after or near the end of the period of calculation.

A useful result of the calculations is an estimate of the ir-

reversible thermodynamic losses in the expansion-recompression cycle. By

integrating PdV over the entire cycle, one may determine the net energy

loss per bubble. For case I, this number turns out to be 3.137×10^3 ergs/

bubble, while in case II it is 1.62×10^2 ergs/bubble. If one assumes an

average of about 1000 bubbles per track (about 30 cm long) and an average

of 100 tracks per picture, this yields 10^5 bubbles per expansion. Such

numbers indicate an energy loss of 31.37 joules for case I while only 1.62

joules for case II. The first number is a significant loss, since the

total energy storage in our chamber is of the order of 700 joules, while

the latter number is essentially negligible.

C. The Bubble Nucleation Process

1. Elements of the Problem

The purpose of the remainder of this chapter is to investigate

in some detail the various proposed mechanisms for the formation of micro-

scopic bubble nucleii and their growth to critical size. These mechanisms

(including some attempts of our own) are examined in the light of available

experimental data and some calculated and empirical parameters of the relevant

liquids.

It is probably safe to state that none of the theories are free from serious objection, although each may be said to help in some way to understand the process of bubble nucleation. To make matters worse, no really definitive experimental data are at hand, even though some experiments have been performed. The difficulty is that in order to fit a given model to experimental data, one must know several parameters fairly accurately, and, preferably, for a number of liquids of different properties. These parameters are the conditions of expanded pressure and temperature, and the number of bubbles per centimeter for particles of known momentum.* It must be stressed that the latter number usually cannot be obtained by a simple counting of bubbles per unit length of track. To illustrate this point, we assume that the probability per unit distance for forming a bubble by a particle of a certain energy is given by $(1/x_0)$. Then the spacing between adjacent bubbles is distributed according to the probability function

$$P(x) = (1/x_0)e^{-x/x_0}$$

where $P(x)$ dx gives the probability that two adjacent bubbles will be separated a distance between x and $x + dx$. Now the parameter x_0 is the quantity which we wish to know. If the bubbles are of infinitesimal size, the average number of bubbles per unit length which would be counted would be given by n, where

$$n = 1/\int_0^\infty xP(x)dx = 1/x_0,$$

as we would expect. However, the bubbles are not of infinitesimal size, and generally have a diameter which is a significant fraction of x_0. One

---

* As is discussed later, the bubble density for fast electrons or positrons is probably adequate for most purposes.

can obtain an estimate of the effect upon the apparent bubble density by
assuming that two bubbles always coalesce if their diameter, a, exceeds
their spacing x. Then an approximation to the observed number of bubbles
per unit length n_c would merely be

$$n_c = \int_a^\infty P(x)dx \Big/ \int_a^\infty xP(x)dx = 1/(x_0 \neq a)$$

or

$$n = 1/x_0 = n_c/(1 - an_c) \tag{II-1-26}$$

However, in an actual experiment the uncertainties as to bubble sizes plus
significant enlargement of the bubble images due to finite optical resolu-
tion make a rough correction such as given above (or even a more accurate
correction) insufficient. A better though more tedious procedure is to
measure the actual distribution of bubble spacings and to take the logarith-
mic slope of the resulting function in the region of large spacings. Such
a procedure with reasonable statistics will give an accurate measure of the
parameter x_0, while simple bubble counting cannot, in general, be trusted.

However, such experimental results as do exist tend to favor at
least one distinct feature of the bubble forming mechanism. It seems
highly probable that most bubbles in a typical case are formed by compara-
tively energetic "knock-on" electrons, (δ-rays) with energies around
1 Kev or greater. Two experiments (60,61) have indicated that the density
of bubbles in a particle track is proportional to $1/\beta^2$, where $\beta = v/c$,
the ratio of particle velocity to that of light, independent of the mass
of the particle. This is the dependence which would be expected, as shown
below, if the bubbles were formed by δ-rays of an energy greater than a
certain threshold value. These results, of course, are not in themselves
conclusive, as this dependence is also that of, say, displaced nucleii.

Until further data is obtained, one also cannot rule out entirely the possibility that the bubble density function may be close to that of the relative ionization of the particles. Over a sensibly large range for slower particles this latter function dE/dx does not deviate enough from $1/\beta^2$ to exclude it completely in the light of present data, although the fit is not as good as for a strict $1/\beta^2$ dependence (61). There are, however, other reasons why one is inclined to accept the δ-ray hypothesis, and these reasons are convincingly presented by Seitz (50). Here we will note, as is shown later, that if one assumes the δ-ray mechanism and calculates the minimum δ-ray energy on the basis of the experimentally observed bubble densities, one finds that the range of the δ-ray is comparable to the diameter of the critical sized bubble (defined earlier). Thus we see that a δ-ray is capable of concentrating its energy in a sufficiently small region. In fact, it is difficult to visualize any other process which is able to localize enough energy to create a bubble of critical radius with sufficiently high probability to produce the observed densities.

Although the δ-ray mechanism must be considered as only highly probable rather than as proven fact, we will none the less hereafter assume its validity. Under this assumption, we may predict the relative bubble density for particles of different energies under constant operating conditions of the chamber. For production of δ-rays of energy between E_1 and E_2, the total cross section σ_e per electron (for "free" electrons) is given by (62)

$$\sigma_e \equiv \left[2\pi e^4 z_e^2 / m_o c^2 \beta^2 \right] \left[(1/E_1) - (1/E_2) \right]$$

where we have neglected spin terms (which are small over the range of

interest) and the atomic binding energies. Here

z_e = charge of incident particle

m_0 = mass of the electron

e = charge of electron

c = velocity of light

$\beta = v/c$; v = velocity of incident particle.

If we assume that a bubble is produced by each δ-ray with energy greater

than E_1, we may assume that $E_2 \gg E_1$, since the experimentally observed

value of E_1 is in the range of 1 Kev, and the energy E_2 must be very much

greater than this in a typical bubble chamber liquid before the range of

the δ-ray is sufficient for the observer to identify it as a distinct

track. Thus we may say, to a good approximation, that the cross section

for producing a bubble per electron in the bubble chamber fluid (assuming

$z_e = 1$) is

$$\sigma_e = \left[2\pi e^4 / m_0 c^2 \beta^2 \right] \left[1/E_1 \right] \qquad \text{(II-1-27)}$$

Note that the only parameter relating to the incident particle is contained

in the term $1/\beta^2$. Hence the number of bubbles per unit length should be

inversely proportional to the square of the velocity of the particle.

However, a rather striking anomaly appears when numbers are inserted into

equation II-1-27 to find the threshold δ-ray energy from the observed

bubble densities. The numbers one obtains for E_1 are an order of magnitude

larger than the energy one estimates is required to form a bubble. To il-

lustrate, let us calculate the energy expended in forming a bubble of

critical radius R_c in a reversible, adiabatic way. That is, we assume

that the bubble is formed with sufficient rapidity that it can obtain no

heat from its surroundings, and all energy must come from that deposited

by the particle. In analogy with equation II-1-2, we may write an energy
equality for the work required as

$$W = [u - c] V_c \rho_v + \mathcal{E}_s + P_H V_c [1 - (\rho_v / \rho_\ell)]$$

where u and c are the internal energies of vapor and liquid as defined for
equation II-1-3, V_c is the volume of the bubble of critical radius and P_H
the hydrostatic pressure in the external fluid. $\mathcal{E}_s$ is the energy due to
surface tension, and is given by $\mathcal{E}_s = 4\pi R_c^2 \sigma$, where σ is the surface
tension. We may find the value of $[u - c]\rho_v$ by use of equation II-1-8,
so we have

$$W = \left\{ L\rho_v + (P_H - P_v)[1 - (\rho_v / \rho_\ell)] \right\} V_c + 4\pi R_c^2 \sigma$$

where P_v is the vapor pressure of the fluid (at the ambient temperature).
If we substitute $V_c = 4\pi R_c^3 / 3$ and $R_c = 2\sigma / (P_v - P_H)$, the above becomes,
where $b = \rho_v / \rho_\ell$,

$$W = 4\pi R_c^2 \left\{ (R_c / 3)[L\rho_v + (1 - b)(P_H - P_v)] + \sigma \right\} \qquad (II-1-28)$$

$$= [16\pi\sigma^3 / (P_v - P_H)^2] \left\{ [2/3(P_v - P_H)] [L\rho_v - (P_v - P_H)(1 - b)] + 1 \right\}$$

The quantities $L\rho_v$ and ρ_v appearing in the above equation can be calculated
in a manner similar to that discussed in the bubble growth problem consid-
ered previously. In order to evaluate this expression, however, we require
numbers taken from experiments.

2. Experimental Data

Table 5 represents a compilation of data extracted from the lit-
erature. Since many of the numbers contained in the table are subject to
great error, a word must be said about them. Those contained in group 1
are from Nagle, Hildebrand, and Plano (63). The authors give here only a
rough count of the bubble density for relativistic particles, but state
the approximate bubble diameter. Thus the number n is their number

TABLE 5 LEGEND

n   = number of bubbles per cm.

T   = operating temperature

P_v = vapor pressure of liquid

P_H = expanded pressure of chamber

σ = surface tension

R_c = critical bubble radius

L   = latent heat per unit mass

ρ_v = density of vapor

ρ_ℓ = density of liquid

W = work required to create bubble

E_1 = threshold δ-ray energy

TABLE 5

$n(cm^{-1})$	T	$P_v(atm)$	$P_H(atm)$	σ dynes/cm	$R_c(cm)$	$L\rho_v$ dynes/cm²	$1-(\rho_v/\rho)$	W(ev)	E_j(ev)
				Group 1 - Hydrogen					
21.5	27°K	4.91	1.2	0.97	5.08×10^{-7}	2.25×10^7	0.882	8.6	355
				Group 2 - Propane					
20	55.5°C	18.4	9.2	3.67	7.88×10^{-7}	1.17×10^8	0.913	158	1800
				Group 3 - n-Pentane					
0	155°C	17.1	12.8	2.62	12.0×10^{-7}	1.11×10^8	0.89	520	---
31.4	155°C	17.1	11.0	2.62	8.48×10^{-7}	1.11×10^8	0.89	187	1170
37.7	155°C	17.1	9.0	2.62	6.39×10^{-7}	1.11×10^8	0.89	79	975
42.5	155°C	17.1	7.0	2.62	5.12×10^{-7}	1.11×10^8	0.89	41	865
				Group 4 - Propane?					
2.5	77.3°C	30.0	23.5	1.43	4.34×10^{-7}	1.74×10^8	0.81	39	14000
6.1	77.3°C	30.0	23.0	1.43	4.03×10^{-7}	1.74×10^8	0.81	31	5700
15.8	77.3°C	30.0	22.58	1.43	3.80×10^{-7}	1.74×10^8	0.81	26	2220
				Group 5 - Isopentane					
30	120°C	10.8	~2.0	4.07	6.28×10^{-7}	0.78×10^8	0.935	56.7	1340
				Group 6 - WF6					
30	136°C	23.1	12.0	3.82	6.80×10^{-7}	1.66×10^8	0.90	140	5450

multiplied by the approximate correction given by equation II-1-26. Also

not given is the value of the expanded pressure P_H. The number included

here is that estimated (close to 1 atm.) from the fact that this chamber

was a "clean" glass chamber, with a very long ($\sim \frac{1}{4}$ sec.) sensitive time.

The values in group 2 are from Willis, Fowler, and Rahm (61). Here the

authors used an accurate bubble counting technique, but do not state the

expanded chamber pressure. The number adopted for P_H is based upon the

observation that most of the propane chambers of the type used by the au-

thors expand to a final pressure believed to be in the vicinity of $\frac{1}{2} P_v$.

Those numbers in group 3 are taken from Bassi, et al. (64), in which the

expanded pressure was believed to be known. However, a simple bubble

counting technique was employed and the bubble diameter (which is stated)

was fairly large. Thus the correction given by equation II-1-26 is used

in obtaining the number n. The values contained in group 4 are taken from

Blinov, et al. (60). In this experiment the expanded pressure is said to

have been accurately known. In addition, the authors used a correct bubble

counting technique. However, the liquid employed is stated to have been

propane, but the number quoted for the vapor pressure of the liquid (30 atm)

at the stated operating temperature (64°C) differs from that of pure pro-

pane (23.7 atm) by about 32%. In deriving the numbers given in Table 5,

we have assumed that the quoted operating temperature is incorrect, and

should be 77.3°C, since the context of the paper makes it clear that the

figure of 30 atm is correct. Another possibility is that the liquid actu-

ally used was severely contaminated with a lower paraffin such as ethane.

In such a case, we can only hope that, in view of the law of corresponding

states between normal paraffins, the numbers used herein would still retain

some validity. Group 5 contains data from Pless and Plano (65). The chamber used here was a negative pressure chamber, and represents something of an extreme operating condition. Therefore it should present an interesting comparison with the other data. Unfortunately the authors quote no bubble density figures so the number n is a rough estimate based upon some of the pictures shown. The final group of numbers is taken from our work with the small WF_6 chamber. The bubble density is approximate only, and the expanded pressure P_H is very uncertain, since this chamber suffered from acute boiling. It is possible that the actual value of P_H was very much higher than that given in Table 5.

In spite of the various uncertainties in values listed, it is evident that the quantity W is smaller than the minimum δ-ray energy by an order of magnitude or greater. This striking discrepancy is the subject of the discussion which follows.

3. Behavior of Stopping δ-rays

Since we are here assuming that bubbles are created by stopping δ-ray electrons, it is pertinent to consider briefly the behavior of these particles. Extensive experimental studies have been conducted upon the range of low energy electrons in aluminum and some work has been done in a cloud chamber (66) on the behavior of these particles in the energy range of 16 Kev. One expects for electrons of this low energy that multiple Coulomb scattering and statistical energy straggling would be very important, and such is found to be the case. For 16 Kev electrons, the average range is found to be about $\frac{1}{2}$ the average path length. Even at this energy, the standard deviation in the path length itself due to statistical fluctuations in the energy loss process amounts to about $\pm$ 22%. Multiple

scattering, which should be even more important for lower energy electrons, has such an additional effect that the actual ranges of the electrons are almost uniformly distributed with a 3 to 1 variation. Katz and Penfold (67) have made a compilation of the experimental data on ranges of electrons versus energy in aluminum, and have fitted the results with an empirical relation which works well down to the lowest measured energies (10 Kev). "Range" as used here is called the "extrapolated" range, and is, approximately, the thickness of material beyond which only a few ($\sim$ 10) percent of the electrons of a given incident energy will penetrate. To the accuracy we require, we may take it as the maximum range of the electrons, while remembering that most electrons of the same energy have shorter ranges than this. Since the actual motion of the stopping electrons is exceedingly complicated, the "range" can be but a semi-quantitative measure at the very best. Thus we have simply continued the empirical relation of Katz and Penfold to lower energies ($\sim$ 1 Kv), even though there is no obvious theoretical justification for doing so. Employing this relation adapted to propane and hydrogen, we then find the (maximum) range of a 2 Kev electron in propane to be about 8×10^{-6} cm, and that of a 400 ev electron in hydrogen to be around 0.7×10^{-6} cm. As can be seen from Table 5, these numbers are comparable with the value of $2 R_c$. Considering that the above are essentially the maximum values of the range of the δ-ray, it seems safe to conclude that the majority of δ-rays of these energies deposit most of their energy within a sphere comparable in size to that of the critical bubble. This energy is, as has been stated, many times that which is adiabatically required, so the question we might ask is why the bubble formatio is so inefficient.

4. Proposed Mechanisms and Calculation of Liquid Parameters

There have been several attempts by various investigators to analyse the underlying mechanism. The viewpoints have been (recently) essentially two. One (45-49) holds that vacancies of critical radius are formed by the ions created during the passage of the charged particle (in particular by the stopping δ-ray). In this mechanism the energy for the formation of a cavity comes from the expansion of the cluster of ions. The other proposal, made by Seitz (50), assumes that the bubble is formed by the explosion of a strictly thermal "spike" left by the δ-ray, and that the energy discrepancy is explained through the inclusion of dynamical factors into the growth process. That is, the bubble formation must be accomplished before the thermal spike is dissipated into the surrounding fluid, and this time proves to be so short that the bubble must be formed in a highly inefficient, irreversible manner. We have investigated quantitatively an alternative mechanism involving the temporary "storage" of the energy in non-thermal processes, and these results are given below.

In attempting to evaluate the validity of these mechanisms, we will find it necessary to have available some estimates of parameters such as the liquid viscosity, diffusivity and mobility of ions in the liquid. Probably, in attempting to explain the mechanism of bubble formation, one would do well to confine attention to the simpler, more elementary liquids such as H_2 or He. However, considerably more data with respect to bubble density is available on hydrocarbons, so the following discussion is restricted to them.

The liquid state is, in general, the most complicated of the states of matter, and as yet only a little progress has been made in treating

its equation of state from a theoretical standpoint. However, there exist both empirical relations and semi-theoretical ones relating to such properties as viscosity. One such relation, of a purely empirical nature, is the approximate equation first proposed by Batchinski (68)

$$\eta = A/(v - b) \qquad (II-1-29)$$

where η = viscosity, $v = 1/\rho_\ell$ = volume per unit mass of liquid, and A and b are empirical numbers nearly independent of temperature and pressure. It turns out that b is comparable to the "molecular volume" constant in Van der Waals equation, so $v - b$ represents, approximately, the "free" volume of the liquid. But regardless of physical meanings attached to this relation, we may regard it as a two parameter equation, to be fitted empirically. Fortunately some data exists in the literature (69) on the viscosities of various paraffins at lower temperatures. From this information, plus the known dependence of density on temperature and pressure, we are able to estimate η at the bubble chamber operating conditions. Alternatively, we may employ a relation proposed by Frenkel (70), among others, on theoretical grounds, which seems to fit experimental data fairly well. This relation is

$$\eta = (6kT\tau_0/\delta^3)e^{E/kT} \qquad (II-1-30)$$

where k = Boltzman's constant, δ = mean distance between adjacent molecules, τ_0 = vibration period of a molecule and E = activation energy per molecule. Now E may be expected to decrease as the "free volume" of the liquid increases, so to account for this we may expand E into powers of the temperature and pressure, as $E = E_0 - a_1 T + a_2 P +$ higher terms. If we retain only the linear terms, and collect the constants, we find

$$\eta \approx [C_1 T/v] \exp[(C_2/T) + (C_3 P/T)] \qquad (II-1-31)$$

where we have set $\delta^3 = $ (Const.)(v), where v is the specific volume of the fluid, and C_1, C_2, and C_3 may be considered as empirical constants. This equation may also be fitted to the known lower temperature data, and a number for η at higher temperatures found. The above two relations give quite comparable answers, equation II-1-31 giving a number about 30% higher than equation II-1-29. We have, somewhat arbitrarily, chosen a number between these two, and in the subsequent discussion, will assume the number $\eta = 0.08$ cp for propane at 55.5°C and pentane at 155°C.

The computation of the mobility and diffusion coefficients is somewhat more dubious. In the discussion which follows, an attempt is made to estimate the order of magnitude of such quantities as the mobility of ions and their recombination coefficients. Because of the almost complete lack of experiments bearing upon the mobilities of ions in liquids, particularly in such conditions of high temperatures and pressures as those encountered in bubble chambers, the numbers obtained here must be considered as semi-quantitative guesses. Some theoretical expressions are employed, but there appears to be no data which can either refute or substantiate them in the case of liquids.

For the case of an ideal gas, it is well known (57) that the diffusion coefficient D_s is related to the viscosity η, approximately as

$$\eta = \rho_v D_s \qquad \text{(II-1-32)}$$

where ρ_v is the density of the gas. Both for liquids and gases, we assume the relation due to Einstein,

$$\mu = D_s / kT \qquad \text{(II-1-32a)}$$

where μ is the mobility of a molecule, defined as the drift velocity under

the influence of unit force.* The combination of the above two equations

leads to

$$\mu = \eta / \rho_v kT \tag{II-1-33}$$

or that the mobility is proportional to the viscosity. However, for liquids

at temperatures and pressures not too high, Frenkel (70) suggests

$$\mu = 1/\eta \delta \tag{II-1-34}$$

where δ is the mean distance between adjacent molecules. Equation II-1-34,

of course, gives the opposite dependence of μ on η. Both expressions may

be approximately valid in the proper region, but difficulty is met in the

application of either of them to the liquids (near the critical point) used

in bubble chambers which are almost "gas-like." For propane at 55.5°C,

equation II-1-34 yields $\mu = 2.2 \times 10^{10}$ sec/gm, while expression II-1-33

gives $\mu = 4.4 \times 10^{10}$ sec/gm. One can, however, estimate the value of μ in

a different way. One may assume that the fluid acts as a highly compressed

gas, and calculate μ directly from the gas expression (71)

$$\mu = \bar{v} \ell / 3kT \tag{II-1-35}$$

where $\bar{v}$ is the arithmetic mean thermal molecular velocity, and ℓ is the

mean free path. If we take $\ell = \delta$, and $\bar{v} = \sqrt{8kT/\pi m}$ where m is the

mass of a molecule, we find, for propane, $\bar{v} = 3.97 \times 10^4$ cm/sec, $\ell = \delta = 5.68 \times 10^{-8}$ cm, $kT = 4.53 \times 10^{-14}$, and $\mu = 1.66 \times 10^{10}$ sec/gm. The

numbers obtained above for mobility are all quite comparable, and since

the validity of the following arguments depends to some extent on a large

---

* Note that this definition of mobility is not the same as that conventionally employed for ionic mobility in gases. The latter is defined as $\mu_I = v_d/E$ where v_d is the drift velocity under the influence of an electric field E. Since, in addition, E is usually expressed in practical volts per cm and v_d in cm/sec, our definition differs from the conventional one by the charge on the ion and some numerical factors for conversion of units. Numerically, $\mu_I = 1.6 \times 10^{-12}\mu$, where we have assumed unit charge per ion.

value for μ, we shall assume a number which is a lower limit to the previous calculations. Hence we will employ $\mu \sim 10^{10}$ sec/gm, yielding $D_s \sim 0.5 \times 10^{-3}$ cm²/sec for the following "order of magnitude" calculations. Note that D_s is within a factor of 4 of D, the thermal diffusivity, given in Table 4.

5. Charge Cluster Theories

Now we are in a position to investigate the probable validity of some of the bubble formation models which have been proposed. One simple model was that first proposed by Glaser (72). In this hypothesis, the critical radius of the bubble is to be modified by the action of charges "lodged" in the walls of the bubble, and is not that given by equation II-1-1. It is clear that a single charge in the center of a bubble will tend only to collapse it, for the dielectric constant of the liquid is greater than that of the vapor. However, if one allows the existence of a number of like charges on the walls of the bubble (or an excess of one sign, which is equivalent), one can show that the resultant condition for a stable bubble of radius of R_0 is modified. The electrical "pressure" P_e on the walls of the bubble is given by (electrostatic cgs units)

$$P_e = N(N - 1)e^2/8\pi \epsilon R_0^4 \qquad (II-1-36)$$

where N = number of excess charges of like sign, ϵ = relative dielectric constant of liquid, and we have assumed we may treat the charges as though spread out uniformly over the walls of the bubble (except for removal of the "self-action" by the term N-1). Then we may define a stable bubble of radius R_0 as that for which the differential pressure across the walls is zero, or $P_e \neq P_v = P_\sigma \neq P_H$ where the subscripts v, σ, and H stand for vapor, surface tension, and hydrostatic, respectively. If we now employ

the expression $P_{\sigma} = 2\sigma/R_0$, and combine with equation II-1-36, we obtain

$$N(N - 1)e^2/8\pi\epsilon R_0^4 - (2\sigma/R_0) / (P_v - P_H) = 0 \qquad \text{(II-1-37)}$$

The above equation has two real solutions for certain values of the constants. We wish the solution for minimum N, such that the quantity on the left is positive for $R > R_0$ (that is, the bubble will expand freely for $R > R_0$). This solution is that for which the derivative with respect to R_0 of the expression on the left is also zero. Omitting the algebraic details, we find

$$R_0 = 3\sigma/2(P_v - P_H) \qquad \text{(II-1-38)}$$

and

$$N(N - 1) = 4\pi\epsilon R_0^3 \sigma/e^2 = 27\pi\epsilon\sigma^4/2e^2(P_v - P_H)^3 \quad \text{(II-1-39}$$

Employing these relations for a typical case in propane (group 2, Table 5) we find $R_0 = 5.91 \times 10^{-7}$cm; $N(N - 1) = 62.3$, $N \approx 8.4$. This theory is, then, a "static" model, in which the bubble is assumed to be created by the mechanical work done in the expansion of the charged sphere. However, there are several serious difficulties with this model. Even if we are allowed to assume the comparatively improbable distribution of ions described above, we must ensure that they remain near the bubble wall. Obviously the latter must expand at least as rapidly as the ions would disperse away from the center of the bubble under the influence of their electric field, or else one could not expect them to stay "lodged" in the wall of the bubble. Suppose we consider this charged sphere to be immersed in the liquid, and let us compute the time required for the ions to move from the center of the bubble to a distance R. The velocity of an ion is given by $F\mu$, where F is the force applied, μ is the mobility, and $F = (N - 1)e^2/2\epsilon R^2$. Then the time required is $t = \int_0^r dR/F\mu = 2\epsilon R^3/3\mu(N - 1)e^2$. If we now put in

the number computed for μ and set $R = R_0$, we find $t \approx 8 \times 10^{-12}$ sec. Such

an extremely short time implies an average wall velocity of $\sim 0.8 \times 10^5$ cm/sec,

about twice the velocity of sound in propane.* A wall expansion velocity

of this magnitude would certainly require very large energies (probably con-

siderably greater than that contained in a δ-ray), and would clearly allow

no time for the cavity to fill with vapor in the "static" model. Further-

more, we may make another calculation which casts additional doubt upon any

such charge cluster model. We assume the recombination coefficient ρ_c of

the ions produced is given (71) approximately by $\rho_c = 4\pi e^2 (\mu^+ \neq \mu^-)$,

where the plus and minus signs refer to positive and negative ions, respec-

tively. If we assume that $\mu^+ = \mu^- = \mu$, we have $\rho_c = 8\pi e^2 \mu \sim 0.5 \times 10^{-7}$

for propane. To calculate the recombination time, we estimate the total

number of ion pairs produced by a 1200 ev δ-ray as ~ 1200 ev/(30 ev/ion

pair) $= 40$ ion pairs. We assume they are distributed uniformly through a

spherical volume of diameter roughly equal to the range of the δ-ray, about

2×10^{-6} cm. This yields a number of ion pairs per unit volume $n \sim 10^{19}$

ions/cm^3. The recombination rate dn/dt is then given by $\rho_c n^2 = 0.5 \times 10^{31}$.

The half-life of the ions is given by $\tau_r = 1/\rho_c n \approx 2 \times 10^{-12}$ sec, even

shorter than the dispersion time calculated before. Of course, the above

number could be in error for several reasons other than the rough estimate

used for the mobility. If there is no electron attachment or many of the

positive ions are free protons rather than charged propane molecules,

---

* Since the concept of mobility depends on the assumption that the
drift velocity is small compared to the thermal velocity, it is clear that
here our use of a constant mobility is not justified. The same comment
probably applies to the ion recombination calculation made later. However,
since this is intended to be an order of magnitude estimate, and for lack
of a better criterion, we will ignore the dependence of mobility upon vel-
ocity. Our estimate for mobility is probably too crude to justify consid-
eration of fine points.

mobilities will be higher than estimated above, and recombination times subsequently shorter.* However, if there exists a "clustering" of neutral atoms about an ion as is evidenced in some gas ionization processes (71), the mobilities will be lower than calculated and recombination will take longer. On the other hand, we have made the above calculation assuming that the ions were uniformly distributed over a fairly large volume rather than concentrated more closely along the path of the δ-ray as is probably more nearly true. Therefore it is possible that recombination will occur in times comparable to the above even in the case of clustering and electron attachment. At any rate, it appears reasonable to conclude that any ionic charge distribution created by a stopping δ-ray will be "thermalized" by dispersion or by recombination in times within an order of magnitude of 10^{-12} sec. There are more detailed theories of bubble formation based upon the charge cluster model (45-49), but we believe that in view of the above conclusion, any such mechanisms are of doubtful validity, and we shall not consider them further.

6. Thermal Spike Theory

We are thus led to the viewpoint proposed by Seitz, in that most of the energy of the δ-ray appears essentially immediately in the form of heat along the path of the stopping particle. An analysis is made by Seitz (50) following this reasoning, to attempt to determine the requirements upon the rate of expansion of the bubble and the energy required in the process. Since the details of this investigation are carefully described

---

* Calculations made by Samuel and Magee (73) indicate that in the passage of charged particles through water, ionic recombination takes place in times of the order of 10^{-13} sec because of electron mobility. Remaining are H and OH (uncharged) radicals, which recombine in times of the order of 10^{-7} sec (74).

in his paper, we wish here only to repeat some of the more pertinent arguments and some of the results. Seitz has analysed both the hydrogen and propane cases, but here we confine our attention, as before, to the hydrocarbons.

One of the crucial factors is the time required for the fluid to dissipate a thermal "spike" left by the δ-ray. The relaxation time for a point heat source over a sphere of radius R_c is given by

$$t_c = R_c^2/4D \qquad (II-1-40)$$

and Seitz takes this as the time in which a bubble must grow to the critical radius R_c if the necessary thermal energy is not to be lost by conduction. Using the numbers in group 1 of Table 5, we find $t_c = 0.93 \times 10^{-10}$ sec. Using the criterion that the bubble walls must expand from the initial spike to radius R_c in time t_c, Seitz then derives an equation of motion for the bubble walls, using the approximation of incompressible fluid flow. He assumes the initial thermal energy is contained in a sphere of volume equal to $2R_c$ (roughly the range of the δ-ray) times the mean molecular area, and assumes the pressure of the vapor it contains is proportional to the energy content per unit volume, in the manner of a perfect gas. Since one would expect the expanding sphere of gas to do a large amount of work against the inertia of the fluid around it, he finds it possible to use the adiabatic pressure law $PV^{\Upsilon} = P_0 V_0^{\Upsilon}$, where $\Upsilon = c_p/c_v$, the ratio of specific heats at constant pressure and volume, respectively. He thus also neglects the conductive heat losses out of the expanding sphere. Using these assumptions, Seitz finds, for propane, the following approximate expressions for the energy of the thermal spike E_1.

$$E_1 = \nu\,(3\rho/2)\,[2/(3\Upsilon+2)]^2\,(R_c/t_c)^2\,(R_c/R_0)^{3(\Upsilon-1)}V_c \qquad (II-1-41)$$

where $V_c = 4\pi R_c^3/3 =$ volume of critical bubble; $V_o =$ volume of initial thermal spike; $R_o =$ radius of initial thermal spike; $\rho_\ell =$ density of the liquid; and $\nu = C_v/R_g$, where R_g is the gas constant per gram, ν taken $= 15$ for propane, and also

$$E_1 = \nu (2/25) \left[1/\log(R_c/R_o)\right] (R_c/t_c)^2 \rho_\ell V_c \qquad \text{(II-1-42)}$$

The first equation (II-1-41) is obtained by neglecting the terms in the equation of motion involving $\partial^2 R/\partial t^2$, the second (II-1-42) is obtained by using an approximation valid if Υ is close to unity as it is for propane, and including the $\ddot{R}$ terms. Now if we employ Seitz's numbers of $\Upsilon = 1.05$, $\nu = 15$, $R_o = 1.233 \times 10^{-7}$ cm, and the numbers taken from Table 5 for R_c and t_c, we find the following values. For equation II-1-41, $E_1 = 2.64 \times 10^{-10}$ ergs $= 165$ ev; and for equation II-1-42, $E_1 = 0.381 \times 10^{-10}$ ergs $= 23.8$ ev. The results in both cases are lower than the empirical value of E_1 (~ 1800 ev) by more than an order of magnitude.* The preceding equations, of course, were derived neglecting the effect of viscosity of the liquid. Seitz also derives an expression for E_1 in which the fluid flow resistance arising from viscosity is considered the dominant term, such that inertial effects are small in comparison. His result is

$$E_1 = \nu (\eta/t_c)(4/3\Upsilon)(R_c/R_o)^{3(\Upsilon-1)} V_c \qquad \text{(II-1-43)}$$

where η is the viscosity of the fluid. Using the same numbers as before and the value for η which we have derived $= 0.8 \times 10^{-3}$ poise, we find

$$E_1 = 4.44 \times 10^{-10} \text{ ergs} = 277 \text{ ev.}$$

---

* It should be remarked here that although we have not calculated the analagous numbers for hydrogen, Seitz does so in his paper. He finds the same general results as for propane. That is, the theoretical values for E_1 are an order of magnitude smaller than the empirical ones.

This number is higher than the ones previously obtained, but still low by almost an order of magnitude. In Seitz's paper, he obtains a much larger number for this case because he uses a value for $\eta = 10^{-2}$ poise. We believe, however, that our number of 0.8×10^{-3} poise is much nearer to the correct value.

Because of the large difference between the number we have calculated above and the one obtained by Seitz, the subject of the viscosity effect merits further discussion. The layer of fluid surrounding the bubble is subject to large pressures and temperatures, both of which influence the value of viscosity, so it is difficult to estimate the effective value for η. Our number was calculated to include the effect of the vapor pressure, and if the viscosity is essentially a function of the free volume (and thus the density) of the liquid, it seems quite improbable that the action of any additional pressure of the expanding sphere could so compress the propane that the density is increased some 70%, which would be necessary to raise its viscosity even to the boiling point value (about 2×10^{-3} poise). This is especially true in view of the fact that the same liquid layer is heated quite significantly both by conduction from the hot bubble and by the effect of the viscosity itself. More specifically we note, as does Seitz in his paper, that an expanding sphere in an incompressible viscous fluid creates a radial compressive stress P_r in the surrounding fluid (which we may consider a retarding pressure) of value

$$P_r = -4\eta R^2 \dot{R}/r^3 \qquad \text{(II-1-44)}$$

where R is the radius of the sphere, and r is the radial coordinate taken from the center of the sphere. The retarding pressure felt by the sphere

is this function evaluated at $r = R$ or $P_R = -4\eta \dot{R}/R$, and the rate of work done by the expanding bubble is

$$\dot{W}_R = -P_R^\prime \dot{V}_R = -4\pi R^2 P_R \dot{R} = 16\pi \eta R \dot{R}^2 \qquad (II-1-45)$$

This work appears as heat in the surrounding fluid, and we ask how it is distributed in the external medium. The answer may be obtained from equation II-1-44 if we differentiate with respect to r, and multiply by $\dot{V}/4\pi r^2$ to obtain $\dot{w}$, the rate of work per unit volume of the surrounding fluid. The result is $\dot{w} = 12\eta R^4 \dot{R}^2/r^6$, or in view of equation II-1-45,

$$\dot{w} = \dot{W}_R (3R^3/4\pi r^6) \qquad (II-1-46)$$

Note that the energy dissipation per unit volume falls off very rapidly with radius, so we expect the liquid in the immediate vicinity of the bubble, where the retarding effect of viscosity is most pronounced, to become hotter. To illustrate, we estimate the temperature rise of the fluid adjacent to the bubble wall when the bubble has expanded to radius R_c. Setting $r = R = R_c$ in equation II-1-46 and replacing $\dot{W}_R$ by $\int_0^{tc.} \dot{W}_R dt \equiv W_R$, we find the energy per unit volume w to be $w = W_R/V_c$, and the temperature rise $= w/c_\ell \rho_\ell$, where $c_\ell \rho_\ell \approx 10^7$ ergs/cm^3. We thus have

$$\Delta T = W_R/V_c c_\ell \rho_\ell \qquad (II-1-47)$$

Now if we employ the number we have obtained from expression II-1-43, $W_R = E_1 = 4.44 \times 10^{-10}$ ergs, $V_c = 2.05 \times 10^{-18}$ cm^3, we find $\Delta T \sim 21^\circ$C, large enough to reduce the viscosity, but probably not significantly considering the approximate nature of the calculation. On the other hand, if the effect of the viscosity is much larger, as Seitz assumes, so that $W_R \sim$ energy of δ-ray $\sim 3 \times 10^{-9}$ ergs, then ΔT above becomes $\sim 150^\circ$C, which raises the temperature of the fluid $\sim 100^\circ$ higher than the critical point! It would appear that it is impossible to attribute the inefficiency of bubble

formation entirely to viscosity. The temperature rise alone should see to it that the viscosity stays low in the vicinity of the bubble.

As Seitz himself has stated, the problem of bubble formation is a complex one, and his analysis is, by necessity, quite approximate. Therefore, we can place only limited stress upon the fact that the numbers obtained are in serious disagreement with experiment. Most of the points made by Seitz are certainly pertinent, and the approach used is very probably in the right direction. However, the order of magnitude disagreement between observed and calculated values of E_1 leads one to suspect that some fundamental effect has been neglected which is in fact quite important. It is the purpose of the following to attempt to discover where such an effect may lie.

7. Energy Storage Effect

If it is possible, as is discussed later, that a portion of the energy is actually stored in the fluid by non-thermal processes (such as ion pairs, dissolution of chemical bonds, etc.), then another attack may be attempted. We assume, for simplicity, that all of the δ-ray energy is stored initially at a point then released thermally with an exponential time constant τ. Since the following analysis does not appear to explain the dominant bubble forming mechanism, the calculation is given in outline form, omitting many details.

The Green's function solution for a spherically symmetric, distributed source of heat in a homogeneous medium of thermal diffusivity D is given by

$$H(r,t) = (1/2r\sqrt{\pi D}) \int_0^t (1/\sqrt{t-t'}) \int_0^\infty r'h(r',t') \qquad \text{(II-1-48)}$$

$$\left\{ \exp[-(r-r')^2/4D(t-t')] - \exp[-(r+r')^2/4D(t-t')] \right\} dr'dt'$$

where $\dot{h}(r',t')$ is the rate of production of heat per unit volume and $H(r,t)$ is the heat contained in the medium per unit volume. Since the carriers of stored energy may be expected to diffuse outward from the point source at the origin with a diffusivity D_s, we may write

$$\dot{h} = (E/\tau)(1/2\sqrt{\pi t' D_s})^3 \, e^{-(t'/\tau)} \, e^{-(r')^2/4t' D_s} \qquad (II-1-49)$$

where E is the total energy contained in the original deposit. If equations II-1-49 and II-1-48 are combined, the integral over r' may be performed explicitly. The result is

$$H(r,t) = E/8\tau\pi^{3/2} \int_0^t \left\{ 1/[(t - t')D + t' D_s] \right\}^{3/2}$$

$$e^{-t'/\tau} \, e^{-r^2/4[(t - t')D + t' D_s]} dt' \qquad (II-1-50)$$

If now we wish to find the heat, Λ, contained within a radius R at time t, we may multiply the above by $4\pi r^2 dr$ and integrate from 0 to R, obtaining

$$\Lambda(R,t) = (E/\tau\sqrt{\pi}) \int_0^t e^{-t'/\tau} \left\{ \sqrt{\pi}\, \text{erf}[R/2\sqrt{(t - t')D + t' D_s}] \right.$$

$$\left. - [R/\sqrt{(t' - t)D + t' D_s}] e^{-R^2/4[(t - t')D + t' D_s]} \right\} dt' \qquad (II-1-51)$$

We would like to maximize the above expression and find the value for τ required to make $\Lambda(R,t)$ (maximum) a small fraction of E. This is extremely difficult in general but in the special case $D = D_s$, it can be done. We note that this approximation may not be too bad, since we have calculated the diffusion coefficient for molecules in section C-4 and found it close to the thermal diffusivity. With this simplification, the integration in equation II-1-51 may be performed explicitly, resulting in

$$\Lambda(\alpha,\beta) = (2E/\sqrt{\pi})(1 - e^{-\beta}) [(\sqrt{\pi}/2)\, \text{erf}(\alpha) - \alpha e^{-\alpha^2}] \qquad (II-1-52)$$

where $\beta = t/\tau$; $\alpha = R/2\sqrt{tD}$. Equation II-1-52 may be differentiated with respect to time and solved numerically to obtain the maximum value of Λ. The result can be approximated by the function

$$[\Lambda/E]_{max} \doteq \lambda \approx A[R_c^2/4\tau D]^B \qquad (II\text{-}1\text{-}53)$$

where A = 0.340, B = 0.920 for $0.01 < \lambda < 0.16$ and A = 0.2865, B = 0.706 for $0.16 < \lambda < 0.5$.

If we employ a value for D of 10^{-3} cm^2/sec, which is between the values of thermal diffusivity and D_s calculated in section C-4, we may compare the predictions of the above with the experimental data in Table 5. If we take for λ simply the ratio between W and E_1 in Table 5, we find that the experimental bubble density is obtained for values of τ of 4×10^{-10} sec, 4.9×10^{-10} sec, and 5.5×10^{-10} sec respectively in the cases of the last three entries in group 3. It is difficult to see physically where a mechanism might exist for storing energies with a release time of this order. The calculation of ionic recombination made earlier indicates thermalization times two orders of magnitude shorter than this. (Chemical processes, as discussed later, would be expected to have much longer decay times than 10^{-10} sec.) Of course, the inclusion of dynamical factors in the formation process could raise the value of λ, perhaps by as much as a factor of two or three, decreasing τ a factor of three or four to $\sim 10^{-10}$ sec. This, however, is not nearly enough to bring it sufficiently close to the estimated ion recombination time to be encouraging. In order for the above mechanism to play an important role in bubble formation, either our ion recombination estimate must be in error about two orders of magnitude, or else another energy storage mechanism must be found.

Energy storage may, however, have an influence on bubble nucleation in another way. In a compound such as propane, the production of ions by a stopping δ-ray results in chemical decomposition of the molecules (75). Although the disassociation products participate thermally almost

immediately, the energy required to break the chemical bonds is probably a permanent loss as far as bubble formation is concerned. One would expect chemical recombination to take very much longer than $10^{-10} - 10^{-11}$ seconds (74,75). The energy "storage" (or loss) is found to be as high as 60% of the total energy produced by stopping particles in a substance such as water (74), and may be comparable to this in a hydrocarbon. The process helps substantially to reduce the energy discrepancy which must be accounted for in the case of liquids with polyatomic molecules. Chemical effects such as the above, however, can hardly help explain bubble formation in such liquids as xenon and helium.

8. Effect of Heat Loss

Another phenomenon which we may investigate is the actual heat loss arising from thermal conduction during the formation of the bubble. This was neglected in Seitz's treatment, but it is possible that it presents a not negligible loss. The actual heat conduction problem is very difficult because of the (perhaps unknown) behavior of the expanding bubble walls, and the variation of thermal conductivity, heat capacity, and density in the region of the bubble. One attempt at a solution could be that due to Zwick and Plesset, equation II-1-15, but its application here is difficult, and of doubtful validity. For lack of a better estimate, we will use the well known solution for a point source of heat in a homogeneous medium, which can be obtained from equation II-1-52 by letting $\tau \rightarrow 0$, or $\beta \rightarrow \infty$. The result, expressed as total heat contained in a volume of radius R as a function of time, is

$$\Lambda(R,t) = E\left[\text{erf}(\alpha) - (2\alpha/\sqrt{\pi})e^{-\alpha^2}\right]$$

Now the time t_c required for a bubble to expand to radius R_c in Seitz's

analysis was such that $\alpha = R/2\sqrt{Dt}_c = 1$. In this case, we have $\Lambda(\alpha = 1)$ = 0.428 E. Therefore if such a crude heat flow estimate has any meaning, we might expect to lose over half of the heat by conduction in the time required for the bubble to expand to radius R_c. It is not obvious whether a better heat flow solution would yield numbers higher or lower than the above, but it seems clear that this source of energy loss could be an important one.

9. Other Considerations

Yet another point which may be important concerns the velocity of the expanding bubble wall. We observe that the order of magnitude of the wall velocity in Seitz's treatment is given by R_c/t_c. For the propane case we are considering, this corresponds to a velocity of $7.88 \times 10^{-7}/0.93 \times 10^{-10} = 0.847 \times 10^4$ cm/sec. Since, by the nature of the expanding ball of hot gas, the wall velocity is probably not at all constant, we would expect it to be considerably higher than the value quoted over part of the expansion. Seitz estimated the velocity of sound in propane in his analysis, and found it to be a factor of 15 higher than the number above, hence the use of the incompressible fluid flow approximation. However, the number he used for the compressibility of propane was 100×10^{-12} cm^2/dyne. We have found while using propane in our bubble chamber that the actual compressibility at the operating temperature is more than a factor of ten larger than the above number, or about 1200×10^{-12} cm^2/dyne. Using our number, we compute the velocity of sound in propane as $v_a = $ (1/density·compressibility)$^{\frac{1}{2}} \approx 4.5 \times 10^4$ cm/sec. This number is on the order of only a factor of five greater than the "average" wall velocity, so it is possible that the incompressible fluid flow approximation may be in serious

error during part of the bubble expansion. Any effect of the finite velocity of sound which delays the expansion will, of course, make the loss of heat by conduction more important.

There are other points which can be considered, although their interpretation is a bit more obscure. For example, it seems fairly certain that the maximum range of the threshold δ-ray as calculated previously is actually greater than the diameter of the critical bubble. Thus it would appear that such a particle does not have a 100% chance of localizing its energy in a sufficiently small region, but rather a smaller value. The same consideration, of course, applies to δ-rays of greater energy. Therefore we would have to include δ-rays of lower energies to obtain agreement with the experimental data, with a consequent reduction of the threshold energy E_1. However, it is doubtful if this effect could lower E_1 a factor of two, since the range falls off so rapidly with energy that δ-rays of this lower value have essentially unity probability of localizing their energy, and there are twice as many of them.

Also, all through the preceding discussion it has been tacitly assumed that the processes take place with spherical symmetry. Actually this is not at all true, as the most likely configuration for an initiating thermal spike is that of a rather coiled, distorted cylinder. What effect this has is not obvious, but it seems certain to initiate some form of non-spherical oscillation as the surface tension acts to shape the vapor region into a sphere. As a result there could be effects upon the average rate of expansion of the walls.

Another assumption has been that the region contains a sufficient number of particles so that the usual results of thermodynamics and

statistical mechanics are applicable. For the worst case listed in Table 5, that of the last entry in group 4, the critical volume contains about 10^3 molecules in the liquid state, but only about 200 in the vapor phase. This is a region in which we may be justified in questioning seriously the applicability of macroscopic statistical laws, especially with regard to the action of the surface tension. The capillary layer in this case becomes comparable in thickness to the bubble radius, so that the definition of R_c may become incorrect or obscure.

10. Functional Dependence of Bubble Density

We would like to close this discussion with some remarks concerning the apparent dependence of bubble density upon the chamber operating parameters. We note from the data in group 3 that there appears to be a sharp threshold for forming bubbles as the expanded pressure is changed. After the sharp threshold is passed, the bubble density appears to increase only slowly with further reduction of the expanded pressure. The data in group 4 show a very strong dependence of bubble density upon expanded pressure, and we are led to believe that the data was taken over a region comparable to the "threshold" noted in group 3. If we examine the expressions II-1-41, 42, and 43 taken from Seitz's analysis, and recall that $t_c \sim R_c^2$ and $V_c \sim R_c^3$ and that (for hydrocarbons), Υ is close to unity and thus $\Upsilon - 1$ is very small, we observe that all three expressions for E_1 are essentially directly proportional to R_c. [Such functions as $(R_c/R_0)^{\Upsilon-1}$ and $\log (R_c/R_0)$ are very weak functions of R_c.] Since E_1, the threshold δ-ray energy, is inversely proportional to the bubble density, we should find that the bubble density goes inversely as R_c. The "energy storage" theory can be seen to give approximately the same prediction, if we note

that $\lambda \sim W/E_1 \sim R_c{}^3 n$ (since the energy required to form a bubble goes roughly $\sim R_c{}^3$). Thus we have $n \sim 1/R_c{}^{1.16}$ for small R_c (large n) and $n \sim 1/R_c{}^{1.488}$ for larger R_c (small n). However, we note in the group 3 data that the "threshold" has a much stronger dependence of bubble density upon R_c than inverse proportionality, while the subsequent values have a markedly weaker one. The data in group 4 also show a dependence stronger than $1/R_c$. A functional dependence similar to $1/R_c$ certainly does not appear to fit the data. Of course, the experimental numbers should be distrusted somewhat for reasons specified earlier, and the theories are quite approximate. Nevertheless, the results are not encouraging. It may be that the process of bubble nucleation must be explained through the combined action of many small effects of comparable importance, in which case the problem looks extremely formidable. Or it may be that we have not yet found the dominant mechanism, or, at least, have not attacked it in a sufficiently quantitative manner.

D. Conclusions

It is pertinent at this point to summarize briefly the results of this chapter. The process of bubble growth in a bubble chamber once the bubbles have attained critical size can be said to be well understood, although somewhat difficult to compute. The samples calculated herein indicate that a practical bubble chamber (at least for hydrocarbons and similar liquids) must be operated so that the expanded pressure is not too low, i.e., in the region of one-half the vapor pressure. Otherwise the bubbles grow too large and too rapidly for accurate location of tracks. The calculations also show that the energy loss caused by track bubbles is quite small for the proper operating conditions.

The mechanism of bubble nucleation, however, is still not fully understood. It is highly probably that δ-rays of energies ~ 1 Kev or greater produce most of the bubbles in a typical particle track, but the reason for this particular energy is not entirely clear. The ionic or "static" model for bubble formation appears untenable in view of ionic mobilities and recombination times. Seitz's theory of thermal explosions caused by δ-rays may be a fundamentally valid concept, but falls short in explaining either the required δ-ray energy or the dependence of bubble density upon bubble chamber operating conditions. An energy storage hypothesis suggested by ourselves also does not predict the proper dependence, and there does not seem to exist an energy storage mechanism with the proper time constant. Other factors discussed herein may explain the required δ-ray energy, but no quantitative formulation exists which predicts the correct bubble density as a function of bubble chamber operating conditions.

Finally, there is a real need for a definitive experiment to determine accurately the bubble density as a function of particle parameters and chamber operating conditions. Present data are inadequate for really conclusive comparison to theory.

ACOUSTICAL TREATMENT OF EXPANSION SYSTEMS

A. Equations of Motion and Solutions

In attempting to find methods to operate very large bubble chambers at high speeds, particularly heavy liquid chambers in which the velocity of sound is small, one may profit by adopting a new approach. The desirability of having high speed expansions and recompressions has been discussed before, and there exists the additional possibility of achieving sufficiently high repetition rates to make counter control of the camera profitable.

One may begin by considering a bubble chamber liquid as a compressible fluid whose boundary conditions are controlled. Then the time required to lower or raise the pressure in the center of the chamber is set by the velocity of transmission of a pressure change initiated at the walls. This is, in general, a very complicated problem, but under certain geometry which may constitute a useful bubble chamber shape, the problem is susceptible to analysis.

Euler's equations of motion for a compressible fluid wherein viscosity is neglected are given by (76)

$$d\underline{v}/dt + (1/\rho)\nabla P = \underline{f} \qquad \text{(II-2-1a)}$$

and the equation of continuity

$$\partial\rho/\partial t + \nabla\cdot(\rho\underline{v}) = 0 \qquad \text{(II-2-1b)}$$

where $\underline{v}$ = velocity of an element of fluid; ρ = density of fluid; P = pressure in fluid; $\underline{f}$ = external force per unit mass of the fluid.

The geometry to which we wish to apply the foregoing equations is that of a uniform cylinder (which may, in fact, be any shape in cross-section) with fixed walls and flat ends. One or both of the ends will be considered to move, acting as a source of plane waves which travel down the cylinder.

This reduces the problem to a one-dimensional one, and is exact in the case of zero viscosity. In a real fluid there are wall effects which interfere with the plane wave approximation, but these will be neglected in this treatment. Note that we are placing no restrictions on the length of the cylinder relative to its lateral dimensions, so that if we imagine the cylinder to be short, with a window at one end and the movable, driving wall at the other, we have a possible bubble chamber geometry.

Under the plane wave approximation, the foregoing vector equations reduce to scalar ones as

$$dv/dt + (1/\rho)\,\partial P/\partial z = 0 \qquad\qquad \text{(II-2-2a)}$$

$$\partial\rho/\partial t + \partial(\rho v)/\partial z = 0 \qquad\qquad \text{(II-2-2b)}$$

where we have set $\underline{f} = 0$ and $v \equiv v_z$, and z is the coordinate parallel to the cylinder walls.

Even with this simplification the equations are difficult to manage because of the total derivative in equation II-2-2a. It would be helpful if we could replace the total derivative with the partial derivative, as is done in acoustics. To see if such a replacement is a good approximation, we must consider a typical bubble chamber pressure wave. For the one dimensional case, the total derivative may be expanded (76) as $dv/dt = \partial v/\partial t + (\partial v/\partial z)(\partial z/\partial t) = \partial v/\partial t + v(\partial v/\partial z)$ and equation II-2-2a becomes

$$\partial v/\partial t + v(\partial v/\partial z) + (1/\rho)(\partial P/\partial z) = 0 \qquad\qquad \text{(II-2-3)}$$

We will now make the same approximations as are made in acoustics, and use the solution to check whether or not the neglected terms are small in a typical bubble chamber case.

We assume a constant compressibility K for the fluid, which is

-183-

a good approximation over a wide range of pressures. Hence

$$\rho \approx \rho_0 [1 + \kappa P] \qquad (II\text{-}2\text{-}4)$$

Using the above, we may rewrite equations II-2-3 and II-2-2b as

$$\partial v/\partial t + (1/\rho_0)\partial P/\partial z = 0 \qquad (II\text{-}2\text{-}5a)$$

$$\kappa \partial P/\partial t + \partial v/\partial z = 0 \qquad (II\text{-}2\text{-}5b)$$

where we have implied

$$|v\,\partial v/\partial z| << |\partial v/\partial t| \qquad (II\text{-}2\text{-}6a)$$

$$|\kappa P| << 1 \qquad (II\text{-}2\text{-}6b)$$

$$|v\,\partial \rho/\partial z| << |\partial \rho/\partial t| \qquad (II\text{-}2\text{-}6c)$$

Equation II-2-6b may be verified immediately, as the maximum value of κP in a bubble chamber is the expansion ratio, which typically is around 2 to 3 percent. In this treatment we shall neglect errors of that order.

If we now differentiate equation II-2-5a with respect to z and equation II-2-5b with respect to t and equate the two, we obtain the familiar wave equation

$$\partial^2 P/\partial t^2 = c^2 \partial^2 P/\partial z^2 \qquad (II\text{-}2\text{-}7)$$

where $c^2 = 1/\rho_0 \kappa$. A plane wave solution which satisfies the above equation is

$$P = P_0 e^{i\omega[(z/c) - t]} \qquad (II\text{-}2\text{-}8a)$$

implying through equations II-2-5a,b that

$$v = (P_0/\rho_0 c)e^{i\omega[(z/c) - t]} \qquad (II\text{-}2\text{-}8b)$$

Application of equations II-2-8a,b directly to the relations II-2-6a and c show that, in both cases, the required condition is

$$v << c \qquad (II\text{-}2\text{-}9)$$

To see if the above criterion is fulfilled in a bubble chamber, we note that the pressure and velocity maxima are related in a plane wave by the

acoustical impedance $\rho_0 c$. That is, independent of the angular frequency ω, we have $v = P/\rho_0 c$ or $v/c = P/\rho_0 c^2 = P\kappa$. As has been remarked, the maximum value of $P\kappa$ is just the expansion ratio of the chamber, which is ~ 2 to 3%. So in using the simple acoustical solutions, we are making an error of only a few percent in a typical bubble chamber, and to the accuracy we require, relations II-1-6a, b, and c are satisfied.

We are now in a position to consider more specific cases in applying the acoustical equations to the expansion of a bubble chamber. These will be listed specifically as separate cases for definiteness.

Case 1. One flat end of the cylinder is a high pressure window, the other end a driven, movable flat wall.

Case 2. One end of the cylinder is a high pressure window, and next to it the sensitive liquid. Farther along the cylinder and containing the sensitive liquid is an undriven, movable thin window. A support fluid then fills the rest of the cylinder and couples to the expansion apparatus.

Case 3. The sensitive fluid in the cylinder is contained on both ends by thin, undriven, movable windows, the remaining part of the cylinder being filled with support fluid. The expansion apparatus may be contained on one or both ends of the sensitive fluid columns.

For clarity, examples of these three arrangements are shown in Fig. 29. For the moment we will not consider the problem of the driving mechanism, and will simply assume that we may force the driving walls to perform any motion we specify. It is evident that plane waves will be reflected to some degree from the interfaces in the models we have listed, so it will be convenient to have first a list of the degree of reflection and transmission in the various cases. These are listed below, and can be

Figure 29
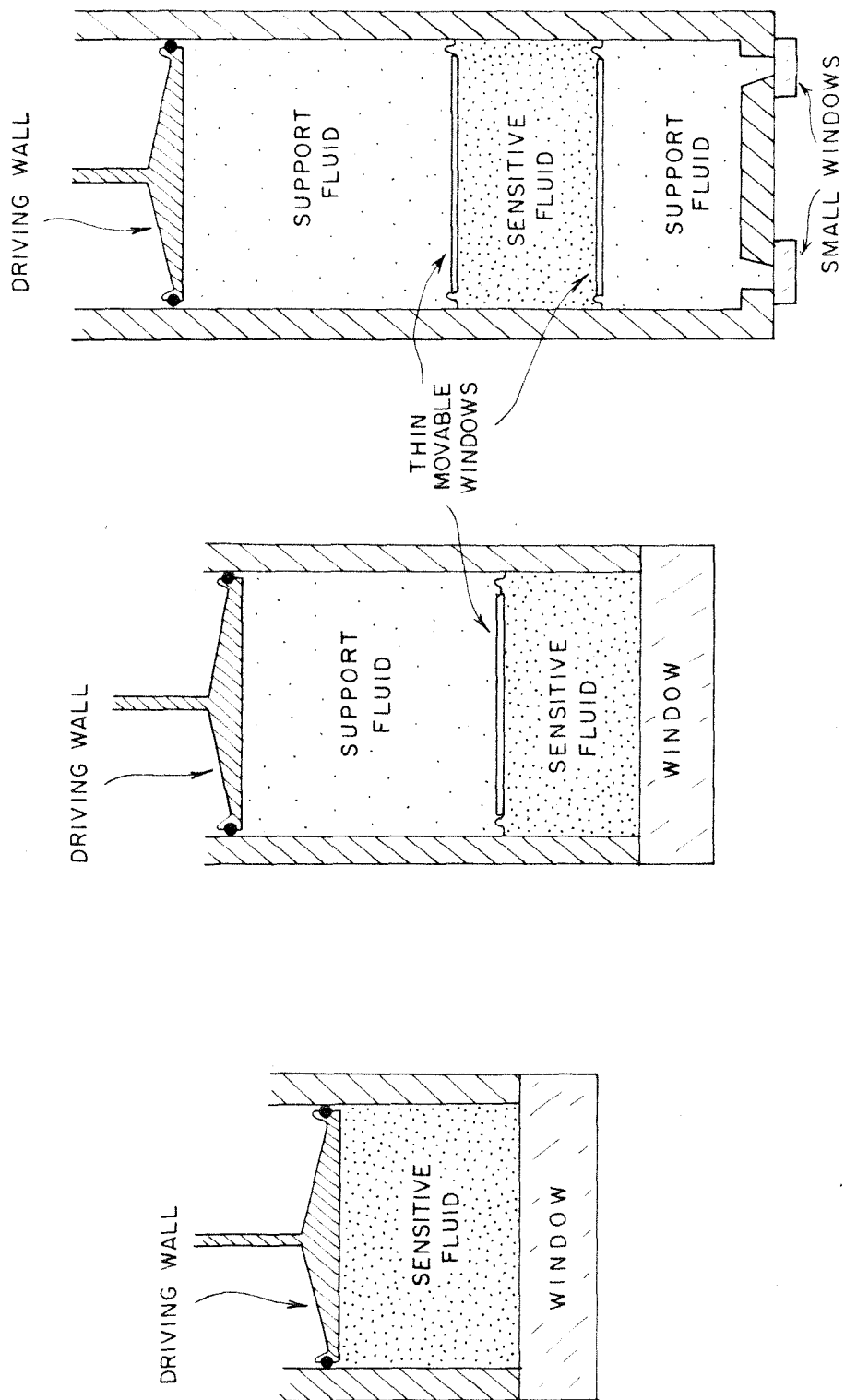
Examples of "Transient" Bubble Chamber Geometry

found by the usual technique of assuming incident, reflected, and transmitted waves of angular frequency ω. Boundary conditions are satisfied at the interface, as well as the equations of motion of the separating plate, if any.

Condition A. A plane wave is incident on an infinitely rigid plate of mass M and area A, attached to the surrounding structure with a stiffness k, where the displacement x and force F required to move the plate define k by F = kx. There is no transmitted wave in this case.

Amplitude of incident pressure wave = P_o

Amplitude of reflected wave = P_o

Phase of reflected wave relative to incident wave at the plate =
$$2 \tan^{-1} \left[A\omega \rho_o c / (k - M\omega^2) \right] \tag{II-2-10}$$

Condition B. A plane wave is incident on a freely movable rigid plate of mass M and area A. On the incident side the fluid has a density ρ_o and sonic velocity c. On the other side the fluid has density ρ_o' and sonic velocity c'.

Amplitude of incident pressure wave = P_o

Amplitude of reflected wave =
$$P_o \sqrt{(1 - r)^2 + \delta^2} / \sqrt{(1 + r)^2 + \delta^2} \tag{II-2-11a}$$
where $r = \rho_o'c'/\rho_o c$; $\delta = \omega M / A \rho_o c$

Amplitude of transmitted wave = $2P_o r / \sqrt{(1 + r)^2 + \delta^2}$ (II-2-11b)

Phase of reflected wave relative to incident wave at interface =
$$-\tan^{-1} \left[\delta / (1 - r) \right] + \tan^{-1} \left[\delta / (1 + r) \right] \tag{II-2-11c}$$

Phase of transmitted wave relative to incident wave at interface =
$$-\tan^{-1} \left[\delta / (1 + r) \right] \tag{II-2-11d}$$

B. Transient Bubble Chambers

We wish first to consider those situations which are suitable for what we will henceforth call a "transient" bubble chamber. By transient is meant that the chamber is pulsed or expanded a single time upon command, as contrasted with what we will henceforth call a "steady-state" bubble chamber. A "steady-state" bubble chamber is one which expands and recompresses continuously at a rate fixed by the time required to expand and recompress once. Most conventional bubble chambers are of the transient type, whereas a steady-state (or free-running) bubble chamber might be the kind which could be employed for camera counter control in conjunction with a high repetition rate accelerator or for cosmic ray study. Case 1 described above is simpler to analyse in the transient case, and illustrates the chief features of this approach to expansion systems. The pertinent point for this geometry is the nature of the sonic reflection from the high pressure window, and for this we need to evaluate the expression II-2-10. We will employ the numbers measured for our high pressure window. We found, approximately, that the window, of a diameter inside the seal of 14 inches, displaces about 0.001 inch per 100 psi of pressure. Therefore the term k/A is given by P/x, and converting to MKS units, we find $k/A = 2.7 \times 10^{10}$. The window itself has a thickness of 4 inches, yielding a mass per unit area $= M/A = 228$ kg/m^2. For a liquid such as propane, $c = 460$ m/s, $\rho_0 \approx 0.4 \times 10^3$ kg/m^3. A typical upper limit for the angular frequency which we will be considering is for $\omega \sim 2000$. These numbers put into expression II-2-10 give a value for the phase shift $\sim 4^0$. This is small enough to neglect, so we may consider the high pressure window as an infinitely rigid wall which reflects incident pressure waves with zero phase

shift, creating a fluid velocity node at the window. It should be remarked that the above is true only if we restrict the angular frequency to values lower than that we have selected. If we consider higher frequencies the phase shift may be quite large. In fact, a frequency some five or six times the one discussed above is the actual resonant frequency of the window. Since we will be including the possibility of high harmonics in the incident wave in our later discussion, it is clear that phase shift may be important. There is no reason, however, why a window could not be mounted much more rigidly than the one on our chamber. In any case, for simplicity we will assume that the window in the model is stiffer than the one on our actual 12 inch chamber, so that we may treat it as a rigid wall even for the higher frequencies.

With the assumptions made above, we may quickly specify the mode of motion of the driving wall to produce the required pressure change in the chamber. The ideal pressure cycle in a bubble chamber is almost a square wave. That is, we would like to drop the pressure rather suddenly to a constant value, keep it there for a short while, and then return it, again abruptly, to its initial value. A pressure wave of this form generated by the driving wall will travel across the chamber, be reflected by the high pressure window so as to double the pressure change in the chamber fluid, and travel back across the chamber. When this wave has returned to the driving wall, the chamber is expanded. Note that the final pressure drop is twice that originally generated by the driving wall. The minimum time to expand the chamber in this case is simply given by 2d/c, where d is the depth of the chamber. The form of motion of the driving wall may be easily found by noting the relationship in a plane wave between the fluid

velocity and pressure, i.e., $v = P/\rho_0 c$. If the chamber is to remain expanded for a short time, the wave must be prevented from reflecting from the driving wall. This requirement determines the motion of the driving wall when the wave returns. Specifically, if the returning wave is of the form $P = P(z \ne ct)$, then there will be no reflection from the driving wall if its velocity is arranged to be $v = (1/\rho_0 c) P(z_0 \ne ct)$ where z_0 is the average coordinate of the driving wall. For illustration, an example of this procedure is shown in Fig. 30, in which is given the driving wall motion as a function of time in units of d/c. For a propane chamber about 20 cm thick, this time is about 1 ms. Also shown is the pressure in the center of the chamber as a function of time.

A similar analysis can be made for cases 2 and 3. The difference here is that the incident plane wave must traverse an interface between two liquids of different properties. It may be easily shown that the condition for perfect transmission of a sonic wave between two liquids in such a case is that the acoustical impedance $\rho_0 c$ be the same for the two. However, the acoustical match is not likely to be perfect between a typical bubble chamber liquid and support fluid, since the compressibility of the former is much higher than that of a typical support fluid. For illustration, $\rho_0 c$ for propane is about 1.84×10^5 kg/m^2 sec, while for a typical paraffin oil it is about 9.1×10^5. This represents an acoustical mismatch of about 5 to 1. The situation is somewhat improved for WF_6 as sensitive liquid and $(C_4F_9)_3N$ as support, owing to the high density of WF_6 and the comparatively large compressibility of the fluorocarbon. Although at the present writing the compressibility of WF_6 at the operating temperature is not known exactly, $\rho_0 c$ is estimated to be about 5×10^5, while the corresponding

Figure 30

Pressure and Driving Wall Waveforms in "Transient" Bubble Chambers

The abcissa of each curve is time in units of d/c', where d is the depth of the chamber and c' is the acoustical velocity in the sensitive fluid.

A. Case 1. Position of driving wall in arbitrary units.

B. Case 1. Pressure of sensitive fluid in center of chamber.

C. Case 2. Position of driving wall in arbitrary units.

D. Case 2. Pressure of sensitive fluid in center of chamber.

E. Case 2. Pressure at driving wall for the case of WF_6 and fluorocarbon.

The scales of pressure are arbitrary, but consistent between the curves. The length of the support fluid column is assumed adjusted in Case 2 so that the acoustical transmission time through it is exactly equal to that through the chamber. Liquids in Case 2 are assumed to be WF_6 and $(C_4F_9)_3N$.
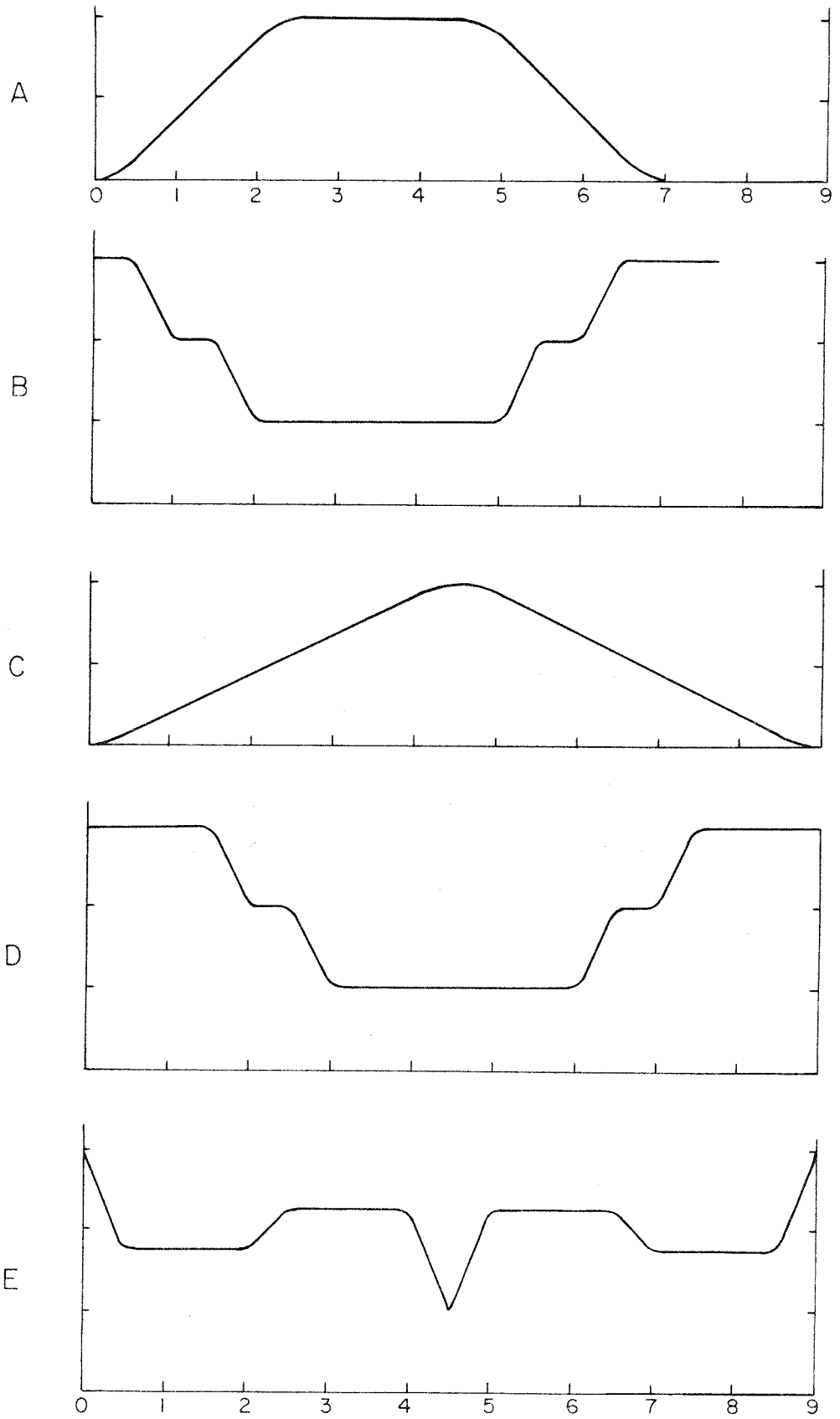
Figure 30

number for the fluorocarbon is about 7.6×10^5. Thus the acoustical match is much better, though not by any means perfect, in this particular case.

One point concerning the effect of the moving windows which separate the support from the sensitive fluids is quite important for the practical design of any chamber such as those we are discussing. We note that the expression II-2-11 concerning the phase of the transmitted wave involves terms $\sim \tan^{-1}(\omega M/A \rho_0 c)$, while those concerning the amplitude of reflected or transmitted wave involve $\sim (\omega M/A \rho_0 c)^2$ compared to unity. In the chamber geometries we are discussing, the movable windows are not, in principle, subject to significant pressure differences, so there seems no good reason why they cannot be quite thin. Even if they are glass, as is likely, a thickness of ~ 1 cm to 1 inch is probably adequate for mechanical strength. Thus $M/A \rho_0 c \sim 10^{-4}$ or smaller, so that a high frequency, $\omega \sim 10^4$ or greater, would be required before the above terms should become significant. We are thus justified in neglecting the effect of the windows in the initial treatment. It should also be noted that any distributed system loosely mounted in the support fluid column with an average mass per unit area comparable to the windows should also have little effect upon the transmission of a pressure wave. An illumination system, for example, could be suspended in the support fluid without deleterious effects if it were properly designed.

Then if we neglect the effect of windows, we may find the value of the transmitted and reflected waves by the simplification of expressions II-2-11 to

$$\text{Transmitted wave} = 2P_0 r/(1 + r) \qquad \text{(II-2-12a)}$$

$$\text{Reflected wave} = P_0(r - 1)/(1 + r) \qquad \text{(II-2-12b)}$$

where we have included the phase change in the sign of expression II-2-12b. Hence we see that in the hydrocarbon case mentioned above, $r \approx 0.2$, yielding a transmission of about $1/3\ P_0$, whereas in the heavy liquid case, $r \approx 0.66$, giving a transmission of $0.8\ P_0$. In the latter case, at least, the pressure transmission is sufficiently good to consider employing a support system such as that illustrated for case 2. The driving function, of course, would have to be arranged to take care of the returning reflected waves from the interfaces, but this could, in principle, be done. To illustrate, we have shown in Fig. 30 a sample of the kind of driving window motion required to give the same chamber pressure vs time function in case 2 as for the one previously given in case 1. It turns out that the motion is greatly simplified if the length of the support column is adjusted so that the sonic transit time through it is exactly equal to the transit time through the sensitive liquid. This is assumed to be the case in Fig. 30, and the liquids are taken to be WF_6 and fluorocarbon.

It may be remarked that from a mechanical standpoint, it might be convenient to reduce the size of the driving windows where possible. Such a thing can be done in cases 2 and 3 without reduction of chamber size by the use of an acoustical horn to couple between the chamber and driving window. However, there are two principal limitations to this technique. One is that there is, in general, a frequency dependent change of phase of a sinusoidal acoustical wave proceeding down a non-uniform horn (77). Therefore a non-sinusoidal pressure wave such as those employed in Fig. 30 would be altered in shape as it proceeded down the horn because of the varying phase shift of its component frequencies. A second limitation is fixed by the requirement upon the absolute pressure of the support medium. In order

to avoid cavitation in the support fluid, one would like to prevent excessive negative pressures. Conservation of energy requires that, in an acoustical horn of slowly varying cross section, a pressure excursion P at a point where the horn has a cross section area A must become an excursion P' = A/A' at another point where the horn has an area A'. Thus if the horn tapers down to too small a cross section at the driving window, excessive negative pressure may be required there in order to achieve the desired pressure change at the chamber.

C. Steady-State Bubble Chambers

An analysis could also be made of case 3, but the principles are the same as for the other two cases, so there is little to be gained. There are, however, some interesting possibilities for the case 3 geometry in conjunction with a steady-state bubble chamber. For this type of device, one would like to set the entire system into resonance, using the driving wall only to replace the energy losses. Such a situation with the geometry we have described is analagous to an organ pipe with the familiar standing waves. We wish to describe such a design in order to show that a very large bubble chamber employing this concept may be feasible which uses the hydrostatic support principle with no large, high pressure glass windows.

One requirement for any bubble chamber which is to be used for precision work is that of uniform expanded pressure. Therefore it is clear that the production of a sinusoidal standing wave of, for example, $\frac{1}{4}$ or $\frac{1}{2}$ wave length in the sensitive fluid itself is not to be desired. In fact, one wishes, in general, to expand as little sensitive fluid as possible consonant with the need for a finite chamber depth in order to avoid the consequent thermodynamic losses. Therefore, the geometry shown in Fig. 31 seems
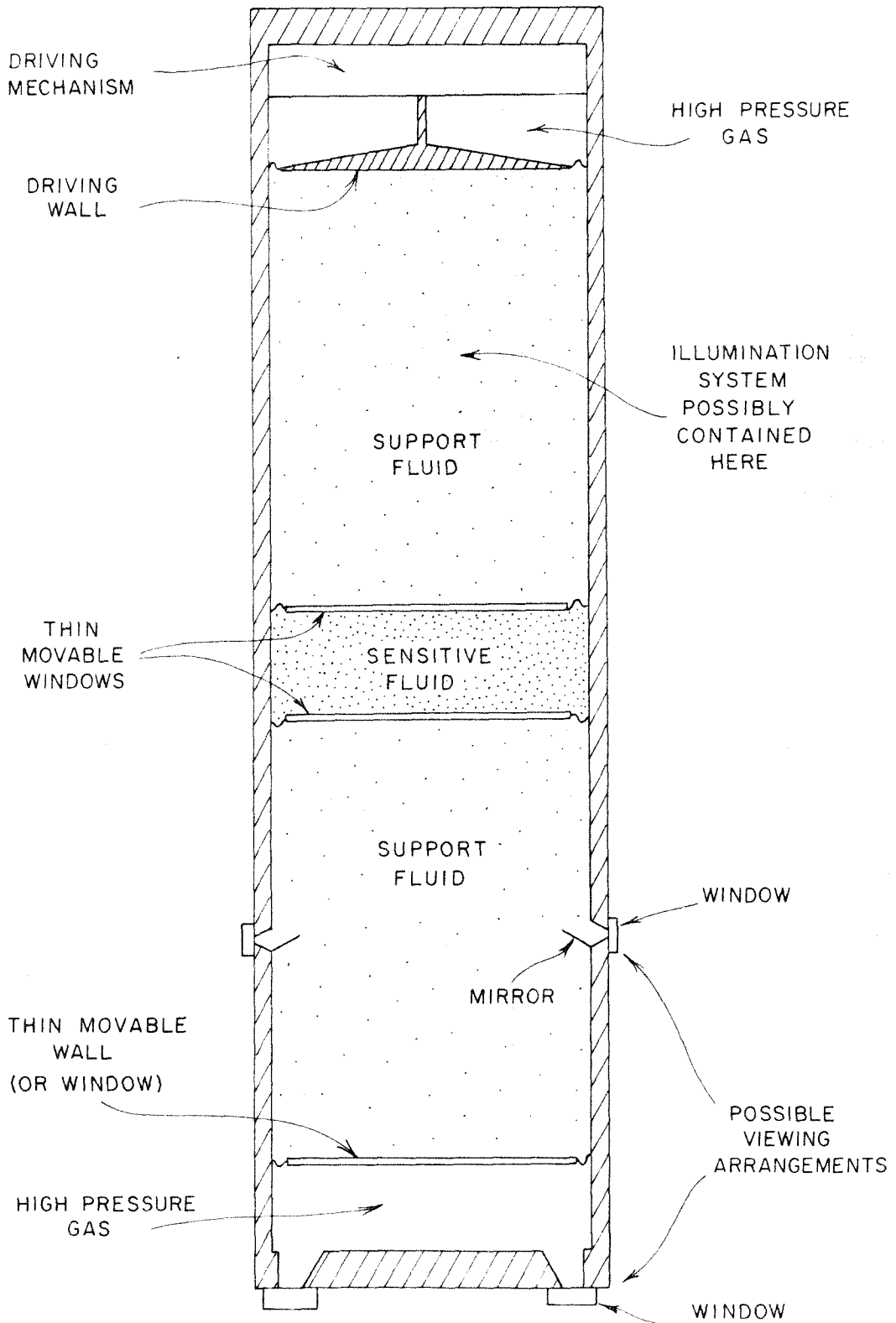
Figure 31

Example of a "Steady-State" Bubble Chamber Geometry
(Scale = 1/20)

a good first choice. The upper end of the tube is the driving wall, and may be thought of as a plate driven by some means (probably electro-mechanical) in a sinusoidal fashion. This plate would be backed by gas at the equilibrium chamber pressure so that it would not have to resist the static pressure in the chamber. The lower end of the tube is also a freely moving (undriven) wall backed by gas at the equilibrium chamber pressure. Taking this pressure as the vapor pressure of the sensitive fluid (in the case of propane or WF_6), ~ 300 psi, we find that $\rho_0 c$ for nitrogen gas is 7.83×10^3, which is a factor of 100 smaller than the corresponding value for any of the support fluids we have discussed. Therefore, the pressure transmission through this boundary is negligible according to expression II-2-12, and the reflection is essentially unity with a 180 degree phase change. The sensitive fluid is placed midway between the two ends of the tube, isolated from the support fluid with thin movable glass windows. It is evident that in the case of a homogeneous medium, this configuration can represent an ideal "open-ended" organ pipe, in which the condition for resonance is that of a pressure node (fluid velocity loop) at either end of the pipe. For the fundamental mode, moreover, the center of the pipe, where the chamber is located, is a pressure loop. The homogeneous case has higher modes which are exact multiples of the fundamental. However, with the actual structure we have shown including the mismatched fluid in the center, the multiple relationship of the higher modes is no longer valid. It is easy to find the condition for resonance of the compound system in the following way. Taking the chamber as symmetric, we note that the spacial distribution of the pressure in the sensitive fluid for a standing wave is given by

$$P = P_0' \cos (2\pi z'/\lambda') \qquad \text{(II-2-13a)}$$

and for the fluid velocity is

$$v' = (P_0'/\rho_0'c') \sin (2\pi z'/\lambda') \qquad \text{(II-2-13b)}$$

where λ' is the wave length and z' the distance from the center of the chamber. (Of course the time dependence includes a 90 degree phase shift between the two functions, but this need not concern us here.) The above expressions are valid only for modes which contain an odd number of pressure loops (the "odd" harmonics in the homogeneous case), but these are the ones with which we are concerned. Similar expressions can be written for the pressure and velocity of the standing wave in the support fluid, as

$$P = \pm P_0 \sin (2\pi z/\lambda) \qquad \text{(II-2-14a)}$$

$$v = \mp (P_0/\rho_0 c) \cos (2\pi z/\lambda) \qquad \text{(II-2-14b)}$$

where λ is the wave length in the support fluid and z the distance from one end of the tube. The required condition is that both pressure and fluid velocity be continuous across the interface. If we equate the right sides of equations II-2-13a and II-2-14a, and the right sides of equations II-2-13b and II-2-14b, and take the quotient of the resultant two equations, we find*

$$\tan (2\pi z_0'/\lambda') = r \, \text{ctn} \, (2\pi z_0/\lambda) \qquad \text{(II-2-15)}$$

where $r = \rho_0'c'/\rho_0 c$, and z_0, $- z_0'$ refer to the position of the interface. (z_0' and z_0 are both to be taken as positive.)

The foregoing equation has only two parameters, z_0' and z_0, so it is in general not possible to find a set of harmonic solutions. That is, z_0 and z_0' cannot, in general, be adjusted so that the series of constants $(2n - 1)\omega_1$ (where $\omega_1 = 2\pi c/\lambda_1 = 2\pi c'/\lambda_1'$ and $n = 1, 2, 3...$) satisfy equation II-2-15. The exceptions to this, of course, (for $r \neq 1$) are such degenerate cases as $z_0 = k\lambda_1/4$, $z_0' = m\lambda_1'/4$, where k and m are integers,

---

* The expression for the modes with an even number of pressure loops is equation II-2-15 with the negative cotangent replacing the tangent in the expression on the left.

but these imply that the fundamental frequency ω_1 generates a pressure loop or node at the liquid interface, a situation we are not seeking. On the other hand, it is possible to adjust z_o and z_o' so as to satisfy two modes, for example the fundamental and the third harmonic, so that $2\pi z_o'/\lambda_1'$ and $2\pi z_o/\lambda_1$ both represent angles in the first quadrant. This may be useful in some cases for obtaining a more nearly "square" pressure function in the sensitive fluid. However, we can more simply restrict our attention to a single frequency, and solve for the lowest mode, which for a given value of λ, λ', is the solution for smallest z_o, z_o', > 0. If we adopt the criterion that we wish pressure uniformity within 5% across the chamber, a simple calculation shows that $z_o' \approx 0.05 \lambda'$, or, since z_o' is $\frac{1}{2}$ the chamber depth, we find that the chamber depth is $0.1 \lambda'$. A direct application of equation II-2-15 (for a given pair of liquids) yields the value for z_o. To illustrate, we have calculated the pertinent parameters in the above fashion for two cases, one with propane as the sensitive fluid and a light paraffin oil as the support, the second with WF_6 as the sensitive fluid and a fluorocarbon as support.* The frequency of operation was selected as 60 cps, for obvious utilitarian reasons, and the results are given in Table 6. It happens, quite fortuitously, that the parameters selected in the WF_6-fluorocarbon case satisfy equation II-2-15 for the third harmonic as well as the fundamental mode. It is then conceivable in this case to excite both modes simultaneously so as to produce a more uniform pressure in the sensitive fluid. For the propane-paraffin oil case, however, the analogous

---

* One support fluid is usable for the 27°K operating temperature of liquid hydrogen. This is neon, which freezes at 24.4°K and boils at 27.2°K. Parameters for this case corresponding to the above have not been calculated owing to uncertainty as to the velocity of sound in liquid neon.

TABLE 6

System	Propane-Paraffin Oil	WF_6-Fluorocarbon
Frequency (cycles/sec)	60	60
Amplitude of Pressure Oscillation* (psi)	200	200
Amplitude of Driving Wall* (cm)	0.73	0.51
Peak Velocity of Driving Wall (m/sec)	2.75	1.94
Depth of Sensitive Fluid (cm)	77	33
Length of Support Column (m)	1.9	1.4
Over-all Length of Tube (m)	4.6	3.1

* "Amplitude" here is $\frac{1}{2}$ the total excursion; e.g., the pressure swing is from 100 psi (expanded) to 500 psi (recompressed).

situation demands a chamber depth of 28 cm (which is satisfactory) and support fluid columns each 3.6 meters long (which is longer than might be desired).

It is to be noted that the length of the chamber structures given in Table 6 are quite within reason, if we assume that the design is to be applied to very large chambers of dimensions comparable to a meter in diameter. The chamber depth is satisfactory for this size chamber for the WF_6 case (33 cm) while it is probably too deep in the propane case (77 cm). The depth of the chamber (and the over-all length of the tube) can, of course, be reduced by raising the operating frequency; doubling it is not out of the question. Furthermore, if one allows the possibility of high pressure windows, two other things could be done for the propane system. The geometry described in Fig. 31 is obviously symmetric about the center of the chamber, so the system could be cut precisely in half and only the upper portion retained, with a high pressure window placed where the center of the chamber now is. This would make the chamber depth a more reasonable 39 cm. One could also consider making the tube of smaller rectangular cross section with windows on either side of the chamber portion. Then the 77 cm dimension becomes the length of the chamber, while the depth and width are determined by the dimensions of the rectangular tube.

The feasibility of the foregoing scheme is not easily evaluated without experiment. The mechanical drive would appear to be conceivable, as the driving window operates in what is ideally a pressure node. The pressure differences developed across it can come only from the dissipation of energy in the chamber, and should be small compared to the pressure excursion developed in the chamber. Many electro-mechanical drives can be

envisioned, one of which might be the magnet configuration used on our expansion engines (see Appendix II). The comparatively small pressure differences developed across the driving window should allow its mechanical design to be light enough so that the mass itself could be adjusted to the resonant frequency of the chamber with the aid of gas reservoirs of the proper size. Since we are dealing here with a single frequency, it is also possible that the acoustical horn might be employed to reduce the size of the driving window.

There is also the question of losses. As far as the loss produced by the track bubbles themselves is concerned, there would appear to be no problem. As shown in Chapter II-1, the energy loss produced by even a fairly heavily "loaded" chamber (100 diametral tracks in a 12 inch chamber) is less than 0.3% of the energy storage in the fluid under the proper expansion conditions, and even this number could be reduced by expanding to a higher pressure than the one used in the calculations. The loss produced by spontaneous boiling from the chamber walls is less predictable, but we have some indication from our tests with the 12 inch chamber that this defect can be eliminated by proper design and choice of materials.

The most difficult question to answer is whether or not the bubbles created during one expansion would have time to collapse completely before the subsequent expansion. The calculations described in Chapter II-1 indicate that they do not under the conditions assumed there, although the equations used are in some error near the end of the recompression cycle. Possibly a much higher recompression pressure than those commonly employed in bubble chambers would be required.

There are other problems as well. For example, the exitation of other (e.g., radial) modes of oscillation might cause trouble in larger diameter chambers, and some form of acoustical wave guides might have to be employed to discourage other modes. The camera viewing ports are possibly not as convenient as one might wish. The places suggested in Fig. 31 are around the periphery of the tube or through the undriven wall on the bottom as shown.

Although there are certainly problems attendant with the system suggested above, the concept might be worth consideration by someone who has a need for such a chamber. The obvious application is to some of the newer machines (e.g., the proposed Pennsylvania-Princeton proton synchrotron) which have repetition rates in the range of 30 cps. In fact it would seem to the writer that there is great promise in a marriage of counter and bubble chamber techniques. The steady-state bubble chamber system proposed in the foregoing offers one method of achieving this fruitful combination, and as such should certainly be investigated.

APPENDIX I

EXPANSION SYSTEM

A. Equation of Motion

In an approximate sense, the expansion system for our 12 inch chamber is analogous to a harmonic oscillator - e.g., a mass on a spring. The spring represents the various fluid and mechanical compressibilities of the system, and the mass that of the pistons, oil, support fluid, and sensitive fluid itself. The mass is to be imagined held with the spring compressed by a mechanical catch. When the catch is released, the mass goes through a single harmonic cycle, and is stopped again by the catch. In order to analyse quantitatively the motion of the expansion cycle, we will use the model shown in Fig. 32. We will further make the following simplifying assumptions, and will discuss their validity later.

1. Incompressible support fluid (except as a correction introduced in the spring constant) of density ρ.

2. Irrotational flow of the liquid.

3. Introduction of an "effective mass" in the expansion of the sensitive fluid.

4. Lossless (conservative) system.

5. Constant compressibility of compressible media.

We refer to Fig. 32 for definitions of the relevant quantities. Because of the incompressibility assumption,

$$xa = XA \qquad (AI-1)$$

In order to write the Hamiltonian for the system, we need the kinetic energy terms. Thus kinetic energy $= T_M + T_m + T_\rho + T_\ell + T_L$, where T_M and T_m refer to the energy of masses M (chamber and sensitive fluid) and m (pistons) respectively, T_ℓ and T_L refer to the energy in the
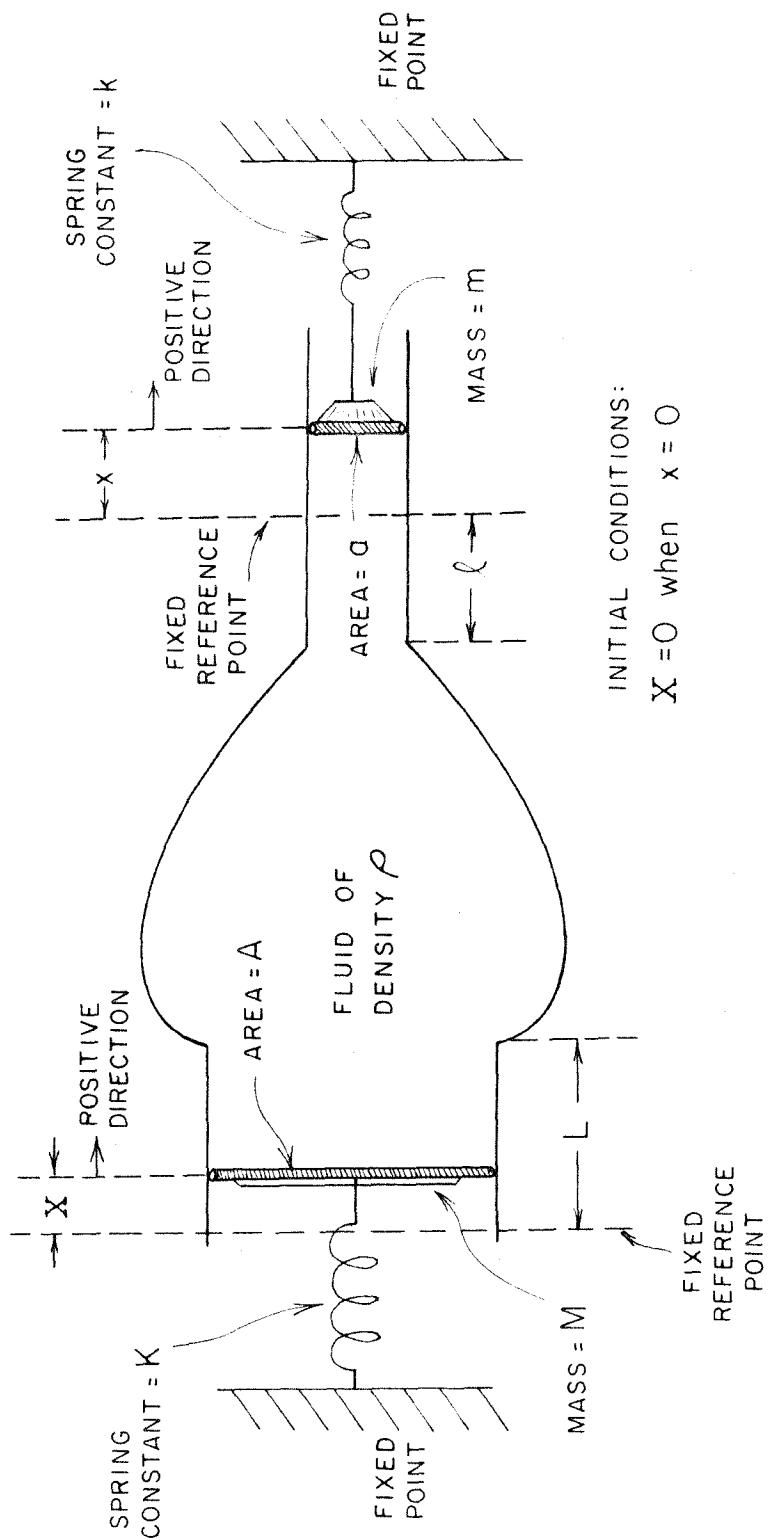
MODEL   FOR   EXPANSION   SYSTEM   CALCULATION

Figure 32

fluid of the "straight sections" $\ell \neq$ x and L - X respectively, and T_ρ refers to the energy of the fluid in the complicated region in between.

The terms are quickly evaluated (the dot denotes differentiation with respect to time). $T_m = \frac{1}{2}m\dot{x}^2$. $T_M = \frac{1}{2}M\dot{X}^2 = \frac{1}{2}M\dot{x}^2 (a/A)^2$, in view of equation AI-1. $T_L = \frac{1}{2}A\rho(L - X)\dot{X}^2 = \frac{1}{2}A\rho[L - x(a/A)] [a/A]^2 \dot{x}^2$, again using equation AI-1. $T_\ell = \frac{1}{2}a\rho(\ell \neq x)\dot{x}^2$. Left to evaluate is T_ρ . It is given by $T_\rho = \int \frac{1}{2}\rho v^2 d\tau$, where $d\tau$ = volume element, v = velocity of the oil, and the integral is taken over the entire volume of oil not included in T_L and T_ℓ . This may be expressed in terms of x by $T_\rho = \frac{1}{2}\rho V \xi (\dot{x})^2$, where V = volume of oil in T_ρ and

$$\xi = (1/V) \int (v/\dot{x})^2 d\tau \qquad\qquad \text{(AI-2)}$$

For this system, ξ is always less than unity.

Summing, then, where $\gamma = $ a/A ,

Kinetic Energy $\equiv T = \frac{1}{2}\dot{x}^2 \Big\{ m \neq \gamma^2 M \neq \rho[A\gamma^2(L - \gamma x)$

$$\neq a(\ell \neq x) \neq V\xi] \Big\} \qquad\qquad \text{(AI-3)}$$

Potential energy terms are also easily determined. Potential energy $\equiv V = \frac{1}{2}KX^2 \neq \frac{1}{2}kx^2$ and using equation AI-1, we have

$$V = \frac{1}{2}x^2 (K\gamma^2 \neq k) \qquad\qquad \text{(AI-4)}$$

where K and k are the "spring constants" shown in Fig. 32.

The Hamiltonian is now given by the sum of T and V, or

$$(\alpha \neq \beta x)\dot{x}^2 \neq \Gamma x^2 = C \qquad\qquad \text{(AI-5)}$$

where

$$\alpha \equiv m \neq \gamma^2 M \neq \rho[AL\gamma^2 \neq a\ell \neq V\xi] \qquad\qquad \text{(AI-5a)}$$

$$\beta \equiv \rho(a - A\gamma^3) = \rho a(1 - \gamma^2) \qquad\qquad \text{(AI-5b)}$$

$$\Gamma \equiv K\gamma^2 \neq k \qquad\qquad \text{(AI-5c)}$$

and C is an arbitrary constant.

If we now solve for ẋ, we may express the solution as the integral

$$t = \int_{x_1}^{x} \sqrt{(\alpha + \beta x)/(C - \Gamma x^2)}\, dx \qquad \text{(AI-6)}$$

The above integral may be performed easily if we employ the approximation that $\beta x \ll \alpha$. (For our system, this is numerically valid, as is shown later.) Then we may expand the integral, and take only the first two terms, as

$$t \approx \int_{x_1}^{x} \sqrt{\alpha/(C - \Gamma x^2)}\, dx + \tfrac{1}{2} \int_{x_1}^{x} \sqrt{\alpha/(C - \Gamma x^2)}\, (\beta x/\alpha)\, dx$$

The first term yields the harmonic solution, (as can be seen directly from the Hamiltonian equation AI-5 by setting $\beta = 0$). Therefore it is convenient to set

$$x_1 = -\sqrt{C/\Gamma} \equiv -x_0 \qquad \text{(AI-7)}$$

whence x_0 is the amplitude of the oscillation. Hence the solution

$$t = (1/\omega)\cos^{-1}(x/-x_0) - \tfrac{1}{2}(\beta/\sqrt{\Gamma\alpha})(\sqrt{x_0^2 - x^2}) \qquad \text{(AI-8)}$$

where

$$\omega \equiv \sqrt{\Gamma/\alpha} \qquad \text{(AI-9)}$$

The second term on the right of equation AI-8 gives a measure of the asymmetry of the perturbed harmonic cycle. If we define Δt as the difference in time between the actual case and that of a pure sinusoid of the same period $2\pi/\omega$ over a quarter of a cycle, we have

$$\Delta t = \beta x_0/2\sqrt{\Gamma\alpha} \qquad \text{(AI-10)}$$

B. Numerical Evaluation

First we evaluate the "spring" term $\Gamma = k + \gamma^2 K$. The term k represents the spring constant in the "bias cylinders" described in Chapter I-3. Since they are gas reservoirs whose volume is large compared

to the volume change during expansion, k is quite small and may thus be accounted for only approximately. To evaluate K, we note that if K_1 is the contribution to K from the sensitive fluid, then

$$K_1 = \Delta \text{Force}/\Delta X = A dP/dX = A dP/(dW/A),$$

where W is the volume of the sensitive medium and P its pressure. If then κ is its compressibility defined by $\kappa = dW/WdP$, we have $K_1 = A^2/W\kappa$. Then Γ_1, the contribution to Γ, is given by $\Gamma_1 = \gamma^2 K_1 = a^2/W\kappa$. Note that the contribution to Γ is independent of the geometry of the sensitive liquid container (in this approximation) and depends only upon its volume and compressibility. If we agree to describe the motion by the variable x, which is essentially the position of the pistons, we then have a convenient way to take into account the compressibility of the support fluid and the flexibility of the vessel itself. That is, we say $\Gamma = k \neq a^2/(\Delta V_p/\Delta P)$, where ΔV_p now refers to the volume change seen at the pistons, and including all sources of compressibility.

The following calculation is based on the parameters as they existed during the second run with butane at 120°C (see Chapter I-4). The term $\Delta V_p/\Delta P$ can be estimated, but poorly. The number ascertained from static measurement of piston positions is 13.3 in^3/100 psi. Converting to MKS units and treating all four pistons as a single piston with area equal to the sum of the four, we find, a = 0.0248 m^2; $a^2 = 6.15 \times 10^{-4}$ m^4; $\Delta V_p/\Delta P = 3.18 \times 10^{-10}$ m^5/Newt; and $\Gamma = 1.94 \times 10^6$ Newt/m $\neq$ k. The term k can be estimated from the volume and pressure of the gas in the bias cylinders, and is about 0.16 $\times 10^6$ Newt/m, so

$$\Gamma \approx 2.1 \times 10^6 \text{ Newt/m}$$

To evaluate β, we assume that only the upper window of the bellows

chamber moves.* Then, since the effective area of the bellows chamber is 150 in^2, and that of the four pistons taken together 38.5 in^2, we have

$$\gamma = 0.256 \text{ and } \beta = \rho a(1 - \gamma^2) = 27.8 \text{ kg/m.}$$

Now we must evaluate α from equation AI-5a. The term L is not strictly applicable to the real chamber, and the effect of the fluid in that portion is included in the term ξ. The constant m is

m (mass of pistons) = 7.2 kg.

The term $\rho a \ell$ includes the expansion engine oil behind the piston, in the valve, and up the neck of the bias cylinders, as well as the mass of the support fluid in front of the pistons. By numerical integration we obtain

$$\rho a \ell = 4.8 \neq 0.8 \text{ kg} = 5.6 \text{ kg}$$

The term M has to include the mass of the flanges, glass, and other fixed parts which are $\approx$ 9 kg. The "effective mass" of the sensitive fluid can be derived in a manner similar to that used in the derivation of the equation of motion, assuming that only the upper window moves, and turns out to be one-third of the actual mass. Assuming butane, we have an effective mass = 2.1 kg. for the sensitive fluid, and

M = 11.1 kg; γM = 0.727 kg.

The term $\rho \nabla \xi$ is not so easy to assess. However, it can be estimated with the aid of an electrical analogue, i.e., an electrolytic tank, and this has been done. If one assumes irrotational flow of an incompressible fluid, it can be shown (54) that it is possible to write a velocity potential φ such that velocity is given by $\underline{v} = -\nabla \varphi$, and obeys Laplace's equation $\nabla^2 \varphi = 0$. A salt tank was set up modeling the

---

* This calculation has been also done for the case in which both windows move equal amounts, and found to differ very little from the results exhibited here. In practice the lower window moves some, but not as much as the upper.

chamber, using copper plates for the pistons and moving windows. The result

of these measurements gave the value of ξ as 0.057. Taking V = 37.5 lit,

ρ = 1.2 kg/lit, we have

$$\rho V \xi = 2.6 \text{ kg.}$$

Summing all terms in α, we have

$$\alpha = 16.1 \text{ kg.}$$

We can now compute $\omega = \sqrt{\Gamma/\alpha}$ as $\omega = \sqrt{2.1 \times 10^6/16.1} = 361.$

Thus τ, the period, is given by $\tau = 2\pi/\omega = 17.4$ ms. A typical period

obtained in the non-boiling runs with the chamber at 120°C (see Chapter I-4)

was 17.0 ms. The excellent agreement with the calculated value is a good

indication that the valve opening is having no constricting influence, and

that the flow is laminar to a high order of approximation.

A calculation of Δt, the asymmetry mentioned earlier, is quickly

made. x_0, typically, is at the most $\sim$ 1.5 inches = 0.038 m. Evaluating

equation AI-10, we have $\Delta t = 0.91 \times 10^{-4}$ sec $\sim 100\mu$ sec; i.e., $(\Delta t)/\tau$

$\approx$ 0.7%. Clearly the approximation in performing the integral AI-6 is

justified and, in fact, for all practical purposes the asymmetry may be

neglected and the harmonic approximation employed.

C. Validity of Approximations

It is now pertinent to discuss the validity of the assumptions

made initially in this treatment. The good agreement with experiment in

itself is an indication that the approximations are not bad, but there are

other arguments as well. Treatment of the support fluid as incompressible,

as long as its actual compressibility is included in the spring constant,

is valid providing the transit time for the velocity of sound in the fluid

is small compared to the period of the oscillation. For glycerine, the

velocity of sound at this temperature of 1600 m/s yields a sonic transit time of about 0.3 ms for the largest chamber dimension. For the fluorocarbon support fluid, however, some error may be introduced, as the velocity of sound of the order of 400 m/s yields a transit time of some 1.2 ms.

The irrotational flow postulate is probably quite good, since this is a pulsed system. Time is usually required to develop vortices in such a low velocity flow system, and the characteristic time estimated for our chamber is of the order of seconds at the flow velocities we encounter.

The use of an effective mass to represent the sensitive fluid is also reasonable, on two counts. First, its effect is small in our system, and second, the approximation in itself is valid if the sonic transit time through the relevant (small) dimension of the bellows chamber is small compared to the period. For butane, this time is calculated to be about 0.38 ms, while for WF_6 it is about 0.6 ms. Although these times might not have much effect on the period of expansion, they may result in a real pressure difference between top and bottom of the chamber, causing some trouble with respect to uniformity of sensitivity.

The assumption that the system is lossless is obviously not valid. The sensitive liquid, upon boiling, may produce large thermodynamic losses. However, as can be seen from the expansions made with only a small amount of boiling (Chapter I-4, Fig. 16), the losses from other sources are really quite small, yielding a mechanical "Q" of about 20. The effect of severe boiling is discussed at length in Chapter I-4. (See Chapter II-1 for a treatment of the losses produced by track bubbles.)

The final assumption made, that of linear compressible media, is an excellent approximation in the pressure ranges we are considering when

the chamber liquid is not boiling. In the boiling region, the complications discussed in Chapter I-4 ensue.

An important point must be made here. The period calculated above is not the actual expansion and recompression time of the chamber. The interval of the pressure cycle which we wish to be small is that portion which is below the vapor pressure of the sensitive fluid. To illustrate, if the starting pressure is 500 psi and the vapor pressure only 250, the actual total "expanded" time may be less than $\frac{1}{2}$ the period calculated above, or smaller than 9 ms.

The effect of the "booster" springs described in Chapter I-3 can be calculated in a manner perfectly analagous to that we have used in the foregoing, the primary difference being that the cycle must be computed in two steps. The initial part of the cycle has a higher spring constant (due to the booster springs), and thus a frequency higher than the middle portion.

D. Applicability to Higher Repetition Rates

A point may be mentioned concerning the applicability of this expansion system to the steady-state bubble chambers discussed in Chapter II-2. For very large heavy liquid chambers the finite velocity of sound would appear to make the approach suggested there more attractive. However, for smaller chambers, particularly those employing lighter liquids, the "lumped constant" approach employed here is probably adequate. There seems no immediate reason why, with the proper driving mechanism attached to the pistons of a chamber such as ours, it could not be made to resonate in a steady-state fashion. Of course the comments made in Chapter II-2 concerning chamber cleanliness and bubble collapse apply here as well. The repetition rate of our present chamber is limited to about one pulse in four

seconds owing to time required to charge the expansion engine condenser bank. This period could be shortened quite easily, of course. The actual pump-up time depends upon the compressibility of the media and the degree of energy loss during an expansion, but should be only around 200 ms under good conditions with our present small 1 hp. pump.

APPENDIX II

EXPANSION ENGINES

A. General Construction

The primary energy storage devices in the expansion engines are gas reservoirs or "springs." These are almost completely non-dissipative, and in principle are simply reservoirs which never require gas supply once they are pressurized. There are two such "springs" on each engine (See Fig. 11, Chapter I-3). Mechanically they consist of a single closed cylindrical vessel divided into two compartments by a piston to which a drive shaft is connected. The rear compartment (B) is called the "bouncer," and contains the smaller volume of the two reservoirs. The position of the back wall is adjustable. The more forward compartment (D) is called the "driver," and contains a comparatively large volume, as well as a supply of oil for lubrication of the "O" ring seal on the piston (P). This piston, with an area of 7 in^2, is made of aluminum, and is in the shape of a flat disk with an "O" ring seal between its edge and the cylinder wall. The rear drive shaft (RS) connects to the piston and extends through the front wall of the driver, where it passes through a Morganite (pressed graphite) bearing and an "O" ring seal.

The front drive shaft (FS) is attached to the rear one by means of a semi-flexible coupling (C). The joint is fundamentally a metallic clamped one, except that the metal pieces are held apart by 1/32 inch rubber washers for flexibility. On the front drive shaft is attached the moving part of the magnet assembly (MMA). This assembly, which is held together by a cast magnesium spider, contains the moving "slug" or armature, and a set of moving coils, described in detail later. The entire assembly is held to the threaded drive shaft by two sets of lock nuts and washers,

one set in front and one behind the assembly. This allows the magnesium piece and its electrical components to rotate slightly, and because of a rubber-asbestos washer between it and one of lock nuts the piece also has some freedom to tilt and make up slight misalignments of the components with respect to the fixed portions of the magnet. The actual orientation (with respect to rotation) of the moving part is maintained by guide rods (not shown).

Adjacent to the moving part of the magnet but shock-mounted to the housing of the valve are the fixed portions of the magnet (FM). These consist of two "E" shaped, laminated magnets with a large coil enclosing the center legs of the E's. When the valve is closed, the moving slug closes the top of the "E," completing a magnetic circuit between the center legs and the outer legs.

Forward of the moving magnet assembly, the front drive shaft passes through an "O" ring seal and a second Morganite bearing, into the valve housing (VH). This housing is normally filled with an oil which is used as the hydraulic medium in the expansion engine portion of the expansion system. Just inside the housing, attached to the front drive shaft and operating in the oil, is a "dash-pot" (DP). The purpose of this device is to arrest the motion of the valve upon closing, so that no large impact is felt upon the magnet assembly. It is, fundamentally, simply a piston-like device which traps a quantity of oil in a small volume during the return, (or closing) stroke of the valve, and forces it to escape through a small orifice. Its operation is explained in more detail later.

The front drive shaft terminates in the sleeve of the valve itself (S). This sleeve is a hollow, open ended cylinder about 5 inches

-215-

in diameter and $3\frac{1}{4}$ inches long. It is attached to the drive shaft at the rear by means of a spider (SP) whose edges are streamlined so that the entire structure is free to move through the oil with little resistance. The sleeve, spider, and both drive shafts are constructed of a hardenable grade of stainless steel.

The seat of the valve, over which the sleeve fits, (ST) is a solid disk of stainless steel attached to the body (or housing) of the valve by a set of metal ribs (R), so that the oil is free to flow between the disk and the body of the valve. The disk contains a rubber "Quad" ring, which provides a sliding seal between the sleeve and the disk. This seal is never disengaged during operation of the valve. The front seals (SS and DS), are engaged by the front portion of the sleeve when the valve is closed. The forwardmost of these (SS) is a rubber "O" ring, and provides a good static seal. Approximately $\frac{1}{2}$ inch back from this is a second seal (DS) which consists of a short Teflon cylinder. The function of the latter seal is twofold. First it acts as a low friction guide to the sleeve to prevent its binding upon the metal parts of the seat. Second, it provides a seal which, though not good statically, is very effective dynamically. Therefore the valve has approximately $\frac{1}{2}$ inch in which to acquire speed before the final seal is broken.

B. Gas "Springs"

The behavior of the "driver" and "bouncer" are readily computable. The action of the valve is sufficiently fast that estimates indicate the deviation of the gas from adiabatic conditions is very small. Thus the equation of state of the gas in the reservoir can be treated, to a good approximation, as that of an ideal adiabatic gas. Then the pressure-volume

relation assumes the form

$$P/P_0 = (V_0/V)^\gamma \qquad\qquad\qquad (AII-1)$$

where P_0 and P are initial and final pressures, respectively; V_0 and V are initial and final volumes, respectively; $\gamma = c_p/c_v$, the ratio of specific heat at constant pressure to specific heat at constant volume. For a diatomic gas such as the nitrogen we are using, γ can be taken with fair approximation to be 7/5.

Now consider the model shown in Fig. 33. The distances are defined in the drawing, and ℓ_1 is taken large enough to include the volume in the actual "driver." ℓ_2 is the distance remaining between the piston and bouncer wall when the valve has stopped on its back stroke, and a the total amplitude of the motion. Now if P_1 is the pressure in the driver, P_2 the pressure in the bouncer, and P_{10} and P_{20} their initial values, then

$$P_1/P_{10} = [\ell_1/(\ell_1 + x)]^\gamma \qquad\qquad (AII-2a)$$

$$P_2/P_{20} = [(\ell_2 + a)/(\ell_2 + a - x)]^\gamma \qquad (AII-2b)$$

The equation of motion of the system is given by

$$\ddot{x} = f_1 - f_2, \text{ where } f_1 = P_1 A/m,$$

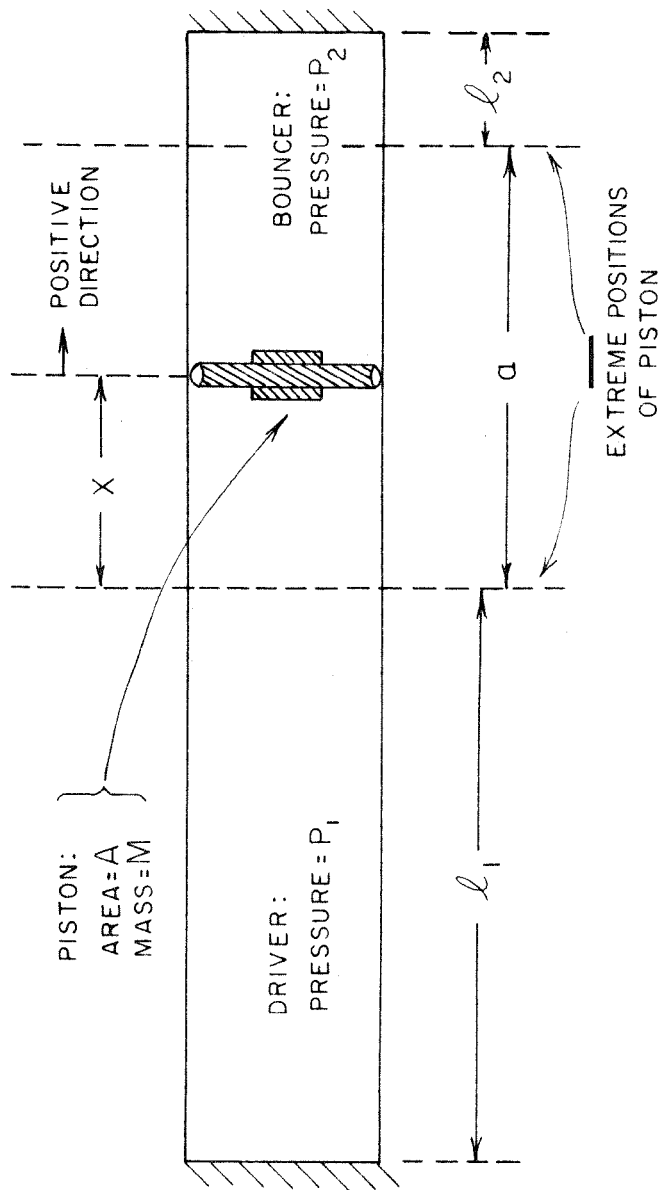A is the area of the piston, m is the mass of the moving system, and i any subscript. The dot denotes differentiation with respect to time. A first integral to this equation can be obtained, where we require $\dot{x} = 0$ at $x = 0$ and $x = a$. The result is

$$f_{10}/f_{20} = P_{10}/P_{20} = [(\ell_2 + a)/\ell_1]\left\{\frac{[(\ell_2 + a)/\ell_2]^{\gamma-1} - 1}{1 - [\ell_1/(\ell_1 + a)]^{\gamma-1}}\right\} \qquad (AII-3)$$

which defines, for a given value of ℓ_2 and a the ratio of pressures that must be used, and

Figure 33

MODEL USED IN EXPANSION ENGINE CALCULATION

$$\tfrac{1}{2}\dot{x}^2 = \left[P_{10}\,\ell_1/(\gamma - 1)\right]\left\{\left[\ell_1/(\ell_1 + x)\right]^{\gamma-1} - 1\right\} \qquad (AII-4)$$
$$+ \left[P_{20}(\ell_2 + a)/(\gamma - 1)\right]\left\{\left[(\ell_1 + a)/(\ell_1 + a - x)\right]^{\gamma - 1} - 1\right\}$$

This equation is of the form $\tfrac{1}{2}(dx/dt)^2 = F(x)$, and the period of the valve can be found as the quadrature $t = \int_0^a dx/\sqrt{2F(x)}$.

Although the integral is difficult, if not impossible, to do analytically, a result can be found by numerical or graphical integration. Some samples of these calculations, some of which were done by the author, some by E. D. Alyea, Jr., and some by J. T. Chang, are indicated in Table 7. Actually the period was calculated only for the total time elapsed between the breaking of the dynamic seal to the return of the valve to this point. Thus the times quoted below are for the function $\tau = 2\int_d^a dt/\sqrt{2F(x)}$ where $d \approx 0.6$ inches, since we are interested only in the effective open period of the valve. The entire moving assembly weighs about 10 pounds. In the examples shown, the ratio of P_{10} to P_{20} is determined according to equation AII-3 in order to fix the stroke to 1.65 inches.

The speed can be increased still more, of course, with a slight loss in orifice area, by simply decreasing the stroke of the valve. The practical limit to the pressure in the driver is set by the holding force of the solenoid.

The oscilloscope traces shown in Figs. 34 are taken from position transducers attached to the moving part of the valve. Figures 34 a and b are typical "free oscillations" of the valve, in which no attempt was made to return it to the closed position. The oscilloscope calibration is given in the caption, as well as the conditions of pressure in the driver and bouncer. Data from the pictures indicate the total initial stroke of the valve in this case as 1.33 inches, with τ as defined above ≈ 11 ms. Note

TABLE 7

| P_{10}(psi)	P_{20}(psi)	ℓ_2(in)	τ(ms)
141	64	1	18.9
141	57	0.75	17.2
141	48	0.5	15.1
212	97	1.0	15.4
212	86	0.75	14.0
212	72	0.5	12.4

Figure 34

Motion of Expansion Engine Valves

Time increases to the right. Up is toward the closed position.

a. Free oscillation, position vs. time. Calibration: vertical is 0.35 inches of valve motion per cm scope deflection. Horizontal is 3 ms/cm. Driver pressure 200 psi, bouncer pressure 68 psi.

b. Free oscillation. Vertical calibration same as in Fig. 34a. Horizontal is 10 ms/cm.

c. Typical valve motion, traveling to closed position. Upper trace is valve motion, lower trace current through four magnets in parallel. Vertical calibration of valve motion approximately the same as above. Current is 100 amperes/cm. Horizontal is 5 ms/cm. (Driver and bouncer pressures were smaller for this pulse than for the ones in Fig. 34a and b.)
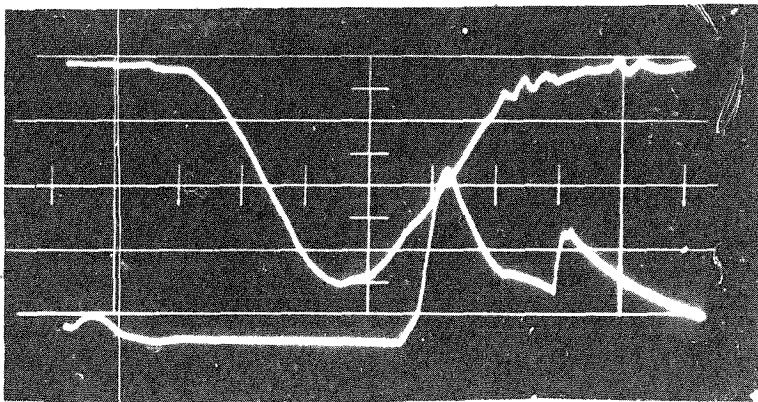
Figure 34
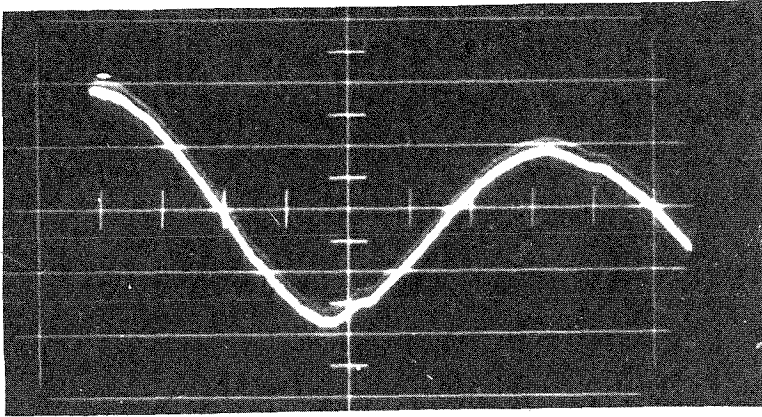
a
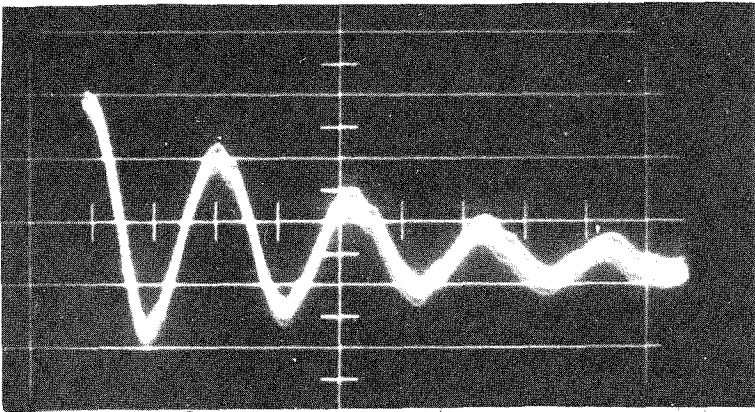
b

c

the extent of the losses in the cycle, indicated by the damping of the oscillation shown in Fig. 34b. The fact that the measured amplitude is considerably smaller than the calculated one is due partly to the losses and partly to the fact that the actual position of the movable back wall of the bouncer was farther forward than was assumed in the calculations.

C. The Magnet

There is a great advantage in having a ferromagnetic magnet material with a very high saturation point for our application. Rapid valve action depends on a large initial differential force from the gas springs and a small mass for the moving system. The large starting force, however, must be held by the magnet. For a magnet of the type we employ, the holding force is proportional to the square of the magnetic field at the gap. Therefore a high saturation magnet results in a very marked reduction in the size and weight of the moving structure, particularly if the magnet itself is a substantial fraction of this weight. The material we employ is Vanadium Permendur, a cobalt alloy which is available in lamination thicknesses. The curves provided by the manufacturer (Allegheny-Ludlum) show a ratio of B/H of 1000 at 20 kilogauss, and a saturation of about 22 to 24 kilogauss. Our experience has indicated, however, that the particular batch we have is probably not that good, although the degradation of its magnetic properties may have resulted from the treatment we have given it.

The fixed part of the magnet consists of two "E" sections (E) spaced on either side of the drive shaft, as shown in Fig. 35. The E's are made up of 0.015 inch laminations which were bonded together with a filled epoxy resin (Briggs R-385), after which the pole tips were ground

Figure 35

Expansion Engine Magnet Assembly

Explanation of Symbols

DS Position of drive shaft
I   Moving portion of magnet (I sections)
CB Magnesium, padded, clamping bars
MC Moving coils of magnet
MS Magnesium spider
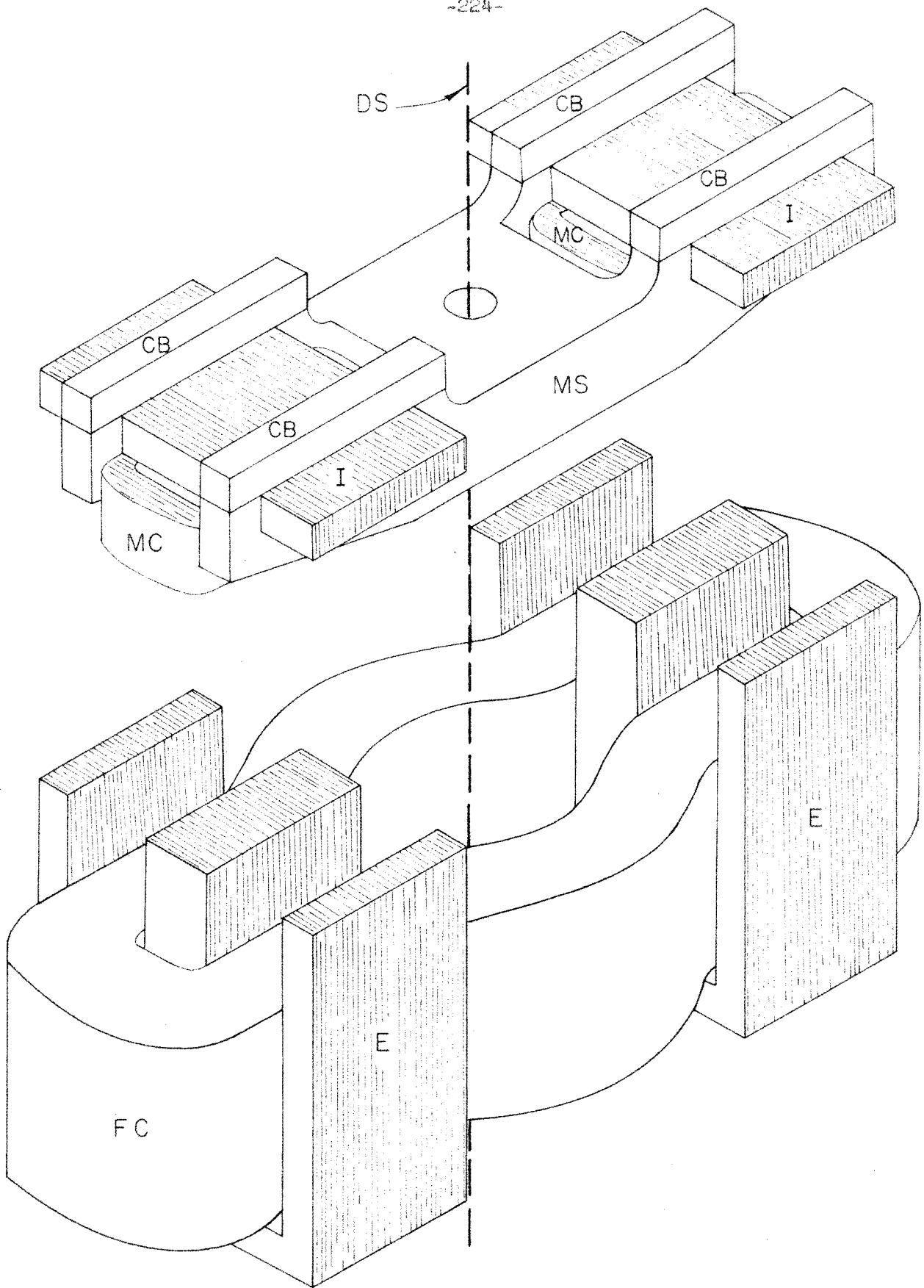E   Fixed portion of magnet (E sections)
FC Fixed coil of magnet

Figure 35

flat and acid etched. The total finished area of all the pole tips of the two E's together is about 9 square inches. The coil (FC) consists of 450 turns of no. 13 square wire, and is wound to include both center legs of the E's and the drive shaft, as shown.

The moving portion of the magnet is made up of the matching "I" sections (I), also made of 0.015 inch Vanadium Permendur, bonded, ground, and etched. The total weight of the two "I" pieces is about $3\frac{1}{2}$ pounds. If we assume a field of 20 kilogauss in the magnet when the valve is closed and the "I" sections rest on the pole tips of the "E's," we can compute the holding force $= \frac{1}{2}(B^2/\mu_o)$ (MKS units) as 230 pounds/in^2. Since the area of the pole tips is about 9 square inches, we should have a holding force in excess of 2000 pounds. Actually, the force is somewhat less than this, partly because the laminations are separated by a finite thickness of material, and partly because the effective air gap of the magnet is larger than it was intended to be, making it impossible for us to energize the magnet fully within the limitations of our current source. There is a real air gap provided by 0.015 inch nylon pads, whose purpose is both to provide shock absorption for the magnet, and to ensure that the flux is not "locked in," making the release erratic and unreliable. The additional effective air gap was apparently created by the grinding and etching of the magnet pole tips.

The moving slugs are fixed to the magnesium spider (MS) by means of padded clamping bars (CB). Below the slugs, fixed to the spider and encircling the center legs of the "E's" when the magnet is closed, are the moving coils (MC). These two coils are each made up of 150 turns of No. 20 round wire, potted in an epoxy resin and bonded to the magnesium piece.

These coils are energized only by the large pulse of current applied to themselves and the fixed coil in series during the "return" of the valve. The moving coils are wound in the same sense as the fixed coil, so that they add to the magnetic field, as well as operating in the leakage flux of the magnet in such a way as to provide a "motor" action from the interaction of their current with the magnetic field.

D. Dash Pot

The operation of the dash pot is best seen with the aid of Fig. 36. The piston (P) is free to slide on the shaft (S) of the valve, but the nut (N) is fixed solidly. The tapered face of the nut mates with the back of the piston and seals several large relief holes (H). During the outward motion of the shaft, the nut is free to leave the piston and open the relief ports. The piston, which is loosely sealed to the cavity walls (C) with a steel piston ring, is then free to move through the oil, and is forced by the spring (SP) against its outer stop (OS) (a distance of about 0.1 in.). When, however, the shaft returns, the nut mates solidly with the piston, sealing the large ports. The oil which is trapped in the cavity must then be forced out through the loose seal at the front of the piston and the adjustable valve (V), transmitting a large retarding force to the shaft.

It is useful to estimate the effect of this type of "dash pot," which depends on kinematical parameters and is more or less independent of the viscosity of the oil. The following analysis is quite approximate, but does illustrate the important parameters. We employ the simple model shown in Fig. 37. The area of the piston is A, and the initial length of its cylinder ℓ. The orifice has an area A_2 and a length ℓ_2, after which the liquid is assumed to escape freely. We assume the liquid to be incompressible.

Figure 36

Dash Pot

Explanation of Symbols

P   Piston
S   Drive shaft
N   Nut (fixed to drive shaft)
H   Large relief holes in piston
C   Cavity walls
SP Spring
OS Outer stop on piston motion
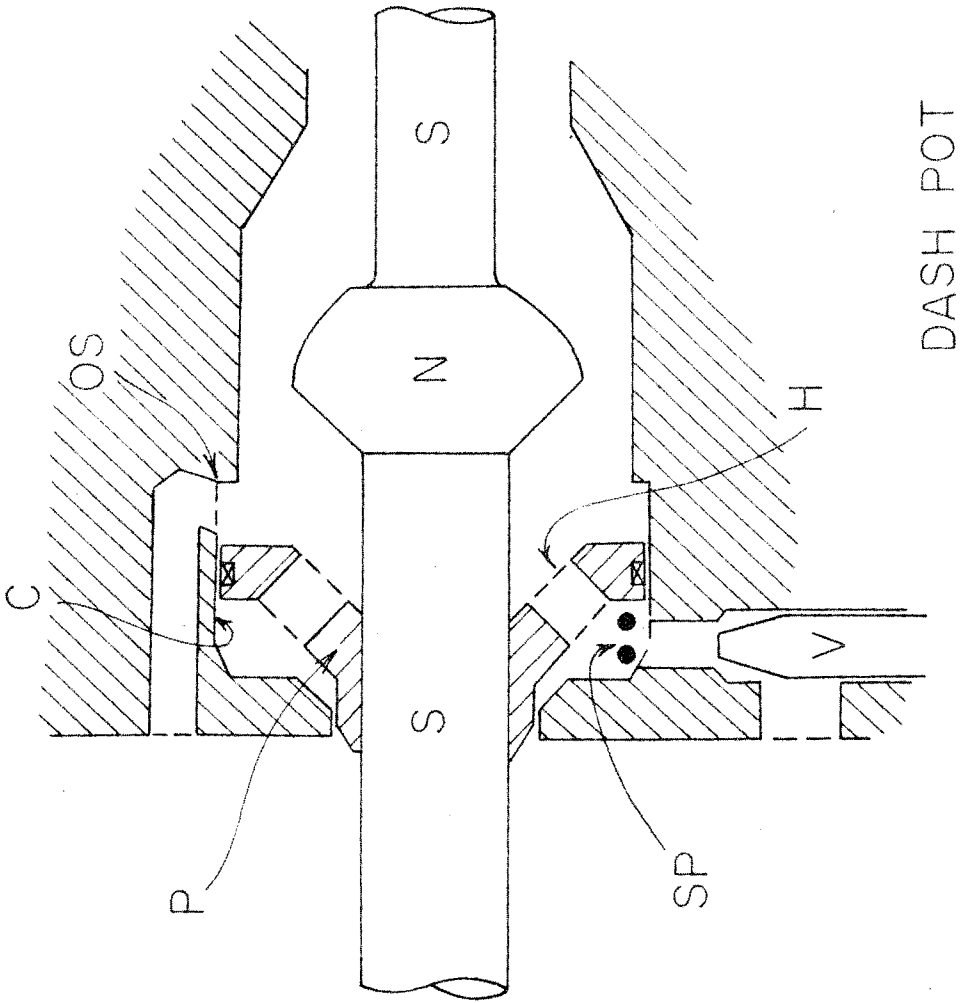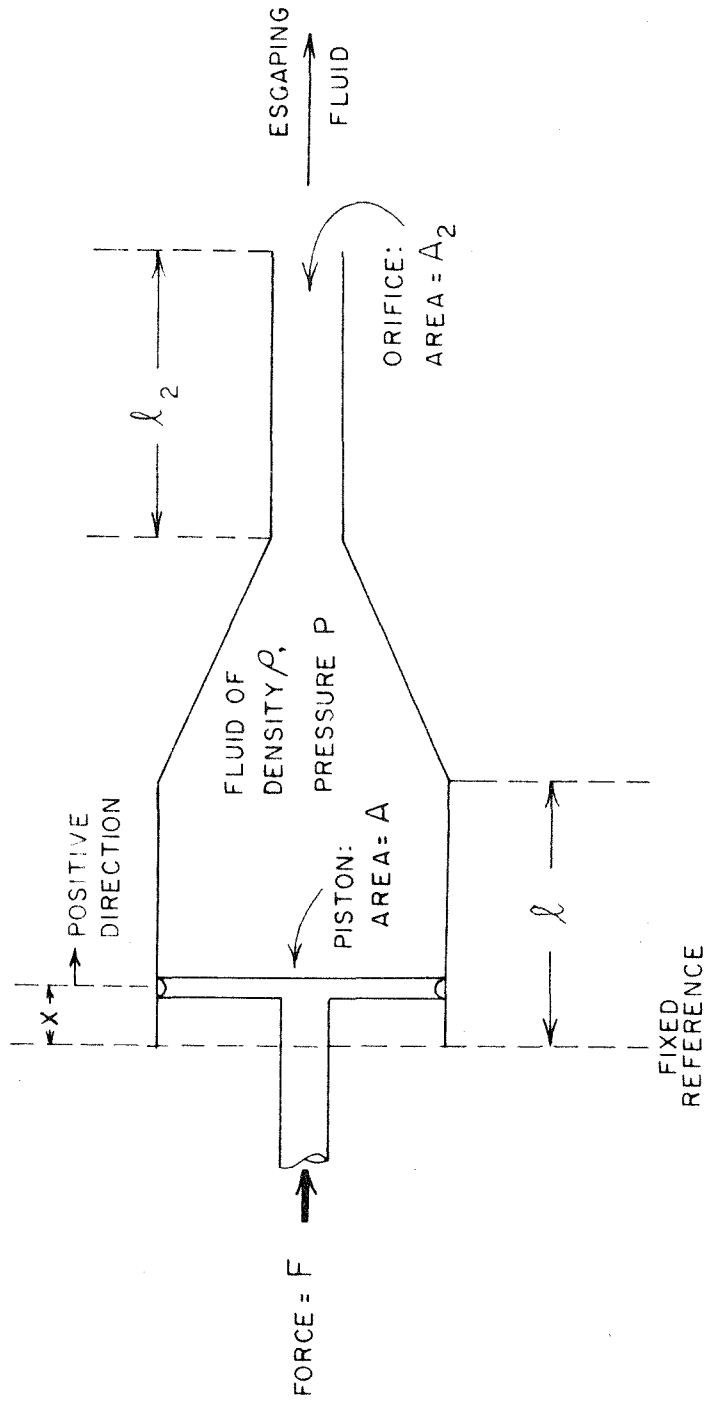V   Valve which provides adjustable orifice

Figure 36

Figure 37

MODEL USED FOR DASH POT CALCULATION

Applying the conservation of energy, we have

$$-A \int_0^x P dx + \tfrac{1}{2} A_2 (\ell_2 - x) \rho v_2^2 + \tfrac{1}{2} A \ell \rho v^2 + \tfrac{1}{2} \rho A_2 \int_0^t v_2^3 dt = \text{Const.} \quad (AII\text{-}5)$$

where v_2 = velocity of the escaping oil; $v = \dot{x}$ = velocity of piston; P = pressure in cylinder; and ρ = density of the oil. The last term on the left represents energy carried away by the escaping oil.

The incompressibility condition implies $v_2 = \sqrt{K} v$; $K = A^2/A_2^2$. Substituting this into equation AII-5, differentiating with respect to time, and dividing through by v, we have

Force on Piston = PA

$$= \rho \dot{v} \left\{ A[\ell - x] + A_2 \ell_2 K \right\} \qquad (AII\text{-}6)$$
$$+ \tfrac{1}{2} \rho A v^2 [K - 1]$$

For the device we are considering, K is a large number, $\sim 4 \times 10^3$, so we may approximate by neglecting $\rho A (\ell - x)$ since this is just the mass of the oil in the cylinder, small compared to the 10 pound mass of the valve, and also neglect 1 compared to K. Therefore,

$$\text{Force} = F_p \approx \tfrac{1}{2} K m \dot{v} + \tfrac{1}{2} \rho K A v^2 \qquad (AII\text{-}7)$$

where m is the mass of the oil in the exit orifice. The firstterm is an "effective mass," which presents an impact to the structure upon contact with the piston. Since $m \sim 1$ gram, then $mK \sim 4kg$, which presents a not negligible effect. To reduce the magnitude of this "impact," the leading edge of the dash pot is tapered, making A_2 much larger at first, and allowing this effective mass to be added to the moving valve structure more slowly.

If we assume that the holding magnet is applying a constant force F to the valve while it is closing (which is approximately true), we can solve the equation of motion of the valve after it contacts the dash pot. The

algebraic details are omitted, but the result is as follows.

Immediately after contact with the dash pot, the velocity of the valve is reduced as

$$v_1 = \sqrt{m/(m + Km)}\, v_0 \tag{AII-8}$$

where m is the total valve mass; v_1 is the velocity after contact; and v_0 is the contact velocity. In the physical structure $v_0 \sim 5$ m/s, $m \approx 4.5$ kg, $Km \sim 4$ kg, so $v_1 \approx 0.69\, v_0 \approx 3.4$ m/s.

Then,

$$v = \sqrt{F/\alpha}\ \operatorname{ctnh}\left[(t + C_1)\sqrt{\alpha F}/M\right] \tag{AII-9a}$$

$$x = (M/\alpha)\ \log\left\{\sinh\left[(t + C_1)\sqrt{\alpha F}/M\right]\right\} - C_2 \tag{AII-9b}$$

and

$$C_1 = (M/\sqrt{\alpha F})\ \operatorname{ctnh}^{-1}\sqrt{\alpha v_1^2/F} \tag{AII-9c}$$

$$C_2 = (M/\alpha)\ \log\left[\sinh(C_1\sqrt{F\alpha}/M)\right] \tag{AII-9d}$$

and $M = m + Km$; $\alpha = \frac{1}{2}\rho AK$.

Pertinent design parameters are represented by several quantities. One is the asymptotic velocity $v_a = F/\alpha$. In our system $F \approx 1000$ lb ~ 4000 Newtons, (the difference between the magnet holding force and the driving force) and $\alpha \sim 8 \times 10^3$. Thus $v_a \sim \sqrt{\frac{1}{2}} \sim 0.7$ m/s.

If we now use the formulas AII-14 a-d to find the actual velocity at the end of the dash pot stroke, taking it as 1/16 in, we find ~ 1 m/s, a decrease from the incoming velocity a factor of 5 in a total distance (including the tapered portion) of about 0.1 inch. The above numbers were evaluated for the case in which the variable orifice ("V" in Fig. 36) was wide open, providing an exit effectively about $\frac{1}{4}$ inch in diameter by about 1 inch long. The dash pot can be made considerably stiffer by reduction of the orifice. This adjustment is made externally, and constitutes a "trim"

on the closing impact of the valve. In practice the dash pots are trimmed
until all four valves have about the same closing characteristics; i.e.,
they all require about the same input energy to "catch" reliably on the
return.

E. Driving and Monitoring Circuits

The requirements of good timing accuracy and synchronizability
of the starting time of the valves place certain demands upon the nature
of the magnet and its power supply. We require that the inductances of
all four holding coils be the same, so that the release times are alike.
Therefore the 0.015 inch nylon pads in the magnetic circuit insure that
the inductance of the solenoids is primarily determined by a reproducible
air gap rather than by the iron characteristics themselves and the exact
way in which the pole tips contact. On the other hand, we would like to
keep the energy storage in the magnets, and thus the thickness of the air
gaps, as small as possible in order to release the solenoids quickly by
application of a large reverse voltage to them. A small inductance for
the magnets and a large reverse voltage pulse are also desirable features,
but the limit to these is set by practical circuit considerations. A small
inductance, of course, implies fewer turns on the magnet but necessitates
a larger current to achieve the desired magnet excitation. Since the recti-
fiers which supply the magnet must be triggerable tubes such as thyratrons
in order to withstand the large reverse voltage pulse, the number of turns
on the coils is determined by the maximum current one can expect to supply
with these tubes. We have compromised by employing four F.G. 105 thyratrons,
which can supply about 24 amperes, or about 6 amperes per magnet. With our

present system the inductance of the four magnets in parallel is about

0.15 hy, and with the release voltage 3KV, the current in the magnets could

be drained in somewhat over 1 ms. (Actual breakaway would occur, however,

in about 0.4 ms, since the holding force falls of roughly as I^2.) In actual

operation the release is somewhat slower, since it turns out to be desirable

electrically (see discussion below) to apply the release voltage through

the moving coils (in series with the fixed coils), with a consequent increase

in the effective inductance of the magnets.

The over-all driving circuit is illustrated in block form in

Fig. 38. The sequence of operations during release of the magnet occurs

as follows, with the magnet current and voltage wave forms shown (idealized)

in Fig. 39. In the quiescent condition, the grids on thyratrons 1a, 1b, 1c,

and 1d are held positive by the control TT-1, and the tubes conduct as simple

rectifiers supplying current to the fixed coils (FC). The condensers shown

are initially charged to, typically, a negative potential of from 2000 to

3000 volts. When the magnets are to be released, TT-2 triggers TH-2 (pt. "a"

in Fig. 39), connecting C-1 (25 μfd) to the fixed coils through the moving

coils MC and an external inductor (IND), of about 0.09 hy. inductance.

Simultaneously, TT-1 drives the grids of TH-1 (abcd) negative. In approxi-

mately 0.5 ms, the current through C-1, IND, and MC has risen to the holding

current value, at which time the condenser has seized control of the magnets,

and, still being negative, depresses the plates of TH-1 (a,b,c,d), so that

they are extinguished (pt. "b" Fig. 39). The LC combination of FC, MC,

IND, and C-1 has a resonant half-period of about 5 ms, so that there still

remain about two milliseconds while the plates of TH-1 (a,b,c,d) are held

negative. During this period they deionize, and are able to tolerate forward
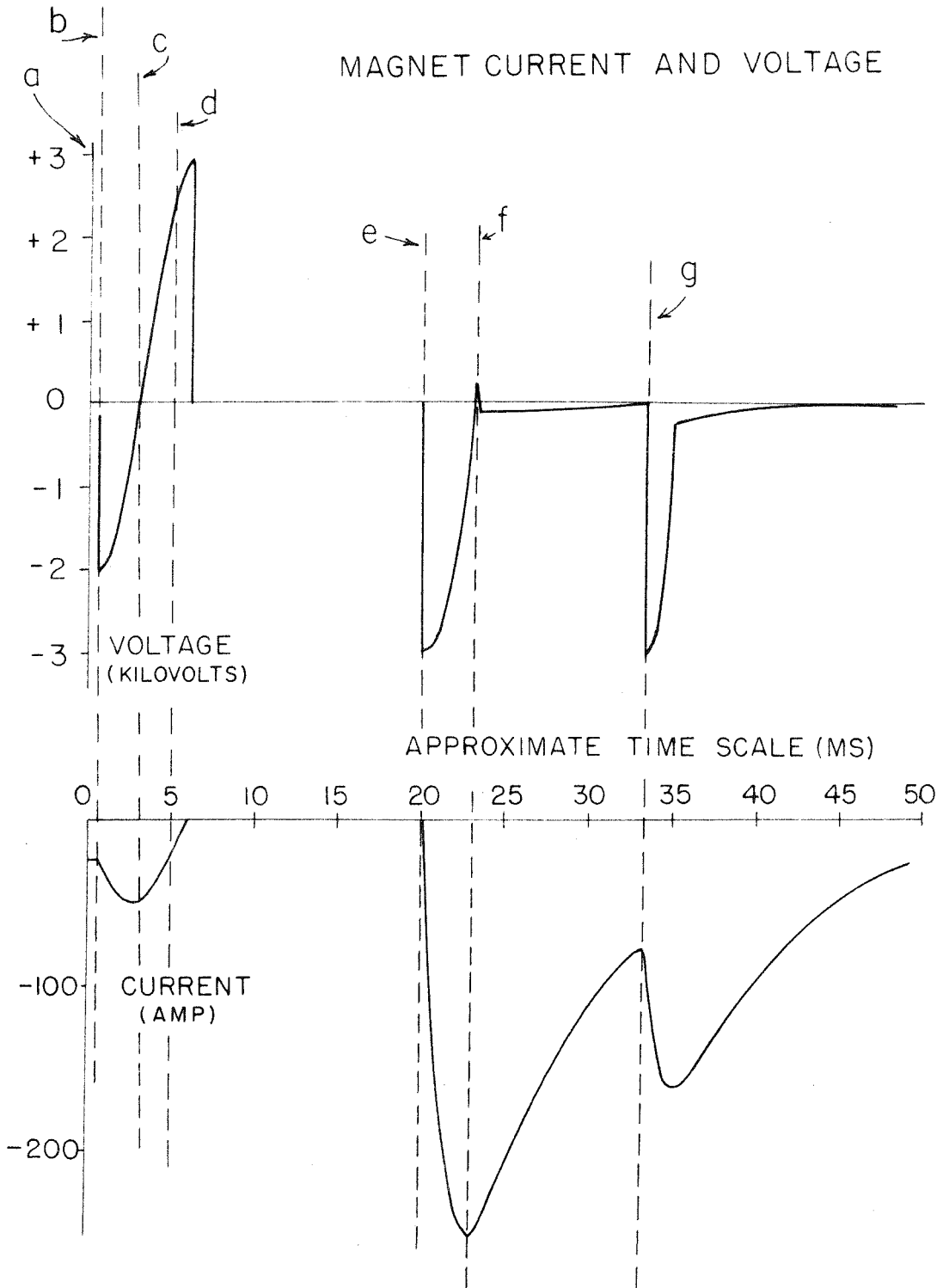
-234-
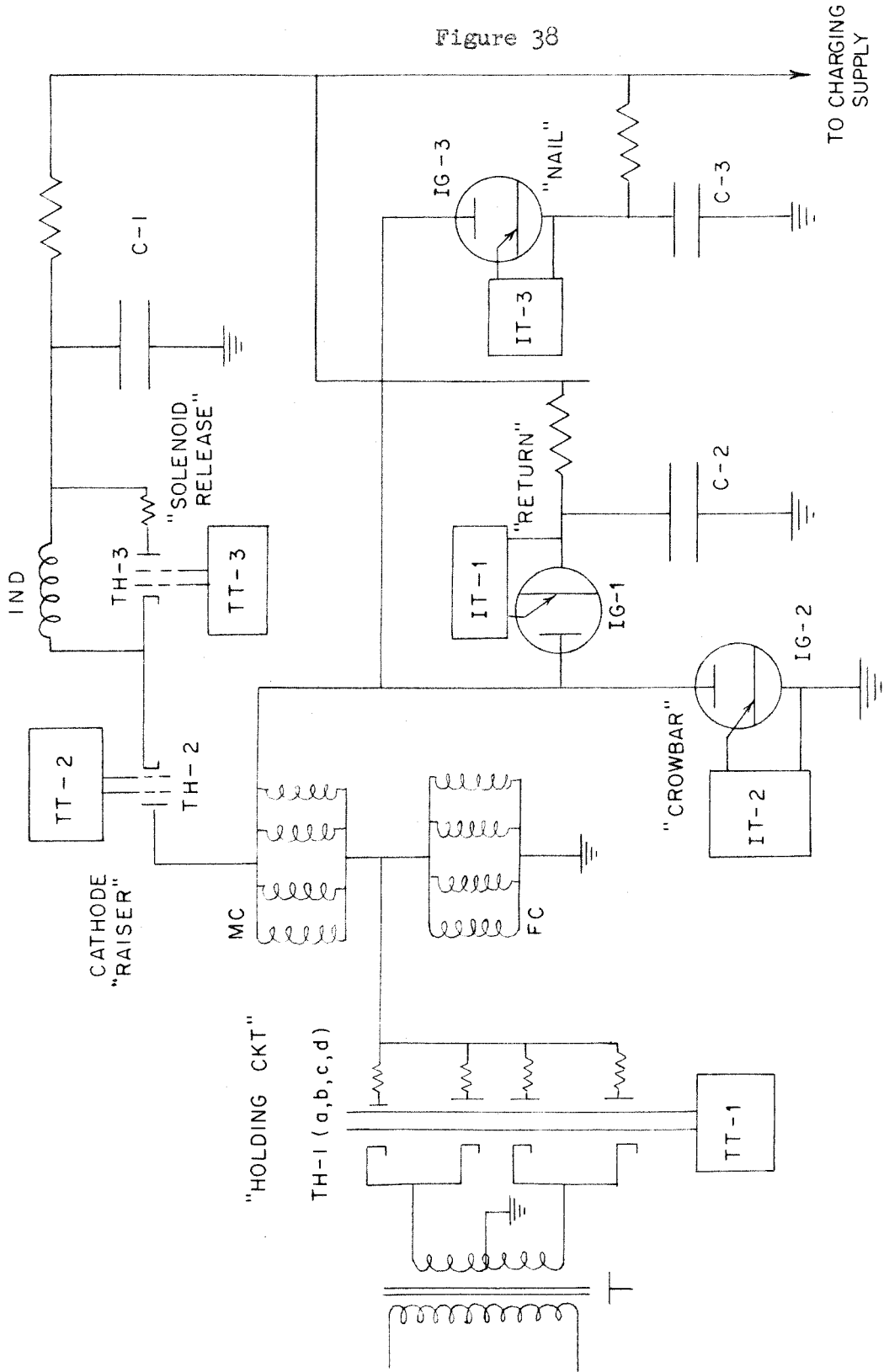
Figure 38

EXPANSION ENGINE POWER CIRCUIT

Figure 39

MAGNET CURRENT AND VOLTAGE

voltages. (These tubes require about 1 ms for deionization.) The resonant LC combination mentioned has a fairly high Q, so that after the current has reached its maximum value of about 40 amperes (pt. "c" Fig. 39), the voltage begins to reverse on C-1, and would reach a positive value of some 3000 volts when the current has vanished. However, when the current has dropped to about 20 amperes again and the potential of C-1 is about 2500 volts positive (pt. "d" Fig. 39), TH-3 is fired, shorting out IND, and reducing the inductance of the LC combination. At this time the current in FC and MC vanishes approximately linearly in about 1.5 ms, TH-2 extinguishes, and the magnets are released.

The reason for applying the releasing voltage pulse through MC rather than directly on to FC is that the two sets of coils are mutually coupled through the magnetic circuit of the solenoid. Were the large voltage pulse applied to the junction of the two sets of coils, the induced voltage in MC would be added to the applied potential, raising parts of the moving coils to a higher potential with respect to ground and putting additional strain on the insulation.

When the valves have traveled to their open condition, "bounced," and are returning, the current pulse is generated to make up mechanical losses. This is done by firing IG-1, which connects the 200 μfd condenser bank C-2 to MC and FC in series (pt "e" in Fig. 39). Since at this stage of valve motion, the magnet is open and has, consequently, a quite small inductance, the current rises to its peak value of about 240 amperes in about 3 - 5 ms. At this time (pt. "f" in Fig. 39) the potential of C-2 is zero, or slightly positive, and the "crowbar," IG-2, is fired, short-circuiting the coils and stopping the LC oscillation. The energy that was stored

in C-2 is then transferred to the magnet, and will there remain until removed either by conversion to mechanical energy or by resistive dissipation.

After the valve has been pulled closed by the return pulse, an additional burst of current is supplied by the 50 μfd condenser C-3 through IG-3 (nail) in the same manner as the return pulse (pt. "g" Fig. 39). This circuit has the function of "securing" the closed position of the magnets. There is no "crowbar" ignitron for this condenser but the function is supplied by the holding thyratrons themselves, as the positive bias is restored to their grids in time to retain the "nail" current pulse in the magnets. This final burst of current then decays to the holding value, and the cycle is complete.

The advantage of operating the magnets in electrical parallel is that they then tend to be self-synchronizing. If, during the return pulse, one of the valves is lagging the others, its magnet will be opened wider, and the inductance correspondingly smaller. Therefore it will accept more current from the return condenser, and it will be found (upon more careful analysis) to have acquired more energy in its magnetic field. This field, upon being destroyed by the closing of the magnet, is converted into mechanical energy. Therefore the lagging valve is driven harder. The same effect is true in reverse of a valve which leads the others.

Each valve has a position transducer, which is simply a carbon potentiometer rotated by a lever actuated by the motion of the valve structure. A DC voltage is impressed across the potentiometer, and the position of the valve read as a voltage from the center tap. In addition there are micro-switches attached to the housing of the engine in such a way that they are actuated when the valve is open. The switches function as safety

indicators, in case any of the valves fail to close.

F. Operation of the Engines

Each of the valves was operated on a test stand several hundred to several thousand times before it was installed, and the four have been operated several hundred times in parallel, under operating conditions. We have encountered a number of troubles with them, most of which appeared after installation. For example, the dash pots seem to change their characteristics somewhat when the valves are operating under internal pressure, and require readjustment in order that the four engines will have the same closing characteristics.

The moving coils have caused trouble owing to shorts between turns. The shorted turns act as secondaries of a transformer and absorb a large fraction of the energy in the condenser bank. The resultant local heating apparently damages the insulation and creates an arc to ground, destroying the coil. Steps have now been taken to eliminate these shorted turns. We first require that all coils undergo a severe testing procedure before being installed in order to eliminate weak or defective ones. In addition, RC terminations have been installed on all the long (50 ft.) cables between the power supply rack and the engines themselves. These terminations serve to reduce insultation damaging action of fast high voltage pulses from the firing of the ignitrons which in the absence of proper cable terminations may double upon reflection from the magnet coils. No new coil troubles have been experienced since the corrective measures were taken, although aging and mechanical shock may eventually cause more shorts. Probably the moving coils should be redesigned.

The most persistent and annoying difficulty with the valves is their propensity for failure to "catch," or remain closed after a cycle. This is usually the result of any of several kinds of maladjustments of the engines, such as the dash pots, electrical timing, or condenser bank voltage. However, now that most of the initial difficulties have been overcome, the valves appear to be quite reliable when properly adjusted, and there seems to be no reason why they cannot be made very reliable.

The oscilloscope trace shown in Fig. 34c was taken during a typical cycle of the valves. The operating conditions are given in the caption. An interesting point is ascertained through analysis of the motion (upper trace) and current (lower trace). The electrical efficiency of the pulsed return circuit can be determined in two ways. One can compare the "free oscillation" motion of the valves to that when they are returned, which, coupled with a knowledge of the gas spring characteristics, yields the energy lost in a single cycle. The picture showing the motion during the returned cycle indicates the velocity and hence kinetic energy which the moving structure has when it contacts the dash pot. The sum of these two quantities is the mechanical energy given to the valve. Alternatively one can integrate with respect to time the square of the current and multiply by the known resistance of the circuit, yielding the electrical energy dissipated during the operation. These measurements have been made on a number of pictures, and the two methods agree quite well. The efficiency figure thus obtained is about 50%, which is unexpectedly high for this type of high-current pulsed system. Of the 500 joules stored in the condenser bank, about 250 joules are converted into mechanical energy. The comparatively high efficiency indicates that this magnetic configuration might be useful in other electromechanical applications.

APPENDIX III

PROPERTIES AND PURIFICATION OF TUNGSTEN HEXAFLUORIDE

A. Physical Properties

      In its pure state, tungsten hexafluoride forms a colorless liquid of high density and comparatively low index of refraction. We have measured the vapor pressure and density of the liquid above its boiling point, and the results are presented in Fig. 40. The vapor pressure measurements were made in the small bubble chamber (Chapter I-2) in the following manner. At a given temperature, measured by a thermocouple, the vapor pressure of the fluid was balanced by helium gas pressure applied to the pop valve side of the expansion diaphragm illustrated in Fig. 3a (Chapter I-2). The volume of liquid was adjusted so that the diaphragm was in its center or unstressed position, and the pressure of helium required to hold it there was read on an external pressure gauge. The accuracy of the curve shown in Fig. 40 is probably about 1 to 2 percent, determined chiefly by the error in the pressure gauge used, since the temperature measurement is believed to have been quite good. The density measurement was made also in the small chamber. The calibrated volume adjuster mentioned in Chapter I-2 was employed to measure the thermal expansion of the liquid (under its vapor pressure) from room temperature to about $150^{\circ}C$. The density at lower temperatures can be found (78) in the literature. The measurement of density was not as accurate as that for the vapor pressure, since it was necessary to correct for the temperature difference between the liquid in the chamber proper and that in the volume adjuster. We have estimated a nominal error of about $\pm 4\%$.

      The estimated critical constants for WF_6 are also shown on Fig. 40, and are: Critical temperature $\cong T_c = 451.3^{\circ}K = 178.2^{\circ}C$ ($\pm 0.5^{\circ}$). Critical pressure $\cong P_c = 46.3$ atm. (± 1 atm). Critical density $\cong \rho_c = 1.4$ gm/cm^3

Figure 40

PROPERTIES OF WF$_6$
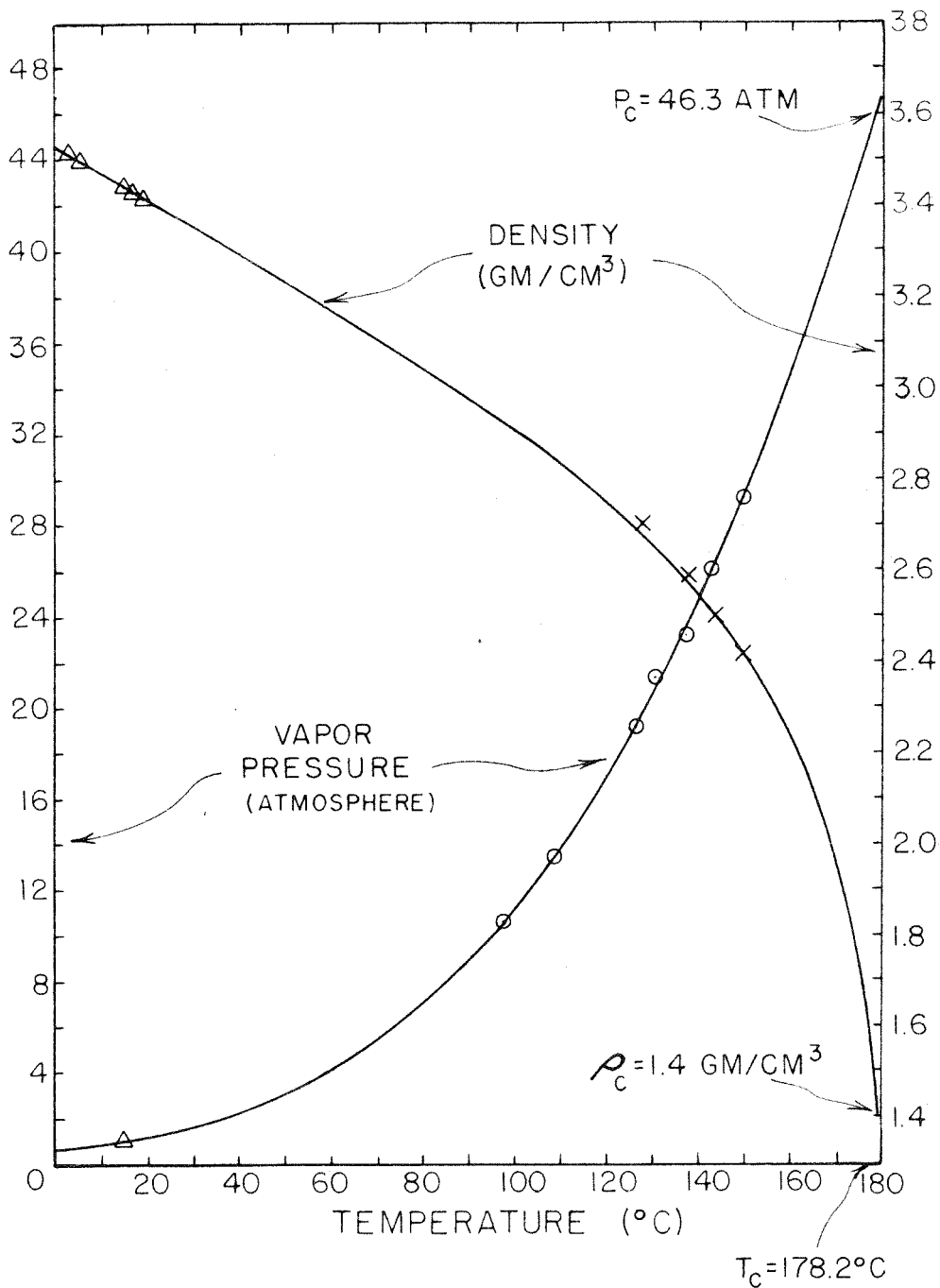
(error not known). The only one of the above constants obtained directly was the critical temperature, as the critical pressure was beyond the range of the pressure supply which we had available. To measure the critical temperature, we heated the chamber slowly, measuring the temperature with a thermocouple. As the liquid approached the critical point, we were careful to keep the liquid meniscus in sight through the chamber windows. At the temperature noted above (which we passed through several times) we observed the conversion of the meniscus into a broad band of critical opalescence. The critical pressure was estimated by noting that our vapor pressure data to the highest value measured fitted within the experimental error the function $P = Ae^{B/T}$ where A and B are constants. This function was then extrapolated to the temperature $T = T_c$. The value of ρ_c was predicted on the basis of the law of corresponding states, in the form of $MP_c/\rho_c T_c$ = universal constant, where M is the molecular weight. The constant is of course not really universal, but the variations in this number seem to be smaller among "non-associating" liquids of high molecular weight like WF_6 than among those of smaller molecular weight, so the foregoing estimate is probably reasonably accurate.

The index of refraction measured at $144^\circ C$ is 1.28 ± 0.02. This value was obtained by observation with a transit of the difference in the apparent depth of the interior of the small chamber above and below the liquid level. The small correction due to the index of refraction of the vapor was estimated from the results of the measurement on the liquid. The result is low for such a dense fluid, but this feature seems common among fluorinated liquids. For example, the fluorinated hydrocarbons in the liquid state seem to have markedly lower indices of refraction than their non-fluorinated counterparts.

B. Chemical Considerations

The chief handling problem with WF_6 for bubble chamber use is the effect of the impure liquid on windows. If WF_6 becomes contaminated with water, it reacts through the chemical process $WF_6 + H_2O \rightarrow WOF_4 + 2HF$. The hydrogen fluoride, especially in the presence of trace quantities of H_2O, will react on silica (or glass) through the reaction $4HF + SiO_2 \rightarrow SiF_4 + 2H_2O$. Therefore, for WF_6 in the presence of glass with a water contaminant, we have the process $2WF_6 + 2H_2O \rightarrow 2WOF_4 + 4HF$; $4HF + SiO_2 \rightarrow SiF_4 + 2H_2O$; $2H_2O + 2WF_6 \rightarrow$ and so forth until either the WF_6 or the SiO_2 is exhausted, as we have a chemical chain reaction (with a unit multiplication). Of course, the situation is really much more complicated than this for an actual bubble chamber, because there are many other compounds around and different impurities may participate in this reaction. All that is really necessary to break the "chain" is to have materials in contact with the liquid that have a strong affinity for HF or H_2O, and combine with them without further production of water or HF. Such a material, for example, is NaF, which combines with HF directly as NaF·HF, producing no water as a byproduct. It is possible that other materials have this function as well. Nevertheless, it is clear that one of the best methods to fight the etching problem is to remove as much as possible of the HF contaminant from the WF_6 and the H_2O traces from the chamber system. Pure WF_6 does not appear to attack quartz or pyrex even at the elevated operating temperature. Therefore a good purification technique is called for. The system we employ is described later.

In the course of our work with WF_6, we have also had an opportunity to study its effect upon various materials, some at elevated

temperatures. We find that inconel and monel (and no doubt also pure nickel) are quite resistant to WF_6, and in fact seem to be quite immune to attack even at high temperatures. Stainless steel also appears to be quite resistant, although we have not tested it to the degree we have inconel and monel. Even copper seems to be reasonably inert to WF_6 at low temperatures, and since the WF_6 was shipped to us in steel tanks, there is reason to believe that steel is also quite resistant (at low temperatures). Possibly most of the metals, if attacked, tend to form fairly impervious fluoride coatings which restrict further reaction. For handling at high temperatures, however, particularly when high purity is desired, the nickel-rich alloys are probably to be preferred.

Among the plastics, Teflon appears to be definitely superior, as one might guess. We have had Teflon gaskets in contact with WF_6 for long periods ($\sim$ two weeks) at the operating temperature ($\sim 145°C$) and have observed some small effect. This is primarily a darkening in color of the Teflon, although the mechanical properties of the plastic do not seem to be at all affected. There is also evidence that the WF_6 penetrated to some extent the 0.030 inch Teflon diaphragm in the expansion system of the small chamber. The conditions of pressure, of course, were extreme, since when the chamber was hot but not operating, the diaphragm was often left holding the 400 psi vapor pressure for long periods. A peculiar effect was also noted when the Teflon parts which had been in contact with WF_6 were removed and exposed to the air. After a period of a few hours, all such surfaces grew "whiskers" (light yellow in color) up to about $\frac{1}{2}$ inch long. No satisfactory explanation for this phenomenon has been found. It should be noted that all Teflon used in the tests was the commercial grade, which is a

sintered material of comparatively large grain size and porosity. A less
porous form which is now available, Teflon 100X, (quite transparent in thin
sheets) may not exhibit the characteristics described above.

Kel-F was also tested. A small piece about 1/16 inch thick which
was quite transparent was kept in contact with hot WF_6 for several days.
At the end of this time it was opaque, and suffered some change in its me-
chanical properties. A small piece of Viton (A Du Pont fluorinated rubber)
subjected to the same test showed severe damage, as did the quartz windows
on the chamber. We have assumed that the window etching was caused by the
products of the chemical action upon the Viton, although this is only a
conjecture.

It must be mentioned that whenever we have filled the small cham-
ber with WF_6, we have found it to be of a marked purplish-pink hue. The
degree of coloration has varied quite widely from one filling to another,
and seems to have nothing to do with the temperature. That it is due to
an impurity and is not a property of WF_6 itself we know because samples
distilled into clean glass tubes have been completely colorless at all tem-
peratures.

C. Purification Techniques

One operation which is important for purification of WF_6 is a
thorough pretreatment of the containers. All handling systems should be
thoroughly evacuated and baked while connected to the vacuum pumps, and
should not be exposed again to air. Of course, the necessity for having a
really leak-free system is obvious, for leaks will almost invariably intro-
duce water vapor. We also pretreat our systems between pumping and baking
operations with a small quantity of WF_6, which we then discard. Such an

operation where possible should materially reduce the traces of H_2O.

The system we employ for purification of the WF_6 was suggested to us by Dr. Bernard Weinstock (37,38). The chief difficulty in separating WF_6 from the usual HF contaminant by distillation is the similarity of their vapor pressures. Their boiling points are within a few tenths degree C of each other, so distillation at room temperature (which is close to their boiling points) is impractical. However, WF_6 freezes about 2.5°C, which is a few degrees below its boiling point, while HF, apparently because of the tendency of its molecules to polymerize, remains liquid to about -96°C. Thus the heat of sublimation of WF_6 is roughly the sum of the heat of fusion plus the heat of vaporization, while that for HF is the heat of vaporization only. Therefore by the Clausius-Clapeyron relation (Equation II-1-19, Chapter II-1), the larger latent heat of WF_6 insures that dP/dT is greater, and the vapor pressures of WF_6 and HF should separate as the temperature is lowered. This is actually the case, and at a temperature (-100°C) just below the freezing point of HF, the vapor pressure of HF (450 μ) is about 20 times that of WF_6 (24 μ). At this temperature the substances should be separable.

The drawing (Fig. 41) illustrates the arrangement of our purification system. WF_6 from the storage tank (ST) is distilled at room temperature through the container (G) containing carefully dried NaF, to remove a large fraction of the HF contaminant, into the first distilling tank (T-1). This tank connects to a large cold trap (CT) which is kept immersed in a temperature bath at -100°C. This bath consists of a freezing eutectic mixture of 2 parts trichlorethylene and one part chloroform. The cold trap itself is constructed primarily of severallengths of thin-walled tubing so that it possesses a very large internal surface area in good thermal contact

---

Figure 41

WF$_6$ "Weinstock" Purification System

Explanation of Symbols

|	
SC	Shipping container for WF$_6$
VL	Valve on shipping container
SV	Special monel valve
G	Getter (NaF or KF)
FL	Float in WF$_6$ tank
T-1	First distilling tank
T-2	Second distilling tank
EB	Container for -100°C eutectic bath
DT	Distilling (Weinstock) cold trap
VV	Vacuum valve (2 inch Globe nickel valve)
V	Vacuum system
DSV	Dual special monel valve
F	Sintered nickel filter
VA	Volume adjuster
C	Chamber filling line
B	Auxiliary chamber filling line
A	Auxiliary line (can be to vacuum system or to Freon-hydrocarbon filling system)
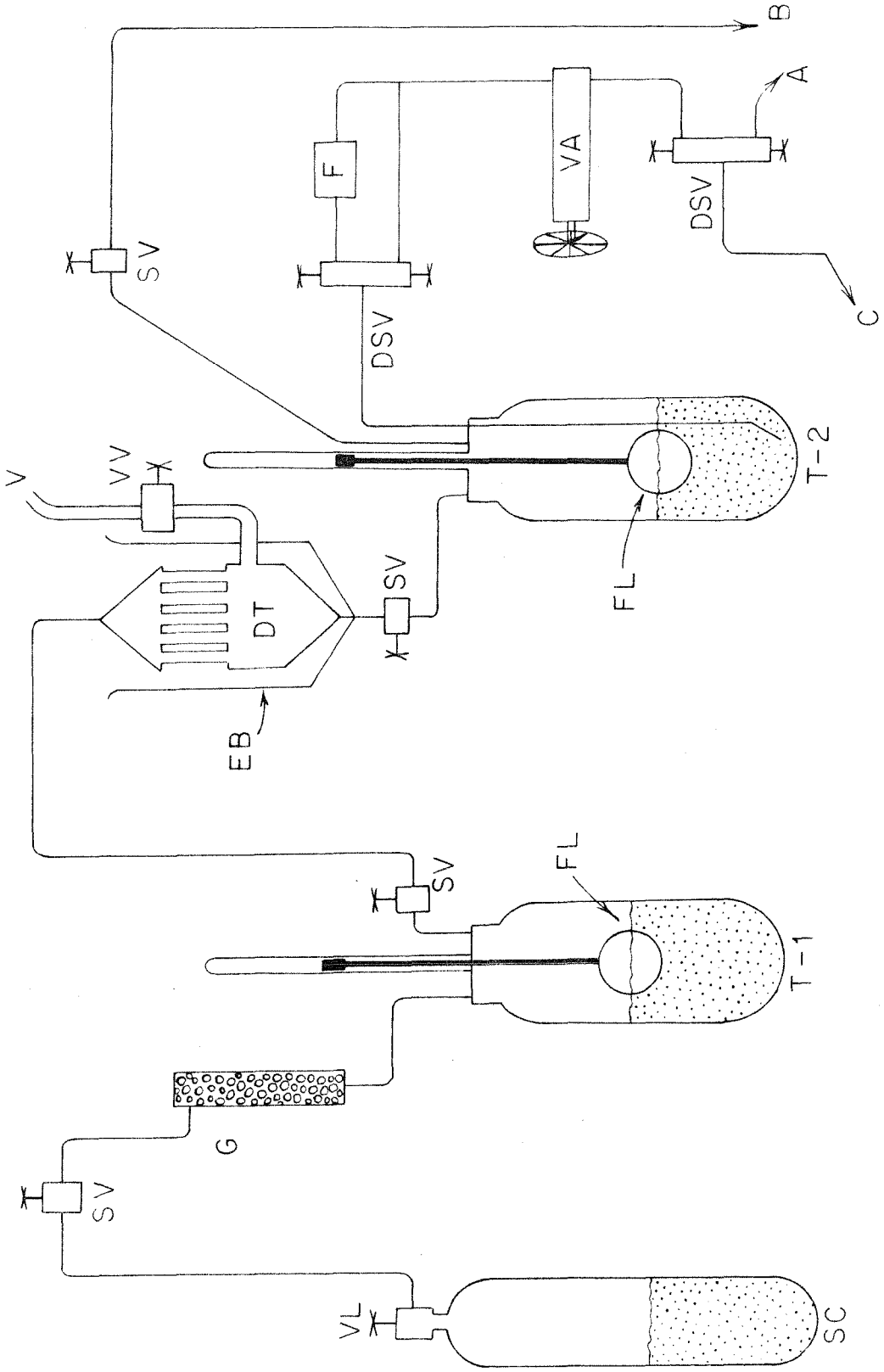
Figure 41

with the bath. A small quantity of WF_6 (measured by the level of the float in T-1) is evaporated into this trap at a time, so that we are assured that the average thickness of frozen WF_6 on the walls is small ($\sim$0.1 - 0.2 mm). T-1 is then valved off and the cold trap is evacuated by way of the vacuum line (VL), which passes through a liquid nitrogen trap before it reaches the vacuum pumps. The length of time the system is pumped is calculated so that about 5 - 10% of the WF_6 is lost. Because of the much higher vapor pressure of HF, essentially all of this contaminant should be pumped away into the liquid nitrogen trap. The coating of material on the walls of the distilling cold trap is required to be thin so that we may avoid trapped pockets of HF beneath the WF_6. This operation is repeated two or three times, and then the eutectic bath is drawn off and the distilling trap (now valved off from the vacuum system) is allowed to warm to room temperature. The melted WF_6 collects in the bottom of the trap, and then is allowed to flow by gravity through a valve into the final distilling tank (T-2). The exact purity of the WF_6 thus obtained is not known, but it should at least be quite free from HF.

References

1. J. J. Lord, Private Communication.

2. E. V. Kuznetsov, M. F. Lomanov, G. A. Blinov, and Chuan Chen-Niang, J. Exptl. Theret. Phys. (USSR) 31, 911 (1956). /Transl. Soviet Physics J.E.T.P., 4, 773 (1957)/.

3. D. C. Oakley and R. L. Walker, Phys. Rev., 97, 1283 (1955).

4. R. L. Walker, J. G. Teasdale, V. Z. Peterson and J. I. Vette, Phys. Rev., 99, 210 (1955).

5. A. V. Tollestrup, J. C. Keck, and R. M. Worlock, Phys. Rev., 99, 220 (1955).

6. J. C. Keck, A. V. Tollestrup, and H. H. Bingham, Phys. Rev., 103, 1549 (1956).

7. E. Knapp, W. Imhof, R. W. Kenney, and V. Perez-Mendez, Phys. Rev., 107, 323 (1957).

8. J. H. Malmberg and C. S. Robinson, Phys. Rev., 109, 158 (1958).

9. R. Smythe, R. M. Worlock, and A. V. Tollestrup, Phys. Rev., 109, 518 (1958)

10. M. Heinberg, W. M. McClelland, F. Turkot, W. M. Woodward, R. R. Wilson, and D. M. Zipoy, Phys. Rev., 110, 1211 (1958).

11. P. C. Stein and K. C. Rogers, Phys. Rev., 110, 1209 (1958).

12. J. W. Dewire, H. E. Jackson, and R. Littauer, Phys. Rev., 110, 1208 (1958).

13. J. L. Uretsky, R. W. Kenney, E. A. Knapp, and V. Perez-Mendez, Phys. Rev. Let., 1, 12 (1958).

14. J. I. Vette, Phys. Rev., 111, 622 (1958).

15. F. P. Dixon and R. L. Walker, Phys. Rev. Let., 1, 142 (1958).

16. R. R. Wilson, Phys. Rev., 110, 1212 (1958).

17. R. F. Peierls, Phys. Rev. Let., 1, 174 (1958).

18. J. J. Sakurai, Phys. Rev. Let., 1, 258 (1958).

19. V. Z. Peterson and I. G. Henry, Phys. Rev., 96, 850 (1954).

20. M. L. Sands, M. Bloch, J. G. Teasdale, and R. L. Walker, Phys. Rev., 99, 652 (1955).

21. R. M. Friedman and K. M. Crowe, Phys. Rev., 105, 1369 (1957).

22. M. Bloch and M. L. Sands, Phys. Rev., 108, 1101 (1957).

23. J. M. Sellen, G. Cocconi, V. T. Cocconi, and E. L. Hart, Phys. Rev., 110, 779 (1958).

24. M. P. Ernstene, Thesis, California Institute of Technology.

25. H. H. Bingham and A. B. Clegg, Phys. Rev., (to be published).

26. P. L. Donoho and R. L. Walker, Phys. Rev., 107, 1198 (1957).

27. A. B. Clegg, M. P. Ernstene, and A. V. Tollestrup, Phys. Rev., 107, 1200 (1957).

28. A. Silverman, R. R. Wilson, and W. M. Woodward, Phys. Rev., 108, 501 (1957).

29. H. M. Brody, A. M. Wetherell, and R. L. Walker, Phys. Rev., 110, 1213 (1958).

30. P. L. Donoho and R. L. Walker, Phys. Rev., 112, 981 (1958).

31. B. D. McDaniel, A. Silverman, R. R. Wilson, and G. Cortellessa, Phys. Rev. Let., 1, 109 (1958).

32. J. M. Teem and E. D. Alyea, Jr., Private Communication.

33. Donald Glaser, Private Communication.

34. J. L. Brown, D. A. Glaser, and M. L. Perl, Phys. Rev., 102, 586 (1956).

35. E. D. Alyea, Jr., L. R. Gallagher, J. H. Mullins, and J. M. Teem, Nuovo Cimento, 6, 1480 (1957).

36. D. V. Bugg, R.S.I., 29, 587 (1958).

37. B. Weinstock and J. G. Malm, J. Inorg. and Nucl. Chem., 2, 380 (1956) and B. Weinstock, Private Communication.

38. Cyril Dodd, Private Communication.

39. R. B. Leighton, R.S.I., 27, 79 (1956).

40. L. Voyvodic and E. Pickup, Phys. Rev., 85, 91 (1952).

41. E. J. Williams, Proc. Roy. Soc. (London) A169, 531 (1939).

42. E. J. Williams, _Phys. Rev._, 58, 292 (1940).

43. W. M. Powell, W. B. Fowler, and L. O. Oswald, _R.S.I._, 29, 874 (1958).

44. W. H. Pearlson (Minnesota Mining and Mfr. Co.) Private Communication.

45. L. Bertanza and G. Martelli, _Nuovo Cimento_, 1, (Series 10), 324 (1955).

46. G. Martelli, _Nuovo Cimento_, 12, (Series 9), 250 (1954).

47. Bertanza, Martelli, and Tollini, _Nuovo Cimento_, 5, 940 (1957).

48. G. A. Askar'ian, _J. Exptl. Theoret. Phys. USSR_, 30, 610 (1956). /Transl. Soviet Physics, J.E.T.P., 3, 4 (1956)/

49. G. A. Askar'ian, _J. Expl. Theoret. Phys._, USSR, 32, 1242 (1957). /Transl. Soviet Physics J.E.T.P., 5, 1011, (1957)/

50. F. Seitz, _Phys. of Fluids_, 1, 2 (1958).

51. M. S. Plesset and S. A. Zwick, _J. Appl. Phys._, 25, 493 (1954).

52. S. A. Zwick and M. S. Plesset, _J. Math. and Phys._, 33, 308 (1955).

53. G. Birkhoff, R. S. Margulies, W. A. Horning, _Phys. of Fluids_, 1, 201 (1958).

54. H. Lamb, _Hydrodynamics_ (Dover Publ., New York, 1945).

55. M. S. Plesset and S. A. Zwick, _J. Appl. Phys._, 23, 95 (1952).

56. _Handbook of Chemistry and Physics_ (Chem. Rubber Publ. Co., Cleveland, Ohio) 36th ed.

57. L. Page, _Introd. to Theor. Phys._ (D. Van Nostr. Co., New York, 1935).

58. P. Epstein, _Textbook of Thermodynamics_ (J. Wiley and Sons, 1954).

59. L. Z. Pollara, _J. Phys. Chem._, 46, 1163 (1942).

60. Blinov, Krestnikov, and Lomanov, _J. Exptl. Theoret. Phys._, USSR, 31, 762 (1956). /Transl. Soviet Phys. J.E.T.P., 4, 661 (1957)/.

61. W. J. Willis, E. C. Fowler, and D. C. Rahm, _Phys. Rev._, 108, 1046 (1957).

62. R. Evans, _The Atomic Nucleus_ (McGraw-Hill, New York, 1955).

63. Nagle, Hildebrand, and Plano, _R.S.I._, 27, 203 (1956).

64. P. Bassi, A. Loria, J. A. Meyer, P. Mittner, and I. Scotoni, _Nuovo Cimento_, 4, 491 (1956).

65. R. J. Pless and I. A. Plano, R.S.I., 27, 935 (1956).

66. E. J. Williams, Proc. Roy. Soc.,(London) A130, 310 (1931).

67. L. Katz and A. S. Penfold, Revs. Mod. Phys., 24, 28 (1952).

68. Batschinski, Z. Phys. Chem., 84, 643 (1913).

69. Selected Values of the Properties of Hydrocarbons, (Cir. of Ntl. Beau. of Stnds. C-461).

70. J. Frenkel, Kinetic Theory of Liquids (Oxford, 1946).

71. J. Von Engel, Ionized Gases (Oxford, 1955).

72. D. A. Glaser, Phys. Rev., 91, 762 (1953).

73. A. H. Samuel and J. L. Magee, J. Chem. Phys., 21, 1080 (1953).

74. F. S. Dainton, The Brit. J. Radiology, 31, 645 (1958).

75. Norman Davidson, Private Communication.

76. A. Sommerfeld, Mechanics of Deformable Bodies, (Academic Press, New York, 1950).

77. P. M. Morse and H. Feshbach, Methods of Theoretical Physics, Part II, (McGraw-Hill, New York, 1953).

78. Quoted in Gmelins Handbuch der Anorganischen Chemie, 8th ed., 54, 156.